UNIVERSITY OF ADELAIDE LIBRARY 19/3/82

THE INTERACTION OF 9-AMINOACRIDINES WITH NATIVE DNA

GARTH BOEHM B.Sc. (Adelaide)

Department of Physical and Inorganic Chemistry,

The University of Adelaide,

South Australia

A thesis submitted for the degree of

Doctor of Philosophy.

June, 1981.

awarded Dec. 1981

CONTENTS

SUMMARY

Binding curves describing the interaction of aminoacridines with DNA have generally been modelled in terms of Langmuir Isotherms. In recent years several more sophisticated mathematical models and modelling techniques, potentially applicable to these systems, have been described. However more accurate experimentally determined binding data are required than have generally been available to date in order to test these models properly. This work has been directed towards the experimental determination of accurate binding data for a series of 9-aminoacridines with native DNA at high ionic strength. A study of the binding of 9-aminoacridines and several 9-alkyl-aminoacridines has been made at several temperatures to determine the effect of 9-aminoacridine structure on the models chosen.

Following an introductory Chapter, a brief review of the literature relevant to the interaction of aminoacridines with DNA is the subject of Chapter II. Chapter III critically examines the experimental determination of binding curves with emphasis on the spectrophotometric method and equilibrium dialysis. The transform of experimental results to binding data is presented in Chapter IV. Chapter V discusses mathematical modelling techniques with emphasis on the Sequence Generating Function method. Several mathematical models potentially applicable to aminoacridine/native DNA systems are derived and their properties examined.

The experimental binding data are consistent with a single type of strong binding site with nearest neighbour site exclusion and next neighbour anti-cooperativity. Several other models are examined and found to be inconsistent with the data. The best fit equilibrium constants and their associated thermodynamic parameters are presented and discussed in Chapter VI.

To the best of my knowledge and belief, this thesis contains no material previously published or written by another person, nor any material previously submitted for a degree or diploma in any University, except where due reference is made in the text.

G. BOEHM

ACKNOWLEDGEMENTS

I wish to express my sincere gratitude to Prof. D.O. Jordan for his supervision, interest and encouragement during the course of this work. I am also indebted to Dr. T. Kurucsev for helpful discussions and a period of supervision. I thank all my fellow research workers for their interest, discussions and suggestions. I am particularly indebted to Dr. D.R. Turner for his keen interest, for innumerable helpful discussions and for critical proof-reading of the text.

I am indebted to Mr. M.G. Wagner, formerly of the Applied Mathematics Department, for his help with the derivation of Sequence Generating Functions and his suggestions concerning fast numerical solutions for the roots of polynomial equations.

Dr. Gillespe of the Department of Obstetrics and Gynaecology kindly permitted the use of an Isocap Liquid Scintillation Counter. Mr. R. Nash of the Department of Electrical Engineering allowed me to use an Intellec EPROM programmer.

I wish to acknowledge the capable and cheerful assistance of the electronics, mechanical and glassblowing workshop staff of this Department and the staff of the University of Adelaide Computing Centre.

Finally, I am personally indebted to my wife, Rosemary, for her continual interest and encouragement.

UNIVERSITY OF ADELAIDE LIBRARY

CHAPTER 1

INTRODUCTION

The role of nucleic acids as the basis of information transfer in life is well established. These compounds constitute the genetic material which enables living organisms to be maintained and propagated. There are two basic kinds of nucleic acids, deoxyribonucleic acid (DNA) and ribonucleic acid (RNA). DNA carries the genetic code, maintaining its integrity, and acts as a template for this code's translation into polypeptides via RNA.* Through the ability of DNA to maintain its integrity life is maintained and its ability to incorporate changes to the individual gene codes, called mutations, is the basis for evolution. Nucleic acids are indeed the remarkable molecules of life.

Although Miescher[1] first discovered nucleic acid in 1869 it was another 84 years until Watson and Crick[2,3] published their detailed account of the secondary structure of natural DNA. Nucleic acids are macromolecules of nucleotide sub-units which themselves are composed of heterocyclic purine or pyrimidine bases linked to pentose sugar-phosphate moieties through the C_1 carbon atom of the sugar. The macromolecule is formed by the condensation of these nucleotides through C_3-C_5 phospho-diester linkages. The primary structure is a sugar-phosphate backbone from which the bases protrude. The pentose sugar group is D-ribose in RNA and D-deoxyribose in DNA. The common bases of DNA are the two purines, adenine (A) and guanine (G) and the two pyrimidines, cytosine (C) and thymine (T). Other bases

---

* In some viruses, such as ØX174, RNA can fulfil both functions.

represent less than 1% of the bases in natural DNA's. In RNA uracil replaces thymine.

The secondary structure of natural DNA, proposed by Watson and Crick[2,3], consists of two strands of polydeoxyribonucleotide arranged side by side and anti-parallel to one another, that is for a given directionality one chain runs in a C_3-C_5 direction and the other in a C_5-C_3 direction. These two chains are paired through a specific, hydrogen bonded arrangement of bases, A paired with T and G with C. This specific pairing explained the earlier observation, known as Chargaff's Rule[4], that the ratio of A to T and G to C found in natural DNA's was indistinguishable from unity. The strands are arranged in a right-handed double helix with one complete turn every ten base pairs and a characteristic interbase spacing of 0.34 nm. The plane in which the base pairs lie is perpendicular to the major helix axis. This model of natural DNA structure is widely accepted although the evidence that it is the correct structure is largely indirect. A general picture of natural DNA is of two intertwined chains of alternating sugar and anionic phosphate groups containing the heterocyclic base pairs within the more hydrophobic core of the molecule.

The study of specific interactions of many kinds of molecules with DNA has become a major and important part of modern chemical and biological science. One of the first groups of chemicals to be studied in detail was the aminoacridines. Acridine itself was first isolated in 1870[5]. Many acridine derivatives, including aminoacridines, have been synthesized since that time. Medical interest in aminoacridines dates from 1888, and in 1913 Browning[6] discovered the effectiveness of Proflavine and Acriflavine as

topical antibacterial agents. This first practical medical use of aminoacridines was followed by the use of Mepacrine in the treatment of malaria. Most recently several 9-aminoacridine derivatives are being investigated as potential antineoplastic agents[7,8]. In addition to their use as chemotherapeutic agents aminoacridines find use as histological stains in a wide variety of applications[9].

The origin of much of the biological activity of aminoacridines is thought to lie in their interaction with nucleic acids[10]. It is not surprising that this interaction has been extensively studied. The most basic observation on the binding of cationic aminoacridines to DNA is that there are two distinct binding processes[11-13]. Cavalieri *et al*[11,12] proposed that the two processes arose from an electrostatic interaction with the primary and secondary phosphate groups of the DNA. However the detailed structure of natural DNA precluded this proposal as there are insufficient secondary phosphate groups to account for the extent of binding. The observation that the binding processes are independent of pH over the range of the pKa of the secondary phosphate groups also militates against this proposal[13]. In 1956 Peacocke and Skerrett[13] determined that the stronger of the two processes, involving a monomer dye-DNA interaction, occurs to the extent of 0.2 aminoacridine cations bound per DNA phosphate residue ($r \simeq 0.2$). The second, weaker process involving bound dye aggregates occurs up to $r = 1.0$, that is electroneutrality for the DNA[13]. Although the importance of the DNA bases to the interaction had been recognised[13-16], the Watson and Crick model[2,3] placed the bases on the interior of the double helix in close van der Waals contact. This seemed to preclude the possibility of direct interaction between the

aminoacridine cations and the DNA bases. In 1961 Lerman[17] made observations that led him to propose a model for the strong interaction. It was observed that, when Proflavine was bound in the strong mode, the length of the DNA molecule increased, with an accompanying decrease in mass per unit length[17]. These observations were consistent with an unwinding of the helix and the insertion of aminoacridine between adjacent base pairs of the DNA helix. This process is called intercalation[17]. Variations to the Lerman model have been proposed[18-20] but the basic concept of a structural change of the DNA allowing insertion of the aminoacridine between adjacent base pairs is generally accepted as the mode of strong binding to DNA.*

The intercalation model can explain the mutagenic activity of aminoacridines. The doubling of the interbase distance at the intercalation site[17,22] may allow the insertion or deletion of a base pair during replication of the DNA. The altered gene which results from this process is called a frame-shift mutant of the original gene[23,24]. One such mutant of the gene that codes for the enzyme lysozyme was used to verify both the triplet nature of the genetic code and the assignment of triplet codes to various amino acids[25]. Since Lerman's proposal of the intercalation model this model has been used successfully to describe the interaction of a variety of biologically active molecules with DNA[26].

The weaker mode of binding of aminoacridines to DNA is thought to be an electrostatic interaction between cationic

---

* At least one exception is known. See Chapter II for a detailed discussion.

aminoacridine and the anionic DNA phosphate residues. The observation that the interaction proceeds to electroneutrality of the DNA supports this hypothesis. The cooperative nature of this mode of binding is probably due to favourable stacking interactions between adjacent bound aminoacridines[21].

Most of the studies of the interaction of aminoacridines with DNA have concentrated on the strong binding mode. Since the late 1960's much of this work has been directed towards the question of possible heterogeneity among strong binding sites[19,20,27] or within one type of site[28-31]. Much of this work has been done with Proflavine or Proflavine-like aminoacridines. A recent kinetic study of the strong binding of 9-aminoacridine to native DNA found no evidence of binding site heterogeneity for this system[32]. Latterly methods for the mathematical modelling of binding data have been developed[33-36]. However, as pointed out by Schellman[36], the sensible use of such methods to model the binding process requires experimental binding data to be more accurately determined than has generally been the case. The work described in this thesis has been undertaken in an attempt to resolve some of the questions which recent work has raised concerning the interaction of 9-aminoacridines with native DNA. The aims of this work are summarized as follows.

(1) To determine the best experimental method, or combination of experimental methods, with which to obtain equilibrium binding data of sufficient precision and accuracy to undertake mathematical modelling of the binding data.

(2) To collect binding data, using the chosen method, for the strong binding of 9-aminoacridine and several substituted 9-aminoacridines to native DNA at a single ionic strength but

at several temperatures so that thermodynamic parameters may be evaluated.

(3) To determine if there is any evidence from absorbance spectrum measurements for the existence of heterogeneity in the strong binding process for the range of compounds studied.

(4) To derive mathematical models of the binding process which are consistent with the experimental observations concerning the binding of these compounds. Subsequently to select the model which best fits the experimental binding data and so obtain values for the thermodynamic parameters which govern the binding process proposed.

REFERENCES

1. Miescher F., *Med. Chem. Unters.*, 4, 441 (1871).
2. Watson J.D. and Crick F.H.C., *Nature*, 171, 737 (1953).
3. Watson J.D. and Crick F.H.C., *Cold Spring Harbour Symp. Quant. Biol.*, 18, 123 (1953).
4. Zamenhof S., Brawerman G. and Chargaff E., *Biochim. Biophys. Acta*, 9, 402 (1952).
5. Graebe C. and Caro H., *Annalen*, 158, 265 (1871).
6. Browning C. and Gilmour G., *J. Path. Bact.*, 18, 144 (1913).
7. Konopa J., Koldej K. and Pawlak J.W., *Chem. Biol. Interactions*, 13, 99 (1976).
8. Fico R.M., Chen T.K. and Canellakis E.S., *Science*, 198, 53 (1977).
9. See for example: Frankel S., Reitman S. and Sonnenwirth A.C., "*Clinical Laboratory Methods and Diagnosis*", Vols. 1 and 2, C.V. Mosby Company, St. Louis (1970).
10. See for example: Albert A., "*Selective Toxicity*", 4th edition, Methuen & Co. Ltd. (1968).
11. Cavalieri L.F. and Angelos A., *J.A.C.S.*, 72, 4686 (1950).
12. Cavalieri L.F., Angelos A. and Balis M.E., *J.A.C.S.*, 73, 4902 (1951).
13. Peacocke A.R. and Skerrett J.N.H., *Trans. Farad. Soc.*, 52, 261 (1956).
14. Michaelis L., *Cold Spring Harbour Symp. Quant. Biol.*, 12, 131 (1947).
15. Oster G., *Trans. Farad. Soc.*, 47, 660 (1951).
16. Heilweil H.G. and Van Winkle Q., *J. Phys. Chem.*, 59, 939 (1955).
17. Lerman L.S., *J. Mol. Biol.*, 3, 18 (1961).

18. Pritchard N.J., Blake A. and Peacocke A.R., *Nature*, 212, 1360 (1966).

19. Armstrong R.W., Kurucsev T. and Strauss U.P., *J.A.C.S.*, 92, 3174 (1970).

20. Ramstein J., Dourlent M. and Leng M., *Biochem. Biophys. Res. Comm.*, 47, 874 (1972).

21. Blake A. and Peacocke A.R., *Biopolymers*, 6, 1225 (1968).

22. Luzzati V., Masson F. and Lerman L.S., *J. Mol. Biol.*, 3, 634 (1961).

23. Waring M.J., *Nature*, 219, 1320 (1968).

24. Lerman L.S., *Proc. Nat. Acad. Sci. Wash.*, 49, 94 (1963).

25. Crick F.H.C., Barnett L., Brenner S. and Watts-Tobin A., *Nature*, 192, 1227 (1961).

26. See for example: Bloomfield V.A., Crothers D.M. and Tinoco I., "Physical Chemistry of Nucleic Acids", Chapter 7, Harper and Rowe (1974).

27. Li H.J. and Crothers D.M., *J. Mol. Biol.*, 39, 461 (1969).

28. Thomas J.C., Weill G. and Daune M., *Biopolymers*, 8, 647 (1969).

29. Ellerton N.F. and Isenberg I., *Biopolymers*, 8, 767 (1969).

30. Duportail G., Mauss Y. and Chambron J., *Biopolymers*, 16, 1397 (1977).

31. Kubota Y. and Steiner R.F., *Biophys. Chem.*, 6, 279 (1977).

32. Turner D.R., Ph.D. Thesis, University of Adelaide (1975).

33. Schwarz G., *Eur. J. Biochem.*, 12, 442 (1970).

34. McGhee J.D. and von Hippel P.H., *J. Mol. Biol.*, 86, 469 (1974).

35. Lifson S., *J. Phys. Chem.*, 40, 3705 (1964).

36. Schellman J.A., *Isr. J. Chem.*, 12, 219 (1974).

CHAPTER II

The interaction of Aminoacridines with Nucleic Acids

CONTENTS

1. Introduction

The interaction of aminoacridines with nucleic acids has been the subject of an extensive research effort on the part of many workers over the last twenty five years. This work has been directed towards gaining a more precise understanding of this interaction both for the insight it may give into the solution structure of nucleic acids and their complexes and as a model for a wider class of interactions of other molecules with nucleic acids, for example antibiotic and mutagenic agents. That such ligand-nucleic acid interactions are of increasing importance throughout the biological sciences has provided the impetus for this field of study.

The literature concerning the interaction of heterocyclic cations, in particular the aminoacridines, with nucleic acids is now so vast that the task of making a complete survey is beyond the scope of this work. Accordingly this brief review is directed specifically towards those interactions which are directly relevant to this research. Only the principal contributions to the understanding of the interaction, particularly the interaction of aminoacridines with native DNA, will be mentioned with emphasis on the most recent work in this field. This will necessarily restrict the survey to the physico-chemical aspects of the interaction. For a survey of the biological role of the interaction the reader is directed to the reviews of Albert[1] and Peacocke[2]. Several reviews of the physico-chemical nature of the interaction have appeared[3-6] which present a comprehensive survey of the period up to the early 1970's. The value of these surveys to the preparation of this review is acknowledged.

2. Binding Sites

(a) Determination

Fundamental to the characterization of the equilibrium and kinetic properties of aminoacridine/DNA complexes is the determination of the number and type of binding sites present on the DNA molecule. The first step towards this end is the determination of a binding curve for a particular aminoacridine and DNA combination. Such a binding curve is determined in terms of the amount of aminoacridine bound per identifiable repeating unit of the DNA molecule, r, in equilibrium with a known concentration of free aminoacridine, C_F. The DNA repeating unit most widely used is DNA phosphorus which is equivalent to a nucleotide residue. Such binding data may be considered in their simplest form to be described by a Langmuir Isotherm[7]:

$$r = \sum_{i=1}^{i=j} \frac{n_i K_i C_F}{1+K_i C_F} \qquad \text{--- 2.1}$$

In this relationship the observed r is the sum of binding to j independent, mutually exclusive classes of binding sites, each with a characteristic association constant, K_i, and number of sites per residue, n_i.

Binding data are usually presented in the form of a Scatchard Plot[8] of r/C_F versus r. An example of such a plot is Fig. 5.1. For a single class of binding site, that is j=1 in Eqn. 2.1, the relationship between r/C_F and r is obtained from 2.1 and is:

$$r/C_F = K(n-r) \qquad \text{--- 2.2}$$

This is the equation of a straight line with an ordinate intercept Kn, an abscissa intercept of n and a slope of -K. If a Scatchard Plot is linear then it can be concluded that

the interaction may be described by a single, non-interacting class of binding sites characterized by K and n.

The interaction of aminoacridines with DNA has generally not yielded linear Scatchard Plots. The observed curvature in such plots may arise from one or more of three causes listed below.

(i) There exists two or more distinguishable classes of binding sites, that is classes of differing characteristic K.

(ii) There is interaction, either direct or induced, between bound ligands.

(iii) There is an electrostatic free energy dependence of the binding with r. e.g. $K = K'\exp(\Delta G_{el}/RT)$.

In case (i) above if two or more classes of sites exist with widely differing K values then linear portions in the Scatchard Plot can be described and the characteristic K and n values obtained from graphical analysis or numerical non-linear fitting procedures.

Case (iii) may be seen as a special case of (ii) and can be suppressed by working with solvents of sufficiently high ionic strength. It will not be considered further here. Case (ii) can arise from cooperative effects between binding sites. Such cooperativity may be either positive or negative in nature resulting in curves concave and convex to be axes respectively. The mathematical description of interactions between binding sites and of cooperativity in binding curves has been the subject of considerable work in recent years. The equations of Schwartz[9,10] and McGhee and von Hippel[11] and the application of the Sequence Generating Function method[12-14] have paved the way for much needed sophistication in the treatment of experimental binding data. Before these methods

can be applied however, more accurate binding curves are required to enable models to be selected[14] to describe the binding process. A full discussion of the methods of treating interactions between bound ligands is contained in Chapter V of this work. Before moving on it is necessary to introduce one further term. In the limit of anti-cooperative interaction, no ligand may be bound to a site subjected to this effect. The term "site exclusion" will be used to describe this situation.

The experimental methods that have been used to determine aminoacridine/DNA binding curves include UV-visible spectrophotometry[15-21], equilibrium dialysis[15,17,18], sedimentation dialysis[22], partition analysis[23] and fluorescence quenching[21,23-27]. The first three methods mentioned above are discussed in detail in Chapter III. A comparative review of all of these methods has appeared elsewhere[3].

(b) Number and type of sites

The work of Peacocke and Skerrett[15] published in 1956 really began the physico-chemical study of the interaction of aminoacridines with DNA. This work remains among the most significant in this field. These workers looked at the interaction of Proflavine, 9-aminoacridine and 9-amino-1,2,3,4-tetrahydroacridine with native DNA. They determined that there is heterogeneity in the binding sites, that the binding is unaffected by pH within the range 3.7-7.4 and that the ionic strength of the solution affects the binding. It is now generally accepted that there are two major classes of binding site. The first of these, usually designated as Complex I, is a strong interaction

having a ΔG° of -25 to -40 kJ/mole. It proceeds to an n value of 0.2-0.25 and is affected by the ionic strength of the solvent, increasing in strength as the ionic strength decreases. The second class of site, designated as Complex II, is a weaker interaction which is greatly affected by ionic strength and proceeds, under favourable solvent conditions to an n of 1.0 (i.e. electroneutrality of the DNA). The formation of Complex II can be largely suppressed by use of high ionic strength solvents. Complex II is associated with the binding of aminoacridine aggregates to the negatively charged phosphate groups of the DNA backbone[3,4,15]. This "outside-bound" complex is predominantly electrostatic in nature and its formation is positively cooperative reflecting the additional favourable free energy change as a result of the formation of stacked dye aggregates.

The first model for Complex I supported by experimental observation was proposed by Lerman[28] on the basis of the observed increase in length and decrease in mass per unit length of DNA on the formation of Complex I. Lerman[29] also observed a decrease in reactivity of the primary amino groups of Proflavine towards an electrophilic reagent, when bound to native DNA as Complex I. To explain his observations Lerman proposed that the aminoacridine was bound between adjacent base pairs of the intact native DNA double helix with the plane of the aminoacridine parallel to the plane of the DNA heterocyclic base pairs. The major axis of the aminoacridine is parallel to the DNA base pair major axis. This intercalation of the aminoacridine will force apart the adjacent DNA base pairs giving rise to the observed hydrodynamic properties of Complex I. The inclusion of the Proflavine primary amino groups within the helix would be

expected to reduce their reactivity to electrophilic reagents.

(c) Effect of ionic strength

While it is obvious why Complex II displays a profound dependence on ionic strength it is less apparent why Complex I should show an ionic strength dependence. Gilbert and Claverie[30] explained this observation purely in terms of electrostatic attractions and repulsions between the cationic aminoacridines and the anionic polyphosphate backbone of the DNA. This explanation seems an oversimplification as it neglects the heterocyclic stacking energies[32] and the effect of ionic strength on the DNA substrate[32]. The dependence on ionic strength of Complex I formation can be explained as the summation of electrostatic interactions, the effect on permanent and induced dipoles within the stacked heterocyclic system and the changes in base-pair separation and backbone stiffness of the DNA which accompany changes in solvent ionic strength[33]. The changes in Complex II formation with ionic strength can also be expected to influence Complex I formation.

3. Structural Effects on the Interaction

In this section the effects of the structure of the components of the interaction is considered. The emphasis is on the strong interaction of aminoacridines with native DNA.

(a) Nucleic Acids

The two extreme structures of naturally occurring DNA *in vitro* are the ordered Watson-Crick double helix, called native DNA, and the disordered, single-stranded random coil, called denatured DNA. Native DNA may be "denatured" by the

effects of temperature, pH or solvent composition. Aminoacridines bind strongly to denatured DNA[34-36] indicating that the intact double helix is not required for strong binding to occur. Although aminoacridines bind with approximately the same strength to either form at room temperature, the denatured DNA is much more sensitive to temperature increases[16,17,35]. Ichimura *et al*[35] showed that although binding of Acridine Orange to either form of DNA occurs with the same ΔG° value at 25°C, the binding to denatured DNA is characterized by a large unfavourable entropy term. Turner[37] showed that a similar situation exists for the binding of 9-aminoacridine to *E Coli* DNA in 0.1 M NaCl. Native DNA, on the other hand, does not release most of the strongly bound aminoacridine until the melting transition[35,38], which itself occurs at a slightly higher temperature indicating that Complex I stabilizes the native DNA structure. There appear to be about twice as many strong binding sites on denatured DNA when compared to native DNA[35,37,38]. Chemical modification of DNA, such as methylation of the heterocyclic bases does not prevent Proflavine intercalating into native DNA[39].

The isosbestic points observed for the interaction of aminoacridines with denatured DNA are in general less well defined than for interaction with native DNA[37,40].

The DNA structural requirements needed to support a strong interaction with aminoacridines appear nebulous. The evidence suggests that both single and double-stranded polynucleotides can bind aminoacridines strongly under a range of conditions of pH and solvent and base composition. Binding to single-stranded polynucleotides is, however, sensitive to temperature. Spectral evidence suggests that

heterogeneity may exist in the strong binding sites of single-stranded polynucleotides. The question of the effect of base composition and heterogeneity of strong binding sites on native DNA is a contentious issue and is examined more fully in section 8 of this Chapter.

(b) Aminoacridines

It is to be expected that the structure of individual aminoacridines, with the attendant effect on the electronic charge distribution within the molecule, will effect the interaction. Steric hinderance can be expected to effect the location of bound aminoacridines.

The two most basic attributes required of aminoacridines in order to bind strongly to DNA are that they be sufficiently basic to be in their cationic form at neutral pH and that they possess a minimum planar area of 0.38 nm^2 (i.e. the three rings of the acridine nucleus should be aromatic). Löber[41] showed that the more basic the aminoacridine the more strongly it binds. Löber and Achtert[42] demonstrated that the alkylation of the ring nitrogen of Acridine Orange and Proflavine further enhances strong binding and that this enhancement was not very dependent on the length of the alkylating group. They also showed that alkylation of the 3 amino or 3,6 amino groups increased the strength of binding provided no steric hinderance to the interaction existed. 3,6-Bis-diethylaminoacridine and 3,6-bis-phenylaminoacridine apparently presented steric hinderance to the interaction since they bound with significantly lower association constants than expected from the trend Löber and Achtert established for these alkylated derivatives[42]. The alkylation of the ring nitrogen

of acridine itself decreased its tendency to bind[42]. These observations suggest that whilst the ring nitrogen is critical to the interaction of acridine itself it is not very important in the interaction of aminoacridines.

The attachment of long bulky side chains to the amino group of 9-aminoacridine does not appear to hinder its binding to DNA[16,43,44]. This would indicate that derivatives of 9-aminoacridine bind in such a way that the 9 position and the groups thereon do not significantly sterically hinder the interaction. Studies[45,46] in which bulky substituents were substituted at various positions around the acridine nucleus of 9-aminoacridine showed that they were able to interact strongly with DNA with evidence of intercalation. Although 9-amino-2,7-di-tert-butyl-acridine shows evidence of intercalation, 3,6-diamino-2,7-di-tert-butyl-acridine does not appear to intercalate[47-49]. It does however bind strongly to native DNA, presumably in an externally bound form.

Hydrogenation of one of the rings of 9-aminoacridine to form 9-amino-1,2,3,4-tetrahydroacridine markedly reduces the extent of its interaction with DNA[16]. It can, however, still intercalate to some extent[16] indicating that complete insertion of the three planar rings is not an absolute requirement of intercalation.

It is apparent from this brief discussion that the structure of individual aminoacridines has a considerable effect upon their interaction with DNA. The available evidence suggests that no one model can satisfactorily explain the intercalation of all aminoacridines[42]. The experimental observations concerning the orientations of individual aminoacridines is reviewed in section 5 of this Chapter.

4. Effects of the Interaction

(a) Effects on nucleic acids

Strong binding of aminoacridines to DNA has a marked effect on the structure of the DNA macromolecule. The increase in intrinsic viscosity[18,28,50] and decrease in sedimentation coefficient[22,28,51] which led Lerman[28] to propose his original model present some of the most compelling evidence in support of the intercalation model. The increase in viscosity occurs up to an r value of about 0.2[18,50], that is the region of Complex I formation, and is associated with an increase in the contour length of the DNA molecule[18]. Drummond *et al*[50] calculated this increase in contour length to be approximately 0.34 nm per bound aminoacridine. This is equivalent to the van der Waal's distance between adjacent base pairs of the Watson-Crick structure. This work was done with high molecular weight DNA which presents some difficulties in quantitative treatment. More recent work[51] on sonicated DNA of lower molecular weight utilizing a rod-like model for the DNA helix estimates the extension of the helix at 84% of the Watson-Crick base pair spacing per bound aminoacridine. An increase in flexibility of the DNA molecule on aminoacridine complexation was also noted[18,51]. An increase in contour length on binding Proflavine has also been observed by autoradiography[52] and light scattering[53], the latter experiments also revealing an increase in the radius of gyration. More recently contour length increases have been measured by electron microscopy[54-56]. Although earlier work[54,55] suggested a contour length increase of less than 0.34 nm per bound aminoacridine, the most recent publication suggests that an increase of 0.34 nm is in fact observed[56].

The increase in contour length is accompanied by a decrease in mass per unit length as shown by low angle X-ray measurements[57], sedimentation rates[38], and light scattering[53]. The decrease in mass per unit length is greater than predicted by Lerman[28] but this can be accounted for by the increased flexibility of the DNA molecule on intercalation of aminoacridine[18,22,38,51].

This increase in length and decrease in mass per unit length is consistent with an unwinding of the double helix. X-ray diffraction studies[28] were consistent with an unwinding of between 12° and 45°. Stereochemical studies[58-60] suggest an unwinding of 12°. The ability of intercalating molecules, including aminoacridines, to unwind the superhelical turns of closed circular DNA's[61,62] and to rewind them in the opposite sense is further support for the suggestion that intercalation unwinds the native DNA double helix.

The changes ascribed to the hydrodynamic properties of native DNA on complexation of aminoacridines are not observed for the binding to denatured DNA. There is no increase in the viscosity[38,50] or decrease in sedimentation coefficient[38] on the binding of 9-aminoacridine or Proflavine to denatured DNA. This indicates that the increase in contour length is specific to the intact double helical DNA structure.

The binding of aminoacridines to native DNA stabilizes the structure towards thermal denaturation as indicated by an increase in the melting temperature of the DNA/aminoacridine complex[17,31,38,63]. The observed increase in T_m is a linear function of r and is a maximum at the limit of Complex I formation[31,64]. Dye bound by complex II does not seem to effect the T_m, being dissociated at lower temperatures[31,63]. The increase in T_m on binding aminoacridines as Complex I

indicates that there is a favourable free energy decrease for the complex compared to DNA alone at the DNA melting temperature.

(b) Effects on aminoacridines

The effect of the interaction on the visible absorbance spectrum of aminoacridines is the most characteristic, experimentally observable feature of the interaction. In general, when aminoacridines are bound as the monomer, the absorbance maximum is shifted to longer wavelengths accompanied by a decrease in apparent molar absorbance[5,15,16,18]. When aminoacridine is bound as Complex II the spectrum generally shifts to shorter wavelengths[65]. This blue shift is similar to that observed for self-association of aminoacridines and has been assigned to the binding of aggregates in Complex II formation. 9-aminoacridine is an exception to this generalization in that both Complex II binding and self-association result in red shifts of the visible absorbance spectrum. The spectral changes associated with strong binding are consistent with interaction of the aminoacridine with the heterocyclic DNA bases[16,66,67]. The spectral changes observed for the strong binding of Proflavine to denatured DNA are similar to those observed for binding to native DNA[66].

The optical properties of complexes of aminoacridines with DNA are potentially a powerful tool in the attempt to elucidate the structure of the complex. The sensitivity of optical rotatory dispersion (ORD) and circular dichroism (CD) to the molecular environment of the optically active species could yield much information on the fine structural features of such complexes. When aminoacridines are bound to DNA they

exhibit extrinsic or induced Cotton effects[34,68-71]. The observation that optical activity is induced in otherwise optically inactive aminoacridines on binding to DNA implies that a definite and regular spacial relationship exists between the chromophore and its binding site[68]. A number of explanations have been proposed to explain such optical anisotropy.

(1) If the chromophores were arranged in a regular helical array the asymmetry required to generate optical activity would be present. Both Complex I and Complex II could yield such an arrangement[72,73]. The observation that Proflavine and Acridine Orange show induced optical activity when bound to denatured DNA[74] suggest that the double helix of native DNA is not a necessary adjunct to the induction of optical activity.

(2) Assymmetry may be induced within the chromophore as a result of an asymmetric environment within the DNA itself[70,75].

(3) Exciton interactions between neighbouring bound aminoacridines could induce optical activity[72,74]. The observation that 1-, 2- and 9-aminoacridines yield optical activity on binding which is independent of the amount bound[76] would suggest that this explanation does not apply to these aminoacridines unless they bind as aggregates. Conversely aminoacridines with a 7-aminoquinoline substructure do display a cooperatively induced C.D.[46].

These observations demonstrate the uncertainty surrounding the interpretation of the optical activity of bound aminoacridines. No single explanation has been able, thus far, to account for all of the observed details. Until

such an explanation is forthcoming only a small part of the potential of these techniques can be realized.

The binding of aminoacridines to DNA induces changes in the fluorescence spectra of the bound dyes. Changes may occur in both the wavelength[67] and intensity[41,77-79] of the observed fluorescence. These changes in fluorescence have been used to determine binding curves, a technique of particular value because of its extreme sensitivity. The conclusions drawn concerning the possible heterogeneity of strong binding sites from fluorescence data are probably the most contentious issues in this field of study. A discussion of these results is contained in Section 8 of this Chapter.

Studies of the diazotization rates of Proflavine when bound to DNA and to synthetic polyelectrolytes by Lerman[29] showed a marked reduction in the rate on strong binding to DNA. He concluded that this was a result of the amino groups of Proflavine being enclosed in the DNA helix and hence less accessible to the electrophilic reagent.

5. Orientation of Bound Aminoacridines

Early work in this area by flow dichroism[80,81] and polarized fluorescence[80] estimated the plane of the bound aminoacridine to be within ±30° of the plane of the DNA base pairs. More recent work has added significantly to these findings. The dichroic spectra of stretched films of Ethidium Bromide[82] and of 9-aminoacridine, Proflavine and Acriflavine[83] with DNA have been studied. Kelly and Kurucsev[83] found that the orientation of Proflavine and Acriflavine, both of which possess a 7-aminoquinoline substructure, were very similar. The plane of the aminoacridine was perpendicular to the major helix axis.

9-aminoacridine however was tilted from the plane perpendicular to the major helix axis by 23° ± 3°. The perpendicular long and short axis transition moments of 9-aminoacridine enabled the determination of the angle of twist between the long axis of 9-aminoacridine and the semi-major axis of the DNA. This angle was found to be 13° ± 3°. Such studies of stretched films, however, are very sensitive to humidity[83]. This must be considered when making extrapolations from observation on stretched films to the solution state.

Very recently a number of X-ray structures, to atomic resolution, have been reported[84-89]. These structures were determined from well hydrated, single crystals of complexes of Ethidium Bromide, Proflavine and 9-aminoacridine with synthetic, self-complementary di- and oligo-ribonucleotides. These structures provide the first visualization of an intercalated complex. The structures show these intercalated complexes to be essentially of the type of Lerman's model. The plane of the intercalated molecule is perpendicular to the direction of the "double helix" axis formed by the stacking of these minature double helices. The major axis of the intercalated molecule is parallel to the semi-minor helix axis with maximum overlap between the ring system of the dye and the base residues in the helix. They are all nearest neighbour excluded structures. The phosphate-sugar backbone of these structures is discontinuous in the sense that the helix is constructed of a stack of minature helices. The complex of 9-aminoacridine with 5-iodocytidylyl(3'-5')guanosine yielded the only exception to the above mentioned general intercalation structure in that every second 9-aminoacridine molecule was severely skewed in the helix.[84] These molecules

however were bound in the site between adjacent helices. It is unlikely that if the backbone were continuous that such a position would be stereochemically feasible.[84] It may therefore be discarded as an artifact of the discontinuous backbone.

Naturally one must be cautious in extrapolating the structures observed in such model systems to the structure of the complexes of these dyes with native DNA in the solution state. These structures do, however, provide the first direct proof that intercalation into a double-helical DNA like structure can occur.

The development of high-field, fourier transform Nuclear Magnetic Resonance (NMR) spectrometers has enabled detailed study of the complexes of aminoacridines with synthetic polynucleotides[90]. The study of complexes with natural DNA is not possible since resonances of nuclei in this material are broadened beyond resolution[91]. Patel's study[90] of the interaction of Proflavine with Poly (dA-dT) and its dissociation over the melting transition of the complex provide a rare insight into the solution structure of an intercalated complex. The data are consistent with a Lerman model of the complex with the amino groups of Proflavine directed towards the backbone chains and maximum overlap between the acridine ring and the nucleotide bases. Patel[90] found that the NMR data were not consistent with the model of Proflavine intercalating into A-T sites proposed by Alden and Arnott[92]. This model, based on valence force field energy minimization calculations, proposed that a Lerman type intercalation existed but with only about $^2/_3$ of maximum π-electron system overlap between the Proflavine and A-T base pair. In this model the C-9 position of the Proflavine is exposed in the groove of the DNA helix. Such calculations[92] are particularly

prone to criticism since the minimization is computed "*in vacuo*", no account being taken of solvent or the field of neighbouring molecules.

The fields of study aimed at determining detailed orientations of intercalated complexes in nucleic acids has developed rapidly in the last few years. The information gained from such studies has given considerable insight into the nature of intercalated complexes. The large majority of studies have shown that Lerman type intercalation models operate in these systems. Most of this work has been with the Ethidium cation and Proflavine, which possess 7-aminoquinoline substructures. The stretched film study[83] suggested that 9-aminoacridine differs from the 7-aminoquinoline containing molecules and more work with 9-aminoacridines would shed more light on these potential differences.

6. General structural models for the complexes

In the preceding sections of this review a brief summary has been made of the experimental observations concerning the interaction of aminoacridines with DNA. In this section the work reviewed will be summarized in terms of current models for the interaction. Similar summaries have appeared elsewhere[2,3,37,38]. The original observation by Peacocke and Skerrett[15] that two types of complex existed has been universally accepted. This summary will treat each of these types in turn.

(a) Complex I - strong binding

The formation of complex I is associated with the following observations.

(1) It is a strong interaction, $\Delta G^{\circ} \simeq -25$ to -40 kJ/mole of bound aminoacridine.

(2) It is more favourable for aminoacridines with three aromatic rings. The presence of one saturated ring does not, however, preclude partial intercalation.

(3) Only cations bind strongly suggesting the interaction is at least part electrostatic in nature. This could also be a mechanistic requirement.

(4) The contour length of double helical DNA is increased and its mass per unit length decreased on formation of Complex I.

(5) These hydrodynamic changes are not observed with denatured DNA provided that the ionic strength of the solution is not significantly altered by adding cationic aminoacridine.

(6) The plane of the bound aminoacridine is approximately parallel to the DNA base pairs and so perpendicular to the double helix major axis.

(7) The reactivity of the amino groups of some aminoacridines is diminished on binding.

(8) At room temperature Complex I has similar stability in both native and denatured DNA. The extent of binding is greater to denatured DNA.

(9) Long side chains attached to the amino group of 9-aminoacridines do not hinder the interaction.

(10) There is an upper limit to the extent of binding (to native DNA) as r for Complex I equals 0.20 - 0.25. That is, one bound aminoacridine per two base pairs.

(11) The stability of double helical DNA is enhanced by aminoacridines bound in Complex I form.

On the basis of observations (4), (6) and (7) Lerman[28] proposed that an aminoacridine cation binds in such a way that the DNA molecule untwists and extends to allow insertion of the aminoacridine between adjacent base pairs. This interaction is called intercalation. The aminoacridine is centrally located within the helix with the ring nitrogen near the central axis of the helix. This arrangement allows maximum overlap of the acridine ring system with the DNA base pairs. The double helical structure of native DNA is an essential requirement of this model which is shown schematically in Fig. 2.1(a).

The model proposed by Lerman satisfactorily explains a number of the general observations concerning Complex I formation. It cannot readily explain observations (2), (5), (8) and (9). To explain these observations, Pritchard *et al*[93] proposed a modified intercalation model. In this model the major axis of the intercalated acridine ring is perpendicular to the helix semi-major axis with the acridine ring nitrogen immediately adjacent to the phosphate-sugar backbone. They suggested that the backbone phosphate group could then take up a position near the positively charged ring nitrogen. This model is shown schematically in Fig. 2.1(b).

The Pritchard *et al*[93] model can satisfactorily explain observations (2), (3), (8) and (9) as well as those of Lerman [(4), (6) and (7)]. This model does not require an intact double helical DNA structure and hence allows for an intercalation type interaction with denatured DNA. In view of the less rigid conformation of denatured DNA an increase in adjacent base-base distance may be possible without increase in the contour length of the DNA molecule. Observations (1) and (11) are a direct consequence of a strong interaction and need no comment.

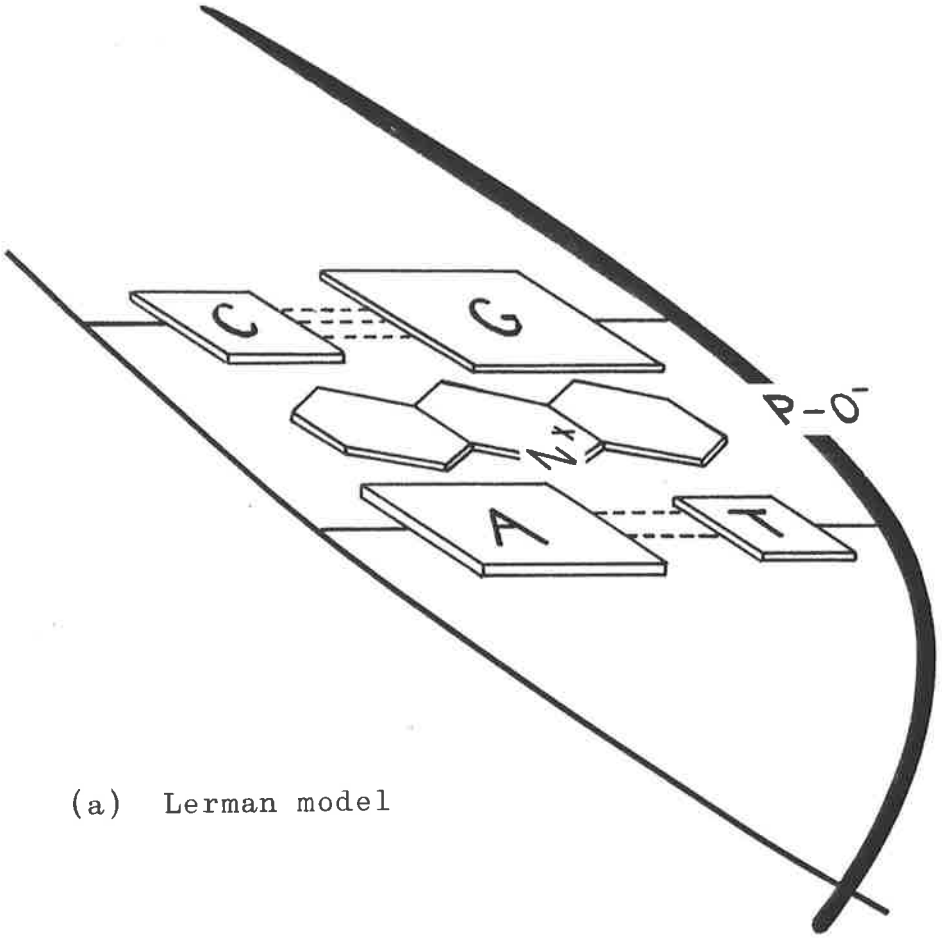

(a) Lerman model

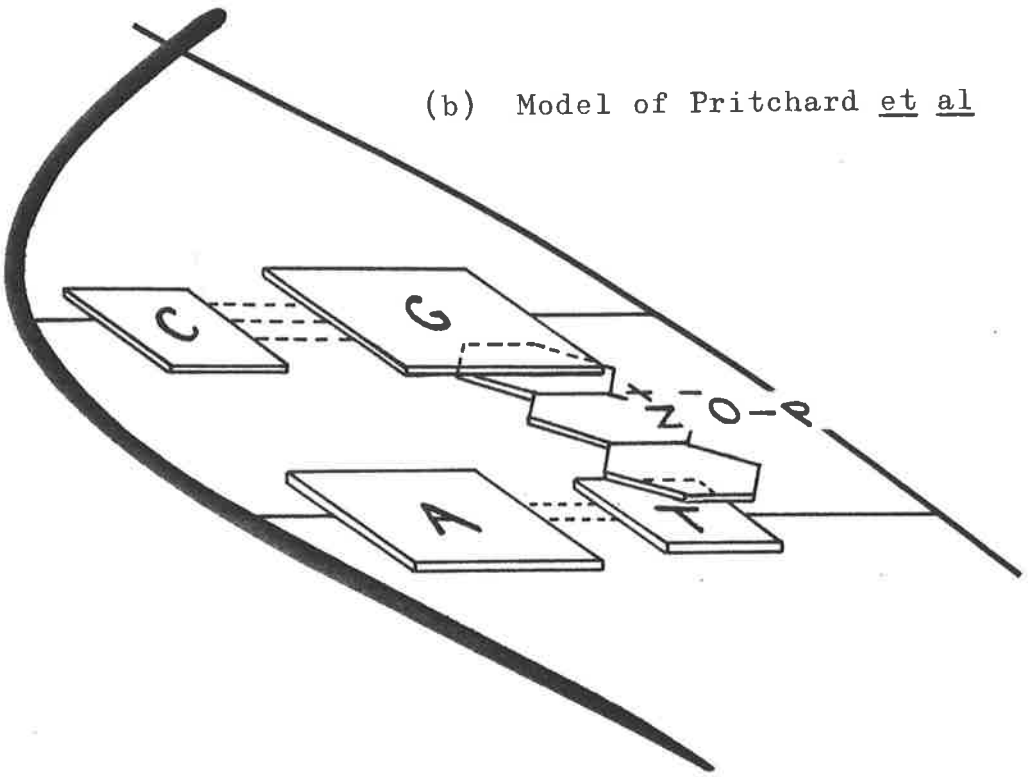

(b) Model of Pritchard *et al*

Figure 2-1. Schematic representations of intercalation models for the interaction of amino-acridines with native DNA.

It is not immediately apparent why the limit of Complex I formation is approximately one aminoacridine bound per two base pairs. In the Lerman model the theoretical upper limit of binding is one dye bound per base pair and in the model of Pritchard *et al* not even this restriction applies. Armstrong *et al*[18] explained this limit by proposing that the slot between every base pair of native DNA is a potential binding site and that aminoacridines bind randomly to these sites with the restriction that intercalation may not occur at sites immediately adjacent to an occupied site. This may be called nearest neighbour site exclusion. A very recent study of the binding of Quinacrine to native DNA[94] proposes such site-exclusion for this system. Whether such sites are actually excluded completely or subject to a very large anti-cooperative effect is difficult to determine. For all practical purposes they are the same since they would only differ at unattainably high free dye concentrations. Work with bis-intercalating 9-aminoacridines and closed circular DNA has only added to the uncertainty of this situation. Le Pecq *et al*[95] studied a series of such compounds in which two 2-methoxy-6-chloro-9-aminoacridine structures were connected by chains of various lengths. These chains contained amine groups. They found that only when the chain was long enough to permit binding two base pairs away from a site occupied by one of the 9-aminoacridine structures did bis-intercalation occur. This suggested that nearest neighbour site exclusion did operate in these systems. However, recently work by Wakelin *et al*[96] on a similar group of compounds but with an alkyl chain interconnecting two 9-aminoacridine molecules showed that nearest neighbour intercalation did occur.

Care must be exercised when extrapolating these findings to mono-functional intercalating molecules since in some respects the statistical distributions governing the location of the second half of a bis-aminoacridine intercalation are different. Once the first aminoacridine ring has intercalated the second ring is constrained to the immediate vicinity of adjacent base-pairs. This makes the concentration of potential intercalating agent in this region effectively infinite. The findings of these studies[95,96] demonstrate that in one case nearest neighbour site exclusion does occur whereas in another similar system intercalation at an adjacent site is possible. In this latter case these experiments[96] provide no information regarding any anti-cooperative effect that may apply to the second intercalation step.

The upper limit of one aminoacridine intercalated per two DNA base pairs may then be explained as arising either from nearest neighbour site exclusion or from a severe nearest neighbour anti-cooperative effect. Such an anti-cooperative effect would impose the observed limit for free dye concentrations which are attainable in practice.

(b) Complex II - weak binding

Aminoacridine bound to DNA to form Complex II has the following characteristics.

(1) It is a weak interaction, ΔG° for the reaction is only a few kJ/mole of bound aminoacridine.

(2) It is principally electrostatic in nature. The ionic strength of supporting electrolyte has a profound effect on the interaction.

(3) It can involve interaction between bound molecules. The binding generally displays a positive cooperativity.

(4) It continues beyond the extent of binding predominated by Complex I formation, which is an internal binding process. It is therefore probably binding to the external, hydrated region of DNA.

(5) It saturates at the condition for electroneutrality of the DNA phosphate group, that is r = 1.0.

The generally accepted model for Complex II binding is one in which the cations bind externally to the helix with the positive ring nitrogen adjacent to the negatively charged phosphate of the DNA backbone. This model explains all of the above observations. Since strong binding predominates in the region of low r it is not possible to make experimental observations of Complex II in isolation. The observation that the viscosity of aminoacridine/DNA complexes is not affected beyond the saturation limit of Complex I binding supports an outside-bound model. Such a model would be expected to result in a cooperative binding process. Aminoacridines binding to the phosphate groups would be expected to bind adjacent to already bound aminoacridine so gaining additional stabilization by forming "sandwich" aggregates with favourable interaction between adjacent bound aminoacridines. Observations of the spectral properties of Complex II suggest they are similar to those of aggregates resulting from self-association of aminoacridines.

7. The kinetics and mechanisms of the interaction

The equilibrium between aminoacridines and DNA is established very rapidly. The study of the kinetics of the reaction awaited the development of perturbation techniques,

such as temperature jump[97], which allow the study of such rapid reactions. In this technique an electrical discharge through a solution produces an increase in temperature with a rise time of a few microseconds. It is then possible to follow the equilibration of the solution to the new temperature using a suitable technique such as absorbance or fluorescence. This technique has been the most widely applied technique in the study of the kinetics of aminoacridine/DNA interaction[98-101].

Li and Crothers[98] studied the interaction of Proflavine with Calf Thymus DNA. They observed two well defined relaxation times, and proposed that two forms of the strongly bound complex exist at equilibrium. The mechanism they proposed is given below.

$$P + DNA \underset{k_{21}}{\overset{k_{12}}{\rightleftharpoons}} (P\text{-}DNA)_{OUT} \underset{k_{32}}{\overset{k_{23}}{\rightleftharpoons}} (P\text{-}DNA)_{IN} \qquad \text{mech. 2.1}$$

$$k_{12} >> k_{21} > k_{23} > k_{32}$$

The first step is a rapid, almost diffusion controlled bimolecular process with a large favourable equilibrium constant. This is assigned to an outside bound Proflavine molecule with an electrostatic component since the amount of Proflavine bound in this way was affected by ionic strength[98]. The second complex, $(P\text{-}DNA)_{IN}$, whose formation was considerably slower, was assigned to intercalation of the outside bound form, $(P\text{-}DNA)_{OUT}$. Li and Crothers[98] suggested that a conformational change occurs in the DNA which allows the outside bound form to intercalate. It should be pointed out that a parallel mechanism in which Proflavine may bind to DNA in either form in parallel fashion rather than in the series mechanism (mech. 2.1) is equally consistent with the kinetic data.

Ramstein and Leng[101] studied the kinetics of the interaction of Proflavine with *Micrococcus Lysodeikticus* DNA. They conclude that the mechanism of Li and Crothers[98] applies but that the $(P\text{-}DNA)_{OUT}$ form of the complex is favoured in G-C rich regions of DNA. They also observed that methylation of the bases of *M.L.* DNA (preferentially on Guanine) while not affecting the formation of $(P\text{-}DNA)_{OUT}$ did increase the amount of intercalated Proflavine. Attempts[20] to fit a mathematical formulation of mech. 2.1 to equilibrium binding data for Proflavine/*M.L.* DNA using K values obtained from the kinetic experiments can only be described as fair. While this model is not inconsistent with the binding data, the fit is not good.

Turner[37] studied the kinetics of the interaction of 9-aminoacridine with highly polymerized *E Coli* DNA. He obtained only one relaxation in the temperature range 45°C - 65°C with an ionic strength of 0.1. This was assigned to a single bimolecular reaction resulting in the intercalation of 9-aminoacridine. The variations in temperature, ionic strength and nucleic acid types used in these studies[37,98-101] make direct comparison difficult. However, the results obtained by Turner[37] suggest that the Li and Crothers[98] mechanism does not apply to the binding of 9-aminoacridine to native DNA.

There has been general acceptance of the Li and Crothers[98] mechanism for the interaction of Proflavine and Proflavine like aminoacridines with native DNA. There is evidence[37] to suggest that this mechanism may not apply to 9-aminoacridines.

8. Heterogeneity among strong binding sites of native DNA

The question of whether heterogeneity exists among the strong binding sites is probably the most contentious issue surrounding the binding of aminoacridines to DNA. Because of its importance to this work I have chosen to examine the evidence under two headings in this section.

(a) Base pair heterogeneity

Since DNA possesses four base residues which occur in two specific pairs there are four base pairs possible in DNA (viz. AT, TA, GC, CG). Considering only the base pairs immediately adjacent to an intercalated aminoacridine, there are then sixteen possible intercalated complexes. This assumes that intercalation may take place in all of these sites. In this sense heterogeneity must exist among the intercalated aminoacridine complexes. The question is not that the individual complexes are chemically different but rather whether any *significant* difference exists between the affinity of an aminoacridine for any of these potential sites. The techniques most applied to this problem have been fluorescence spectra and, more latterly, nanosecond fluorescence decay.

The majority of aminoacridines exhibit a decrease in fluorescence intensity[77-79] on strong binding to DNA. However Acridine Orange and its derivatives[77,79] and the intercalating phenanthridine Ethidium Bromide[108] show enhancement of fluorescence on binding to DNA. The mechanism of the fluorescence quenching, which is not satisfactorily understood, is the crux of the argument surrounding base-pair specific binding. Some workers[24,25,104] have suggested the existence of quenching and non-quenching binding sites, assigned to GC-rich and AT-rich sites respectively. The

general observation that the degree of quenching appears to increase with increasing r has led some workers[24,25] to suggest that aminoacridine binds more strongly to AT base pairs. This suggestion has been challenged by others[26,27] who propose that the variation in fluorescence quantum yields can be explained by near neighbour interactions between randomly bound dye molecules. This challenge of the base pair specific binding explanation has itself been criticised by Daune[105] who suggests that at the very low r values employed in these studies, the aminoacridines would be bound too far apart for nearest neighbour interaction. However, if the binding were truly random, then a certain portion of the dye molecules would occur as near neighbours while others would be essentially isolated from other bound molecules. Moreover the fraction of dye bound as near neighbours would inevitably increase as r increases, even at low total r values. An examination of the properties of random binding to a linear lattice using the Sequence Generating Function method[12-14] would be of great value in determining the increase in near neighbours as r increases at low r values. In this way it would be possible to calculate the number of, and distances over which dye-dye interactions would have to take place to explain the observed increase in total quenching.

More recent work[106-109] using the nanosecond fluorescence decay technique suggests that two or more decay processes make up the decay curve of bound Proflavine and 9-aminoacridine. The variation of the relative amounts of these individual contributors to the observed decay curve with changes in r, and between DNA's of differing GC content, has been assigned to base-specific heterogeneity among the binding sites[109]. Conversely, Duportail *et al*[107] did not

observe this variation and suggested a non base-specific strong binding site heterogeneity. The total quantum yield from bound 9-aminoacridine is very low, of the order of a few percent, and hence the resolution of these curves is poor. There is disagreement[109] over the number of decay processes and the measured fluorescence spectrum of bound 9-aminoacridine. The situation regarding the nanosecond fluorescence decay measurements on bound 9-aminoacridine is confused.

During any discussion of fluorescence spectra and fluorescence decay it must be remembered that the fluorescence properties of a molecule are the properties of an excited state of that molecule. Such an electronic excited state will involve changes in the charge distribution of the molecule with concomitant changes in dipole moment magnitude and direction. Such changes could result in changes in the position of the intercalated dye within the helix. Indeed just such a suggestion was made by Ellerton and Isenberg[26] to explain the fluorescence polarization properties of bound Proflavine. One must be careful when extrapolating the fluorescence data to the ground state of a bound molecule. If such positional changes occur they would be on the nanosecond time scale and hence cast doubt on the fluorescence decay measurements. It has been reported that the spectra of bound Proflavine[106] and bound 9-aminoacridine[109] are independent of time over the nanosecond time scale although in neither case was the evidence for these statements presented. The development of picosecond fluorescence decay techniques would circumvent this short-coming since the excitation and decay process will occur on a time scale too short for molecular movement to occur simultaneously. This technique should resolve some of the problems of the other fluorescence techniques.

The current evidence for base specific heterogeneity among strong binding sites is not conclusive. Alternate explanations of the fluorescence properties of bound aminoacridines are available and at this stage it is not possible to state unambiguously that base-pair heterogeneity exists for bound aminoacridines.

(b) Binding site heterogeneity

Armstrong *et al*[18] studied the binding of Proflavine and Acridine Orange to native DNA using equilibrium dialysis and spectrophotometry. At low ionic strength they observed two modes of strong binding which they assigned to an intercalated monomer acridine and to a bound dimer (inferred from spectral evidence). They propose that monomer dye intercalates into the helix and subsequently another dye may bind immediately adjacent to the intercalated dye with partial overlap of the acridine ring systems. This model is shown schematically in Fig. 2.2(a).

Li and Crothers[98] proposed from kinetic studies that a strong "outside" bound form exists for proflavine. That such non-intercalated strong binding is possible has been demonstrated by study of the binding of the sterically hindered 3,6-diamino-2,7-di-tert-butylacridine. This does not necessarily imply that such outside bound forms are thermodynamically stable for dyes which can intercalate. This model is shown in Fig. 2.2(b).

Ramstein *et al*[100] studied the interaction of Proflavine with DNA's of differing GC content both by viscometry and T-jump kinetics. They concluded that a strong outside bound form existed but that it was preferred in GC-rich regions, and that intercalation was preferred in AT-rich regions of the

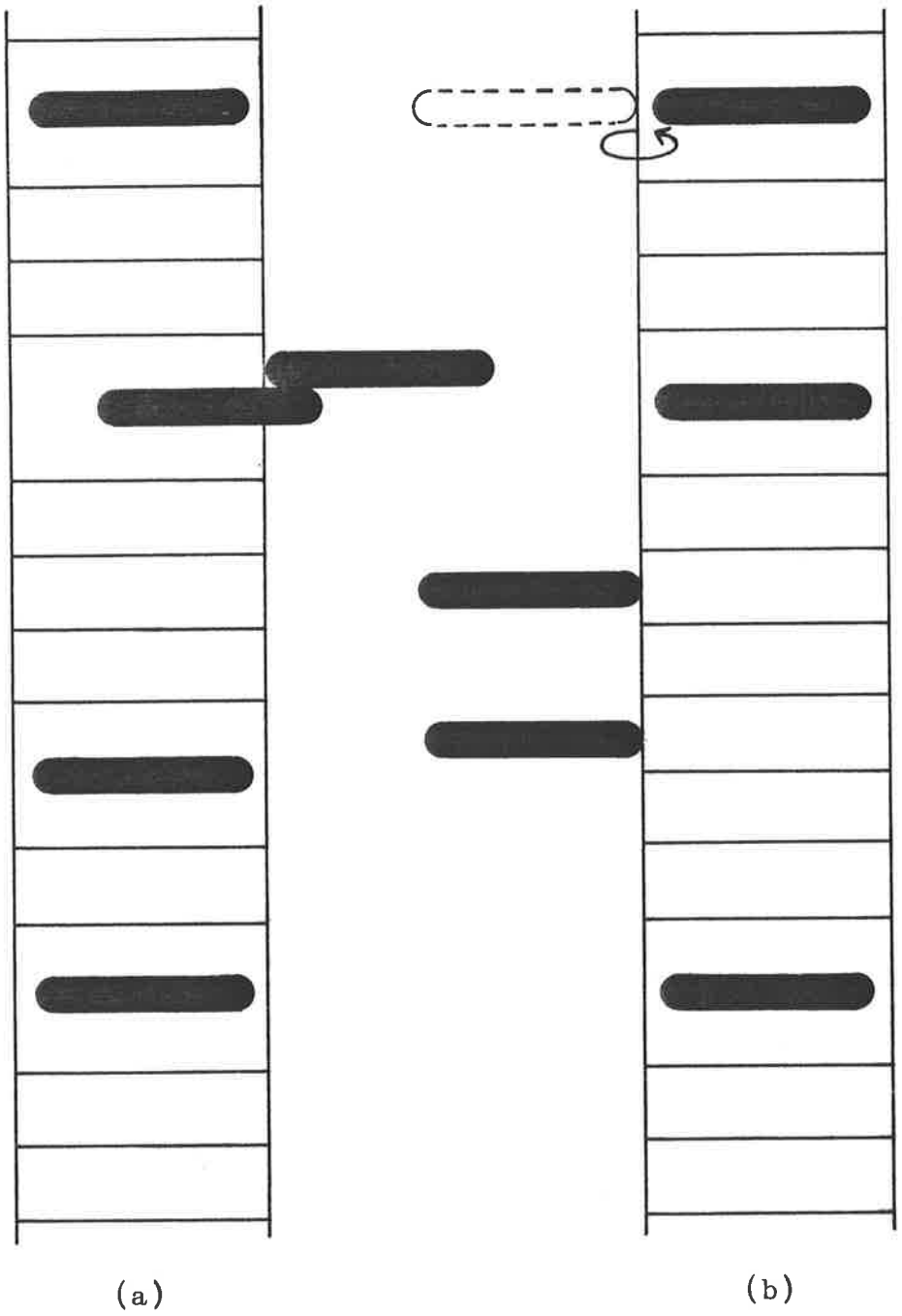

Figure 2-2. Schematic representations of binding site heterogeneity for the strong binding of aminoacridine to native DNA.

(a) The model of Armstrong et al.
(b) The model of Li and Crothers.

DNA. This model is schematically similar to Fig. 2.2(b) except that the local base composition of the DNA now influences the relative amounts of intercalated and outside bound forms which exist in a given DNA segment.

These studies of the binding of Proflavine and Proflavine-like aminoacridines to DNA suggest that some strongly outside-bound form is possible either as a separate entity (as in Fig. 2.2(b)) or as a dimer formed with an already intercalated molecule (Fig. 2.2(a)). Furthermore such forms are not favoured in solvents of high ionic strength. No study of which I am aware suggests that 9-aminoacridine or its derivatives display such site heterogeneity. Indeed recent studies of the binding of Quinacrine[94,110] and 9-aminoacridine[37] to DNA do not suggest either base-pair or binding site type heterogeneity.

REFERENCES

1. Albert A., "The Acridines", 2nd ed., Arnold (publishers) Ltd., (1966).
2. Peacocke A.R., *Chem. Heterocycl. Comp.*, 9, 723 (1973).
3. Blake A. and Peacocke A.R., *Biopolymers*, 6, 1225 (1968).
4. Löber G., *Z. für Chemie*, 9, 252 (1969).
5. Löber G., *Z. für Chemie*, 11, Part 1 pp 92, Part 2 pp 135 (1971).
6. Georghiou S., *Photochem. Photobiol.*, 26, 59 (1977).
7. Langmuir, I., *J.A.C.S.*, 38, 2221 (1916).
8. Scatchard G., *Ann. N.Y. Acad. Sci.*, 51, 660 (1949).
9. Schwarz G., *Eur. J. Biochem.*, 12, 442 (1970).
10. Schwarz G., Klose S. and Balthasar W., *Eur. J. Biochem.*, 12, 454 (1970).
11. McGhee J.D. and von Hippel P.H., *J. Mol. Biol.*, 86, 469 (1974).
12. Lifson S., *J. Phys. Chem.*, 40, 3705 (1964).
13. Bradley D.F. and Lifson S., in "Molecular Associations in Biology", B. Pullman (ed.), Academic Press, New York, (1968), p. 261.
14. Schellman J.A., *Isr. J. Chem.*, 12, 219 (1974).
15. Peacocke A.R. and Skerrett J.N.H., *Trans. Farad. Soc.*, 52, 261 (1956).
16. Drummond D.S., Simpson-Gildemeister V.F.W. and Peacocke A.R., *Biopolymers*, 3, 135 (1965).
17. Chambron J., Daune M. and Sadron C., *Biochim. Biophys. Acta*, 123, 306, 319 (1966).
18. Armstrong R.W., Kurucsev T. and Strauss U.P., *J.A.C.S.*, 92, 3174 (1970).
19. Jordan D.O. and Sansom L.N., *Biopolymers*, 10, 399 (1971).

20. Ramstein J., Leng M. and Kallenbach N.R., *Biophys. Chem.*, 5, 319 (1976).

21. Löber G., Schütz H. and Kleinwächter V., *Biopolymers*, 11, 2439 (1972).

22. Lloyd P.H., Prutton R.N. and Peacocke A.R., *Biochem. J.*, 107, 353 (1968).

23. Heilweil H.G. and van Winkle Q., *J. Phys. Chem.*, 59, 939 (1955).

24. Tubbs R.K., Ditmars W.E. and van Winkle Q., *J. Mol. Biol.*, 9, 545 (1964).

25. Thomes J.C., Weill G. and Daune M., *Biopolymers*, 8, 647 (1969).

26. Ellerton N.F. and Isenberg I., *Biopolymers*, 8, 767 (1969).

27. Chan L.M. and van Winkle Q., *J. Mol. Biol.*, 40, 491 (1969).

28. Lerman L.S., *J. Mol. Biol.*, 3, 18 (1961).

29. Lerman L.S., *J. Mol. Biol.*, 10, 367 (1964).

30. Gilbert M. and Claverie P., *J. Theor. Biol.*, 18, 330 (1968).

31. Gersch N.F. and Jordan D.O., *J. Mol. Biol.*, 13, 138 (1965).

32. See for example: Bloomfield V.A., Crothers D.M. and Tinoco I., "Physical Chemistry of Nucleic Acids", Harper and Rowe (1974).

33. Schildkraut C. and Lifson S., *Biopolymers*, 3, 195 (1965).

34. Blake A. and Peacocke A.R., *Biopolymers*, 5, 383 (1967).

35. Ichimura S., Zama M., Fujita H. and Ito T., *Biochim. Biophys. Acta*, 190, 116 (1969).

36. Jordan D.O. and Sansom L.N., *Stud. Biophys.*, 24/25, 225 (1970).

37. Turner D.R., Ph.D. Thesis, University of Adelaide (1975).

38. Sansom L.N., Ph.D. Thesis, University of Adelaide (1972).

39. Ramstein J. and Leng M., *Biochim. Biophys. Acta*, 281, 18 (1972).

40. Kharintonenkov I.V. and Drynov I.D., *Biofizika*, 16, 1008 (1971). (English Translation).

41. Löber G., *Photochem. Photobiol.*, 8, 23 (1968).

42. Löber G. and Achtert G., *Biopolymers*, 8, 595 (1969).

43. Peacocke A.R., *Stud. Biophys.*, 24/25, 213 (1970).

44. Filipski J., Chorazy M. and Mendecki J., *Stud. Biophys.*, 24/25, 249 (1970).

45. Unpublished observations quoted in reference 2.

46. Dalgleish D.G., Peacocke A.R., Fey G. and Harvey C., *Biopolymers*, 10, 1853 (1971).

47. Müller W. and Crothers D.M., *Stud. Biophys.*, 24/25, 279 (1970).

48. Löber G., *Stud. Biophys.*, 24/25, 233 (1970).

49. Dalgleish D.G., Feil M.C. and Peacocke A.R., *Biopolymers*, 11, 2415 (1972).

50. Drummond D.S., Pritchard N.J., Simpson-Gildemeister V.F.W. and Peacocke A.R., *Biopolymers*, 4, 971 (1966).

51. Cohen G. and Eisenberg H., *Biopolymers*, 8, 45 (1969).

52. Cairns J., *Cold Spring Harbour Symp. Quant. Biol.*, 27, 311 (1962).

53. Mauss Y., Chambron J., Daune M. and Benoit H., *J. Mol. Biol.*, 27, 579 (1967).

54. Freifelder D., *J. Mol. Biol.*, 60, 401 (1971).

55. Dasgupta S., Misra D.N. and Dasgupta N.N., *Biochim. Biophys. Acta*, 294, 38 (1973).

56. Butour J.L., Delain E., Couland D., Le Pecq J.B., Barbet J. and Roques B.P., *Biopolymers*, 17, 873 (1978).

57. Luzzati V., Masson F. and Lerman L.S., *J. Mol. Biol.*, 3, 634 (1964).

58. Fuller W. and Waring M.J., *Ber. Buns. Physik. Chem.*, 68, 805 (1964).

59. Neville D.M. and Davies D.R., *J. Mol. Biol.*, 17, 57 (1966).

60. Pigram W.J., Fuller W. and Davies M.E., *J. Mol. Biol.*, 80, 361 (1973).

61. Bauer W. and Vinograd J., *J. Mol. Biol.*, 33, 141 (1968).

62. Waring M., *J. Mol. Biol.*, 54, 247 (1970).

63. Kleinwachter V., Bakarova Z. and Bohacek J., *Biochim. Biophys. Acta*, 174, 188 (1969).

64. Kleinwachter V. and Koudelka J., *Biochim. Biophys. Acta*, 91, 539 (1964).

65. Michaelis L., *Cold Spring Harbour Symp. Quant. Biol.*, 12, 131 (1947).

66. Walker I.O., *Biochim. Biophys. Acta*, 109, 585 (1965).

67. Weill G. and Calvin M., *Biopolymers*, 1, 401 (1963).

68. Neville D.M. and Bradley D.F., *Biochim. Biophys. Acta*, 50, 397 (1961).

69. Blake A. and Peacocke A.R., *Nature*, 206, 1009 (1965).

70. Yamaoka K. and Resnik R.A., *J. Phys. Chem.*, 70, 4051 (1966).

71. Li H.J. and Crothers D.M., *Biopolymers*, 8, 217 (1969).

72. Gardner B.J. and Mason S.F., *Biopolymers*, 5, 79 (1967).

73. Stryer L. and Blout E.R., *J.A.C.S.*, 83, 1411 (1961).

74. Blake A. and Peacocke A.R., *Biopolymers*, 4, 1091 (1966).

75. Aktipis S. and Martz W.W., *Biochim. Biophys. Res. Comm.*, 39, 307 (1970).

76. Dalgleish D.G., Fujita H. and Peacocke A.R., *Biopolymers*, 8, 633 (1969).

77. Weill G., *Biopolymers*, 3, 567 (1965).

78. Löber G., *Photochem. Photobiol.*, 4, 607 (1965).

79. Löber G., *Photochem. Photobiol.*, 8, 23 (1968).

80. Lerman L.S., *Proc. Nat. Acad. Sci. U.S.A.*, 49, 94 (1963).

81. Nagata C., Kodama M., Tagashira Y. and Imamura A., *Biopolymers*, 4, 409 (1966).

82. Houssier C., Hardy B. and Fredericq E., *Biopolymers*, 13, 1141 (1974).

83. Kelly G.R. and Kurucsev T., *Biopolymers*, 15, 1481 (1976).

84. Sakore T.D., Jain S.C., Tsai Chun-che and Sobell H.M., *Proc. Nat. Acad. Sci. U.S.A.*, 74, 188 (1977).

85. Tsai C.C., Jain S.C. and Sobell H.M., *Proc. Nat. Acad. Sci. U.S.A.*, 72, 628 (1975).

86. Tsai C.C., Jain S.C. and Sobell H.M., *J. Mol. Biol.*, 114, 301 (1977).

87. Jain S.C., Tsai C.C. and Sobell H.M., *J. Mol. Biol.*, 114, 317 (1977).

88. Neidle S., Achari A., Taylor G.L., Berman H.M., Carrell H.L., Glusker J.P. and Stallings W.C., *Nature*, 269, 304 (1977).

89. Berman H.M. Stallings W., Carrell H.L., Glusker J.P., Neidle S., Taylor G. and Achari A., *Biopolymers*, 18, 2405 (1979).

90. Patel D.J., *Biopolymers*, 16, 2739 (1977).

91. Bradbury E.M. and Rattle H.W.E., *Eur. J. Biochem.*, 27, 270 (1972).

92. Alden C.J. and Arnott S., *Nucleic Acid Res.*, 2, 1701 (1975).

93. Pritchard N.J., Blake A. and Peacocke A.R., *Nature*, 212, 1360 (1966).

94. Wilson W.D. and Lopp I.G., *Biopolymers*, 18, 3025 (1979).

95. Le Pecq J.B., Le Bret M. Barbet J. and Roques B., *Proc. Nat. Acad. Sci. U.S.A.*, 72, 2915 (1975).

96. Wakelin L.P.G., Romanos M., Chen T.K., Glaubiger E.S., Canellakis E.S. and Waring M.J., *Biochemistry*, 17, 5057 (1978).

97. See for example: Eigen M. and De Maeyer L., "Techniques of Organic Chemsitry", Vol. 8, part 2; Freiss, Lewis, Weisberger, eds., *Interscience*, New York (1963).

98. Li H.J. and Crothers D.M., *J. Mol. Biol.*, 39, 461 (1969).

99. Schmechel D.E.V. and Crothers D.M., *Biopolymers*, 10, 465 (1971).

100. Ramstein J., Dourlent M. and Leng M., *Biochem. Biophys. Res. Comm.*, 47, 874 (1972).

101. Ramstein J. and Leng M., *Biophys. Chem.*, 3, 234 (1975).

102. Le Pecq J.B. and Paoletti C., *J. Mol. Biol.*, 27, 87 (1967).

103. Fornasiero D., personal communication.

104. Bidet R., Chambron J. and Weill G., *Biopolymers*, 10, 225 (1971).

105. Daune M., quoted in reference 2.

106. Georghiou S., *Photochem. Photobiol.*, 22, 103 (1975).

107. Duportail G., Mauss Y. and Chambron J., *Biopolymers*, 16, 1397 (1977).

108. Kubota Y. and Steiner R.F., *Biophys. Chem.*, 6, 279 (1977).

109. Kubota Y., Motoda Y. and Fujisaki Y., *Chem. Lett.*, 1979, 237.

110. Borisova O.F., Razjivin A.P. and Zaregorodzev V.I., *FEBS. Lett.*, 46, 239 (1974).

CHAPTER III

The experimental determination of equilibrium binding data.

CONTENTS

1. Introduction

In order to determine the parameters which characterize the interaction of 9-aminoacridines with native DNA it is necessary to determine the extent of binding to the DNA as accurately as possible using available experimental techniques. In this chapter I will examine the advantages and limitations of the two main techniques chosen from those available to study this interaction. These two techniques are UV-visible spectrophotometry of solutions and equilibrium dialysis. A third technique, that of sedimentation velocity, will be briefly discussed. The purpose of these studies is to determine which technique, or combination of techniques, offers the best accuracy and reproducibility for determining equilibrium binding parameters. In this discussion 9-aminoacridine is frequently used as a representative of the properties and behaviour of the substituted 9-aminoacridines studied.

2. Spectrophotometric analysis

All of the 9-aminoacridines studied in this work, and indeed most aromatic heterocyclic cations which interact strongly with DNA, undergo modification of their characteristic UV-visible absorbance spectra on binding to DNA[1,2]. Under certain conditions it is possible to use these absorbance changes to determine the amount of the ligand bound to DNA in ligand/DNA mixtures.

In a system containing only two spectrally distinct forms of the same chromophore in equilibrium with each other, the observed absorbance at some wavelength, λ, may be expressed as:

$$\varepsilon^{\lambda}_{OBS} = (1-\alpha)\varepsilon^{\lambda}_{F} + \alpha\varepsilon^{\lambda}_{B} \qquad \text{--- 3.1}$$

where $\varepsilon^{\lambda}_{OBS} = A^{\lambda}_{OBS}/C_T$

In this equation, $\varepsilon^{\lambda}_{OBS}$, $\varepsilon^{\lambda}_{F}$ and $\varepsilon^{\lambda}_{B}$ are the observed, free and bound molar absorptivities at wavelength λ, A^{λ}_{OBS} is the observed absorbance, C_T is the total concentration of the chromophore and α is the fraction of the chromophore in the bound form. Equation 3.1 will be valid at all wavelengths at which the chromophore absorbs. If any three of the parameters in Eqn. 3.1 are known at any wavelength λ, then the fourth may be obtained. It is then only necessary to know two parameters at any other λ, or for any other mixture of the ligand with DNA, to obtain the other two. This arises because any given mixture has a constant α, and ε_B will be fixed at any given wavelength. In practical terms the problem is two-fold:

(1) To decide whether Eqn. 3.1 holds for the system under consideration.

(2) Can one solution (and hence all solutions) to a set of equations, of the type of Eqn. 3.1, be determined?

(a) Internal linearity

It has long been considered that the occurrence of an isosbestic point in a series of spectra is indicative of there being only two absorbing species in the system[3,4,5]. However Brynestad and Smith[6] have shown that this is not the case. They show that isosbestic points may be generated in multi-component systems and moreover that an isosbestic point need not arise in a two component system. An additional and better test for a two component system arises from the consideration of Eqn. 3.1. The spectrum of any member of a set of spectra composed of mixtures of only two components may be generated as a linear combination of the concentrations and absorptivities of the components. If this holds true then:

$$\varepsilon^{\lambda}_{2} = (1-\beta)\varepsilon^{\lambda}_{1} + \beta\varepsilon^{\lambda}_{3} \qquad \text{--- 3.2}$$

where ε_1, ε_2 and ε_3 are the apparent molar absorptivities of any three members of a two component set and β is a number independent of the wavelength of the observation. Brynestad and Smith[6] refer to this property of such a set of spectra as "Internal Linearity". All that is required to confirm that a given set of spectra are internally linear is to determine that the value of β found at one wavelength is invariant at all other wavelengths in the absorption band for combinations of spectra taken three at a time. The range of mixtures for which this holds, defines the range over which only two experimentally distinct chromophores exist in the solution.

(b) Choice of spectral band

The UV-visible spectra of 9-aminoacridine HCl, 9-(cyclohexyl)-aminoacridine HCl and *E Coli* DNA all in 0.10 M NaCl as solvent are shown in Fig. 3.1. These two acridines are chosen because they represent the extremes of the wavelength range within which fall the spectra of all the other 9-aminoacridines studied in this work. There are three bands in the UV-visible spectra of the acridines. The two visible/near UV bands are labelled ^1L_a and ^1L_b on Fig. 3.1 after the assignment of Zanker and Schiefele[7]. The DNA has a strong UV absorption centred around 260 nm and no visible region absorption bands as such. The choice of spectral band to study then is straight-forward. The UV band is rejected because of the strong absorption of DNA in the same region which would lead to a multi-component system. Of the remaining two bands the ^1L_a band is chosen because:

(i) It is more intense.

(ii) It is at longer wavelength and so suffers less from the background absorbance of DNA in the visible region.

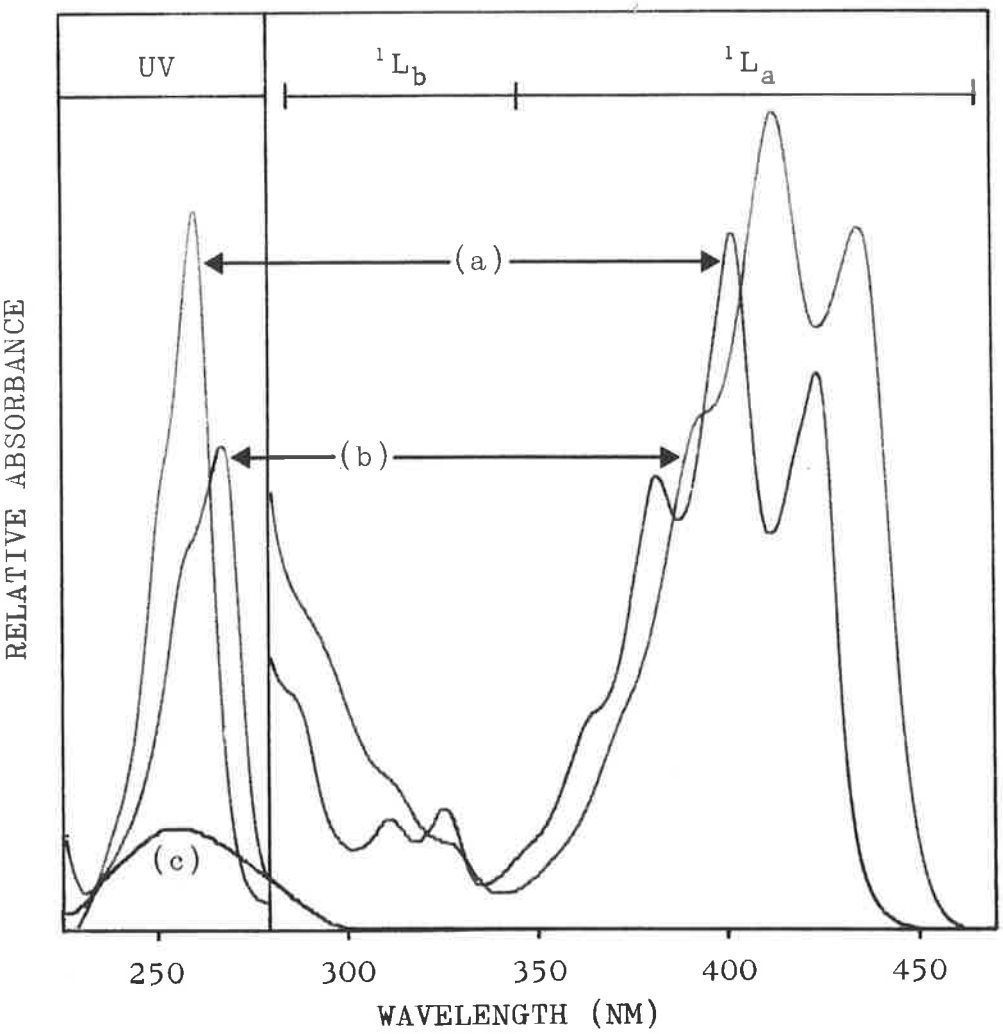

(a) 9-aminoacridine HCl/0.10 M NaCl

(b) 9-(cyclohexyl)-aminoacridine HCl/0.10 M NaCl

(c) Native *E Coli* DNA/0.10 M NaCl

Figure 3-1. The UV-visible spectra of two 9-aminoacridines and *E Coli* DNA all at the same concentration. Note that the relative absorbance scale of the UV section of the spectrum (225 - 280 nm) is one eighth of the scale of the near-UV/visible section of the spectrum (280 - 470 nm).

Point (i) is obvious. A more intense band enables work over a greater range of concentration of the dye with greater precision in measuring absorbances. Point (ii) merits more attention. The interfering apparent absorbance of DNA solutions in the visible region of the spectrum has often been mentioned[2,8] but not explained. It warrants attention since it may present a serious limitation to the accuracy of the spectrophotometric method of determining binding parameters.

(c) DNA background absorbance

The spectrum of this apparent absorbance is shown in Fig. 3.2. It is seen to decrease monotonically in intensity with increasing wavelength. Bacterial DNA's, both prepared in this Department and commercially obtained samples, show apparent molar absorptivities (based on DNA phosphate) of between 2.5 and 10 at 400 nm. It is observed that DNA samples which yield "water bright" solutions at a concentration of 1 mg/ml tend to have lower absorbances in the visible region than those samples whose solutions have a more "grainy" appearance. It has been suggested that the absorbance may be due to light-scattering from the DNA molecules, or small aggregates of them, or from minute air-bubbles trapped in the solution[24]. Sonication of solutions of high molecular weight samples had no significant effect on the absorbance. Solutions which were centrifuged for 1 hour at 10,000 RCF and carefully decanted into spectrophotometer cells also showed little change in absorbance. The apparent molar absorptivity appears to be invariant, within the uncertainty of measurement, up to about 1.5×10^{-3} M DNA phosphorus. Above this concentration it decreases slightly. Variation of temperature within the range 10°C to 50°C and of neutral salt

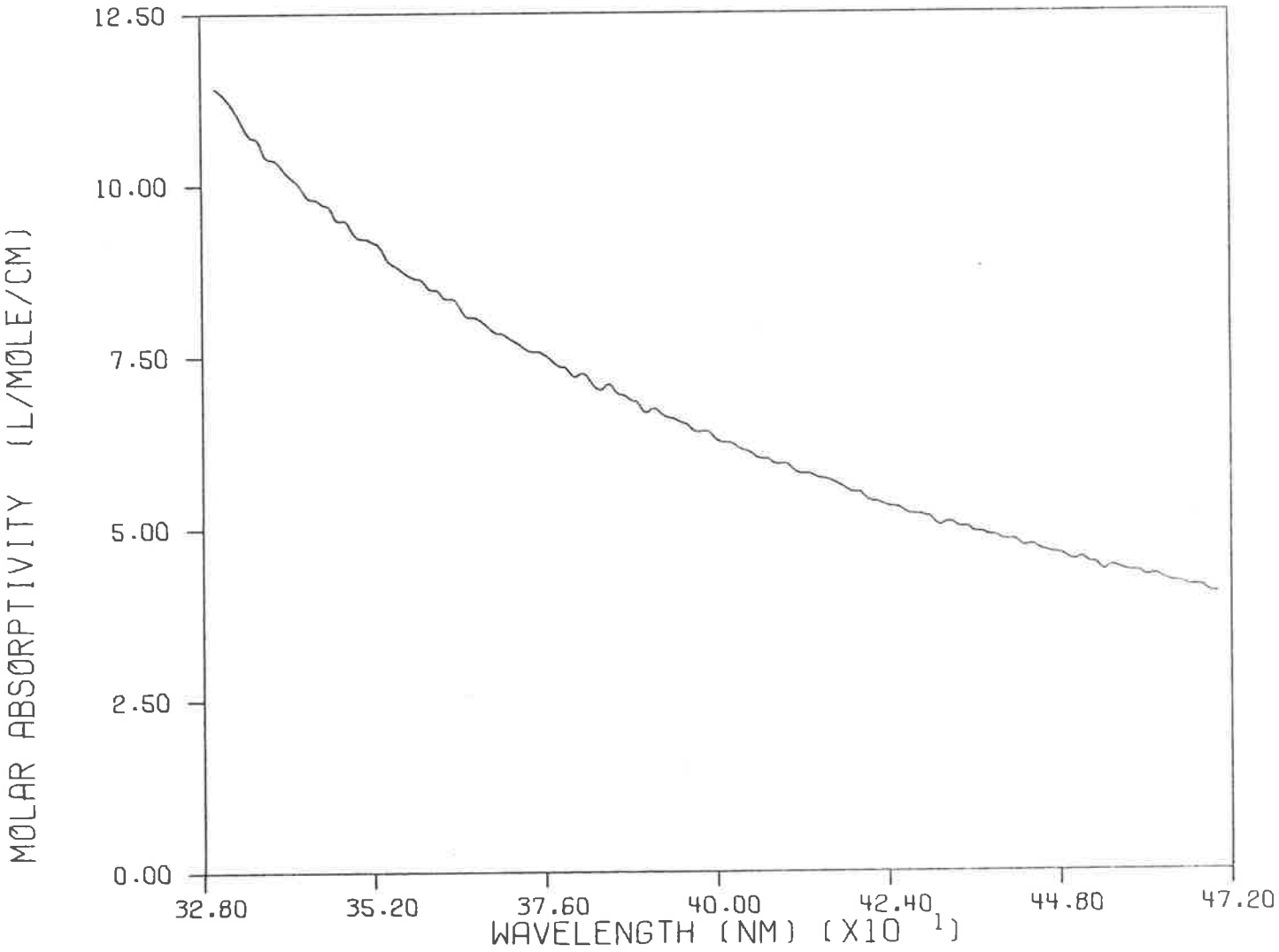

Figure 3-2. The apparent absorbance spectrum of *E Coli* DNA in a solvent of 0.10 M NaCl in the region 330 nm to 470 nm. Average of five concentrations in the range 1 x 10^{-4} M to 1 x 10^{-3} M DNA phosphorus.

concentration in the solvent between 0.001 M NaCl to 0.10 M NaCl had little effect. It was observed that the geometry of the various spectrophotometer cells used had some effect. The use of narrow long pathlength microcells leads to a lower apparent absorbance than when using wider cells. The optical geometry of the different spectrophotometers used also affected the absorbance. The use of the DMR-10 double-beam spectrophotometer yielded lower absorbances than the PMQ-II single-beam spectrophotometer. Variation of the beam width in the PMQ-II using masks at the entrance to the sample housing produced lower absorbances when the beam was narrowed. Experiments conducted using another PMQ-II spectrophotometer equipped with a wide-window photomultiplier[9] in place of the normal detector also yielded lower absorbances for the same beam widths when compared to an un-modified PMQ-II.

It is extremely unlikely that this absorbance is the tail of the UV absorption band of the DNA. It is possible that it could be some absorbing impurities in the sample carried over from the bacterial cells from which the DNA was extracted. In view of the exhaustive purification procedures and of the featureless nature of the absorbance, this explanation also seems unlikely. The best explanation in view of the observations reported here is that the DNA molecules, or aggregates of them, act as Rayleigh scatterers. This light-scattering is apparently sufficient to lead to a measurably reduced light transmittance through DNA solutions and hence an apparent absorbance of light. The dependence of the absorbance at any particular wavelength on the optical geometry of the measuring system is particularly significant as support for this explanation.

The correction for such a non-specific absorbance in dye/DNA mixtures presents some difficulty. The absorbance of a DNA solution of equal DNA concentration can be measured under the same conditions and then subtracted from the total absorbance of a mixture as has been reported[2,8]. This does not make allowance for the possibility that the DNA absorbance correction may change in the presence of a ligand. For mixtures of DNA and the 9-aminoacridines studied in this work, the only region in which the dyes are non-absorbing is at wavelengths above 455 - 465 nm. In this region any residual absorbance should be due to the dye/DNA complex alone. The apparent molar absorptivity at these wavelengths is of the order of 2 which yields very low absorbances and so makes accurate estimation of any change to the absorbance difficult to measure. The uncertainty of absorbance measured for a 1.0×10^{-3} M DNA solution in a 2 cm cell is of the order of 25% of the measured absorbance value. Absorbances measured for dye/DNA solutions at 470 nm varied within the uncertainty of measurement and on average increased slightly when compared to the values for DNA alone. This indicates that no major change in absorbance occurs at these wavelengths. It gives no indication whether the apparent "spectrum" of the DNA in the region below 470 nm has changed. A small correction at 470 nm will be larger in the region of 400 nm and below, where the apparent molar absorptivity is higher.

A second indication of whether the correction is too small can be seen from plots of $\varepsilon^{\lambda}_{OBS}$ versus T_L/T_A, where T_L is the total dye concentration and T_A the total DNA concentration. In Fig. 3.3 several such plots are shown for the system 9-aminoacridine/*E Coli* DNA. The curves in Fig. 3.3 labelled

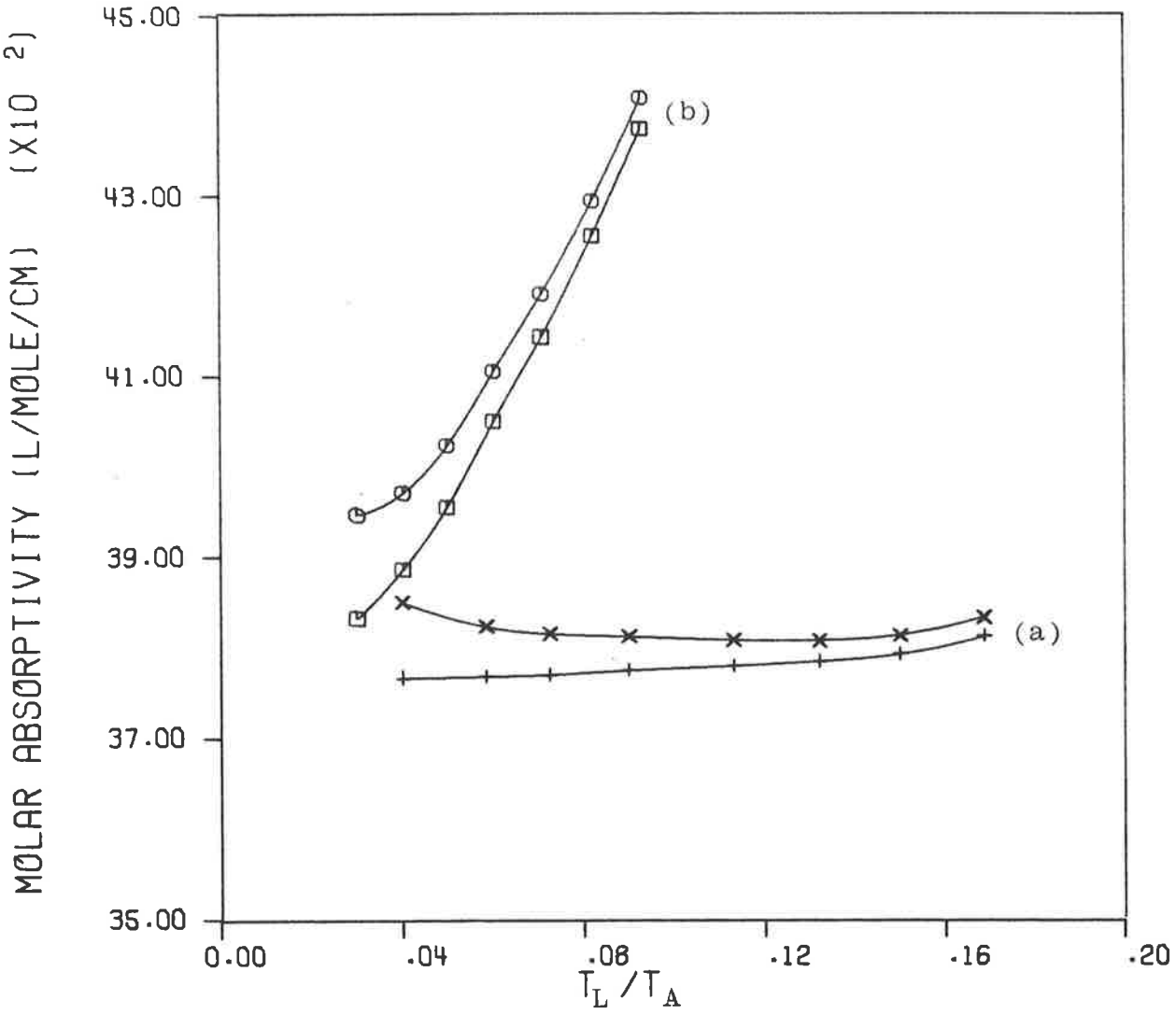

(a) 9AA/*E Coli* DNA/0.001 M NaCl.

$T_L = 4.895 \times 10^{-5}$ M

× before DNA background absorbance correction.
\+ after DNA background absorbance correction.

(b) 9AA/*E Coli* DNA/0.10 M NaCl.

$T_L = 5.297 \times 10^{-5}$ M

⊙ before DNA background absorbance correction.
⊡ after DNA background absorbance correction.

Figure 3-3. Plots of observed molar absorptivity at 401 nm versus T_L/T_A for 9AA/*E Coli* DNA mixtures.

(a) show the result with 0.001 M NaCl as solvent. This particular system is chosen to illustrate this point since the absorbance of the dye reaches a constant value at DNA concentrations sufficiently low for the background absorbance correction to be negligible when followed at 400 nm. It is then possible to follow the total apparent absorbance as the DNA concentration is further increased, any change being due to the DNA alone. The minimum correction for DNA background absorbance must be such that no nett increase in total absorbance occurs with increasing DNA concentration. This minimum correction however only specifies a lower limit to the magnitude of the correction and does not limit the maximum value it may take. Fig. 3.3(a) illustrates that the correction applied in that case, the apparent absorbance of the DNA in the absence of 9-aminoacridine, meets the minimum correction criterion. The curves in Fig. 3.3 labelled (b) show the situation with 0.10 M NaCl as solvent. For these systems the dye absorbance continues to decrease with increasing DNA concentration and no final plateau region is obtained. While the minimum correction criterion still applies there is no limit to the maximum correction that may be used in these cases.

(d) Determination of fraction bound

The solution of equations of the type given in Eqn. 3.1 must be found to determine the fraction of dye bound in a dye/DNA mixture. If the spectra of n dye/DNA mixtures are recorded at j wavelengths, then (n x j) simultaneous equations in (n x j + 1) unknowns may be formulated as follows:

$$\varepsilon^{\lambda}_{OBS} = (1-\alpha_k)\varepsilon^{\lambda}_{F} + \alpha_k\varepsilon^{\lambda}_{B} \qquad \text{--- 3.3}$$

where $\varepsilon^{\lambda}_{F}$ and $\varepsilon^{\lambda}_{B}$ are fixed at wavelength λ and α_k is the

fraction bound in the k^{th} mixture. For the spectrum of the k^{th} mixture, α_k remains constant and ε_F^λ and ε_B^λ vary with wavelength. All values of ε_F^λ are determined from the spectrum of the dye alone in the same solvent as used for the mixtures and at sufficient dilution to ensure only monomer dye is present in the solution. In the absence of a value for any α_k or ε_B^λ no unique analytical solution to the equations is possible since there will always be one more unknown than there are simultaneous equations to describe the system. It is necessary then to determine one or more values of α_k and/or ε_B^λ to solve the equations and so obtain the fraction of dye bound in any given mixture.

Values of α_k can only be determined by an independent method such as equilibrium dialysis. Experiments can be conducted with a mixture of dye/DNA giving values for α_k and total dye concentration, T_L, and total DNA concentration, T_A, in equilibrium on the DNA side of the membrane. The spectrum of a mixture of identical T_L and T_A can then be recorded and, in conjunction with known values of ε_F^λ, solutions to equations of the type of Eqn. 3.3 obtained since ε_B^λ is now the only unknown. This approach is limited by the accuracy with which α_k may be determined by an independent technique such as dialysis. The precision of this method may be checked for a given system by evaluating α_k for several mixtures and using these values to obtain ε_B^λ from each solution. The spread of the values of ε_B^λ will provide an estimate of random experimental errors, although not of any systematic errors. The possibility of dye loosely associating with the DNA without any measurable spectral change to the dye could also produce error in α_k values. This situation can be largely avoided by not using high dye to DNA ratios in the estimations of α_k. Conversely

the occurrence of increasing α_k estimates with increasing T_L/T_A may indicate that such an interaction does occur. A detailed discussion of the limitations of the equilibrium dialysis method is contained in the latter part of this chapter.

A second approach to the solution of the equations is to determine a value for ε_B^λ and use this to generate α_k values. It has often been assumed[2,8,23] that ε_B may be obtained by preparing mixtures of sufficiently low T_L/T_A so that all the dye is in the bound form to within the resolving power of the spectrophotometer. Modern UV-visible spectrophotometers have reproducibilities of about 0.5% so the association constant for the formation of the complex would have to be sufficiently high for > 99% of the dye to be bound. High molecular weight bacterial DNA's of the type used in this work have a solubility limit of $2 - 3 \times 10^{-3}$ M DNA phosphate above which homogeneous solutions cannot be obtained in a solvent of 0.10 M NaCl. The maximum DNA/dye ratio which may be used is governed by this solubility limitation and by the molar absorptivity of the dye in the mixture. To maintain precision of measurement, the absorbance of the mixture should be maintained above 0.1 absorbance units. For aminoacridines such as Proflavine[10,11] and Acridine Orange[11] molar absorptivities of $1.5 - 3 \times 10^4$ are observed when the dyes are bound to DNA. In the case of 9-aminoacridines these are of the order $3.5 - 4 \times 10^3$ which means a five-fold increase in dye concentration is required to obtain the same absorbance in DNA mixtures of low T_L/T_A. In order to see how these factors will influence the ability to directly measure ε_B, I will assume a simple model to describe the interaction. For low T_L/T_A the equilibrium may be written as:

$$\text{dye} + \text{DNA} \rightleftharpoons \text{complex}$$

$$\text{and} \qquad K = \frac{[\text{complex}]}{[\text{dye}][\text{DNA}]} \qquad \text{--- 3.4}$$

This model is valid for $T_L/T_A < 0.08$ where bound dye molecules on average are separated by at least 6 DNA base pairs and so represents "binding in isolation" to the DNA helix. The assumption is made that the dye does not bind to specific base pairs or sequences of base pairs but rather in a random manner and that the binding in this region is not cooperative in nature. The results of these calculations are presented in Fig. 3.4. This shows that if the association constant is high enough or if very low dye concentrations can be used then mixtures can be prepared in which all of the dye is bound to within the uncertainty of measurement. This however is not the case for the 9-aminoacridines used in this work.

In the absence of directly measured values of ε_B, a method of extrapolating to the value must be used. Turner[12] has suggested a graphical estimation obtained by extrapolating a plot of $\varepsilon_{OBS}/\varepsilon_F$ versus T_L/T_A to zero T_L/T_A, which represents an infinite DNA/dye ratio, so obtaining the ratio $\varepsilon_B/\varepsilon_F$ and hence ε_B. Figure 3.5(a) shows such a plot for the 9AA/*E Coli* DNA/0.10 M NaCl system at 22°C. Firstly it is evident that $\varepsilon^{\lambda}_{OBS}/\varepsilon^{\lambda}_F$ has not reached $\varepsilon^{\lambda}_B/\varepsilon^{\lambda}_F$ within experimentally accessible T_L/T_A values. Secondly it is evident that the extrapolation is not a simple straight line, but rather a curve convex to the T_L/T_A axis. The extrapolation is then rather subjective in nature. To reduce the uncertainty in this procedure several curves may be generated in the region $T_L/T_A < 0.09$ using different T_L values. The Law of Mass Action dictates that the ratio $\varepsilon^{\lambda}_{OBS}/\varepsilon^{\lambda}_F$ should be greater for lower T_L values since the concentration of free dye will be

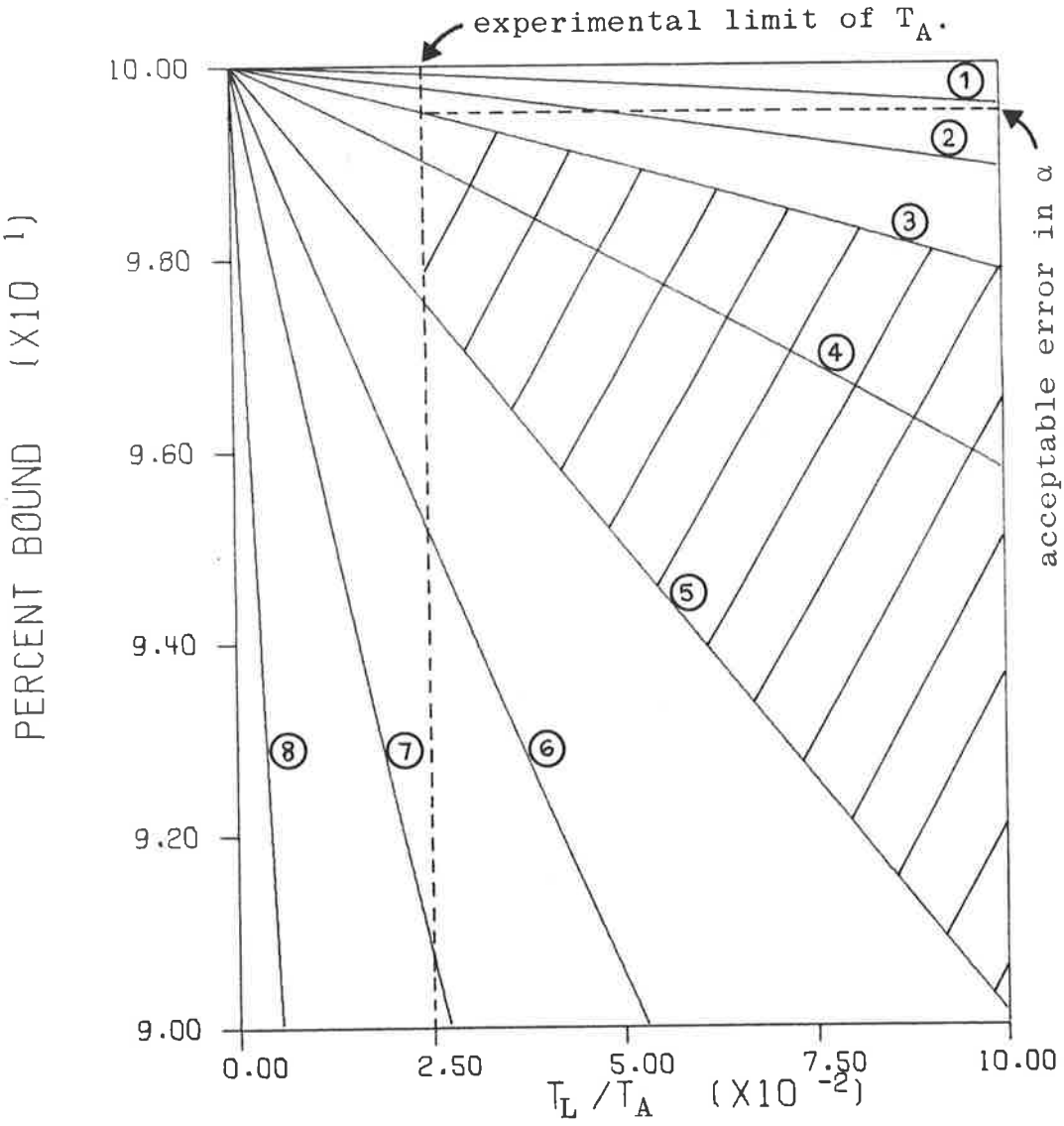

Curve No.	K (M^{-1})
1	5×10^5
2	2×10^5
3	1×10^5
4	5×10^4
5	2×10^4
6	1×10^4
7	5×10^3
8	1×10^3

Figure 3-4. Plots of % dye bound versus T_L/T_A computed from the binding in isolation model. T_L taken as 5×10^{-5} M. The cross-hatched area represents the range of reported K values for 9AAs.

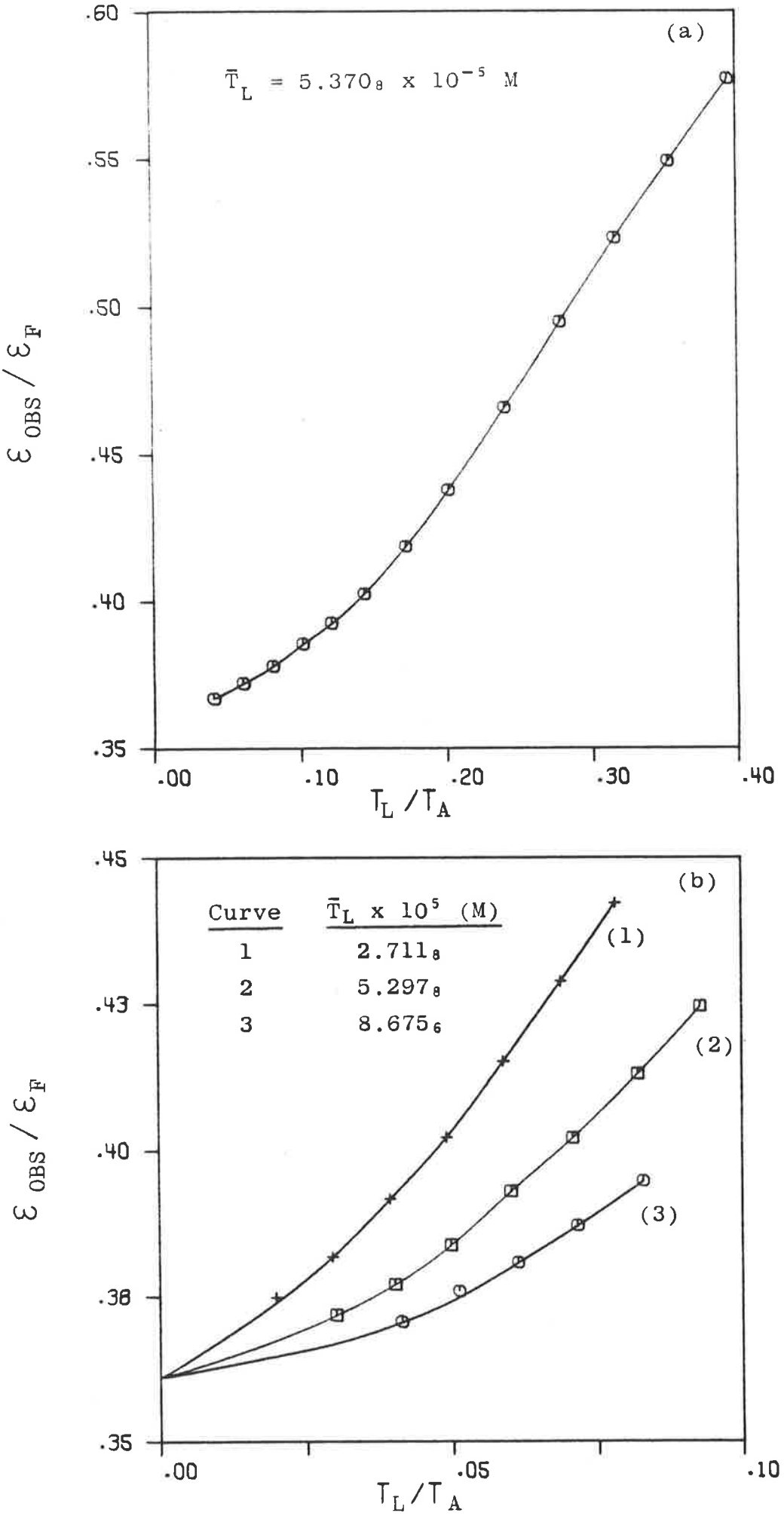

Figure 3-5. Plots of $\varepsilon_{OBS}/\varepsilon_M$ at 401 nm versus T_L/T_A for the 9AA/*E Coli* DNA/0.10 M NaCl system at 22°C.

higher relative to the total dye concentration. Hence a family of curves should be generated which only meet when $\epsilon^{\lambda}_{OBS} = \epsilon^{\lambda}_{B}$. Figure 3.5(b) shows such a family for the 9AA/*E Coli* DNA/0.10 M NaCl system at 22°C. The uncertainty of the extrapolation has been reduced but still remains larger than is desirable given the precision with which ϵ^{λ}_{OBS} values can be determined at $T_L/T_A \leq 0.05$.

In an attempt to further reduce the subjective nature of the extrapolation a non-linear fitting procedure was employed to fit values of ϵ^{λ}_{B} and an association constant, K, to this data. If the simple "binding in isolation" model is assumed to operate in this region then a relationship between ϵ^{λ}_{OBS} and T_A in terms of known values of T_L and ϵ^{λ}_{F} and parameters ϵ^{λ}_{B} and K may be derived. This derivation is given in Appendix I. A computer program, PROGRAM NONLIN which is briefly described in Appendix V, was used to obtain best fit values of ϵ^{λ}_{B} and K for a family of curves expressing ϵ_{OBS} as a function of T_A. Typical results from this procedure are shown in Fig. 3.6. These results are expressed as $\epsilon^{\lambda}_{OBS}/\epsilon^{\lambda}_{F}$ versus T_L/T_A to enable direct comparison with the subjectively drawn curves. While the result of fitting a family of curves together were good, attempts to fit values of ϵ^{λ}_{B} and K to single curves were poor. It is apparent from the results obtained that the fitted parameters, ϵ^{λ}_{B} and K, are highly correlated. The use of several curves fitted together, constraining the least squares fit to single values of ϵ^{λ}_{B} and K, markedly reduced this correlation and resulted in a more satisfactory fit for the data.

Another approach to the determination of a binding curve from incomplete spectral data has been proposed by Gatti *et al*[13]. These workers based the determination of

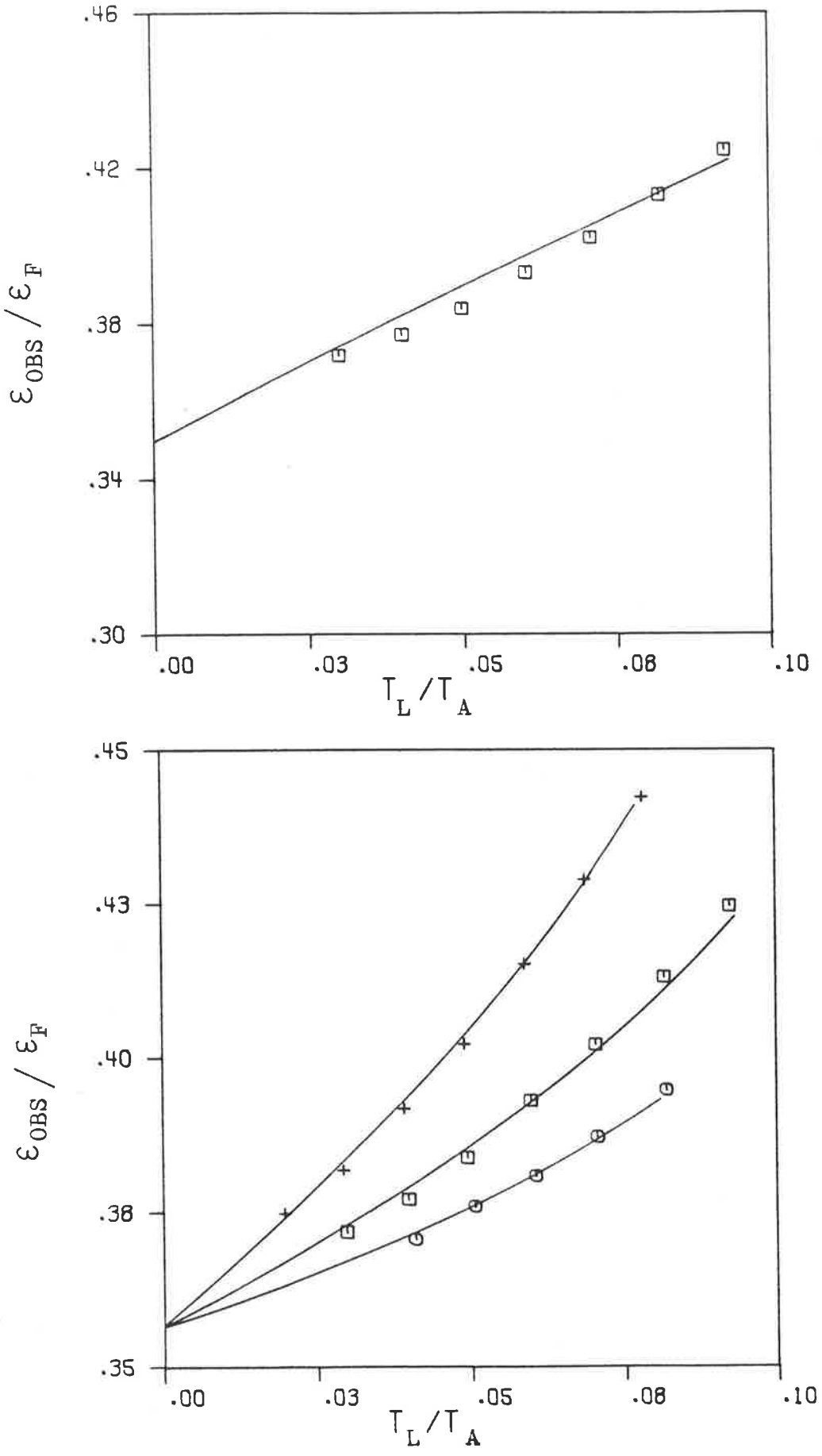

Figure 3-6. Plots of $\varepsilon_{OBS}/\varepsilon_M$ at 401 nm versus T_L/T_A for the 9AA/*E Coli* DNA/0.10 M NaCl system at 22°C. The curves were generated by non-linear fitting assuming a "binding in isolation" model (see text).

binding curves for the ethidium bromide/r-RNA system on a development of the more general work of Halfman and Nishida[14] concerning the binding of small molecules or ions to proteins. The essence of the method is to eliminate unknown parameters in the system by finding a relationship between the change in a measurable physical property of the system, whose change depends only on the binding process, and the known bulk concentrations in which one or more of the unknown parameters is constant. Such a relationship between change in absorbance on binding and total macromolecule concentration, where a single binding process is assumed, may be derived as follows. Consider the quantity

$$\Delta A_k^\lambda = A_0^\lambda - A_k^\lambda \qquad \text{--- 3.5}$$

where A is absorbance measured at wavelength λ, k refers to the k^{th} ligand/macromolecule mixture and A_0^λ is defined as:

$$A_0^\lambda = A_F^\lambda = C_T \epsilon_F^\lambda \qquad \text{--- 3.6}$$

where the subscript F refers to the free ligand and C_T is the total ligand concentration. We may also write:

$$A_k^\lambda = C_{F(k)} \epsilon_F^\lambda + C_{B(k)} \epsilon_B^\lambda \qquad \text{--- 3.7}$$

where the subscript B refers to the bound species. Substituting Eqns. 3.6 and 3.7 into 3.5 and dividing by the total macromolecule concentration, T_A, yields:

$$\frac{\Delta A_k^\lambda}{T_{A(k)}} = \frac{C_T \epsilon_F^\lambda - (C_{F(k)} \epsilon_F^\lambda + C_{B(k)} \epsilon_B^\lambda)}{T_{A(k)}} \qquad \text{--- 3.8}$$

Since:
$$C_T = C_{F(k)} + C_{B(k)} \qquad \text{--- 3.9}$$

Then:
$$\frac{\Delta A_k^\lambda}{T_{A(k)}} = \frac{C_{B(k)}}{T_{A(k)}} (\epsilon_F^\lambda - \epsilon_B^\lambda)$$

$$= r_k \Delta \epsilon^\lambda \qquad \text{--- 3.10}$$

Several curves of $\Delta A^{\lambda}/T_A$ versus T_A may be constructed using ΔA^{λ} values obtained with constant C_T and differing T_A to plot each individual curve. Now provided all absorbing species satisfy Beer's Law over the concentration range used, then $\Delta\varepsilon^{\lambda}$ will be independent of C_T and the intercepts with the curves of a line drawn such that $\Delta A^{\lambda}/T_A$ is constant will yield values of C_T and T_A at constant r. The ratio r may be written as:

$$r = {}^{C_B}/_{T_A} \qquad \text{--- 3.11}$$

and combining this with Eqn. 3.9 yields:

$$C_T = rT_A + C_F \qquad \text{--- 3.12}$$

A plot of ordered pairs (C_T, T_A) obtained at constant r should be linear with a slope, r, and an ordinate intercept, C_F. The values of r and C_F so obtained can be used to construct a binding curve for the ligand/macromolecule system.

This derivation presented above is valid provided the binding process is not influenced by the extent of the reaction or the concentrations used to obtain suitable mixtures. If these conditions are not met then the C_T versus T_A curves *may* not be linear. Values of r may still be obtained from any linear portion of the curve but accurate values of C_F would not be obtained.

Before applying this method the data should be tested to check that it conforms to Eqn. 3.10. From this equation we may write:

$$\frac{\Delta A_k^{\lambda}}{T_{A(k)}} \Big/ \frac{\Delta A_{\ell}^{\lambda}}{T_{A(\ell)}} = \frac{r_k}{r_{\ell}} \qquad \text{--- 3.13}$$

The right-hand side of this relationship is a constant independent of wavelength. The ratio on the left-hand side may be evaluated at several different wavelengths to verify

that this condition is met. This requirement, that the ratio $\Delta A_k^\lambda / \Delta A_\ell^\lambda$ be independent of wavelength, is however equivalent to a necessary condition for internal linearity within a set of spectra (see Chapter III (2) (a)). Hence data from internally linear systems will satisfy Eqn. 3.13.

This method has been applied to data for the 9AA/*E Coli* DNA/0.10 M NaCl system. The data used is the same as that presented for the extrapolative method, both to allow direct comparison of the results and because only data gathered at low T_L/T_A will approximately conform to the condition mentioned above concerning the effect of the extent of binding upon the binding process. Figure 3.7 shows plots of $\Delta A^\lambda/T_A$ versus T_A for three total dye concentrations. The (C_T, T_A) pairs obtained from these curves at $\Delta A^\lambda/T_A$ values between 4.5×10^3 M^{-1} and 2.75×10^3 M^{-1} (the full extent of the usable range for these curves) are plotted in Fig. 3.8. The lines drawn on this figure were obtained by linear regression analysis of these data sets. Table 3.1 presents the results of this fitting procedure together with some statistical parameters for the fits.

This method of determining the binding curve has some disadvantages when compared to the extrapolative method. More data must be collected to obtain a suitable number of datum points on the C_T versus T_A curves. A minimum of three data sets must be collected and preferably more to increase the number of points on which the linear regression is performed. As shown in Table 3.1, the standard errors of the slope are erratic. To improve this situation it is necessary to obtain more points on the C_T versus T_A curves. The erratic standard errors observed may be a function of the low number of degrees of freedom resulting from the small number of points on each

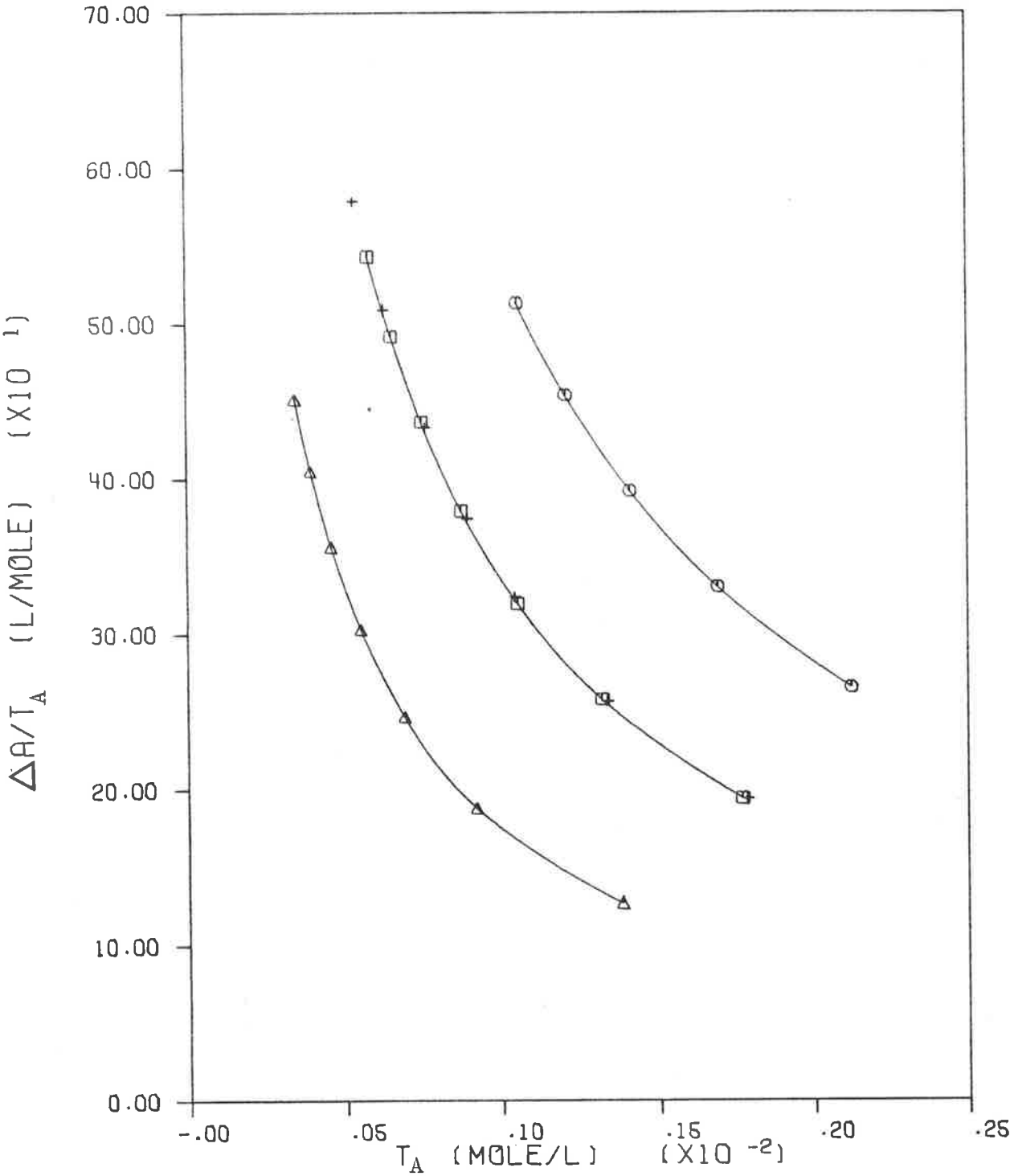

Symbol	$\bar{T}_L \times 10^5$ (M)
△	2.711_8
□	5.297_8
+	5.370_8
○	8.675_6

Figure 3-7. Plots of $\Delta A/T_A$ at 401 nm versus T_A for the 9AA/*E Coli* DNA/0.10 M NaCl system at 22°C.

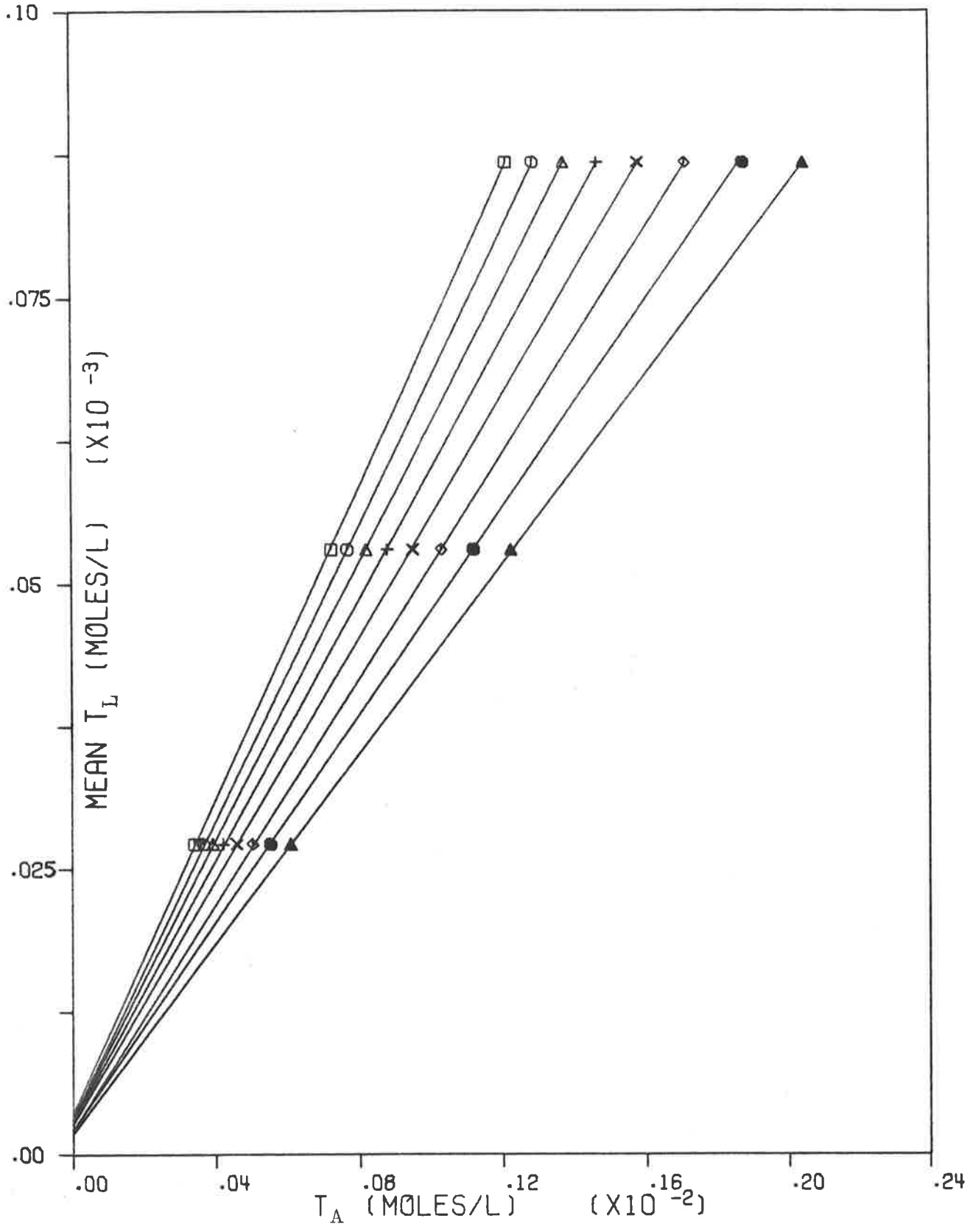

Figure 3-8. Plots of ordered pairs of $(\bar{T}_L, T_A)$ obtained from Fig. 3-7 at 8 $\Delta A/T_A$ values between 450 M^{-1} and 275 M^{-1}. See Table 3.1 for the regression coefficients of the fitted lines.

TABLE 3.1

The linear regression coefficients and their standard errors for plots of T_L versus T_A at constant $\Delta A/T_A$ for the 9AA/*E coli* DNA/0.10 M NaCl system at 22°C.

$\Delta A/T_A$ x 10^3 (M^{-1})	r (1)	S.E.	C_F (2) x 10^6 (M)
4.50	0.0685_0	2.87×10^{-3}	3.44_4
4.25	0.0647_6	1.75×10^{-8}	3.18_1
4.00	0.0608_7	6.79×10^{-5}	2.96_8
3.75	0.0570_3	1.95×10^{-3}	2.86_4
3.50	0.0532_2	7.18×10^{-8}	2.48_6
3.25	0.0494_2	3.48×10^{-4}	2.06_3
3.00	0.0454_1	8.62×10^{-9}	1.99_9
2.75	0.0415_4	4.30×10^{-8}	1.83_4

(1) Obtained directly from the slope of the linear regression line.

(2) Obtained directly from the intercept of the linear regression line.

(3) The measure used to assess the goodness of fit to a straight line is the coefficient of determination (r^2). Its value was greater than 0.99996 in all cases.

curve. It should be noted that as T_A increases the $\Delta A^{\lambda}/T_A$ versus T_A curves asymptote towards the abscissa. This makes the determination of T_A at constant $\Delta A^{\lambda}/T_A$ difficult in this area where the system is most likely to meet the required conditions. This is the converse of the situation with the extrapolative method where data points of high T_A will be most useful. Despite these largely experimental drawbacks this method is sound and represents a valuable cross-check of the extrapolative method.

Finally, the method of Li and Crothers[15] must be mentioned since it has been often applied[16]. This analysis was originally formulated by Benesi and Hildebrand[17] and is based on a simple equilibrium such as that of Eqn. 3.4; in the nomenclature of this work:

$$\frac{1}{\varepsilon_F-\varepsilon_{OBS}} = \frac{1}{\varepsilon_F-\varepsilon_B} + \frac{1}{\varepsilon_F-\varepsilon_B}\cdot\frac{1}{K}\cdot\frac{1}{T_A-T_L} \qquad \text{--- 3.14}$$

where it is assumed that $T_A - rT_A \simeq T_A - T_L$ when $T_A >> T_L$. This is the equation of a straight line from which ε_B is obtained from the intercept of a plot of $1/(\varepsilon_F-\varepsilon_{OBS})$ versus $1/(T_A-T_L)$. The slope of this line will yield a value of the association constant, K. when the reciprocal of the slope is multiplied by the intercept. Such a plot for the 9AA/*E Coli* DNA/0.10 M NaCl system at 22°C is presented in Fig. 3.9. It is apparent that the data plotted do not represent straight lines but rather curves convex to the abscissa. Attempts to fit linear regression lines to these data result in grossly underestimated values of ε_B and K when compared to those obtained by the other methods discussed previously. In the light of this result it is concluded that the systems studied in this work cannot be adequately described by the assumptions inherent in the derivation of

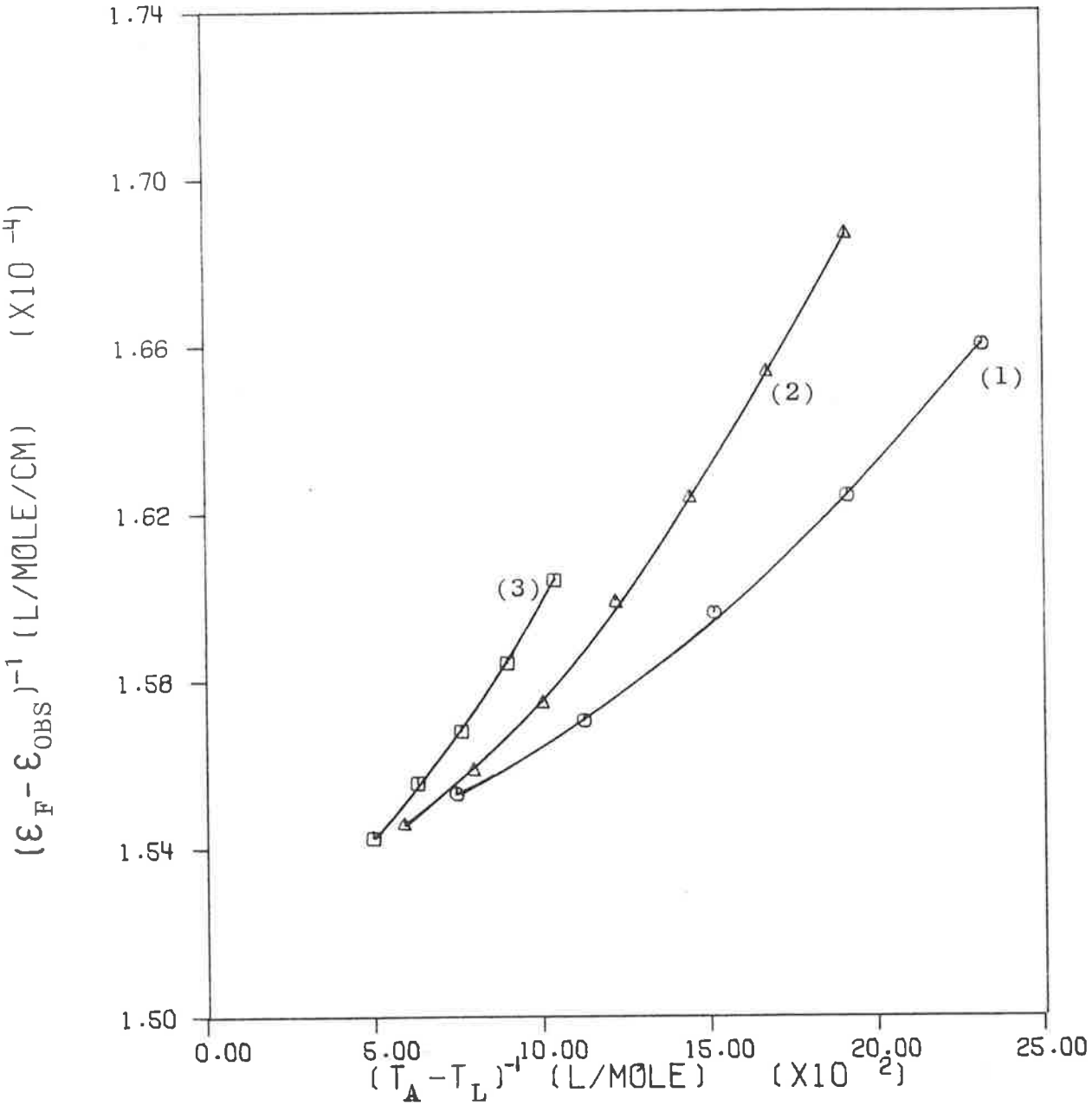

Curve No.	$\bar{T}_L \times 10^5$ (M)
1	2.711_8
2	5.297_8
3	8.675_6

Figure 3-9. Plots of $(\varepsilon_F - \varepsilon_{OBS})^{-1}$ at 401 nm versus $(T_A - T_L)^{-1}$ for the 9AA/*E Coli* DNA/0.10 M NaCl system at 22°C.

Eqn. 3.14. This result is consistent with the observations concerning the attempt to fit spectral data directly using the non-linear equations derived in Appendix I. This attempt also resulted in grossly underestimated values of ε_B and K.

(e) Analysis of errors

The ultimate accuracy of binding data collected by spectrophotometry will depend on the linearity and reproducibility of the UV-visible spectrophotometer. Provided all the data used to obtain the binding curves are taken on the same spectrophotometer its absolute absorbance accuracy is not crucial; however a measure of this accuracy against some standard will enable data collected on one spectrophotometer to be used in conjunction with measurements taken on another. The instruments used in this study were a Zeiss DMR-10 double beam recording spectrophotometer and a Zeiss PMQ-II single beam spectrophotometer. The DMR-10 was further equipped with a microprocessor based data collection and control facility designed by the author and described in Appendix IV.

The best check of linearity and absolute absorbance accuracy available is that described by Burke *et al*[18] using acidic potassium dichromate as a liquid absorbance filter. This test is superior to solid filters since it employs the actual conditions used to record absorbances of liquid samples. Table 3.2 shows typical results of this test which was made regularly during the course of this work. Wavelength accuracy was checked using the 486.1 nm line of the deuterium lamp. The PMQ-II was accurate to within 0.05 nm and the DMR-10 showed no deviation to within 0.02 nm, the step size of the monochromator. These tests established that the

TABLE 3.2

Calculated and measured absorbances for KCr_2O_7 in 0.001 M $HClO_4$.

Cell pathlength = 10.00_3 mm

Concn. (mg/ℓ) \ λ (nm)	235	257	313	350	Source
21.235_7	0.2644 0.264_5 0.2639	0.3046 0.304_5 0.3056	0.1030 0.103 0.1034	0.2278 0.228 0.2289	Calc. PMQ-II DMR-10
39.498_1	0.4887 0.489 0.4876	0.5686 0.568_5 0.5682	0.1915 0.192 0.1914	0.4242 0.424 0.4247	Calc. PMQ-II DMR-10
59.580_2	0.7401 0.740 0.7346	0.8613 0.861 0.8597	0.2891 0.289 0.2895	0.6406 0.641 0.6413	Calc. PMQ-II DMR-10
79.413	0.9907 0.992 0.9949	1.1526 - 1.154	0.3858 0.386 0.3861	0.8548 0.855 0.8553	Calc. PMQ-II DMR-10

absolute accuracy and linearity of both instruments are very good.

The reproducibility of the instruments was checked using a 9-aminoacridine/DNA mixture, readings being recorded several times at several wavelengths over a period of 3 days. This check encompasses both the reproducibility of the instruments, the cleaning and positioning of the curvettes, and in the case of the PMQ-II, the subjectivity of the operator. The results show a standard deviation of 0.0006 for the PMQ-II for absorbances between 0.2 and 0.5 and 0.0003 for the DMR-10 for absorbances between 0.1 and 0.7. Allowing two standard deviations, the precision of measurement is 0.5% at 0.200 absorbance.

Spectra collected from systems containing only two chromophores should show internal linearity to within the error of 0.5% on each absorbance measurement. For dye/DNA systems there are two areas which may show greater deviation. The first is at high T_L/T_A where appreciable amounts of free dye exist in solution and the formation of dye aggregates may produce lower absorbances than expected. This presents no problem to determining accurate binding data since the actual free dye concentration may be determined by an iterative procedure using a plot of absorbance versus concentration obtained for the dye in the absence of DNA. The procedure for this correction is detailed fully in Chapter IV (4). The second region where greater than expected deviation might occur is at very low T_L/T_A where the DNA concentration is high enough to contribute significantly to the total absorbance. Correction for this absorbance is made as described earlier in this Chapter. If deviation from internal linearity persists this may be due to the uncertain

nature of this correction. If this is so then deviations will be higher at shorter wavelengths. Absorbance readings taken on solutions with high DNA concentrations will have an additional uncertainty of about 0.5% - 1.0%.

Potentially the most serious source of error is in the estimation of ε_B^λ for systems such as the 9-aminoacridines at high ionic strength where this quantity cannot be obtained directly from measurement. Methods of subjective graphical extrapolation or objective non-linear fitting of data at low T_L/T_A to a simple model for the behaviour in this region can be used. Accurate estimation of the error involved in these procedures is difficult, however it is in the range of 1% - 3% uncertainty in the value of ε_B^λ determined. The effect of this uncertainty on the calculation of the fraction of dye bound, α, depends on the value of this fraction and is discussed in Chapter IV (4). The use of an independent technique, such as equilibrium dialysis, to obtain values for α and hence ε_B^λ is subject to similar errors as those discussed for the extrapolative methods. It does, however, provide a useful check of the uncertainty in the estimate of ε_B^λ providing systematic experimental errors can be kept to a minimum. Limitations of the technique of equilibrium dialysis are examined in the latter part of this chapter.

Finally, the contribution of the technique used to collect spectrophotometric data must be considered. The two principal techniques employed are the use of individual solutions of fixed T_L and varying T_A, or the titration of an aliquot of dye solution in a cuvette with a concentrated solution of DNA. In theory both methods should produce adequate results however I believe that for the determination of ε_B^λ the first method, the use of discrete solutions, offers

several practical advantages. Each solution of a set has the same T_L and will be related to any other set by a constant difference in T_L. When using extrapolative plots of the type $\varepsilon^{\lambda}_{OBS}/\varepsilon^{\lambda}_{F}$ versus T_L/T_A this will ensure that a family of curves so generated will maintain a constant relation to one another throughout the range of T_L/T_A values used. When the titration technique is employed, both T_L and T_A change on each addition to the cuvette and the relationship of data sets collected at differing initial T_L is more complex. Unless very high initial T_L values are chosen, the T_L values obtained in the crucial region of low T_L/T_A are low and will lead to steeper extrapolations to a T_L/T_A of zero than is desirable. The errors incurred in making multiple additions to a cuvette are inevitably higher than when using discrete solutions where only single additions are required and larger volumes may be employed. A further potential source of error is the anomalous behaviour of the DNA background scattering at high T_A values. I have observed that in some cases considerable time was required after stirring dye/DNA solutions of high T_A for the absorbance to equilibrate to a time independent value. Since the order of this change is small and the time required to equilibrate is several minutes, this drift in absorbance value is easily missed, particularly if a rigid time schedule is observed while making additions and taking readings for such titration experiments.* However once a

---

* Indeed I have obtained reproducible but incorrect binding data sets while employing such a schedule. A good test for this source of error is to leave a much longer time period between two successive readings toward the end of the titration. If insufficient time has been allowed between the other additions, a discontinuity in the resulting binding curve is observed at that point.

value of ε_B^λ has been obtained the titration technique may be employed provided the last mentioned point is taken into consideration. It offers considerable economy of solution use and time when compared to the discrete solution method.

3. Equilibrium dialysis

The technique of equilibrium dialysis depends upon an inert semi-permeable membrane which allows the free passage of small molecules, such as aminoacridines, across the membrane but precludes the free passage of large molecules such as highly polymerized DNA. Figure 3.10 is a diagram of a small volume equilibrium dialysis cell of the type used in this work. In a typical experiment a dye/DNA mixture is loaded into one side of the assembled cell and solvent into the other. The cell is then immersed into a thermostated water bath and slowly rotated to provide stirring of the contents. After sufficient time has elapsed to allow equilibrium to be established across the membrane, the cell is removed from the thermostat bath and the contents of one or both sides assayed for dye concentration. Since the DNA is only present on one side of the membrane any dye bound to it is also retained on that side of the membrane. Only unbound dye is free to cross the membrane and establish equilibrium within the system. In the presence of excess neutral salt to suppress the Donnan Equilibrium[19], and assuming unit activity coefficients, the concentration of dye on the DNA-free side of the membrane is equal to the free dye concentration throughout the system. The distribution of dye in the system may be described thus:

$$\text{Side A:} \quad T_{L(A)} = C_B + C_F$$

$$\text{Side B:} \quad T_{L(B)} = C_F$$

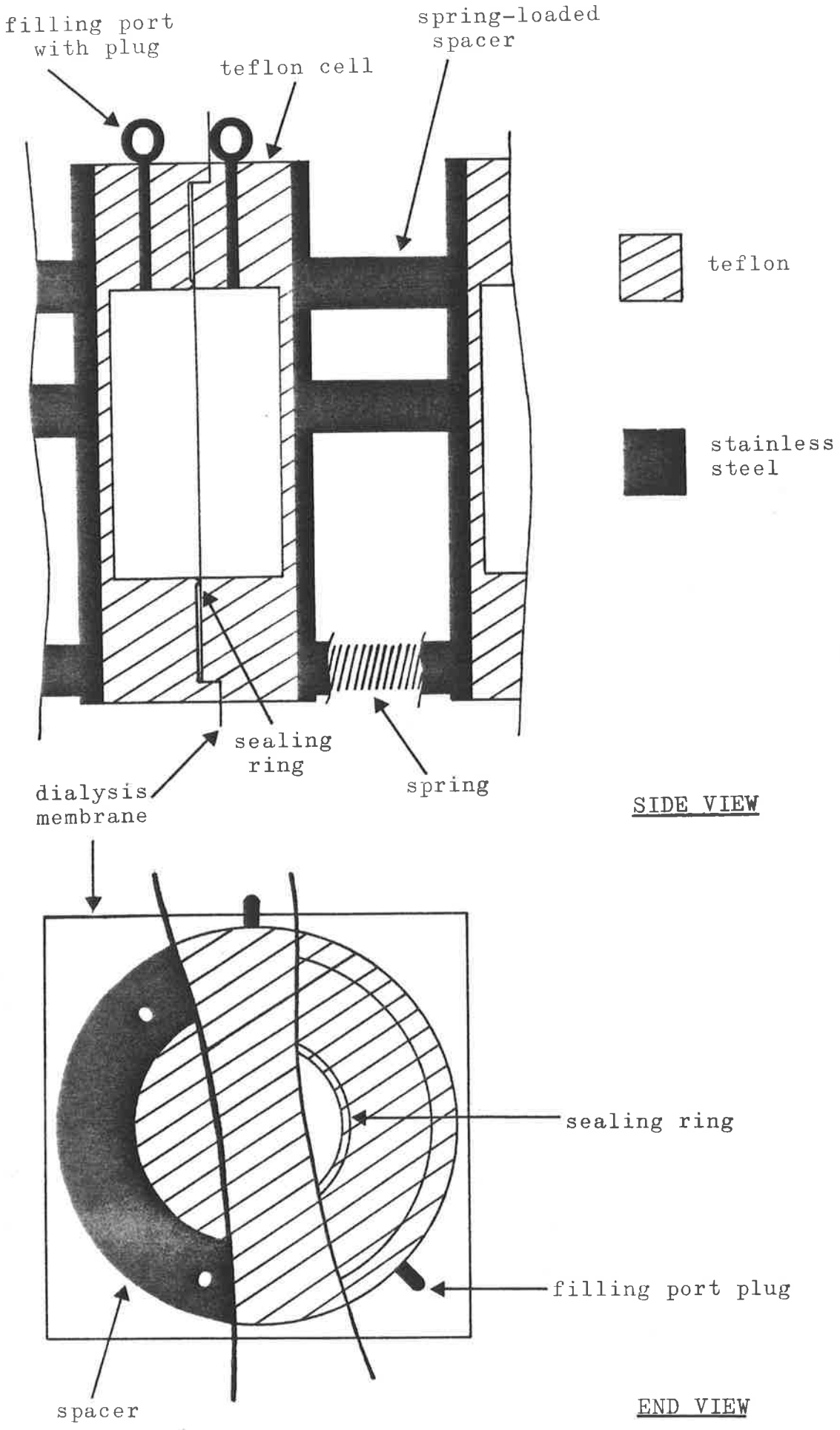

Figure 3-10. Schematic representation of the small volume Dialysis Cell.

For equal volumes on Side A and Side B and since:

$$T_L = T_{L(A)} + T_{L(B)}$$

then $$C_B = T_L - 2C_F$$

If T_L is known and C_F is determined on Side B at equilibrium, then C_B may be calculated. In cases where $T_{L(A)}$ can be determined, the value of C_B obtained as above may be checked.

The dialysis cells shown in Fig. 3.10 have the advantage of small volume to large membrane surface area when compared to the traditional equilibrium dialysis technique using a cylindrical dialysis membrane sack immersed in a container of solvent. These cells result in smaller volumes required, faster equilibration time and more effective stirring of the cell contents. Figure 3.11(a) shows the approach to equilibrium of a solution of 9-aminoacridine in 0.10 M NaCl. The approach to equilibrium in a closed equilibrium dialysis system may be adequately described as a first order rate process. As such the following equation may be used to obtain a value for the rate constant, k, and hence a value for the half-life of the system.

$$\ln(C_x/0.5C_T) = -kt \qquad \text{--- 3.15}$$

where C refers to the concentration of the membrane permeable species. In a typical experiment a known concentration of aminoacridine is loaded on one side of the cell and solvent on the other. The appropriate value of C_x, depending on whether the half cell being assayed at time t initially contained solvent only or the aminoacridine, is given by $0.5C_T - C_t$ or $C_t - 0.5C_T$ respectively. Figure 3.11(b) shows the rate plot which yields a k value of 0.0124 min^{-1}. Hence the half-life for the system used in this work is 56 minutes at 22°C. If 10 half-lives are allowed then 99.9% equilibrium is attained.

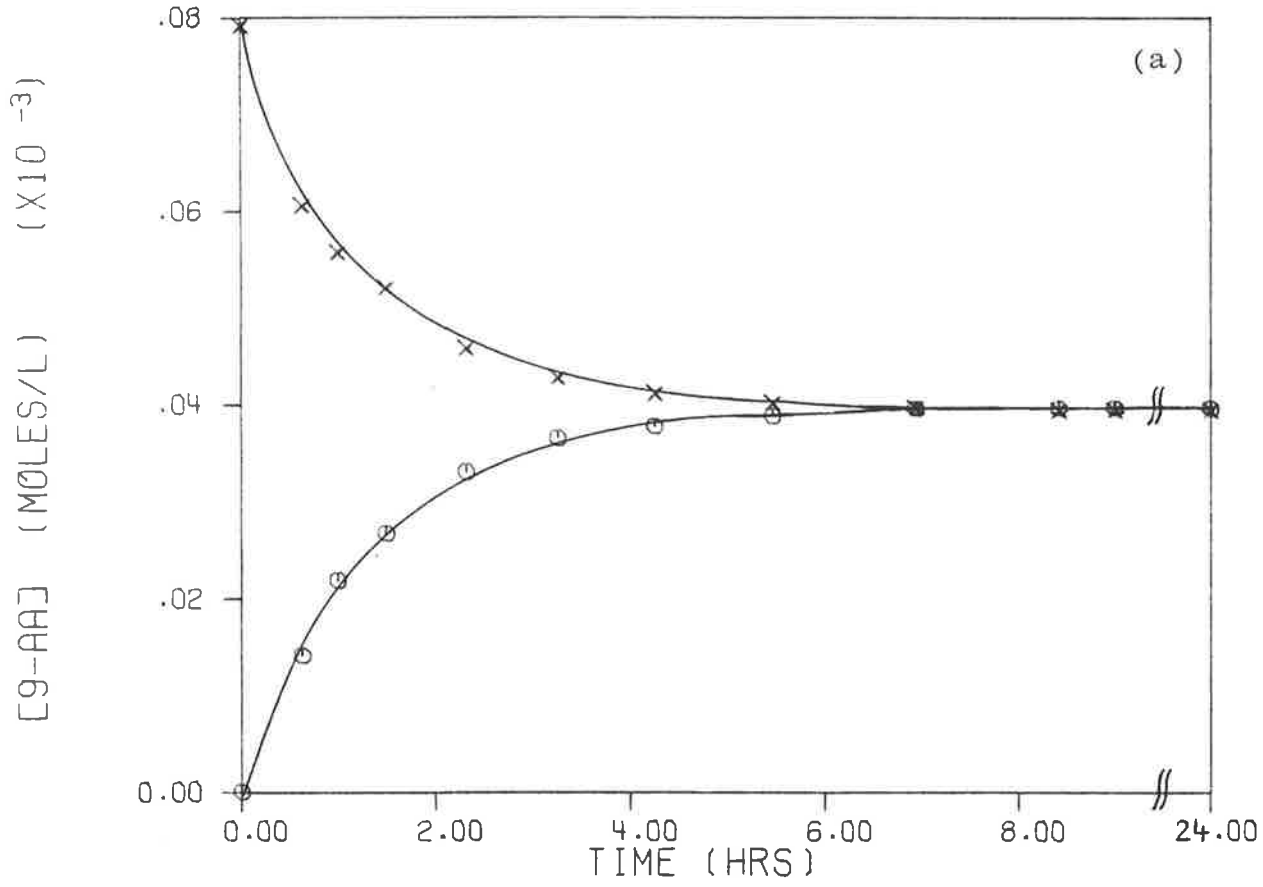

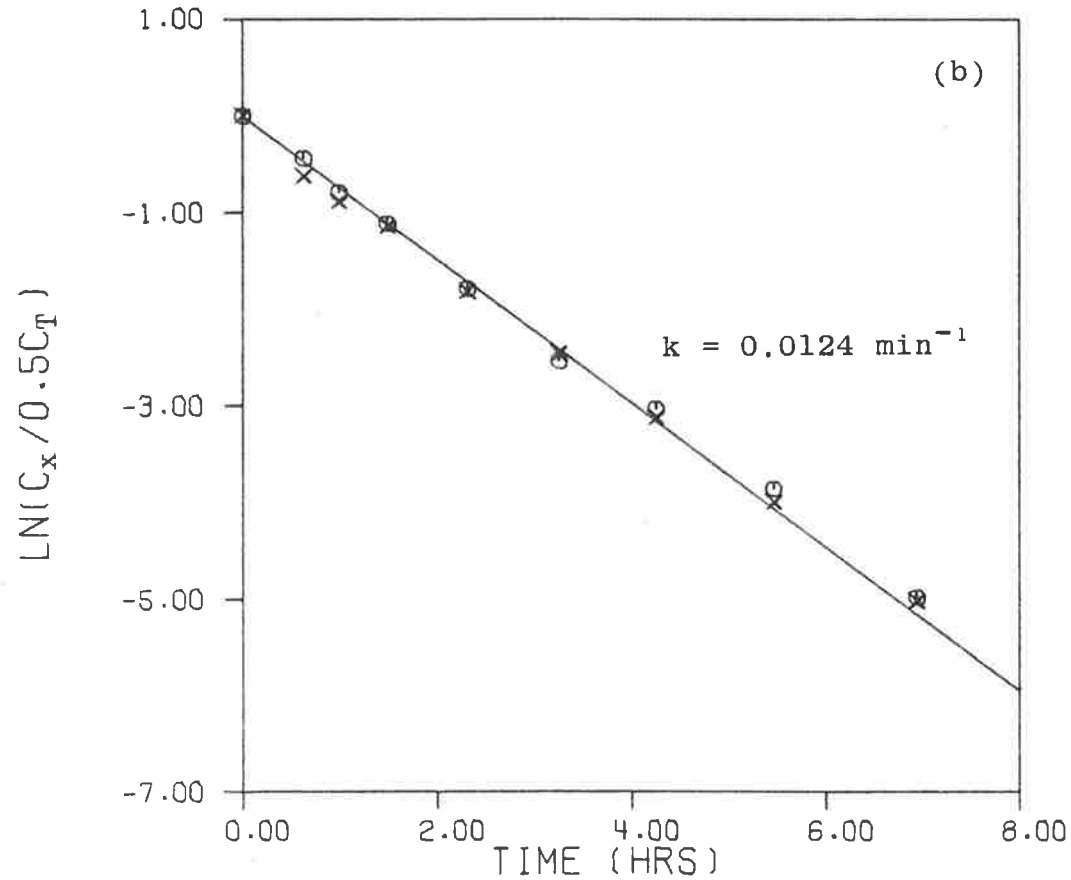

Figure 3-11. The approach to equilibrium of 9AA in 0.10 M NaCl dialysed against 0.10 M NaCl in the small volume dialysis cells.
(a) Plot of [9AA] versus time.
(b) Rate plot according to Eqn. 3.15 of data from (a).

This was the minimum equilibration time allowed in all experiments described in this work. In order to determine the sources of error and any corrections that may be required, the following investigations were made.

(a) Membrane selection

Most membranes used for equilibrium dialysis are of regenerated cellulose. The properties of two types of cellulose membranes were investigated. The first type was supplied by the manufacturer of the dialysis apparatus (Kontron) and the second was the range of "Visking" dialysis tubing (Union Carbide). The first type was thinner and had a larger pore size than all types tried from the second source. After initial use they were rejected because tubing of similar or larger pore size could not be obtained to exhaustively pre-dialyse the DNA solutions. The second source supplies tubing in a range of diameters from $^{8}/_{32}$ inches to $^{50}/_{32}$ inches. The pore size varies from size to size and batch to batch as judged by the amount of UV-absorbing material which leaks through the membrane when DNA is dialysed against solvent. This observation confirms the findings of Craig *et al*[20] regarding the properties of this type of dialysis tubing. It was concluded that the best compromise is to use the same membrane stock for DNA pre-dialysis as for the equilibrium dialysis itself so ensuring that at least equal permeability to DNA was achieved for both. "Visking" $^{25}/_{32}$ tubing was chosen as it provided the most convenient size for the pre-dialysis and the equilibrium dialysis experiments. The tubing was cut on one edge and to length using a perspex jig constructed for the purpose. The pieces were treated as described in Chapter VII and folded out when wet to give the square, single

thickness membrane required for the equilibrium dialysis unit.

(b) Treatment of DNA samples

Despite the use of the same dialysis membrane for pre-dialysis as for the equilibrium dialysis itself, initial results were poor. Considerable UV-absorbing material leaked through the membrane in the course of equilibrium dialysis experiments. This material accounted for up to 4% of the total UV absorbance of the DNA solutions after 72 hours dialysis of DNA solutions against solvent. If the solvent in the solvent side of the cell was changed the leakage continued, again to a maximum of 4% in the worse cases. The DNA used was extracted from *E Coli* cells by the method of Marmur[21] with an additional phenol extraction, method 1 outlined in Chapter VII. Figure 3.12 shows the UV spectrum of this material compared with the spectrum of the whole DNA solutions. Sedimentation Velocity experiments showed the material to have a M.W. of approximately 20,000. It is concluded that this material was short chain length DNA and as such capable of binding dye when equilibrated on the "solvent" side of the membrane. In view of the exhaustive pre-dialysis and the observation that the concentration of this short chain length DNA rose to a maximum value, it is probably due to an endonuclease impurity in the DNA prepared by method 1.

Various modifications to the DNA preparation were investigated to try to rid the DNA samples of this property. The method chosen as a result of this work is outlined as method 2 in Chapter VII. DNA prepared by this method and exhaustively pre-dialysed showed no detectable leakage of UV-absorbing material across the membrane after 72 hours dialysis in the cells. These preparations were used for all

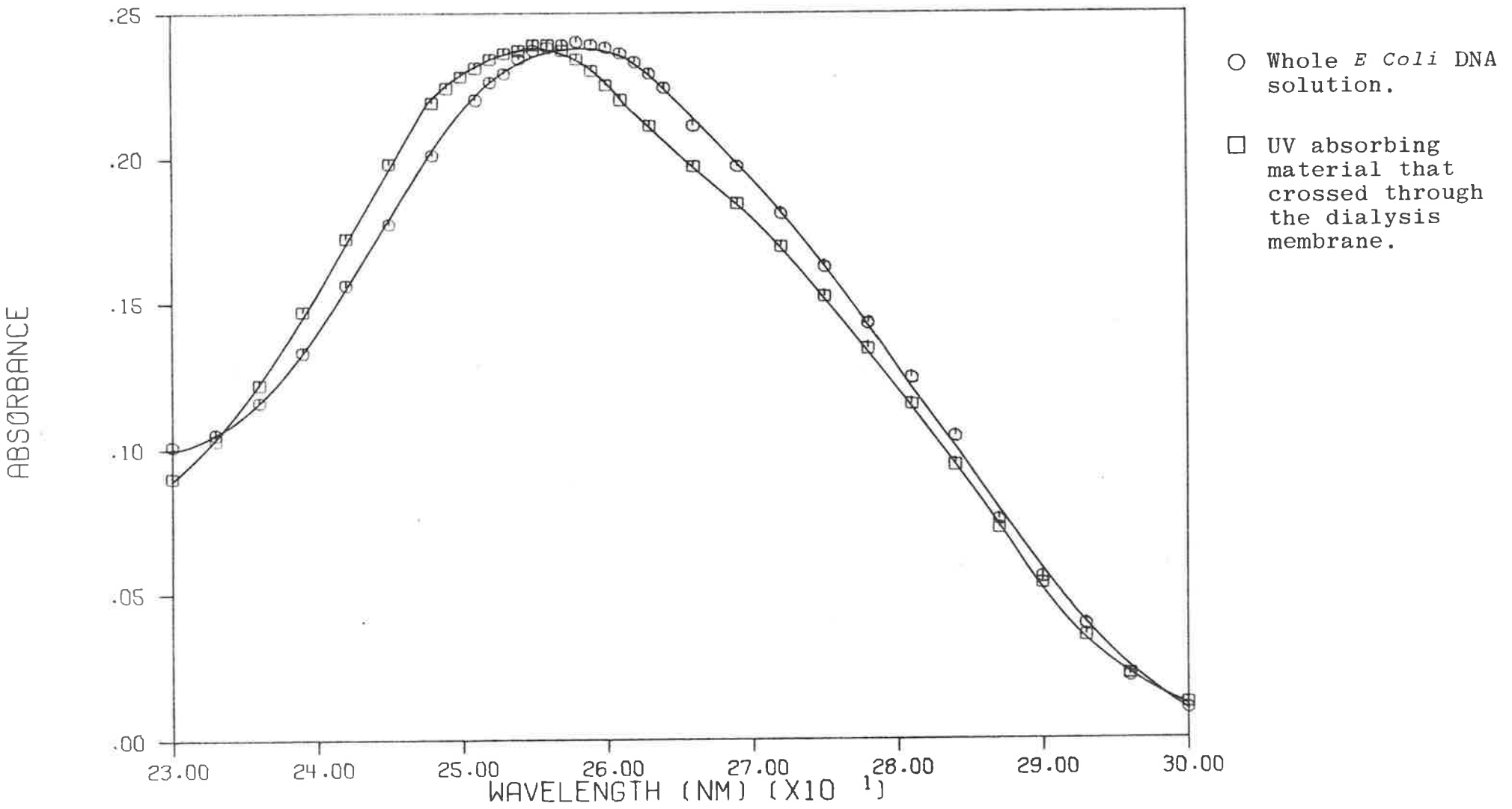

Figure 3-12. The UV absorbance spectra of whole *E Coli* DNA solution and the UV absorbing material that crossed the dialysis membrane after 24 hours dialysis, both normalized to the same peak absorbance.

subsequent dialysis experiments on dye/DNA mixtures. In addition the usual precautions to avoid mechanical shearing of the DNA were observed whenever handling DNA solutions, particularly when filling the dialysis cells.

(c) Adsorption of components

In this section I shall consider the effect of the teflon cell and membrane on each of the two principal components in turn.

(i) DNA

DNA solutions of various concentrations were dialysed against the solvent, 0.10 M NaCl, for periods of 48 hours. The DNA-containing side of the cell was then assayed for DNA concentration, using the method described in Chapter VII, and the resulting concentrations compared with the initial concentration of the DNA solution. Table 3.3 shows the results of one such experiment. It can be seen that the DNA concentration is always lower after dialysis by a constant number of moles of material. Since no UV absorbance crossed the membrane this is interpreted as a surface area related adsorption of DNA, either by the dialysis membrane or the teflon cell walls. Correction for such an adsorption is difficult because although the DNA has been removed from the bulk solution it remains in the half-cell adsorbed onto a surface. It will still be able to bind dye but probably not in the same way as the DNA in the bulk solution. The loss of DNA from solution in this way is minimized by using high initial DNA concentrations where the effect is negligible. Other than this loss of concentration, the DNA solutions were unchanged by 48 hours dialysis as assessed by their spectral properties, melting temperature and hyperchromicity.

TABLE 3.3

The concentration of DNA before and after equilibrium dialysis against solvent.

Concn. x 10^5 (M) \ Time (hrs)	24	48	72	ave Δ x 10^6 (M)
0.9981	0.8036	0.8040	0.8035	1.94
5.321	5.141	5.130	5.156	1.79
10.37	10.16	10.19	10.17	1.97
51.14	50.91	50.89	50.93	2.3
107.6_2	107.3_9	107.5_0	107.4_6	1.7

Temperature 25°C. All concentrations moles of DNA phosphorus. Absorbance of solvent side at 260 nm ≤ 0.002 in all cases.

(ii) 9-aminoacridine

9-aminoacridine solutions in 0.10 M NaCl were dialysed against solvent to determine if the dialysis cell or membrane bound any of the dye. The result of one such experiment is shown in Table 3.4. It is apparent that a small but nearly constant percentage of the 9-aminoacridine has been lost in each case. This observation is inconsistent with either binding of the 9-aminoacridine to the cellulose membrane or a surface adsorption phenomenon. Further experiments were conducted using tritiated water in the solvent of 0.10 M NaCl, and following the effective loss of solvent by determining the concentration of tritiated water in 1 ml aliquots of the

TABLE 3.4

The concentration of 9-aminoacridine HCl before and after equilibrium dialysis.

(1) initial Concn. x 10^5 (M)	(2) 24 hr Concn. x 10^5 (M)	(2) 48 hr Concn. x 10^5 (M)	average % decrease
0.527_3	0.507_5	0.505_2	3.9_7
0.987_9	0.957_8	0.955_3	3.1_7
2.465_2	2.378_9	2.377_7	3.5_3
5.135_2	4.976_5	4.969_8	3.1_6
7.457_2	7.220_1	7.209_6	3.2_4
10.278	9.928_5	9.946_0	3.3_2
19.876	19.317	19.298	2.8_6
mean % decrease			$3.3_2 \pm 0.3_5$

(1) The initial 9-aminoacridine HCl solution was loaded on both sides of the cell.

(2) Average of assay of both sides of the cell.

solvent before and after dialysis. The details of these experiments are described in Chapter VII. Table 3.5 shows the result of these experiments which show a similar percentage loss of tritiated water after dialysis. This loss is in fact a dilution of membrane permeable molecules by the solvent contained in the wet membrane. The dilution of approximately 3% when 6 ml total volume is used in the cells is consistent with the amount of solvent contained in the 7 cm^2 area of membrane in contact with the solution. This dilution applies only to membrane permeable components of the system. The membranes must be prepared and installed in the cells while wet in order to ensure membrane integrity. With careful handling and draining of each membrane before use, the dilution can be held constant to within 0.2%. When this dilution correction is applied there was no detectable loss of 9-aminoacridine when concentrations in the range 0 to 2×10^{-4} M were tested.

(d) Analysis of errors

The sources of error discussed above, together with uncertainty in determining DNA concentrations and volumes of solution used will produce errors in the range 1% to 2%. Any additional errors will result from the method of analysis of dye distribution at equilibrium. Peacocke and Skerrett[8] have proposed an analysis of relative errors in the fraction bound, r, with the variables C_T, C_F, T_A and the volumes used. They point out that, in general, the maximum accuracy in r results from the largest change in redistribution across the membrane due to dye binding to the DNA. Errors in C_T, T_A and volumes used are minimal since these quantities may be determined and checked independently of the dialysis

TABLE 3.5

The activity of tritiated water before and after dialysis.

Before dialysis (1)	Standard Deviation		After dialysis (1)	% decrease
	obs. (1)	calc.(1)(2)		
10559	34	32	10204	3.3_6
10732	31	33	10338	3.6_7
25157	87	50	24304	3.3_9
25200	92	50	24298	3.5_8
47077	139	69	45401	3.5_4
47787	127	69	46311	3.0_9
Average obs. S.D. as % of count = 0.31%			Average % decrease = 3.4_4	

(1) Average counts per minute for 1.000 ml of water. Obtained from the average result of at least ten 10 minute counting periods.

(2) Calculated as $\sqrt{N}$ where N is the average count for the ten minute counting period. Note that $\sqrt{N}$ is actually the standard error of the count but approximates the standard deviation.

apparatus. The only quantity obtained from the dialysis experiment is C_F. Within the constraint of maintaining a homogeneous dye/DNA solution, the best conditions to use will be a compromise between maintaining a large ratio of bound dye to total dye and the precision with which free dye may be determined. The assay technique employed is absorptivity hence the sensitivity of assay depends on the molar absorptivity of the dye. In the case of 9-aminoacridine a minimum concentration of 5×10^{-6} M is required if errors are to be maintained at 2% or less in the concentration of 9-aminoacridine. Overall uncertainty for the 9-aminoacridine/DNA system will be in the range 2% to 5% being highest at low r values.

(4) Sedimentation velocity

The technique of sedimentation velocity applied to aminoacridine/DNA systems to determine quantitative information about the binding was first reported by Lloyd *et al*[22]. These workers used a photographic technique to determine the absorbance of Proflavine/DNA mixtures spun in an analytical ultracentrifuge. In this method, which they called "Sedimentation Dialysis", the boundary of the sedimenting DNA replaces the semi-permeable membrane in a dialysis experiment. The dye molecules are so small that they do not sediment in the centrifugal field used in these experiments. Since the concentration of DNA is constant in the plateau region below the sedimentation boundary, after applying a correction for the radial dilution effect, and it carries the bound dye with it in the region below the boundary represents bound plus free dye and the region above the boundary yields the free dye concentration. In this manner

binding curves may be determined in the same way as for equilibrium dialysis except that an optical assay technique must be used. However this method does have an advantage over equilibrium dialysis in that the sedimentation coefficient of the dye/DNA complex may be obtained at the same time. This can yield information about the hydrodynamic properties of the complex.

In this work a Beckman model E analytical ultracentrifuge equipped with a scanner and multiplexor was used. In the trial system of 9-aminoacridine/DNA the centrifuge cells used had double-sectored carbon-filled epoxy centre-pieces and sapphire windows. No adsorption of 9-aminoacridine or DNA to the cell components was observed. The light source, a high pressure mercury/xenon lamp, was replaced with a high pressure xenon lamp since the intense spectral lines in the mercury lamp caused skewed bandwidth envelopes when used with the Beckman DU monochromator fitted to the centrifuge. This effect made observed absorbances in the centrifuge difficult to compare with absorbances measured using the centrifuge cells in a Zeiss PMQ II spectrophotometer. Measurements were made at speeds between 30,000 r.p.m. and 45,000 r.p.m. using 3 cells and a counter-balance piece in a 4 hole titanium rotor. The 3 cells were scanned sequentially until the sedimenting boundary was $^2/_3$ of the way down the cell at which stage it was too broad to obtain useful results. Wavelengths of 400 nm (the peak absorbance of 9-aminoacridine at the bandwidths used) and 427 nm (the isosbestic point for 9-aminoacridine/DNA mixtures) were used to follow the 9-aminoacridine in the cells.

The accuracy of this method of determining binding data depends on the precision with which absorbances can be

measured in the centrifuge. Lloyd *et al*[22] observed errors of up to 10% using their photographic method. The results we obtained using the scanner were disappointing. The measured absorbances of 9-aminoacridine solutions alone were poor when compared to measurements taken on the PMQ-II spectrophotometer. The scanner system displayed a speed dependence, low signal to noise ratio at low total absorbances and was irreproducible on successive runs with the same cells, by as much as 20% in some instances. The use of the isosbestic point at 427 nm was abandoned since the band width required to obtain acceptable signal to noise ratios was too large to yield meaningful data. This isosbestic point is difficult to work with because of the very large change in the slope of the absorbance around this wavelength between the free 9-aminoacridine and the bound 9-aminoacridine. Use of 400 nm was better although no estimate of the 9-aminoacridine in the DNA containing region of the cell is possible at this wavelength. The use of this technique to obtain accurate binding data was abandoned in view of the imprecision in determining absorbances using the scanner system.

The effect of these absorbance inaccuracies on the determination of sedimentation coefficients is difficult to estimate. Any error would be due to error in determining the mid-point of the sedimenting boundary which is in turn related to the sharpness of and speed with which the boundary moves. The results we obtained for the effect of 9-aminoacridine on the sedimentation coefficient of native *E Coli* DNA were qualitatively similar to those reported by Sansom[23].

In view of these difficulties it was concluded that good quantitative binding data cannot be obtained using the

standard scanner/multiplexor system provided for the Beckman model E analytical ultracentrifuge. Despite the potential advantages of this method, until more accurate and reproducible methods of determining absorbances of solutions within the ultracentrifuge cells are available, it is restricted to the determination of sedimentation coefficients for dye/DNA systems.

REFERENCES

1. Löber G., *Z. für Chemie*, 9, 252 (1969).
2. Blake A. and Peacocke A.R., *Biopolymers*, 6, 1225 (1968).
3. Cohen D.M. and Fischer E., *J. Chem. Soc.*, 3044 (1968).
4. Morrey J.R., *J. Phys. Chem.*, 66, 2169 (1962).
5. Morrey J.R., *J. Phys. Chem.*, 67, 1569 (1963).
6. Brynstad J. and Smith G.P., *J. Phys. Chem.*, 72, 296 (1968).
7. Zanker V. and Schiefele G., *Berichte Bungs. Physik. Chem.*, 62, 86 (1958).
8. Peacocke A.R. and Skerrett J.H.N., *Trans. Farad. Soc.*, 52, 261 (1956).
9. Kelly G.R. and Kurucsev T., *Eur. Polymer J.*, 11, 581 (1975).
10. Armstrong R.W., Kurucsev T. and Strauss U.P., *J.A.C.S.*, 92, 3174 (1970).
11. Li H.J. and Crothers D.M., *Biopolymers*, 8, 217 (1969).
12. Turner D.R., Ph.D. Thesis, University of Adelaide (1975).
13. Gatti C., Houssier C. and Fredericq E., *Biochim. Biophys. Acta*, 407, 308 (1975).
14. Halfman C.J. and Nishida T., *Biochemistry*, 11, 3493 (1972).
15. Li H.J. and Crothers D.M., *J. Mol. Biol.*, 39, 461 (1969).
16. Ramstein J., Leng M. and Kallenbach N.R., *Biophys. Chem.*, 5, 319 (1976).
17. Benesi H.A. and Hildebrand J.H., *J.A.C.S.*, 71, 2703 (1949).
18. Burke R.W., Deardorff E.R. and Menis O., *J. Research Natl. Bureau Stand. A. Physics and Chemistry*, 76A, 469 (1972).
19. See, for example: Tanford C., "Physical Chemistry of Macromolecules", J. Wiley and Sons Inc. (1961).
20. Craig L.C., King T.P. and Stracher A., *J.A.C.S.*, 79, 3729 (1957).
21. Marmur J., *J. Mol. Biol.*, 3, 208 (1961).

22. Lloyd P.H., Prutton R.N., and Peacocke A.R., *Biochem. J.*, 107, 353 (1968).

23. Sansom L.N., Ph.D. Thesis, University of Adelaide (1972).

24. Kurucsev T., Personal Communication.

CHAPTER IV

Spectral properties of 9-aminoacridines and their DNA complexes and the calculation of binding curves.

CONTENTS

1. Introduction

The first step in the application of the spectrophotometric method to the determination of binding curves for dye/DNA systems is to define the spectral properties of the dyes and their complexes with DNA. Provided the system displays the internal linearity discussed in the previous Chapter, it may be further treated to determine the fraction of dye bound, α, and hence the binding curves. In this Chapter the spectral properties of 9-aminoacridine and six 9-alkylaminoacridines and their DNA complexes are examined. The various methods of calculating binding curves from spectrally suitable dye/DNA systems are applied and the resultant binding curves presented. The errors in these curves are discussed with a view to examining possible models to describe the system.

2. 9-aminoacridines

A series of 9-substituted 9-aminoacridines have been prepared and purified as described in Chapter VII. The names, structures and abbreviations used in this text, together with the pKa values for the protonation of the acridine ring nitrogen are presented in Fig. 4.1. The pKa values are such that in the pH range used in this study, 5.8 - 6.5, all will exist in solution as the mono-protonated cations. The solvent used to study the interaction with DNA was 0.10 M NaCl. This solvent was chosen because it has a sufficiently high ionic strength to suppress the purely electrostatic binding of the ligand to DNA[1]. It can also be used as a solvent for equilibrium dialysis where a solvent of lower ionic strength may produce complications[2] due to the Donnan Equilibrium. All the 9-aminoacridines prepared and 9-aminoacridine itself,

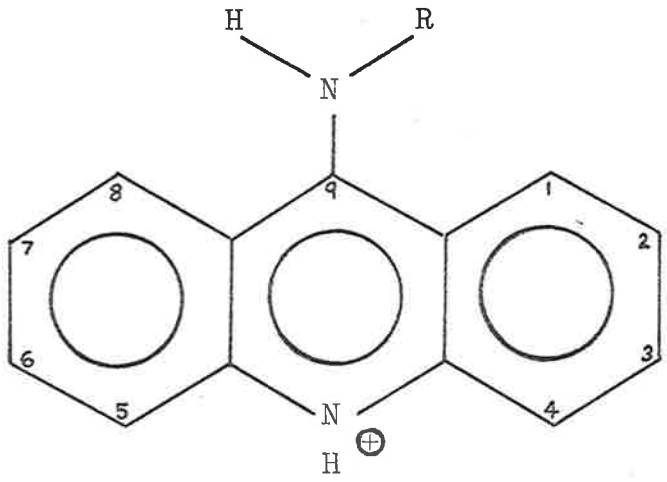

R Group	NAME	ABBREVIATION	pKa
Proton	9-aminoacridine HCl	9AA	9.99[b]
Methyl	9(methyl)aminoacridine HCl	9(Me)AA	10.31[b]
Butyl	9(butyl)aminoacridine HCl	9(Bu)AA	9.89[b]
Hexyl	9(n-hexyl)aminoacridine HCl	9(n-Hex)AA	>9.2[c]
cyclo-Hexyl	9(cyclo-hexyl)aminoacridine HCl	9(cyc-Hex)AA	9.32[b]
Octyl	9(n-octyl)aminoacridine HCl	9(n-Oct)AA	>9.2[c]
tert-Octyl	9(tert-octyl)aminoacridine HCl	9(t-Oct)AA	>9.2[c]

(a) These pKa values refer to the acridine ring nitrogen atom.

(b) Taken from Albert A. and Goldacre R., *J.C.S.*, 706 (1946).

(c) Determined in this work. See Chapter VII.

FIGURE 4.1 The structure and pKa values of several 9-aminoacridines.

were sufficiently soluble in this solvent to be studied with the exception of 9(t-oct)AA. This material proved to be very insoluble in aqueous solvents hence it could not be studied. The solutions of all these compounds in 0.10 M NaCl were stable towards light and heat. There was however, a very slow loss of material from solution. Very old solutions often contained an insoluble precipitate. To guard against this slow loss, the absorbance of solutions was monitored periodically and solutions were discarded if any change in absorbance occurred. A loss was usually detected after 2 - 3 months standing at room temperature.

All the 9-alkylaminoacridines had spectra similar to 9-aminoacridine, although the ^1L_a band was red-shifted and the ^1L_b band blue-shifted (see Chapter III, Fig. 3.1). A summary of the spectral properties of the five compounds studied in detail is contained in Appendix II. Deviation from Beer's Law ideality was detectable for all compounds. The $\varepsilon_{\lambda max}$ values quoted in Appendix II are the average of several dilutions in the range 5×10^{-6} M to 1×10^{-5} M. Values of absorbance at several concentrations in the range 5×10^{-6} M to $1\text{-}2 \times 10^{-4}$ M were recorded for each compound and fitted to quadratic or cubic polynomials with absorbance as a function of concentration. These polynomials were used to calculate true concentrations at any measured absorbance within that range.

Each of the compounds showed a dependence of $\varepsilon_{\lambda max}$ with solvent composition and temperature. The spectra were sharper at lower temperatures and at lower ionic strengths of the solvent. This leads to correspondingly higher molar absorptivities at the wavelengths of the peaks. Furthermore the deviations from Beer's Law, resulting from the formation of aggregates in solution, were lower at higher temperatures

which would oppose the observed decrease in absorbance with increasing temperature. In view of these observations, the temperature effect is interpreted as a solvent effect on these compounds in solution. It is therefore necessary to determine molar absorptivities and absorbance versus concentration curves for each solvent/temperature combination used if the maximum available precision is required.

3. 9-aminoacridines/DNA mixtures

Spectra of 20 to 30 mixtures of ligand/DNA, having T_L/T_A values within the range 10 to 0.02 with a constant T_L, were recorded from 470 nm to 330 nm at 1 nm intervals at each of 4 different temperatures. This procedure was applied for each of the five 9-aminoacridines studied. The preparation of these solutions and the recording and processing of the spectral data are described in Chapter VII. The apparent absorbance of the *E Coli* DNA used was recorded at several DNA concentrations, in the range 2×10^{-4} M to 1×10^{-3} M DNA phosphate, over the same wavelength range and the resultant molar absorptivities averaged to provide a background DNA spectrum. These absorptivities, together with the known DNA concentration of each ligand/DNA mixture, were used to correct the absorbance of each mixture for DNA background absorbance at each wavelength. An indication of the accuracy of this correction was obtained from the wavelength range in which the ligand does not absorb. This range usually encompassed 10 data points between 460 nm and 470 nm. Since the absorbances at these wavelengths should be zero in all mixtures, the actual absorbances calculated when the DNA correction was applied provided a guide to the accuracy of the correction. Figure 4.2 shows the higher wavelength isosbestic point for

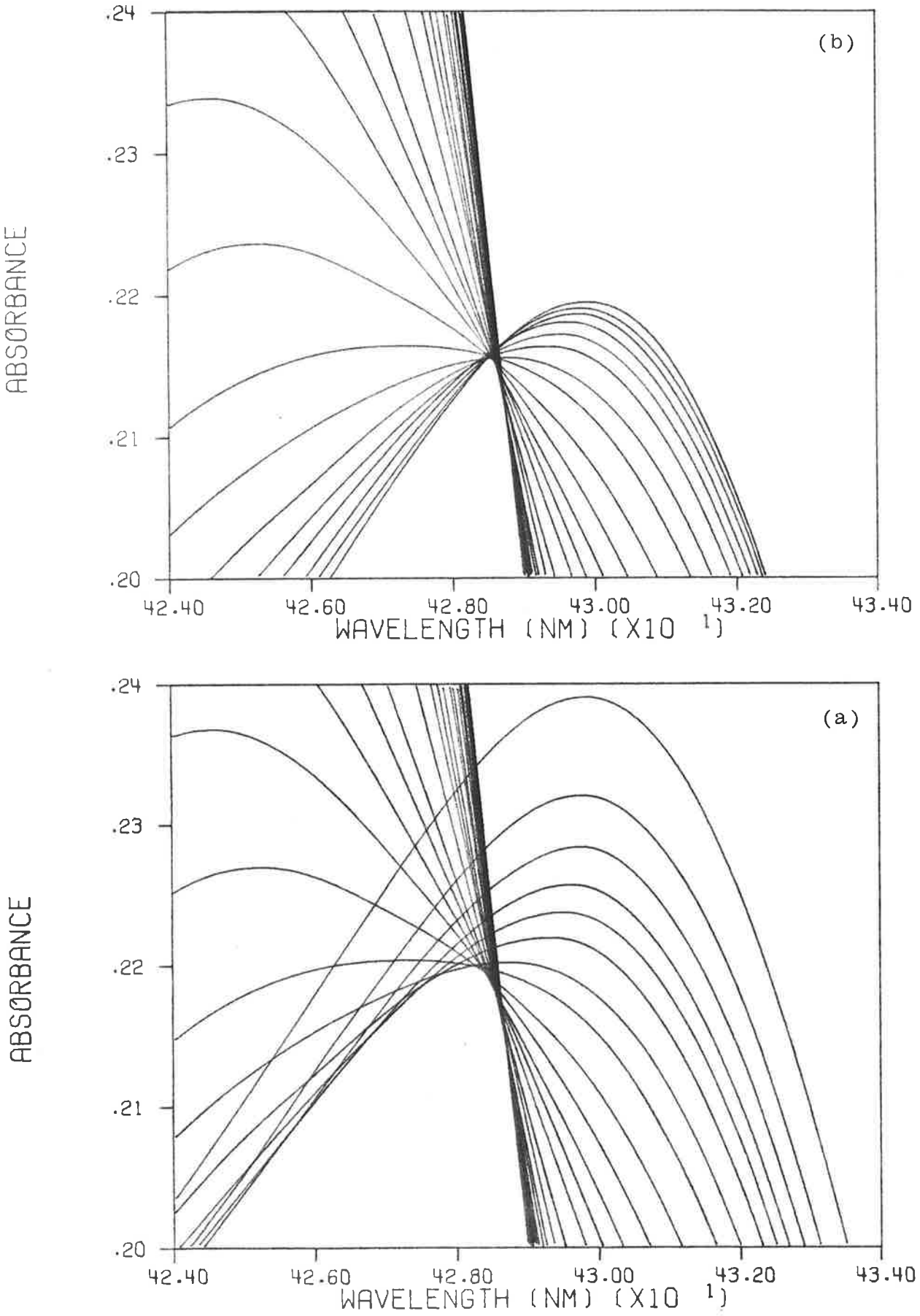

Figure 4-2. The higher wavelength isosbestic point for the 9AA/*E Coli* DNA/0.10 M NaCl system at 22°C.

(a) before DNA background absorbance correction.

(b) after DNA background absorbance correction.

the 9AA/*E Coli* DNA/0.10 M NaCl system at 22°C, both before and after the DNA background correction. Figure 4.3 shows the isosbestic point for the 9(Me)AA/*E Coli* DNA/0.10 M NaCl system at 35°C. The DNA sample used in the former case had a much higher background absorbance than the sample used with the 9(Me)AA. These two cases represent the extremes of the DNA background absorbance encountered during this work. In both cases the correction applied appears to be satisfactory.

(a) Internal linearity

The conditions for and significance of internal linearity has been fully discussed in Chapter III (2)(a). Each set of spectra was tested for internal linearity in the following manner. The condition which must be met is:

$$A_j^\lambda = (1-\beta_j)A_k^\lambda + \beta_j A_\ell^\lambda \qquad \text{--- 4.1}$$

where A_j, A_k and A_ℓ are the absorbances of any 3 members of a set at some wavelength λ, and β_j is a number independent of λ. Furthermore this relationship must hold for any randomly chosen j, k and ℓ from the set such that $j \neq k \neq \ell$. The number, β_j, is computed from:

$$\beta_j = \frac{A_k^\lambda - A_j^\lambda}{A_k^\lambda - A_\ell^\lambda} \qquad \text{--- 4.2}$$

at several wavelengths and averaged to give $\bar{\beta}_j$. This mean value, $\bar{\beta}_j$, is then used to compute an error function, δ, as follows:

$$\delta^\lambda = A_j^\lambda - [(1-\bar{\beta}_j)A_k^\lambda + \bar{\beta}_j A_\ell^\lambda] \qquad \text{--- 4.3}$$

This function, which has the units of absorbance, is computed at each wavelength and may be plotted to show the deviation from internal linearity with wavelength. If a set of spectra displays internal linearity, the error function should be zero

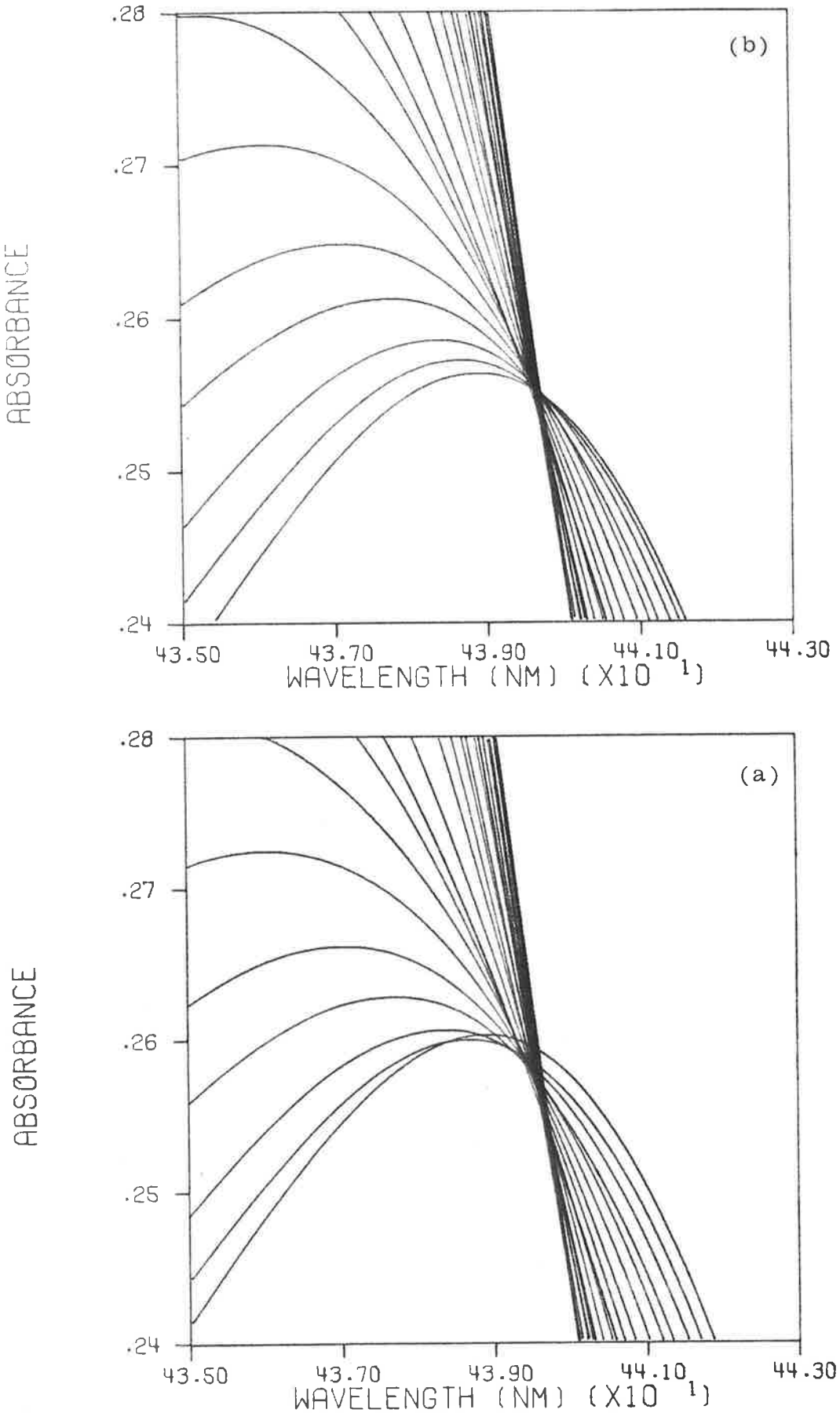

Figure 4-3. The higher wavelength isosbestic point for the 9(Me)AA/*E Coli* DNA/0.10 M NaCl system at 35°C.

(a) before DNA background absorbance correction.

(b) after DNA background absorbance correction.

within the precision of measurement of the absorbance at all wavelengths tested.

All possible combinations of 3 members of a set of 20 to 30 members could not be computed, so a reasonable selection of linear combinations were made. Generally about 200 combinations were made, arranged about 6 spectra from the middle of the set. These spectra were taken in all possible combinations with 6 spectra from both ends of the set. This procedure includes spectra of very high and very low T_L/T_A, although these regions are least accurate for the reasons discussed in Chapter III. The separately determined monomer spectrum of the ligand was included in each set. The "absorbances" for this spectrum were obtained as the product of the molar absorptivity of the monomer and the average ligand concentration of the set. A FORTRAN EXTENDED computer program, PROGRAM INTLIN, was written to make the calculations. For each combination made the program first calculates the individual β_j values in order to calculate the mean value, $\bar{\beta}_j$. A β_j value is calculated for each wavelength for which $|A_k^\lambda - A_j^\lambda| \geq 0.04$ and $|A_k^\lambda - A_\ell^\lambda| \geq 0.04$. The reason for this condition can be seen by considering Eqn. 4.2. As ΔA becomes small the random errors due to errors of measurement become relatively large and so can produce grossly erroneous β_j values which weigh heavily in the mean $\bar{\beta}_j$ value (if more than half the β_j values calculated are rejected, then the entire combination is rejected). The program calculates $\bar{\beta}_j$ and uses this value to recompute the linear combination at all wavelengths, and hence the error function, δ. This process is repeated until all possible combinations of the three sub-sets of spectra are exhausted. The resultant δ^λ values are then averaged. These $\bar{\delta}^\lambda$ are plotted against λ to confirm:

(1) Deviations from internal linearity are within the precision of measurement.

(2) No systematic deviations exist.

If these conditions are met, the set of spectra are internally linear throughout the T_L/T_A range used. Where these conditions are not met, the process can be repeated to determine if a region of internal linearity exists within the set.

For every combination of ligand and temperature used, the sets of spectra so generated were internally linear with the exception of 9(n-hex)AA and 9(n-oct)AA. In the case of 9(n-hex)AA the spectra were approximately internally linear at 50°C with increasing deviation by the members of low T_L/T_A as the temperature decreased. 9(n-oct)AA showed considerable deviation at all four temperatures, with greater deviation at lower temperature. The set of spectra for 9(Me)AA with *E Coli* DNA in 0.10 M NaCl at 10°C is shown in Fig. 4.4 together with the plot of $|\bar{\delta}^{\lambda}|$ against λ. This set is representative of the internally linear sets. Figure 4.5 shows similar plots for the 9(n-hex)AA/*E Coli* DNA/0.10 M NaCl system at 10°C, representing a system which shows some departure from internal linearity. A complete summary of the spectra for all the ligands and temperatures used is given in Appendix II.

All the internally linear sets showed isosbestic points at around 430 nm and between 360 nm and 320 nm. The higher wavelength points for the 9(Me)AA/*E Coli* DNA/0.10 M NaCl system at 10°C, 22°C, 35°C and 50°C are shown in Fig. 4.6 and 4.7. Although these isosbestic points arise as a consequence of internal linearity in these cases, they do not in themselves show that this linearity exists, nor do they

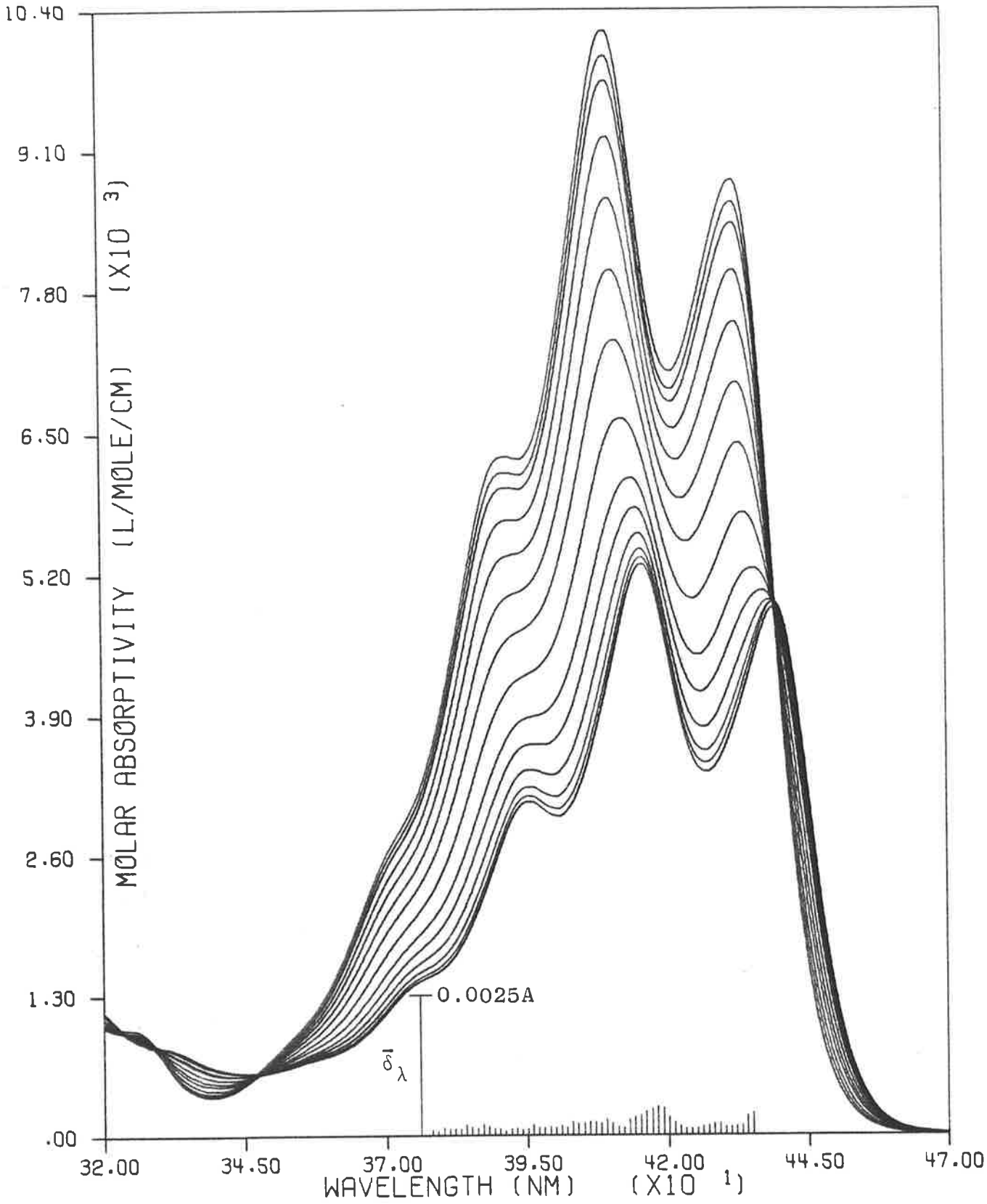

Figure 4-4. Spectra of the 9(Me)AA/*E Coli* DNA/0.10 M NaCl system at 10°C and the associated plot of $\bar{\delta}_\lambda$ versus λ. The spectrum of highest ε^{410} is the 9(Me)AA monomer spectrum and that of lowest ε^{410} is the generated *E Coli* bound spectrum of 9(Me)AA. Note that every alternate spectrum of the set has been omitted from the plot for the sake of clarity.

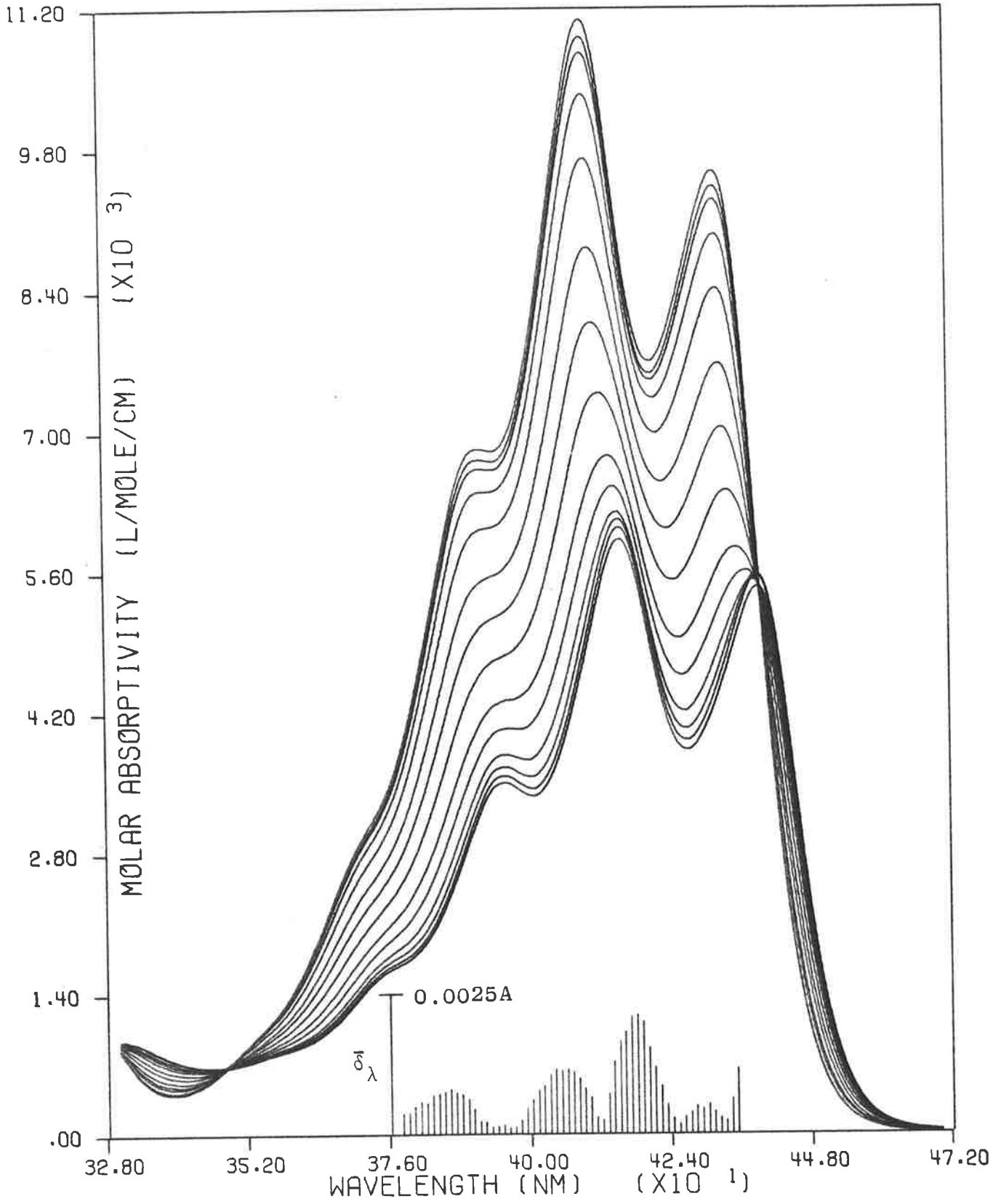

Figure 4-5. Spectra of the 9(n-Hex)AA/*E Coli* DNA/0.10 M NaCl at 10°C and the associated plot of $\bar{\delta}_\lambda$ versus λ. The spectrum of highest ε^{410} is the 9(n-Hex)AA monomer spectrum and that of lowest ε^{410} is the generated *E Coli* bound spectrum of 9(n-Hex)AA. Note that every alternate spectrum of the set has been omitted from the plot for the sake of clarity.

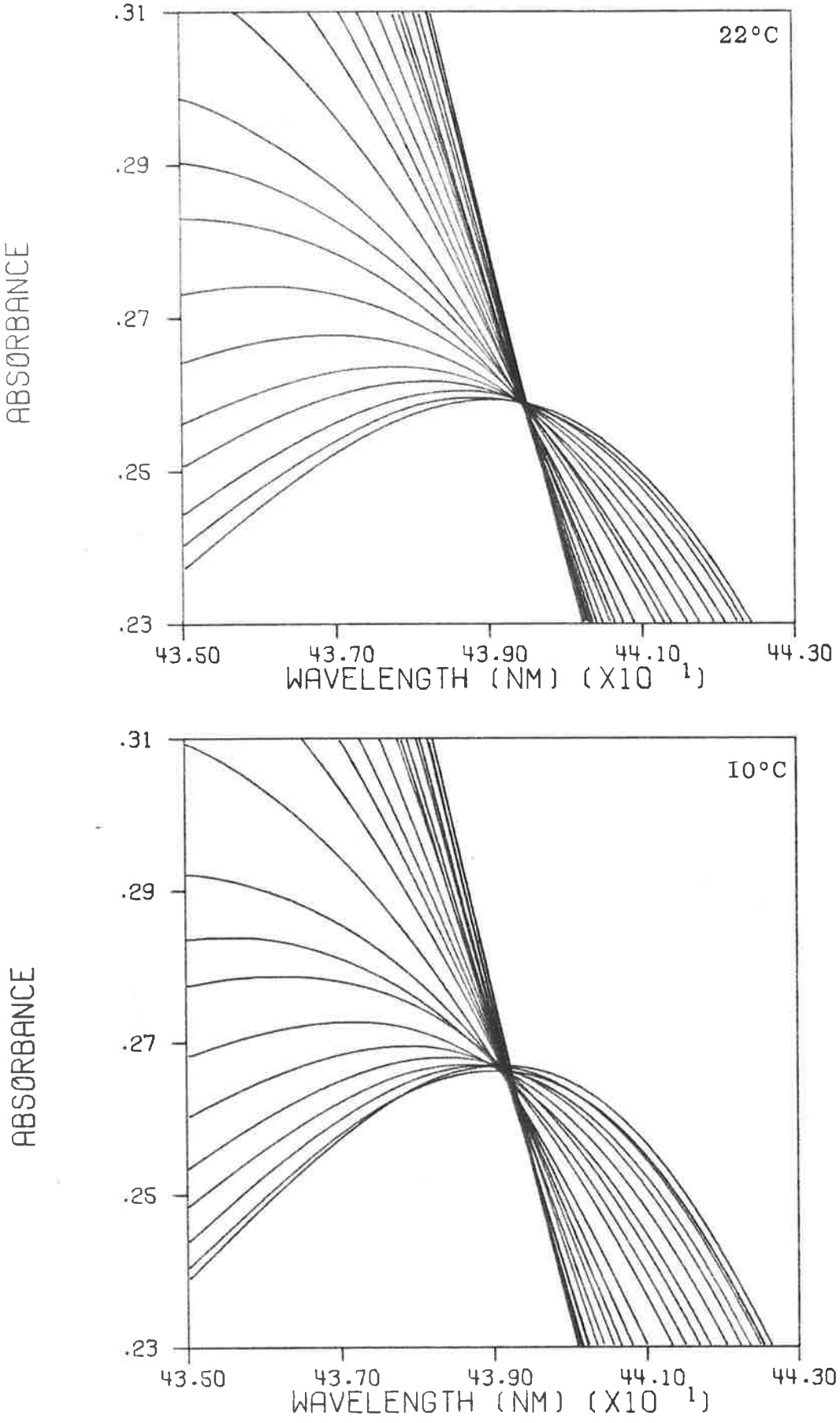

Figure 4-6. The higher wavelength isosbestic points for the 9(Me)AA/*E Coli* DNA/0.10 M NaCl system at 10°C and 22°C, corrected for DNA background absorbance.

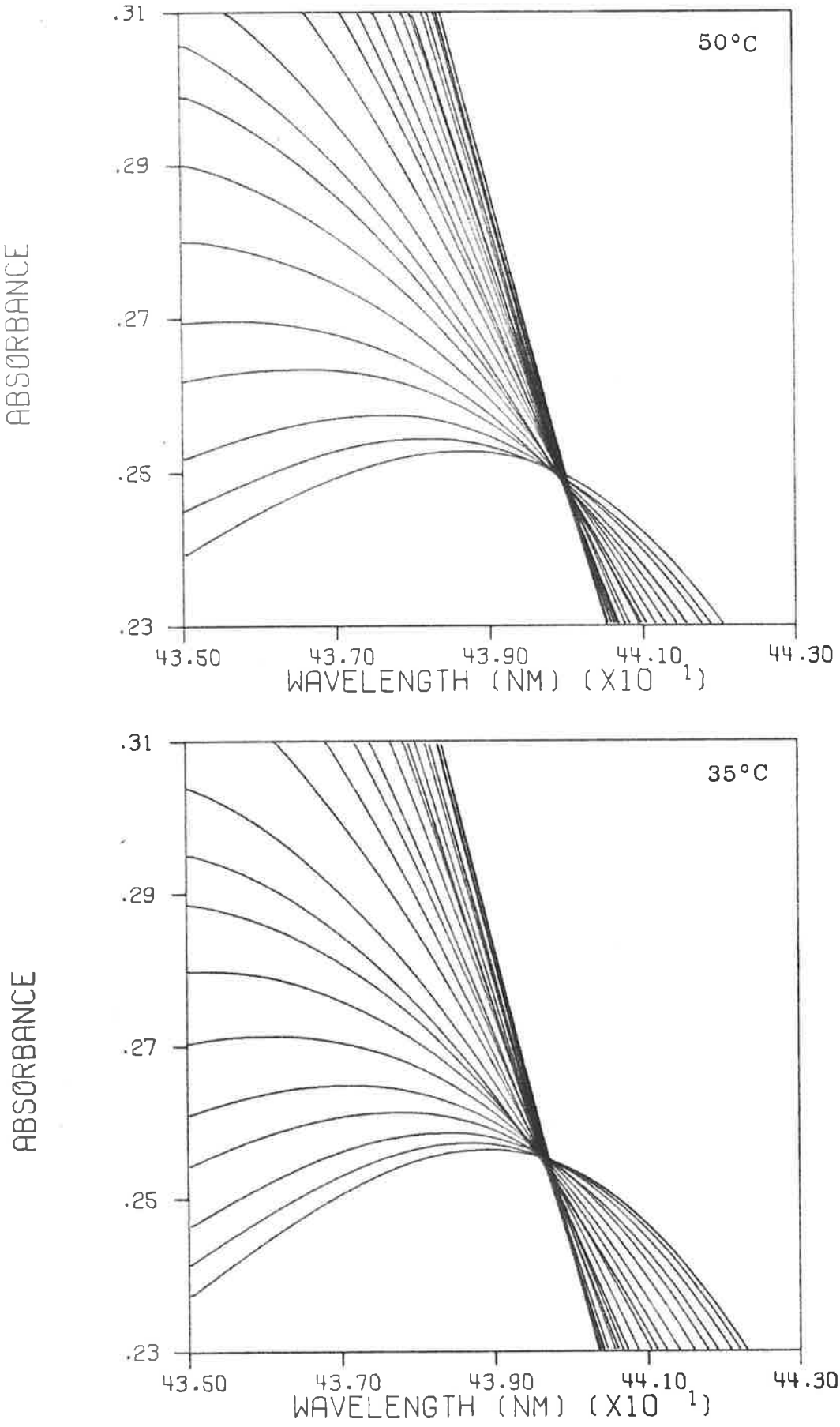

Figure 4-7. The higher wavelength isosbestic points for the 9(Me)AA/*E Coli* DNA/0.10 M NaCl system at 35°C and 50°C, corrected for DNA background absorbance.

provide the quantitative information of the degree of any deviation from such linearity that the error function, δ, can provide.

(b) Determination of bound ligand spectrum

The bound ligand spectrum could not be determined directly for any of the combinations of ligand and temperature studied in this work. A complete discussion of methods to determine this spectrum indirectly is contained in Chapter III. The method of choice, extrapolation of plots of $\varepsilon^{\lambda}_{OBS}/\varepsilon^{\lambda}_{M}$ versus T_L/T_A to an ordinate intercept, yields values of the bound species molar absorptivity, $\varepsilon^{\lambda}_{B}$, at the wavelength λ. If internal linearity exists then this value may be used together with the monomer molar absorptivity, $\varepsilon^{\lambda}_{M}$, to calculate an *apparent* fraction bound, α', for the ligand.

$$\alpha'_k = \frac{\varepsilon^{\lambda}_{M} - \varepsilon^{\lambda}_{k}}{\varepsilon^{\lambda}_{M} - \varepsilon^{\lambda}_{B}} \qquad \text{--- 4.4}$$

$$\text{where} \qquad \varepsilon^{\lambda}_{k} = A^{\lambda}_{k}/T_L \qquad \text{--- 4.5}$$

for the k^{th} spectrum of the set. The α' values so obtained are then used to compute $\varepsilon^{\lambda}_{B}$ at all other wavelengths, λ, as follows:

$$\varepsilon^{\lambda}_{B} = \frac{\varepsilon^{\lambda}_{k} - (1-\alpha'_k)\varepsilon^{\lambda}_{M}}{\alpha'_k} \qquad \text{--- 4.6}$$

The $\varepsilon^{\lambda}_{B}$ values so obtained are the bound ligand molar absorptivities at all wavelengths for which $\varepsilon^{\lambda}_{M}$ and $\varepsilon^{\lambda}_{k}$ values are known. The precision of the $\varepsilon^{\lambda}_{B}$ values may be checked by performing the extrapolative procedure at various wavelengths and comparing the $\varepsilon^{\lambda}_{B}$ values so obtained. Table 4.1 contains the values of $\varepsilon^{\lambda}_{B}$ calculated in this way at 5 wavelengths for the 9AA/*E Coli* DNA/0.10 M NaCl system. It can be seen that

TABLE 4.1

Values of ε_B^λ obtained from extrapolation of Plots of $\varepsilon_{OBS}^\lambda/\varepsilon_M^\lambda$ versus T_L/T_A.

λ (nm)	422	418	401	393	381
ε_M^λ ($M^{-1}cm^{-1}$)	8187.7	7276.5	10300	7516.3	6696.7
ε_B^λ ($M^{-1}cm^{-1}$)	3070.4	2812.4	3718.3	2770.0	2384.9

Values of ε_B^{401} calculated using the ε_M^λ and ε_B^λ values tabulated, from Eqn. 4.6.

λ (nm)	ε_B^{401} (1) ($M^{-1}cm^{-1}$)	Standard Deviation	% Deviation (2)
422	3722.2	6.98	-0.105
418	3712.0	11.20	+0.169
401	3718.3	-	-
393	3707.4	4.71	+0.293
381	3709.7	7.33	+0.231

(1) These values of ε_B^{401} are the average of 18 such values, calculated using the values of ε_M^λ and ε_B^λ listed in the first tabulation, from the spectra of 18 mixtures. The ε_B^{401} values so calculated for each of the wavelengths (excepting 401 nm) are presented to enable a direct comparison of the results obtained.

(2) The percentage deviation is with respect to the ε_B^{401} value obtained by extrapolation of data collected at that wavelength, namely 3718.3 M^{-1} cm^{-1}.

these results are self-consistent to within the expected deviations due to the errors in the extrapolations and in the absorbance measurements.

Two further checks of the ε_B^λ values determined have been performed. The first is the use of dialysis results to calculate free and bound ligand concentrations, C_F and C_B respectively, for ligand/DNA mixtures. These values, combined with the absorbances for equilibrium mixtures identical to those determined by dialysis, are used to calculate ε_B^λ values. These results are contained in Table 4.2. The second check is to use the method of Gatti *et al*[3], described in Chapter III, to obtain values of r and C_F. These values, obtained at a specific $\Delta A/T_A$ value, are used with the known T_L value to calculate ε_B^λ through Eqn. 3.10 where ε_B^λ is the only unknown. Table 4.3 shows the results obtained by this method. The results obtained from both these methods are in excellent agreement with the results of the extrapolative method.

The monomer spectrum and the *E Coli* DNA bound spectrum for 9-aminoacridine at 22°C in 0.10 M NaCl are shown in Fig. 4.8. The bound spectrum shows a red shift and broadening of the component peaks when compared with the monomer spectrum. The relative magnitude of the longest wavelength peaks has also changed, the peak at 424 nm having become more intense. These general features of the DNA bound spectrum relative to the monomer spectrum are seen in all the 9-aminoacridines used in this work.

Having obtained the bound ligand spectrum for all the internally linear systems, we may now proceed to calculate binding curves to describe these systems. These curves will enable mathematical models of the binding process to be fitted and the interaction may then be characterized in terms of the thermodynamic parameters obtained from these models.

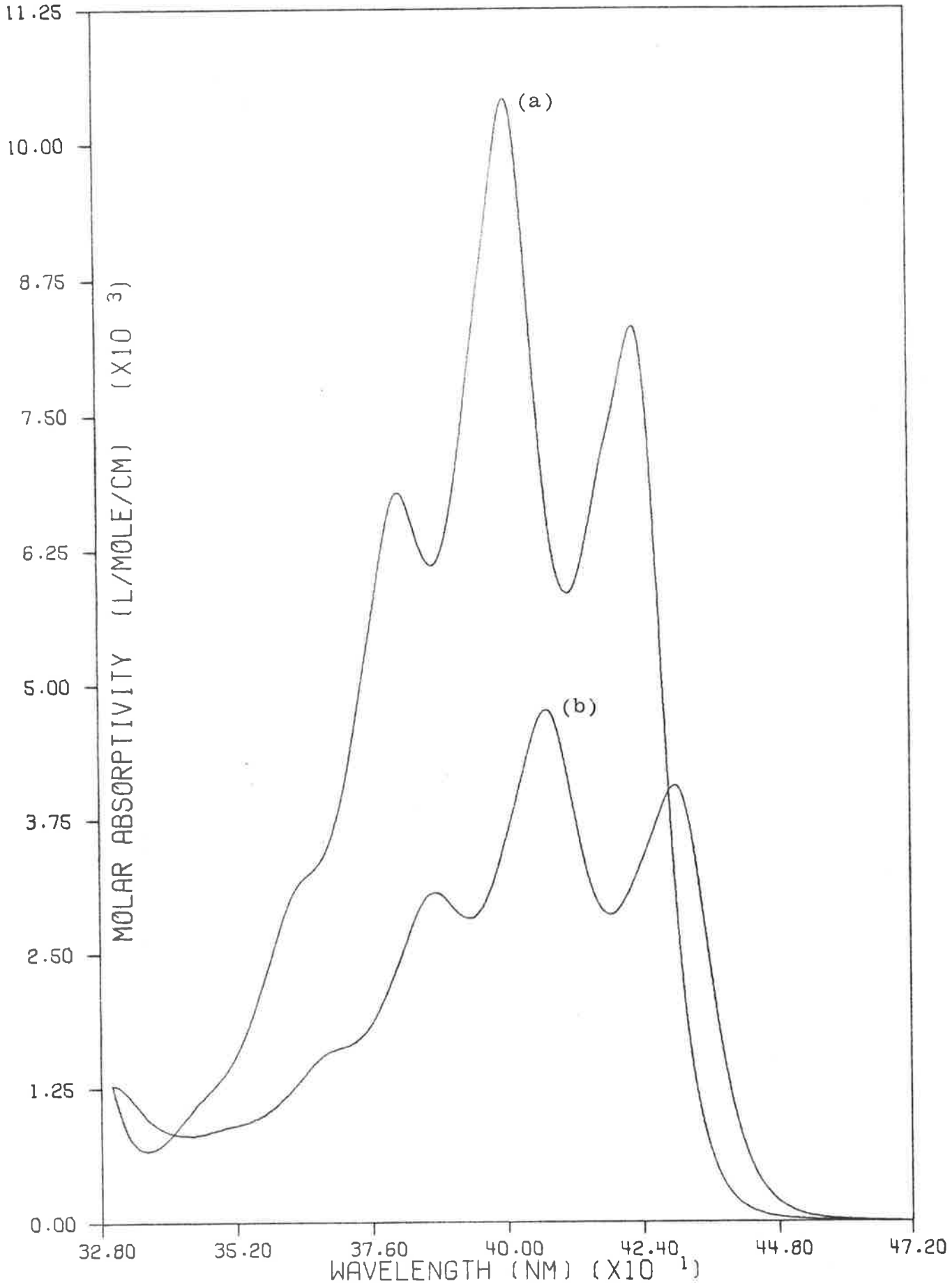

Figure 4-8. The observed monomer spectrum, a, and the generated *E Coli* DNA bound spectrum, b, of 9AA in 0.10 M NaCl at 22°C.

TABLE 4.2

ε_B^{401} values calculated from dialysis experiments.

C_F (1) x 10^6 (M)	C_B (1) x 10^5 (M)	T_L x 10^5 (M)	T_A x 10^4 (M)	α (2)	A_{OBS}^{401} (3)	ε_B^{401} (4) (M^{-1} cm^{-1})
1.7271	4.5688	4.7415	4.8406	0.9636	0.1875	3714.5
2.6457	6.7318	6.9964	5.5550	0.9622	0.2777	3720.4
5.2142	4.7693	5.2907	2.7642	0.9015	0.2313	3723.7
12.826	11.397	12.679_5	4.8332	0.8889	0.5568	3726.4
26.855	7.5060	10.191_5	2.5278	0.7365	0.5569	3734.3

$\bar{\varepsilon}_B^{401} = 3723.8 \pm 7.33$

(1) Calculated from the dialysis experiment.

(2) Equals C_B/T_L.

(3) Measured absorbance of the DNA containing side corrected for DNA background absorbance.

(4) From Eqn. 4.6.

TABLE 4.3

ε_B^{401} values calculated from the method of Gatti *et al*[3].

$\Delta A^{401}/T_A$ (1) (M^{-1})	r (1) (from slope)	ε_B^{401} (2) (M^{-1} cm^{-1})
450	0.06850	3730.7
425	0.06476	3737.3
400	0.06087	3728.6
375	0.05703	3724.5
350	0.05322	3723.5
325	0.04942	3723.7
300	0.04541	3693.5
275	0.04154	3679.9

(1) Data taken from Table 3.1.

(2) The average ε_B^{401} value is 3717.7 ± 20.0. A value of 3728.1 ± 5.8 is obtained if the last two points are omitted.

4. Binding curves

Binding curves are usually defined in terms of the fraction of ligand bound per macromolecular unit and the free ligand concentration in equilibrium with that complex. When the macromolecule involved in the interaction is naturally occuring DNA, the DNA is heterogenous with respect to molecular weight and so no discrete molecular weight can be defined, but only an average. In such cases molecular weight is normally expressed in terms of some repeating unit of the macromolecular structure. For DNA the unit chosen is usually moles of DNA phosphorus, which is equivalent to moles of single nucleotide residue. For reasons explained in detail in Chapter V, it is more appropriate to use moles of DNA base pairs as the DNA concentration unit. This will have no effect on the numerical values of C_F and will exactly double the values of r obtained from the data when compared to those values calculated using the units of moles of DNA phosphorus.

(a) Graphical representation

The graphical expression of ligand/macromolecule binding curves may take many forms[2], the most common being the Scatchard Plot[4]. This transform is most often used to display ligand/macromolecule binding data for three reasons.

(1) It is a closed form plot having intercepts on both the ordinate (r/C_F) and the abscissa (r).

(2) In many cases it is amenable to graphical analysis to obtain some or all of the parameters characterizing the binding process.

(3) The shape of the curve provides valuable clues as to the number and nature of the binding processes.

With the advent of modern digital computers it is now possible to analyse binding data more objectively using linear or non-linear fitting algorithms to find model parameters. While this has removed the need for subjective graphical analyses, the Scatchard plot remains the best general visual presentation of ligand/macromolecule binding data and will be used in this work to present results.

(b) Formal requirements for the calculation

The calculation of binding data from complete spectral data has generally been made using the expression due to Peacocke and Skerrett[5], presented below:

$$\alpha = \frac{A_F^\lambda - A_{OBS}^\lambda}{A_F^\lambda - A_B^\lambda} \qquad \text{--- 4.7}$$

$$r = \alpha(T_L/T_A) \qquad \text{--- 4.8}$$

In the above expression the absorbances are all for the same wavelength and total ligand concentration. From the ratio, r, so found the corresponding free ligand concentration is calculated as:

$$C_F = T_L - rT_A \qquad \text{--- 4.9}$$

Blake and Peacocke[1] listed four conditions which must be met before Eqn. 4.7 may be used. These conditions may be reformulated as:

(1) The nucleic acid is non-absorbing at all wavelengths used in Eqn. 4.7.

(2) Both free and bound ligand absorbance obey Beer's Law over the whole concentration range used.

(3) Both ε_F^λ and ε_B^λ do not vary with r.

(4) Either there is only one spectrally distinct species of bound ligand, or if more than one distinct species

(4) (Continued)

exists, the relative proportions of bound species are invariant with r.

Two further observations were presented as a consequence of conditions (1) to (4).

(5) There should be a clear isosbestic point through which all spectra of mixtures of equal T_L will pass at a wavelength where $\varepsilon_F^\lambda = \varepsilon_B^\lambda$.

(6) The value of r calculated from the spectral data will be the same for all wavelengths which meet conditions (1) to (4).

The fundamental importance of these conditions to the calculation of binding curves from spectral data warrants discussion in the light of this work. The first condition is usually not met in practice and methods of correcting for this absorbance have been presented in Chapter III. The second condition, that ε_F^λ and ε_B^λ are constant to within available spectrophotometric precision, has also been discussed in Chapter III. ε_F^λ will not generally meet this condition for aminoacridines at the higher free ligand concentrations. The method of making correction for these deviations is presented in a following section of this Chapter. The question of the constancy of ε_B^λ is more complex, involving both conditions (2) and (3). The proposition put by condition (2) is that ε_B^λ values due to one or more distinct bound species are constant over the range of concentrations of those species occuring during the experiments. This implies that these species have a unique, reproducible spectroscopic identity under some given set of experimental conditions. The effect of experimental conditions brings us to the third condition, which requires

that the spectroscopic properties of these species are invariant of the number of ligands bound per unit of macromolecule. This condition must be met to experimentally observe condition (2), except where r is confined to a small range. The problem of the effect of ligands binding close to an already bound ligand, and so possibly altering the nature of the binding sites by introducing strain into the DNA secondary structure, could cause a dependence of ε_B^λ on r. The question of the existence of such a cooperative effect is discussed fully in Chapter V. Two additional sources of a dependence of ε_B^λ on the amount of ligand bound are that natural DNA is heterogenous in base composition, there being 16 different combinations of nearest neighbour base pairs alone, so that any difference in the way a ligand is bound to different base pair combinations could produce a dependence of ε_B^λ on r. The second source is the possibility of the binding of aggregates of ligand which may produce an observed dependence of ε_B^λ with the amount of ligand bound. It must be emphasized that any of the above situations *may* produce a dependence of ε_B^λ on r. Any one or indeed all of these situations can exist and not produce a dependence of ε_B^λ on r, if the relative contributions that the various bound forms make to the overall ε_B^λ is invariant over the experimentally accessible range of r. This is the origin of the fourth condition.

The problem of determining that all these conditions are met in an experimental situation is considerable, especially so when deviations in ε_B^λ values are observed. Since, as we have seen, bound species usually cannot be isolated in an experimental system and are never isolated for high r values, any resolution of the causes of deviation from

ideal spectral behaviour must be indirect. Fortunately however the degree of any deviation may be quantified. Blake and Peacocke[1] presented the two experimental observations, numbered (5) and (6) above, as evidence that the necessary conditions had been met by a system under study. These observations taken together imply that internal linearity, as presented earlier in this Chapter, should replace these observations as the experimental condition to be met in order to apply Eqn. 4.7. This test not only overcomes the problem that spectral data may meet conditions (1) to (4) but not display an isosbestic point, but also provides direct quantitative information on any deviations and the wavelength range over which they occur. Observation (6) is a necessary condition for the existence of internal linearity, and so is redundant if this test is used.

(c) Non-ideal spectral data

Before applying Eqn. 4.7, it is instructive to examine the effect of non-ideal spectral data on the binding curves calculated from such data. Most real systems will not yield ideal data and it is inevitable that corrections will have to be applied to some or all of the parameters used in the calculations. The total concentration terms, T_L and T_A, will be known to good precision if solutions are prepared by weighing and so not contribute to errors in observed absorbances, nor in the calculation of r and C_F values. This leaves the absorbance ratio as the prime source of error. The precision and accuracy of recording absorbances has been discussed in Chapter III.

The absorbance ratio, Eqn. 4.7, may be considered in three sections.

(1) $\alpha \rightarrow 0$, $A_F^\lambda \simeq A_{OBS}^\lambda$, $T_L > T_A$

In this region any small errors in A_F^λ, or indeed in A_{OBS}^λ, will have a large effect on the ratio and so on r. T_A is small compared to T_L, hence the effect of a large error in r upon the value of C_F is small as $C_F \simeq T_L$.

(2) $\alpha \simeq 0.5$, $A_{OBS}^\lambda \simeq \frac{1}{2}(A_F^\lambda + A_B^\lambda)$, $T_L \leqslant T_A$

Here the effect of errors in absorbances on α is smaller although errors in the numerator will still weigh more heavily in the resultant α. The values of both r and C_F will be most accurate in this region.

(3) $\alpha \rightarrow 1$, $A_{OBS}^\lambda \simeq A_B^\lambda$, $T_L < T_A$

Errors in α in this region are smallest since the absorbance differences are at their maximum. However in contrast to the first region, small errors in r will have a profound effect on the value of C_F, since $T_A >> T_L$.

In order to appreciate the effect of errors in the values of A_F^λ and A_B^λ on the magnitude of errors in r and C_F in each of these three regions, I will use spectral data collected for the 9AA/*E Coli* DNA/ 0.10 M NaCl system to calculate binding data for each region in turn. Before proceeding however it is necessary to transform the equation defining α and to consider the problem of determining the correct free ligand absorbance at high r values.

(c) (i) The correction of ε_F^λ

A more tractible form of Eqn. 4.7 is obtained by dividing all the absorbance terms by T_L to yield:

$$\alpha = \frac{\varepsilon_F^\lambda - \varepsilon_{OBS}^\lambda}{\varepsilon_F^\lambda - \varepsilon_B^\lambda} \qquad \text{--- 4.10}$$

The value of ε_F^λ used for any single calculation must be the apparent molar absorptivity of the free ligand for the free ligand concentration actually in the solution for which $\varepsilon_{OBS}^\lambda$ was obtained. That this is so can be simply shown from the following derivation assuming the existence of aggregates in the free dye solution. In the following derivation the subscript M refers to the monomer free dye D to a dimer species and N to a N-mer species. The total observed absorbance may be written as:

$$A_{OBS} = C_T\varepsilon_{OBS} = C_B\varepsilon_B + (C_M\varepsilon_M + 2C_D\varepsilon_D + \ldots + NC_N\varepsilon_N) \quad \text{--- 4.11}$$

where $C_F = C_M + 2C_D + \ldots + NC_N$; $\varepsilon_N = A_N/NC_N$

and $C_T = C_F + C_B$

We may now define the apparent molar absorptivity of the total *free* dye as:

$$\varepsilon_F = \frac{C_M\varepsilon_M + 2C_D\varepsilon_D + \ldots + NC_N\varepsilon_N}{C_F} \quad \text{--- 4.12}$$

Now we may write:

$$C_F\varepsilon_F = C_T\varepsilon_{OBS} - C_B\varepsilon_B$$

$$= C_T\varepsilon_F - C_B\varepsilon_F$$

hence $$C_T(\varepsilon_F - \varepsilon_{OBS}) = C_B(\varepsilon_F - \varepsilon_B)$$

and $$\frac{C_B}{C_T} = \alpha = \frac{\varepsilon_F - \varepsilon_{OBS}}{\varepsilon_F - \varepsilon_B} \quad \text{--- 4.13}$$

Equation 4.13 is identical to Eqn. 4.10.

For all of the 9-aminoacridines used in this work $\varepsilon_F^\lambda = \varepsilon_M^\lambda$, where ε_M^λ is the monomer molar absorptivity, for concentrations below 1×10^{-5} M in 0.10 M NaCl. For higher concentrations measurable deviations are observed, almost certainly due to self-association of the ligand. Since the

value of C_F is not known, but is to be obtained from the calculation, the solution to finding the correct value of ε_F^λ to use is an iterative procedure. Previously and separately determined values of A_F^λ for many C_F values covering the desired range of concentrations, are fitted to a polynomial, usually a quadratic, to obtain an empirical expression relating A_F^λ and C_F. This enables ε_F^λ to be accurately determined for any given C_F in the range. The iterative procedure is then applied as follows.

(1) A zeroth order approximation to C_F is obtained by assuming that $\varepsilon_F^\lambda = \varepsilon_M^\lambda$ and then calculating r^0 and C_F^0.

(2) A first order approximation is then obtained by assuming the value of ε_F^λ indicated by C_F^0 and so calculating r^1 and C_F^1.

(3) The second and subsequent order approximations are calculated in the same way as the first order approximation, only the value of ε_F^λ is corrected each time using the C_F^{n-1} approximation for the true value of C_F in the n^{th} approximation.

(4) The procedure is terminated when $C_F^{n-1} = C_F^n$ to the accuracy expected from random experimental errors in the data.

The procedure converges quickly and only a few iterative cycles are required to obtain satisfactory results. It may be applied to all binding data although when C_F is low, no "corrected" value is generated as $\varepsilon_F^\lambda = \varepsilon_M^\lambda$. This enables the same algorithm to be applied to all data and so simplifies any computing programs used to calculate binding data.

Table 4.4 presents the results of this iterative procedure for two data points from the 9AA/*E Coli* DNA/0.10 M NaCl system. It can be seen that the algorithm is stable and

converges quickly to a solution. The effect of this correction on the value of r obtained when C_F is high is quite dramatic. An error of a few percent in ε_F^λ can produce errors of several hundred percent in the calculated values of r when C_F approaches T_L*. In contrast the error in C_F is comparable to the relative error in ε_F^λ. It should be noted that the data used in Table 4.4 and the succeeding tables in this Chapter are taken from the data used to calculate the four binding curves for the 9-aminoacridine system. This data is not directly comparable with the data used earlier in this work which was collected before the DMR-10 spectrophotometer was available. The narrower spectral bandwidth of the DMR-10 and the use of 401 nm rather than 400 nm accounts for the differences in ε_M and ε_B when compared to the earlier data, which was used to validate the determination of ε_B. Binding data collected from both sets of spectral data fall on the same curve.

(c) (ii) The effect of error in ε_F^λ and ε_B^λ

Having overcome the problem of choosing appropriate ε_F^λ values, we may now examine the effect of errors in calculated and observed molar absorptivities on calculated binding parameters in each of the three regions. For this purpose an error of 1% in ε_F^λ and 2% in ε_B^λ will be used. These magnitudes reflect the relative difficulty in obtaining precise values for these two parameters. The error in $\varepsilon_{OBS}^\lambda$ is small and the errors in T_L and T_A are taken to be negligible.

---

* This effect of the value of ε_F^λ on r explains why the observed initial value of ε_F^λ is preferred by many workers to ε_M^λ. The use of ε_F^λ values observed for a particular T_L will indeed better approximate the correct ε_F^λ for C_F when $C_F \simeq T_L$. This avoids the extremely large errors in r at high r when compared to using ε_M^λ, but of course progressively introduces errors in r and hence C_F as C_F decreases. The only way to obtain correct binding parameters is to use the real ε_F^λ for each C_F.

TABLE 4.4

The iterative procedure for calculating ε_F^λ.

For the following data is from the 9AA/*E Coli* DNA/0.10 M NaCl system at 22°C. Run no. BS059.

$\varepsilon_M = 10400$; $\varepsilon_B = 3765$; $\lambda = 401$ nm; $A_F^{401} = aC_F^2 + bC_F + c$ where $a = -6.74106 \times 10^6$, $b = 1.03717 \times 10^4$, $c = 3.57829 \times 10^{-5}$.

(1) For $\varepsilon_{OBS}^\lambda = 9908.3$; $T_L = 5.3768 \times 10^{-5}$ M; $T_A = 2.9019 \times 10^{-6}$ M.

N	ε_F^λ ($M^{-1}cm^{-1}$)	α	C_B x10^6(M)	C_F x10^5(M)	r	r/C_F x10^{-4}(M^{-1})
0	10400	0.0741	3.9846	4.9783	1.373_1	2.7581
1	10036.8	0.0249	1.1018	5.2666	0.379_7	0.7209
2	10017.4	0.0174	0.9378	5.2830	0.323_2	0.6117
3	10016.2	0.0173	0.9285	5.2839	0.319_9	0.6055
4	10016.2	0.0173	0.9279	5.2840	0.319_8	0.6052

(2) For $\varepsilon_{OBS}^\lambda = 9374.8$; $T_L = 5.3855 \times 10^{-5}$ M; $T_A = 1.7938 \times 10^{-5}$ M.

N	ε_F^λ ($M^{-1}cm^{-1}$)	α	C_B x10^6(M)	C_F x10^5(M)	r	r/C_F x10^{-4}(M^{-1})
0	10400	0.1545	8.3214	4.5534	0.463_9	1.0188
1	10065.5	0.1096	5.9042	4.7951	0.329_1	0.6864
2	10049.2	0.1073	5.7796	4.8075	0.322_2	0.6702
3	10048.4	0.1072	5.7732	4.8082	0.321_8	0.6694
4	10048.3	0.1072	5.7728	4.8082	0.321_8	0.6693

Table 4.5 shows calculations in the region where α is near zero. As previously indicated an error in ε_F^λ has a great effect on the value of r. The relative error induced in C_F is constant and somewhat smaller. The propagation of these errors into the value of r/C_F is additive. The accuracy of ε_B^λ is much less critical in this region producing only small errors in the calculated results. The results obtained when α is around 0.5 are presented in Table 4.6. The errors induced in r and C_F are small and the relative weights of ε_F^λ and ε_B^λ in contributing to error are nearly equal. The value of ε_F^λ affects the value of r as a function of α in this region and ε_B^λ affects C_F as a function of α. The final region of the curve, that where α approaches unity, is shown in Table 4.7. In this region the errors induced through ε_F^λ are small and have little effect upon the calculated parameters. The error produced by ε_B^λ on r is small, however the error in C_F is large. This arises since $T_A >> T_L$ and the small errors in r are magnified enormously as the value of T_A increases. These errors are propagated into the calculated values of r/C_F producing erratic results.

In summary, the error in r is greatest when α is near zero and least as α approaches unity. Conversely the error in C_F is effected by the error in r least when r is high (i.e. α is near zero) and greatest as α approaches unity, since $T_L >> T_A$ in this region. This complex dependence of errors in calculated binding data on the absorbance values used to calculate the data must be considered when assessing the reliability of the binding curves and the relative precision of their component sections to one another. In practice, the precision of the values of ε_F^λ used throughout the range of the binding curve is limited only by the precision of the

TABLE 4.5

Errors in calculated binding data as $\alpha \rightarrow 0$.

The following data is from the 9AA/*E Coli* DNA/0.10 M NaCl system at 22°C. Run no. BS059; $\varepsilon_M^\lambda = 10400$; $\varepsilon_B^\lambda = 3765$; $\lambda = 401$ nm.

$\varepsilon_{OBS}^\lambda$ ($M^{-1}cm^{-1}$)	ε_F^λ (1) ($M^{-1}cm^{-1}$)	T_L x10^5(M)	T_A x10^6(M)	T_L/T_A
9772.6	10025.6	5.3607	6.8125	7.869
9529.1	10039.5	5.3768	13.474	3.991
9374.8	10048.3	5.3855	17.938	3.002

r	C_F x10^5(M)	r/C_F x10^{-4}(M^{-1})	$\Delta r/r$ (%)	$\Delta C_F/C_F$ (%)	$\frac{\Delta(r/C_F)}{r/C_F}$ (%)
		- - - - NO ERROR - - - -			
0.318_0	5.1440	0.6183	-	-	-
0.324_6	4.9395	0.6571	-	-	-
0.321_8	4.8082	0.6693	-	-	-
		- - - - ε_F^λ + 1% - - - -			
0.437_0	5.0630	0.8631	37.4	1.57	39.6
0.382_3	4.8616	0.7864	17.8	1.58	19.7
0.364_0	4.7326	0.7692	13.1	1.57	14.9
		- - - - ε_B^λ + 2% - - - -			
0.321_9	5.1414	0.6260	1.23	0.05	1.25
0.328_6	4.9341	0.6659	1.23	0.11	1.34
0.325_7	4.8012	0.6784	1.21	0.15	1.36

(1) As determined by the iterative procedure.

TABLE 4.6

Errors in calculated binding data for $\alpha \simeq 0.5$.

The following data is from the 9AA/*E Coli* DNA/0.10 M NaCl system at 22°C. Run no. BS059; $\varepsilon_M^\lambda = 10400$; $\varepsilon_B^\lambda = 3765$; $\lambda = 401$ nm.

$\varepsilon_{OBS}^\lambda$ ($M^{-1}cm^{-1}$)	ε_F^λ (1) ($M^{-1}cm^{-1}$)	T_L $x10^5$(M)	T_A $x10^5$(M)	T_L/T_A
7346.6	10171.2	5.3530	8.1390	0.6577
7006.0	10190.0	5.3810	9.2945	0.5789
6553.5	10217.2	5.3564	11.0895	0.4830

r	C_F $x10^5$(M)	r/C_F $x10^{-4}(M^{-1})$	$\Delta r/r$ (%)	$\Delta C_F/C_F$ (%)	$\frac{\Delta(r/C_F)}{r/C_F}$ (%)
		- - - - NO ERROR - - - -			
0.289_9	2.9928	0.9689	-	-	-
0.286_9	2.7144	1.0570	-	-	-
0.274_3	2.3149	1.1848	-	-	-
		- - - - ε_F^λ + 1% - - - -			
0.295_7	2.9460	1.0039	2.00	1.56	3.60
0.291_5	2.6720	1.0908	1.60	1.56	3.20
0.277_5	2.2788	1.2178	1.17	1.56	2.79
		- - - - ε_B^λ + 2% - - - -			
0.293_4	2.9647	0.9898	1.21	0.94	2.15
0.290_3	2.6827	1.0821	1.19	1.17	2.38
0.277_5	2.2790	1.2177	1.17	1.55	2.77

(1) As determined by the iterative procedure.

TABLE 4.7

Errors in calculated binding data as $\alpha \to 1$.

The following data is from the 9AA/*E Coli* DNA/0.10 M NaCl system at 22°C. Run no. BS059; $\varepsilon_M^\lambda = 10400$; $\varepsilon_B^\lambda = 3765$; $\lambda = 401$ nm.

$\varepsilon_{OBS}^\lambda$ ($M^{-1}cm^{-1}$)	ε_F^λ (1) ($M^{-1}cm^{-1}$)	T_L $x10^5$(M)	T_A $x10^4$(M)	T_L/T_A
4081.1	10368.2	5.3831	4.4657	0.1205
4007.2	10377.1	5.2837	5.2210	0.1012
3928.7	10389.6	5.3905	6.6785	0.0807

r	C_F $x10^6$(M)	r/C_F $x10^4(M^{-1})$	$\Delta r/r$ (%)	$\Delta C_F/C_F$ (%)	$\frac{\Delta(r/C_F)}{r/C_F}$ (%)
		- - - - NO ERROR - - - -			
0.114_8	2.5769	4.4539	-	-	-
0.097_5	1.9354	5.0374	-	-	-
0.078_7	1.3321	5.9097	-	-	-
		- - - - ε_F^λ + 1% - - - -			
0.114_9	2.5371	4.5273	0	1.54	1.65
0.097_5	1.9055	5.1194	0	1.55	1.63
0.078_7	1.3115	6.0047	0	1.55	1.61
		- - - - ε_B^λ + 2% - - - -			
0.116_1	1.9857	5.8466	1.13	22.9	31.3
0.098_6	1.3491	7.3101	1.13	30.3	45.1
0.079_6	0.7276	10.944	1.14	45.4	85.2

(1) As determined by the iterative procedure.

spectrophotometer, which is discussed in Chapter III. Provided due care is exercised and the same conditions used to measure the ε_F^λ values as are used for the measurement of the binding curve data, the precision of ε_F^λ should be better than 0.5%. Similar reasoning applies to the $\varepsilon_{OBS}^\lambda$ values measured except that in regions of high T_A the background absorbance correction for the DNA must be applied. The method of making, and restrictions applying to this correction are discussed in Chapter III. The determination of ε_B^λ is more uncertain. Since extrapolative procedures are used it is difficult to accurately estimate the error involved. Perhaps the best guide to the likely precision of this value is the comparisons in Tables 4.1, 4.2 and 4.3 of this Chapter. These would indicate that the precision of this value is also of the order of 0.5% or better. These errors in the absorbance values are fortunately much less than the 1% and 2% used for the purpose of illustration of the effect of errors on binding data. They do, however, serve to illustrate that considerable care is required if precise binding data is to be obtained from the spectrophotometric method.

(d) Accuracy of the binding curves

In order to assess the accuracy of the binding curves produced from spectral data, binding data for the 9AA/*E Coli* DNA/0.10 M NaCl system have been collected using equilibrium dialysis. The preparation of materials and corrections applied to the curves are presented in detail in Chapter III. These data are used to provide a comparison between curves obtained by different experimental methods although the curves calculated from spectral data are more precise and potentially more accurate.

The curves displayed in Fig. 4.9 are those obtained both from dialysis and spectral data at 22°C. The agreement between the two independently obtained curves is good, indicating that the accuracy of the experimental methods is good. Both curves show good precision within the curve. This demonstrates the validity of the method used to obtain binding curves from spectral data. Binding data for all the systems which showed spectral internal linearity have been calculated and are presented in Appendix III. The significance of the lines drawn on these plots is explained in Chapter V.

Having calculated binding curves for these systems, the next step is to use these data to test various mathematical models of the binding process and so obtain a suitable model, and thermodynamic parameters, with which to characterize the processes. The derivation of mathematical models of binding processes is the subject of the next Chapter.

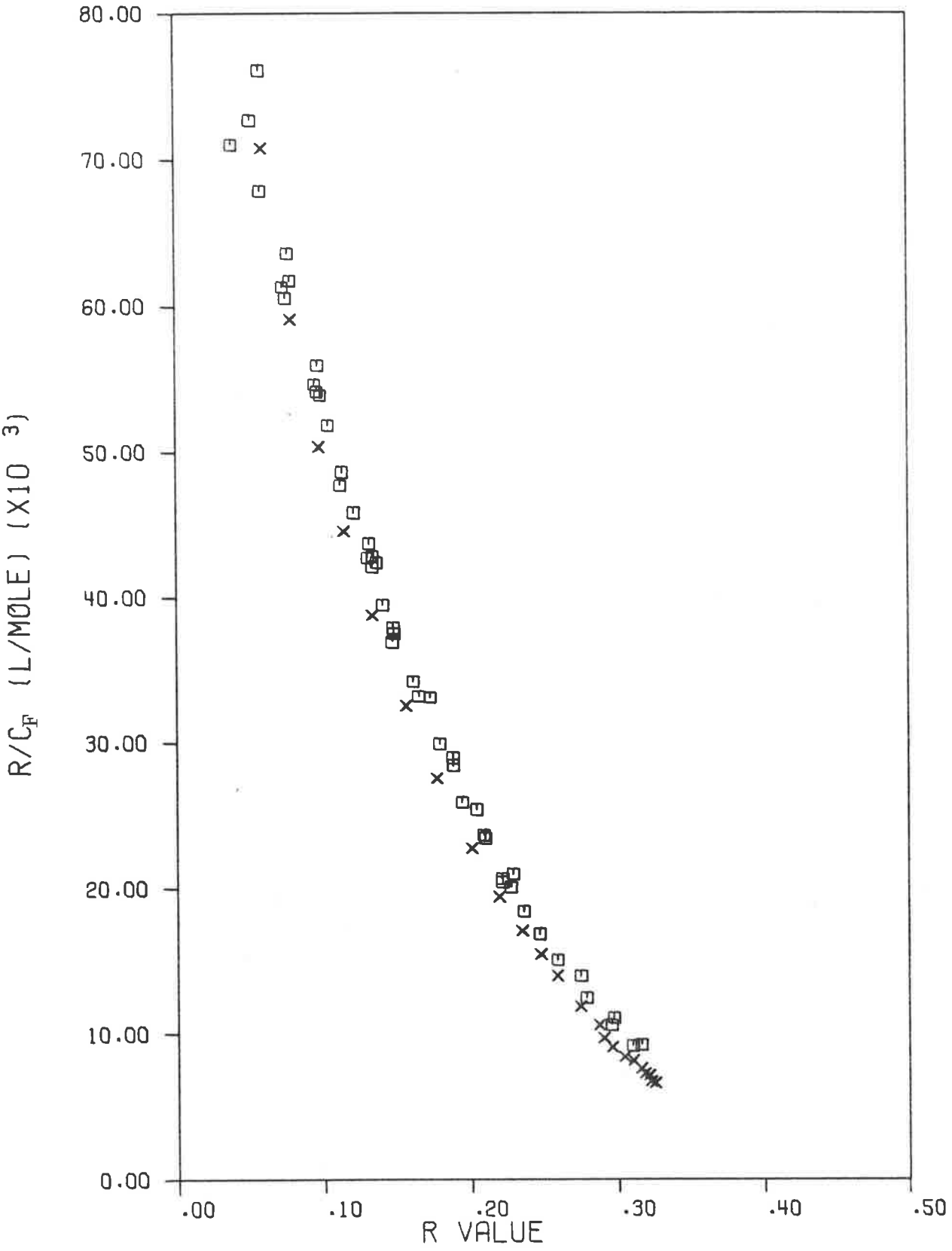

Figure 4-9. Scatchard plot of binding data for the 9AA/*E Coli* DNA/0.10 M NaCl system at 22°C. The square symbols are the data from dialysis experiments and the cross symbols are data from the spectrophotometric method.

REFERENCES

1. Blake A. and Peacocke A.R., *Biopolymers*, 6, 1225 (1968).
2. See, for example: Tanford C., "The Physical Chemistry of Macromolecules", J. Wiley and Sons Inc., New York (1963).
3. Gatti C., Houssier C. and Fredericq E., *Biochim. Biophys. Acta*, 407, 308 (1975).
4. Scatchard G., *Ann. N.Y. Acad. Sci.*, 51, 660 (1949).
5. Peacocke A.R. and Skerrett J.N.H., *Trans. Farad. Soc.*, 52, 261 (1956).

CHAPTER V

Mathematical models for the binding process.

CONTENTS

1. Introduction

The mathematical modelling of binding processes for ligand/DNA interactions has been the subject of considerable interest in the last 5 years. Prior to this resurgence of interest in mathematical models, data from these systems was generally analysed in terms of the Langmuir binding isotherms[1,2] as originally used by Peacocke and Skerrett[3]. Although there have been some instances of more sophisticated treatments[4,5], they have remained relatively isolated examples. The development of more sophisticated treatments was prompted by the requirement for methods to model the binding of multivalent ligands and the need to describe co-operative interactions in general. The advent of the Sequence Generating Functions method[6,7] has aided these developments, which have been primarily of a theoretical nature. Only a few examples of the application of these models have appeared to date[11,12].

In this Chapter we will examine the methods for deriving models of the interaction of ligands with a linear matrix of binding sites, defining a number of models in the process. These models, together with other available models, will provide a basis from which to determine the model that best fits experimentally observed binding data for 9-aminoacridines and native DNA.

2. Historical perspective

The interaction of a ligand with a macromolecule may be described, at the most basic level, as a stepwise equilibrium. In such a treatment each succeeding ligand binds to an existent ligand/macromolecule complex, formed in the initial nucleation step, and is associated with a discrete set of equilibrium parameters. However there are two problems

associated with such a treatment. The first is the need for very accurate, reproducible data with which to identify and define each individual association. Such data are almost impossible to obtain for systems involving natural DNA. The variations in samples arising through the extraction and purification procedure, the resulting distribution of molecular weights and the very large number of ligands which may bind to each molecule combine to make experimental observation of individual association steps extremely difficult. The second problem concerns the usefulness of the data obtained from this treatment. In many instances the individual ligand/macromolecule associations are not sufficiently different from one another to enable them to be properly resolved, and more importantly, to enable any conclusions to be drawn concerning the nature of the individual association complexes. A full discussion of this point, together with a simple example, has been presented by Tanford[8].

The difficulties involved with the stepwise equilibrium method may be partly overcome by utilizing the theory developed by Langmuir[1,2] to describe the adsorption of gases at an interface. This adsorption isotherm may be written as:

$$r = \sum_i r_i = \sum_i \frac{n_i K_i C_F}{1+K_i C_F} \qquad \text{--- 5.1}$$

where r = total fraction of all sites occupied.

r_i = the fraction of the i^{th} binding sites occupied.

n_i = the saturation fraction for the i^{th} sites.

K_i = the association constant for the i^{th} sites.

C_F = the concentration of free ligand.

This expression is valid for i independent, mutually exclusive classes of binding site. Only groups of sites with

significantly differing n_i and/or K_i are distinguished by this method. This overcomes many of the disadvantages of the multiple equilibria treatment and has been widely applied to the description of the interaction of aminoacridines with DNA[9], generally as the more familiar transform due to Scatchard[10]. A Scatchard plot of a binding isotherm for a case where $i = 2$ is shown in Fig. 5.1. The parameters which may be obtained graphically are marked on the figure. The reasons for displaying binding data using the Scatchard plot are fully discussed in Chapter IV.

A Scatchard plot will be linear for a single type of binding site, any curvature being taken as an indication of the existence of multiple classes of sites. However curvature in a binding isotherm may arise for reasons other than the existence of independent, mutually exclusive classes of sites and it is in this that the Langmuir equation is deficient as a description of the binding process. If it is suspected that this is the case, then models capable of accounting for interacting binding sites are required. Before proceeding to derive such models we must first define carefully the type of system that is required and consider the assumptions and simplifications which are necessary to allow meaningful mathematical models to be formulated.

3. Definition of the system

The Langmuir isotherm has a wide applicability to many types of absorption systems. The system we are concerned with, that of the interaction of aminoacridines with DNA, may be described as the binding of ligands to an infinite linear lattice. This lattice is taken to be infinite to enable end-effects to be neglected and is a lattice of

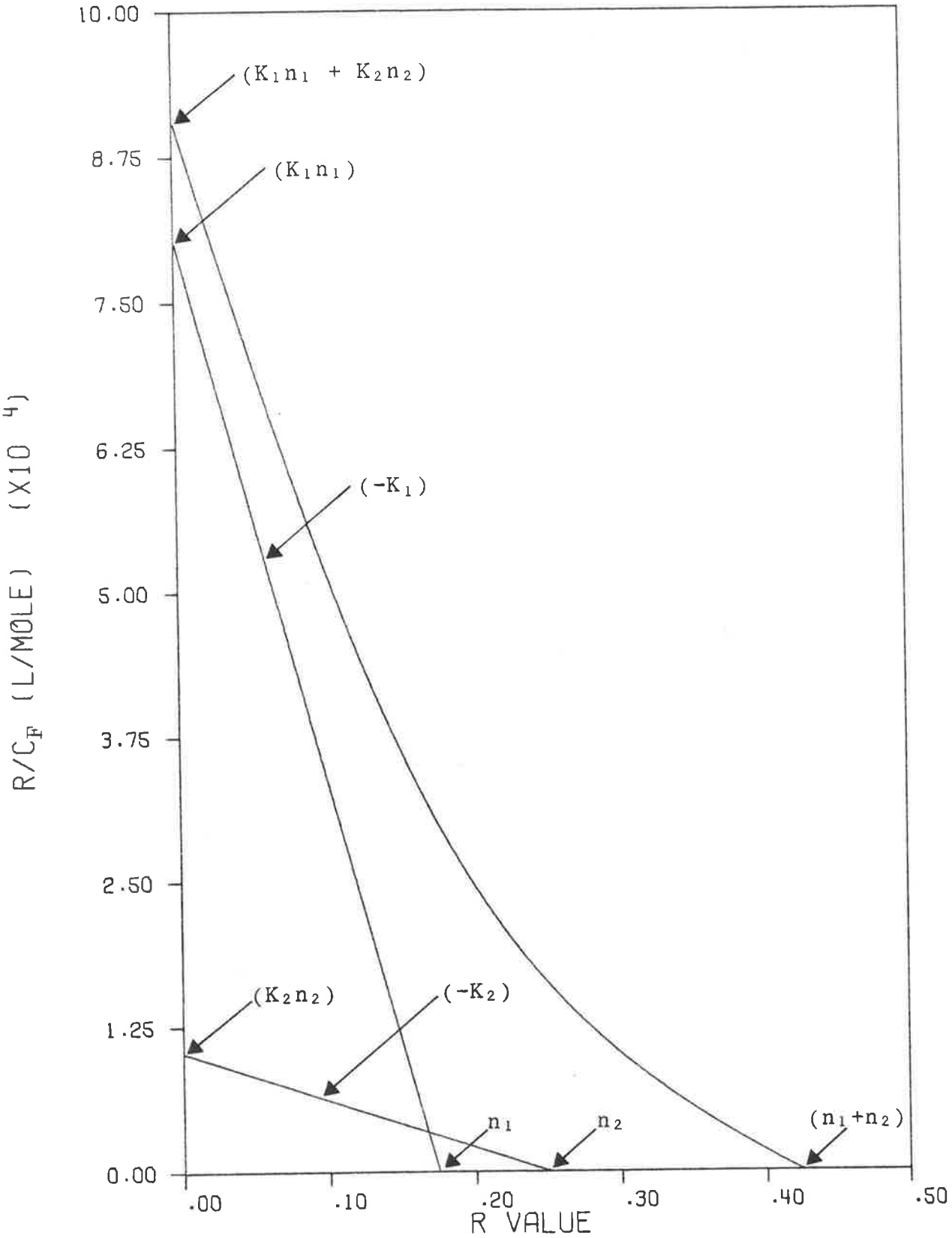

$K_1 = 4.60 \times 10^5$; $n_1 = 0.175$

$K_2 = 4.10 \times 10^4$; $n_2 = 0.250$

Figure 5-1. Scatchard plots for two classes of binding site; each class shown separately and as their sumation. The parameters that may be obtained graphically are marked on the plots.

binding sites and *not* a lattice of repeating macromolecular units. This distinction, which is not drawn when applying the Langmuir equation, is essential for the case of more complex models. When applying the Langmuir equation, macromolecular repeating units may be used initially as lattice sites since all sites are independent and mutually exclusive. The lattice saturation values, n_i, then indicate the number or fraction of repeating units involved in one site of the i^{th} kind. For one type of site, this may be written as:

$$L + RU \rightleftharpoons \text{complex} \qquad \text{--- 5.2}$$

and

$$K = \frac{[\text{complex}]}{[L][RU]} \qquad \text{--- 5.3}$$

where L is the ligand, RU is any macromolecular repeating unit and K is the association constant. Where interaction between adjacent sites occurs, the value of RU must be replaced by the actual concentration of sites. The probability expressions used to define inter-site interaction only maintain their integrity if this restriction is rigidly observed. This is because sites are allowed to be occupied or vacant and no allowance can be made for fractionally occupied sites, a concept which has no meaning in a static mathematical model. This difference in the definition of macromolecular concentration units may lead to differing values between the Langmuir parameters, n_i and K_i, and their equivalents from more complex models. Any such differing values will be related to one another as the value of RU chosen for the Langmuir treatment is related to actual site concentration.

The lattice of binding sites defined above is taken to be homogeneous. This is a simplification since DNA is not homogeneous in base sequence however it is a necessary constraint placed on the lattice to enable the derivation of

models for a binding system. Although the methods I will describe allow more than one type of binding to exist, there may only be *one* type of vacant site. Hence these methods do not embody the essence of a heterogenous lattice, which ideally should reflect the real DNA sequence. The only treatment of heterogenous lattices which has appeared is that due to Crothers[4]. This treatment is a purely numerical procedure which uses Monte Carlo methods to generate a random heterogenous lattice of appropriate base-pair mixture as a model for the DNA used. I will have more to say about this constraint later in this Chapter.

In summary the problem is to mathematically describe the interaction of ligands with an infinite, homogeneous, linear lattice of binding sites in such a way as to allow inter-site interactions to occur.

4. Sequence Generating Functions

The method of the Sequence Generating Function (SGF) was proposed by Lifson[6,7] as a straight-forward way of determining the partition function for a long, linear chain of binding sites. From this, the stochastic equations describing the system may be obtained without the use of matrix algebra. This method is very flexible, being capable of modelling a wide variety of binding systems and yielding a great deal of information concerning the behaviour of these models. Some models have been proposed by Schellman[11] and by Ramstein *et al*[12] using the SGF method to derive the equations. All of the models which have been proposed in the literature for homogeneous, linear lattices can be derived using SGFs. Because of the importance and relative newness of the SGF method, I will now describe in some detail the derivation of models using this method.

(a) The functional form

Firstly, we define the allowable states for each binding site in the lattice. If N different types of binding are possible, then there will be (N + 1) allowable states for each site, including the unbound state. Sequences of adjoining sites in the same state are assigned a statistical weight proportional to the probability of their occurrence, depending on the physical model chosen. A microstate of the system is defined if we can list the length and type of each sequence in the linear lattice. From statistical mechanics we may write:

$$Z^{(n)} = \Sigma W^{(n)} \qquad \text{--- 5.4}$$

and

$$G = -kT\ln Z^{(n)} \qquad \text{--- 5.5}$$

where Z is the partition function of the lattice, W the statistical weight of a microscopic state and n the number of sites in the whole lattice. The free energy of the molecule, G, increases linearly with n. Now if n is sufficiently large, a constant, X_1, may be defined to be independent of n such that:

$$Z^{(n)} \simeq X_1^{(n)} \qquad \text{--- 5.6}$$

X_1 then is the contribution of one site on the lattice to the partition function $Z^{(n)}$. In this case a power series may be defined as:

$$\Gamma(X) = \sum_{n=0}^{\infty} Z^{(n)} X^{-n} \qquad \text{--- 5.7}$$

This series is convergent for $X > X_1$ and will just diverge in the limit as $X \to X_1$.

$\Gamma(X)$ is evaluated by first defining a SGF, $U_m(X)$, for the sequences of empty sites and for each type of binding as:

$$U_m(X) = \sum_{\ell=1}^{\infty} U_m^{\ell} X^{-\ell} \text{ for } m = 0,1,2,\text{---},N \qquad \text{--- 5.8}$$

where ℓ is the length of the sequence and U_m is the statistical weight for a site bound in the m^{th} mode. $U_0(X)$ is used to represent a SGF for an empty site. We may also define a parameter k_{ij} to account for interaction between *adjacent* sites binding types i and j. A matrix can now be written whose elements represent all possible types of SGFs as follows.

$$M(X) = \begin{bmatrix} 0 & k_{01}U_1(X), & k_{02}U_2(X), & ---, & k_{0N}U_N(X) \\ k_{10}U_0(X) & 0 & , k_{12}U_2(X), & ---, & k_{1N}U_N(X) \\ & & & & \\ k_{N0}U_0(X), & k_{N1}U_1(X), & k_{N2}U_2(X), & ---, & 0 \end{bmatrix} \quad --- 5.9$$

It should be noted that the row of M represents the type of sequence *preceding* that specified by the column (that is $M_{ij}(X)$ is the SGF for a sequence of sites in the j^{th} mode that was preceded by a sequence in the i^{th} mode). Now since $k_{ij} = k_{ji}$ by definition, M(X) can be written as a product of a symmetric and a diagonal matrix.

$$M(X) = \begin{bmatrix} 0 , & k_{01}, & k_{02}, & ---, & k_{0N} \\ k_{10}, & 0 , & k_{12}, & ---, & k_{1N} \\ & & & & \\ k_{N0}, & k_{N1}, & k_{N2}, & ---, & 0 \end{bmatrix} \begin{bmatrix} U_0(X), & 0 , & 0, & ---, & 0 \\ 0 , & U_1(X), & 0, & ---, & 0 \\ & & & & \\ 0 , & 0 , & 0, & ---, & U_N(X) \end{bmatrix}$$

--- 5.10

The generating functions for the sequences at the ends of the lattice will, in general, differ from those for interior sequences. By defining a column vector, $\underset{\sim}{e}$, such that e_j is the right-hand end sequence for sites in the j^{th} mode, then the row vector, $\underset{\sim}{e}^T$, will represent the left-hand end effects. We may now write the matrix product, $[M(X)]^{\ell}.[M(X)]^{\ell}_{ij}$, which represents the sum of all possible combinations of (ℓ-1) successive sequences that separate a

sequence of type i from a sequence of type j. This is shown diagramatically in Fig. 5.2. Hence the sum of all products of ℓ successive SGFs is given by $[M(X)]^{\ell}$. Referring back to Eqn. 5.7, we may now write:

$$\Gamma(X) = \sum_{\ell=0}^{\infty} \underset{\sim}{e}^{T} M(X)^{\ell} \underset{\sim}{e} \qquad \text{--- 5.11}$$

$$= \underset{\sim}{e}^{T} [1 - M(X)]^{-1} \underset{\sim}{e} \qquad \text{--- 5.12}$$

The step from Eqn. 5.11 to 5.12 is possible because $\sum_{\ell=0}^{\infty} M(X)^{\ell}$ converges and $\Gamma(X)$ is decreasing monotonically for all $X > X_1$. $\Gamma(X)$ will diverge at $X = X_1$ so that $|1 - M(X)|$ vanishes at this point and X_1 is obtained as the largest root of:

$$|1 - M(X)| = 0 \qquad \text{--- 5.13}$$

We are now in a position to derive formulae describing the average properties of the system when the form of the SGFs, $U_m(X)$, has been found.

(b) The statistical weights

The first step to evaluating the SGFs, $U_m(X)$, is to determine the corresponding statistical weights, U_m, by relating them to the thermodynamic parameters of the physical system we wish to describe. The statistical weights, U_m, are given by:

$$U_m = q_m a_F \qquad \text{--- 5.14}$$

and

$$U_0 = q_0 \qquad \text{--- 5.15}$$

where a_F is the activity of the free ligand and the values of q_0 and q_m are related to the free energies of empty and bound sites respectively by:

$$q_m = e^{(-G_m/RT)} \qquad \text{--- 5.16}$$

and

$$q_0 = e^{(-G_0/RT)} \qquad \text{--- 5.17}$$

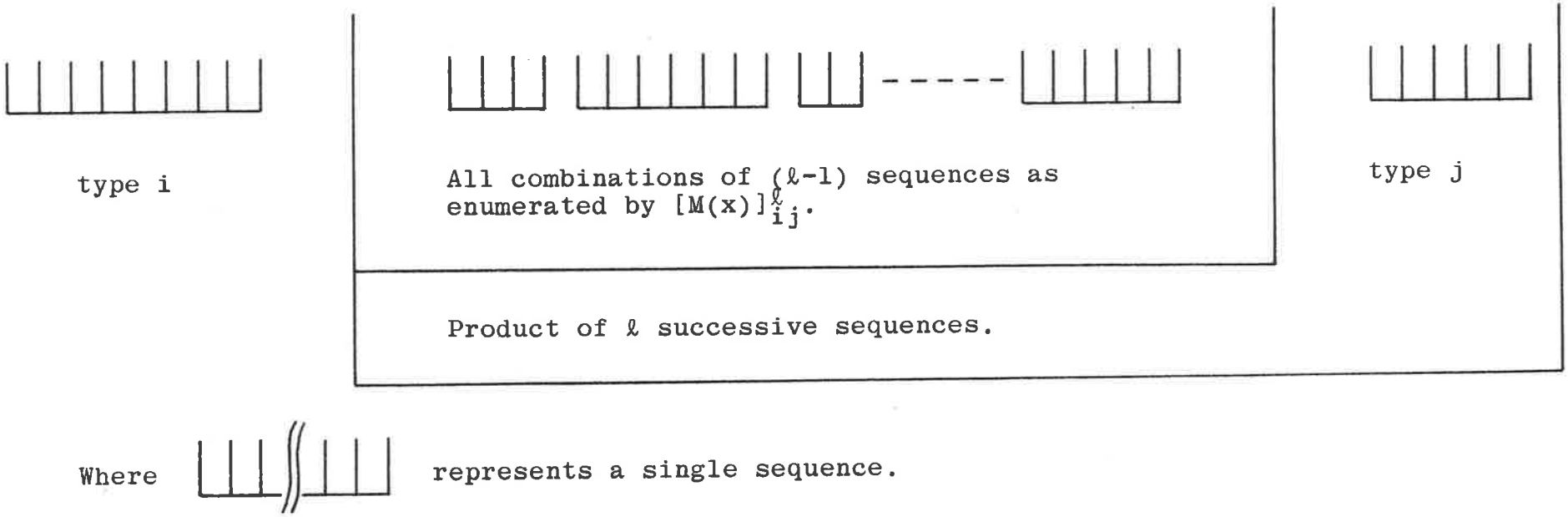

Figure 5-2. Schematic Representation of $[M(x)]^{\ell}_{ij}$.

The free energy of a site bound in the m^{th} mode, G_m, can be related to the free energy of an empty site, G_0, by:

$$G_m = G_0 + \Delta G_m^\circ \qquad \text{--- 5.18}$$

If we now arbitrarily define G_0 as zero, we may rewrite Eqns. 5.16 and 5.17 as:

$$q_m = e^{(-\Delta G_m^\circ/RT)} \qquad \text{--- 5.19}$$

and

$$q_0 = 1 \qquad \text{--- 5.20}$$

so relating the q_m values to the free energy changes on binding to a site. Using the familiar relationship between the equilibrium constant, K_m, and free energy change,

$$\Delta G_m^\circ = -RT\ln K_m \qquad \text{--- 5.21}$$

we may rewrite Eqn. 5.19 as:

$$q_m = K_m \qquad \text{--- 5.22}$$

Now making the usual approximation of unit activity coefficients for dilute solutions, Eqns. 5.14 and 5.15 become:

$$U_m = K_m C_F \qquad \text{--- 5.23}$$

and

$$U_0 = 1 \qquad \text{--- 5.24}$$

Interactions between adjoining sites, bound in the same mode, m, for example, are obtained by multiplying the statistical weight for the pair of sites, $U_m^2X^{-2}$ (remembering that any site, whether bound or empty, has a contribution of X^{-1}), by a factor k_m. This factor will be defined by the relation:

$$k_m = e^{(-\Delta G_m^E/RT)} \qquad \text{--- 5.25}$$

where ΔG_m^E is the excess free energy, and k_m the equilibrium constant, for the process of bringing a ligand from a remote site on the lattice to a site adjacent a ligand bound in the same mode. Where interactions occur between adjacent sites

bound in different modes, k_{ij} is:

$$k_{ij} = e^{(-\Delta G^E_{ij}/RT)} = k_{ji} \qquad \text{--- 5.26}$$

It should be noted that binding in any mode, m, adjacent to an empty site has a statistical weight of U_m, so any parameters of the type k_{m0} or k_{0m} are unity.

Three possible types of behaviour may be discerned from the k values. They are as follows.

(i) $\Delta G^E > 0$, $k < 1$: anti-cooperative binding.

(ii) $\Delta G^E = 0$, $k = 1$: no interaction between adjacent sites.

(iii) $\Delta G^E < 0$, $k > 1$: cooperative binding.

Finally the statistical weights associated with another common binding phenomenon, that of site-exclusion, must be defined. In this form of binding a ligand bound to a single site excludes any form of binding at t adjacent sites on either side of the bound ligand. The statistical weight associated with a site bound in this manner is simply $U_m X^{-(t+1)}$, since the ligand effectively occupies (t+1) sites when bound. The reason the factor is (t+1) and not (2t+1) may be visualized by considering the situation at saturation binding on the lattice. In this case a ligand is bound every (t+1) sites as each excluded block of length t is "shared" by the bound ligands on either side of it. Each ligand then effectively excludes only t sites on the lattice. This situation is illustrated in Fig. 5.3 (4) (ii).

To summarize, we have used parameters of the type K_m, k_m, k_{ij} and t to define statistical weighting factors. The processes these factors govern are represented schematically in Fig. 5.3.

(1) The process characterized by the equilibrium constant, K_m.

(2) The process characterized by k_m.

(3) The process characterized by k_{ij}. Note that $k_{ij} = k_{ji}$.

(4) The site exclusion case for t = 3

(i) The situation for low lattice saturation. The bound ligand excludes 3 sites either side of its site.

(ii) The situation at lattice saturation. Although each ligand has excluded 3 sites on either side, there is one ligand bound every 4 lattice sites, ie. (t + 1) sites.

Figure 5-3. Schematic Representation of the binding parameters K_m, k_m, k_{ij} and the site-exclusion case for 2 binding modes represented by O and X. The ladder symbols represent a segment of an infinite lattice.

(1)

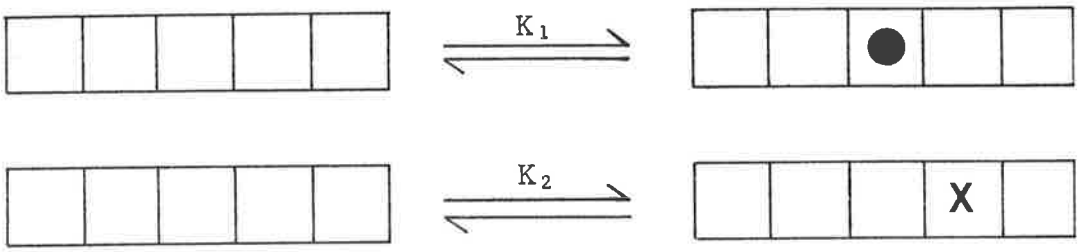

(2)

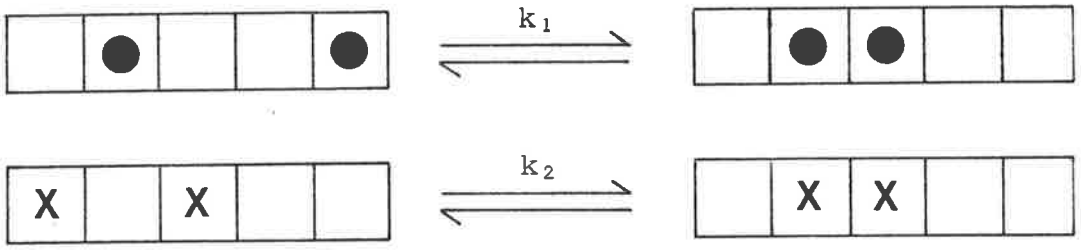

(3)

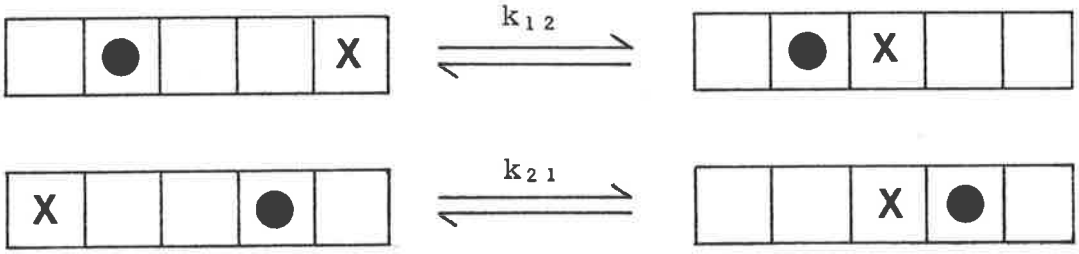

(4)

(i)

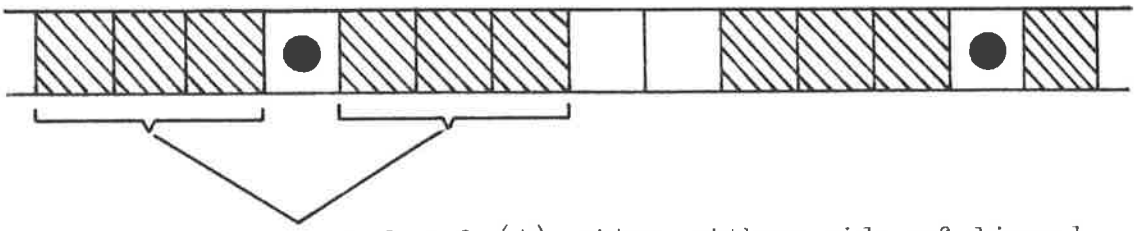

excludes 3 (t) sites either side of ligand.

(ii)

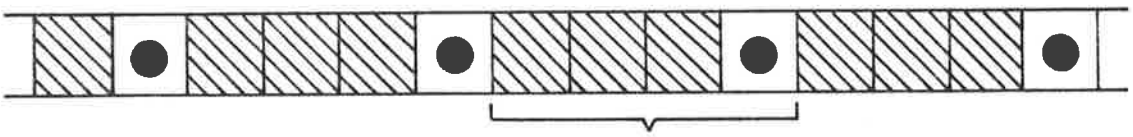

effectively excluded block
at saturation of length (t+1)

(c) The average properties

Now that the form of the statistical weighting factors is known, the SGFs for empty and bound sites may be represented as $U_0(X)$ and $U_m(X,K_m,k_m,C_F)$ and Eqn. 5.13 rewritten as:

$$f(X,K_m,k_m,C_F) = \begin{bmatrix} 1 & -U_1 & -U_2 & \cdots & -U_N \\ -U_0 & 1 & -k_{12}U_2 & \cdots & -k_1NU_N \\ -U_0 & -k_{21}U_1 & 1 & \cdots & -k_2NU_N \\ & & & & \\ -U_0 & -k_{N1}U_1 & -k_{N2}U_2 & \cdots & 1 \end{bmatrix} = 0 \qquad \text{--- 5.27}$$

The required formulae to represent the average properties of the system may now be derived as partial differentiations of $f(X,K_m,k_m,C_F)$ evaluated for the critical value of X, X_1, which is the largest root of Eqn. 5.27. In making these equations we use the general rule that the partial derivative of $f(X,K_m,k_m,C_m)$ with respect to a parameter representing a particular state is proportional to the average number of occurrences of that state[7]. To illustrate this procedure we will derive some average property relationships.

(i) For N different modes of binding, the fraction bound is usually written as:

$$r = \sum_{m=1}^{N} r_m \qquad \text{--- 5.28}$$

$$\text{where} \qquad r_m = \frac{C_B^{(m)}}{T_A} \qquad \text{--- 5.29}$$

In our case we interpret r_m as the ratio of the number of ligand molecules bound to sites in the m^{th} mode to the total number of sites on the lattice. The parameters involved are K_m, governing the m^{th} mode binding, and X^{-1} which represents

any site on the lattice. r_m can now be written as:

$$r_m(K_m,k_m,C_F) = \left[\frac{\partial f}{\partial \ln K_m}/\frac{\partial f}{\partial \ln X^{-1}}\right] X = X_1 \qquad \text{--- 5.30}$$

which is quite literally the ratio of the occurrence of sites bound in the m^{th} mode to the occurrence of all sites on the lattice. This equation may be simplified to:

$$r_m(K_m,k_m,C_F) = \left[-\frac{K_m}{X}\left(\frac{\partial f}{\partial K_m}/\frac{\partial f}{\partial X^{-1}}\right)\right] X = X_1 \qquad \text{--- 5.31}$$

(ii) The average number of ligands bound as nearest neighbours in the m^{th} mode, n_m, is obtained similarly as:

$$n_m(K_m,k_m,C_F) = \left[\frac{\partial f}{\partial \ln k_m}/\frac{\partial f}{\partial \ln K_m}\right] X = X_1$$

$$= \left[\frac{k_m}{K_m}\left(\frac{\partial f}{\partial k_m}/\frac{\partial f}{\partial K_m}\right)\right] X = X_1 \qquad \text{--- 5.32}$$

(iii) As a third and final example, the average fraction of the m^{th} mode bound sequences of length ℓ, m_ℓ, may be obtained as follows. Firstly, the following mathematical tool is used to separate the desired sequence. The m^{th} mode SGF is rewritten as:

$$U_{(m)}(X,K_m,k_m,C_F,\Theta) = U_{(m)}(X,K_m,k_m,C_F) + (\Theta_\ell - 1)k^{\ell-1}(K_m/X)^\ell \qquad \text{--- 5.33}$$

In this way the desired term $k^{\ell-1}(K_m/X)^\ell$ is replaced by $\Theta_m k^{\ell-1}(K_m/X)^\ell$ in $U_{(m)}$. Now differentiation with respect to $\ln\Theta_\ell$ and then setting $\Theta_\ell = 1$ yields the result.

$$m_\ell = \left[\frac{\partial f}{\partial \ln \Theta_\ell}/\frac{\partial f}{\partial \ln K_m}\right] \Theta_\ell = 1$$

$$= \left[\frac{\Theta_\ell}{K_m}\frac{\partial f}{\partial \Theta_\ell}/\frac{\partial f}{\partial K_m}\right] \Theta_\ell = 1 \qquad \text{--- 5.34}$$

This average property is not easily obtained by methods other than the SGF method. It could be of considerable

importance to the interpretation of fluorescence and circular dichroic spectral studies of these systems.

As these examples have shown the SGF method is a powerful technique for the determination of average properties of a system. A more complete list of such average properties has been given by Schellman[11].

(d) The evaluation of SGFs

The SGF's may now be evaluated. The statistical weight for an empty site, U_0, is defined as unity (Eqn. 5.24) and $U_0(X)$, the corresponding SGF, is obtained from Eqn. 5.8 as:

$$U_0(X) = \sum_{\ell=1}^{\infty} U^{\ell} X^{-\ell} \qquad \text{--- 5.35}$$

and the solution of this series is:

$$U_0(X) = \frac{1}{X-1} \qquad \text{--- 5.36}$$

Evaluation of the SGF for the m^{th} binding mode, assuming no site-exclusion effect is:

$$\begin{aligned} U_m(X,K_m,k_m,C_F) &= \sum_{\ell=1}^{\infty} U_m^{\ell} k_m^{\ell-1} X^{-\ell} \\ &= \sum_{\ell=1}^{\infty} (K_m C_F)^{\ell} k_m^{\ell-1} X^{-\ell} \\ &= \frac{K_m C_F}{X - k_m K_m C_F} \end{aligned} \qquad \text{--- 5.37}$$

The $(\ell-1)$ exponent of k_m arises since, in any sequence of ℓ contiguous bound ligands, there will be $(\ell-1)$ *adjacent* bound ligand pairs.

For the case of a site-exclusion effect the SGF evaluates as:

$$\begin{aligned} U_m(X,K_m,k_m,C_F) &= \sum_{\ell=1}^{\infty} U_m^{\ell} k_m^{\ell-1} X^{-(t+1)\ell} \\ &= \sum_{\ell=1}^{\infty} (K_m C_F)^{\ell} k_m^{\ell-1} X^{-(t+1)\ell} \\ &= \frac{K_m C_F}{X^{(t+1)} - k_m K_m C_F} \end{aligned} \qquad \text{--- 5.38}$$

The definition of a further SGF will now be considered as it will be required later in this chapter when we consider suitable models for the aminoacridine/DNA system. This involves extending the cooperative effect to a further site by introducing a second cooperativity factor, s. The statistical weight of this factor is defined in the same way as for the factor k (see Eqns. 5.25 and 5.26). This SGF is then:

$$U_m(X,K_m,k_m,s_m,C_F) = \sum_{\ell=1}^{\infty} U_m^{\ell} k_m^{\ell-1} s_m^{\ell-2} X^{-(t+1)\ell}$$

$$= \sum_{\ell=1}^{\infty} (K_m C_F) k^{\ell-1} s^{\ell-2} X^{-(t+1)\ell}$$

$$= \frac{K_m C_F + (K_m C_F)^2 k_m (1-s_m) X^{-(t+1)}}{X^{(t+1)} - k_m s_m K_m C_F} \qquad \text{--- 5.39}$$

The derivation of the formulae to describe average molecular properties presented above differs from that proposed by Schellman[11]. He was principally concerned with developing models to describe the binding of multi-valent ligands and to this end he used a parameter to describe the interaction between adjacent ligands bound into a sequence of *unbound* sites. A single mode of binding is considered and a parameter y is defined as the additional weight of an unoccupied site due to the effect of bound ligand on either side. So for anti-cooperative binding such a site will be favoured to remain unbound and $y > 1$. This is in contrast to our parameter k which for anti-cooperativity $o < k < 1$. The evaluation of the empty site SGF, $U_0(X)$, now becomes:

$$U_0(X,y) = \frac{y}{X} + \sum_{i=z}^{\infty} X^{-i}$$

$$= \frac{y-1}{X} + \frac{1}{X-1}$$

$$= \frac{y(X-1) + 1}{X(X-1)} \qquad \text{--- 5.40}$$

This result may be compared with Schellman's equation 5 where z has not been included. It is immediately apparent that this approach has increased the order of Eqn. 5.27 which must be solved to obtain the critical value X_1. This will inevitably involve more complex numerical procedures for evaluation than are required for the derivation presented in this Chapter, despite the number of parameters being equivalent in both methods. To formulate models to describe monovalent ligand/DNA interactions the approach presented here, which aims to describe bound sequences on the lattice, is preferable to that of Schellman. The derivation I have presented is more closely aligned with that given by Ramstein *et al*[12] who presented models similar to models I and II in the following section.

(e) The models

It remains now to define the attributes of the physical process we wish to model, write SGFs in terms of the model and find the best parameter values to fit an experimentally obtained binding curve. Based on the parameter values so obtained, and on any other information known about the physical system, we can then determine if a given model fits the data and which of several possible models represents a best fit. As a first step, three models of increasing complexity which may possibly describe aminoacridine/DNA systems will be written and their behaviour with varying parameter values examined. This will aid us in choosing suitable models.

The three models I will describe are shown schematically in Fig. 5.4. Both models I and II contain cases of k = 1 which in effect yield two additional models so that five

(a)

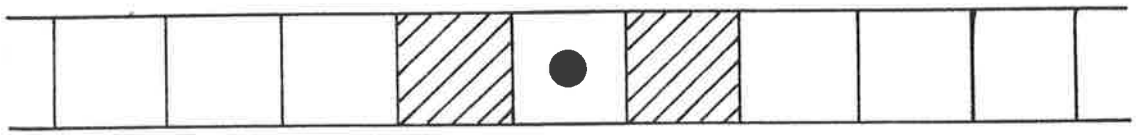

Two State model with cooperativity. Model I

(b)

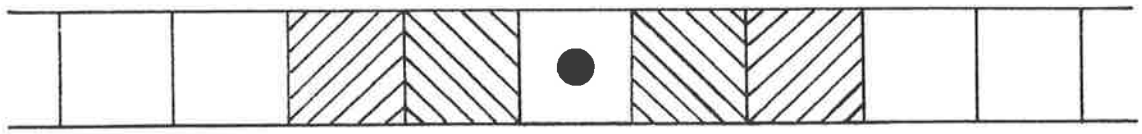

Two State model with nearest neighbour site-exclusion and cooperativity. Model II

(c)

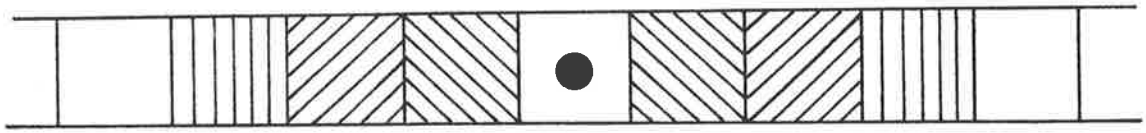

Two State model with nearest neighbour site-exclusion and dual cooperativity. Model III

LEGEND

Bound Ligand

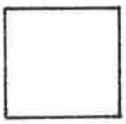

Vacant Site

Excluded Site

Cooperativity affected Site (k)

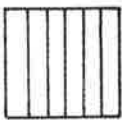

Cooperativity affected Site (s)

Figure 5-4. Schematic representation of binding models.

possible descriptions of binding behaviour will be dealt with in these models.

(1) MODEL I - Two state model with cooperativity.

If only one type of binding exists then there are only two types of site on the lattice, bound and empty, and Eqns. 5.27 and 5.31 become:

$$f(X,K,k,C_F) = \begin{vmatrix} 1 & -U_1 \\ -U_0 & 1 \end{vmatrix}$$

$$= 1 - U_0(X)U_1(X,K,k,C_F)$$

$$= 1 - \frac{U_1(X,K,k,C_F)}{X-1} = 0 \qquad \text{--- 5.41}$$

and $$r(K,k,C_F) = \left[- \frac{K}{X}\left(\frac{\partial f}{\partial K}/\frac{\partial f}{\partial X}\right)\right]_{X = X_1} \qquad \text{--- 5.42}$$

Substituting Eqn. 5.37 into 5.41 we get

$$f(X,K,k,C_F) = 1 - \frac{KC_F}{(X-1)(X-KkC_F)}$$

$$= X^2 - (1+KkC_F)X + (k-1)KC_F = 0 \qquad \text{--- 5.43}$$

The roots of this quadratic can be found utilizing the usual formula, which in this case becomes:

$$X = \tfrac{1}{2}(1 + KkC_F \pm \sqrt{\Delta})$$

where $$\Delta = (1 - KkC_F)^2 + 4KC_F \qquad \text{--- 5.44}$$

As both K and C_F must be positive in any real physical system, the largest root of Eqn. 5.43 is given as:

$$X_1 = \tfrac{1}{2}(1 + KkC_F + \sqrt{\Delta}) \qquad \text{--- 5.45}$$

This result and Eqn. 5.43 are now combined with Eqn. 5.42 which, on differentiation, yields:

$$r(K,k,C_F) = \left[-\frac{K}{X} \cdot \frac{-kC_FX + (k-1)C_F}{2X - (1+KkC_F)} \right]_{X = X_1}$$

$$= \left. \frac{[f(X,K,k,C_F) - X(X-1)]}{-X_1\sqrt{\Delta}} \right|_{X = X_1}$$

$$= \frac{X_1 - 1}{\sqrt{\Delta}} \qquad \text{--- 5.46}$$

thus $$r(K,k,C_F) = \tfrac{1}{2}\left[1 + \frac{KkC_F - 1}{\sqrt{\Delta}}\right] \qquad \text{--- 5.47}$$

To check the validity of this expression, consider the case of $k = 1$. In this instance there is no interaction between adjacent ligands so that the binding is independent. For this situation Eqn. 5.47 reduces to:

$$r(K,k,C_F) = \frac{KC_F}{1 + KC_F} \qquad \text{--- 5.48}$$

which is, of course, the Langmuir equation for one type of binding and $n = 1$. This is a necessary condition since the expressions used here are for lattice binding sites and *not* macromolecular repeating units.

Further examination of Eqn. 5.47 shows that for anti-cooperative binding, $k < 1$, values of r will be lower than for independent binding and that for cooperative binding, $k > 1$, values of r will be higher than for independent binding. It may be noted that this equation corresponds to the infinite, one-dimensional Ising model with nearest neighbour interactions.

This equation has been evaluated for several values of the parameters K and k and the results are presented as Scatchard Plots in Fig. 5.5. The value of K used, 9×10^4 M^{-1}, was chosen as typical of K values observed for the systems studied. The values of the cooperativity factor, k, cover the range 0.0001 to 3 so encompassing anti-cooperative, non-cooperative and cooperative behaviour. The ordinate

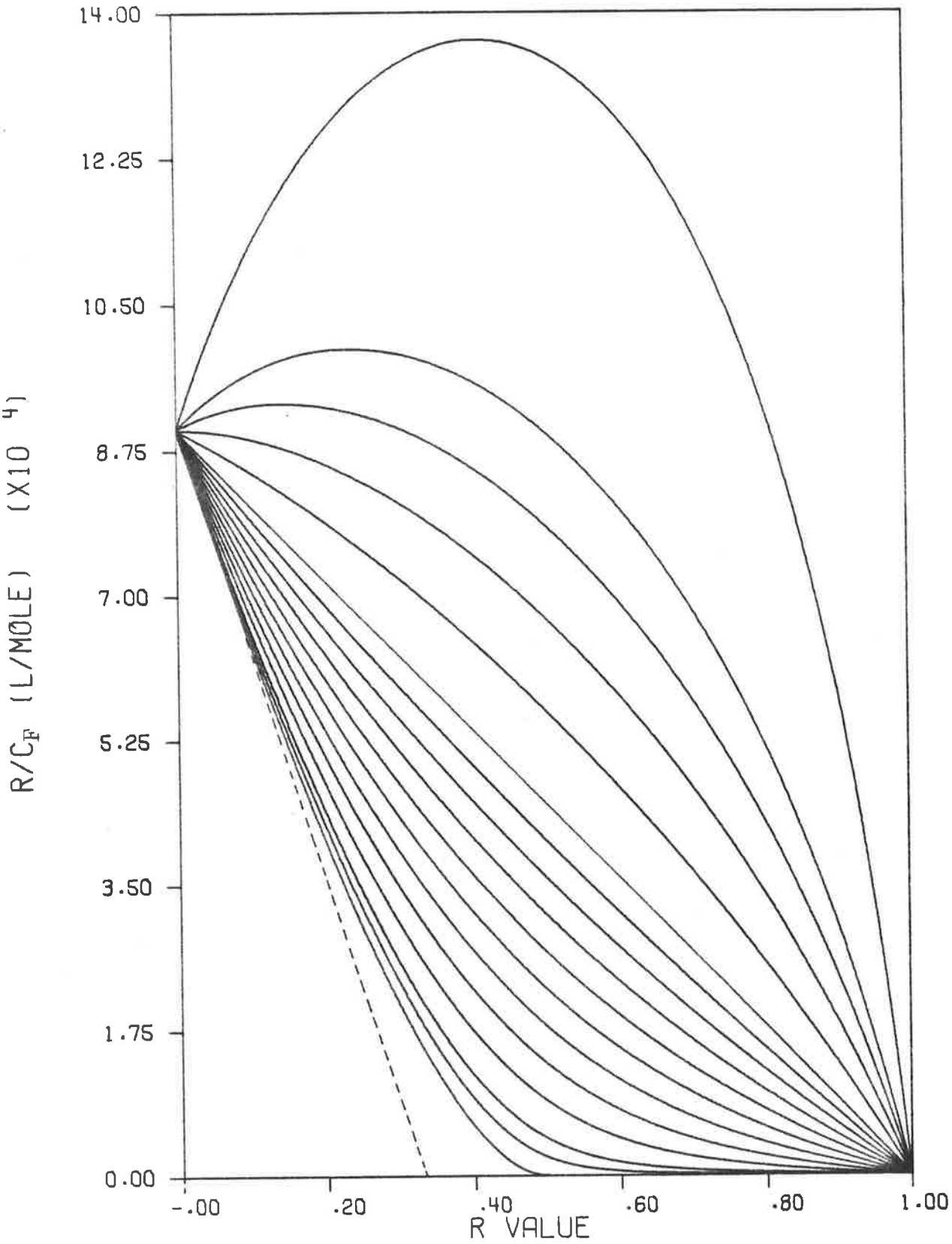

K = 9.0 x 10^4 M^{-1}; k values are 3, 2, 1.75, 1.5, 1.25, 1, 0.9, 0.8, 0.7, 0.6, 0.5, 0.4, 0.3, 0.2, 0.1, 0.05 and 0.0001 from top to bottom respectively. The dashed line is the upper limiting slope of the k = 0.0001 curve.

Figure 5-5. Scatchard plots of SGF model I.

intercept, which corresponds to K, is invariant however, the apparent abscissa intercepts decrease below the saturation value of r = 1 as the strength of the anti-cooperative interaction increases, i.e. as $k \to 0$. For $0 < k < 1$ a value of r = 1 is reached at sufficiently high C_F, however in practical cases visual inspection of experimentally obtained curves will always indicate an intercept of less than unity. The lower limiting abscissa intercept is 0.5 as k approaches zero. The approximately linear region of this curve at low r extrapolates to an intercept of 0.33. These observations of the behaviour of the function as $k \to 0$ can be explained in terms of the physical model. Since the anti-cooperative effect is of importance in aminoacridine/DNA systems, we shall examine this feature of the model in more detail. Three limiting behaviour cases for anti-cooperativity can be defined, for the limiting value of $k \to 0$, as follows.

(i) For small r, the binding is of the form shown in Fig. 5.6(a). The ligands tend to bind at sites remote from one another and so each ligand effectively occupies 3 lattice sites. The upper limit of this binding will correspond to an r value of $\frac{1}{3}$, the observed limiting slope for small r.

(ii) At higher r overlap of the anti-cooperativity affected sites will occur, since the anti-cooperative effect does not occur until the ligand actually binds to the lattice and is not propagated beyond the nearest neighbour. This is illustrated in Fig. 5.6(b) and leads to the apparent intercept of r = 0.5.

(iii) At very high C_F ligand may, in the limit, bind to every site (since $k \neq 0$) and so a value of r = 1 will be attained. It is highly unlikely that values of $r > 0.5$ will be observed in an experimental situation where k is very small.

(a)

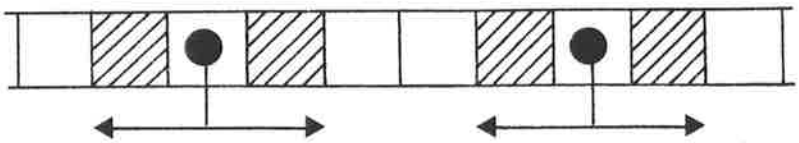

k → 0, low r. This demonstrates the apparent "site-exclusion" effect when ligands can bind in isolation from one another. Each ligand effectively occupies 3 sites.

(b)

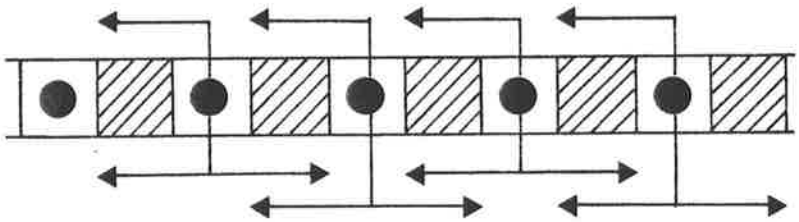

k → 0, high r. This demonstrates how the anti-cooperativity affected sites may overlap so that each ligand now effectively occupies 2 sites.

(c)

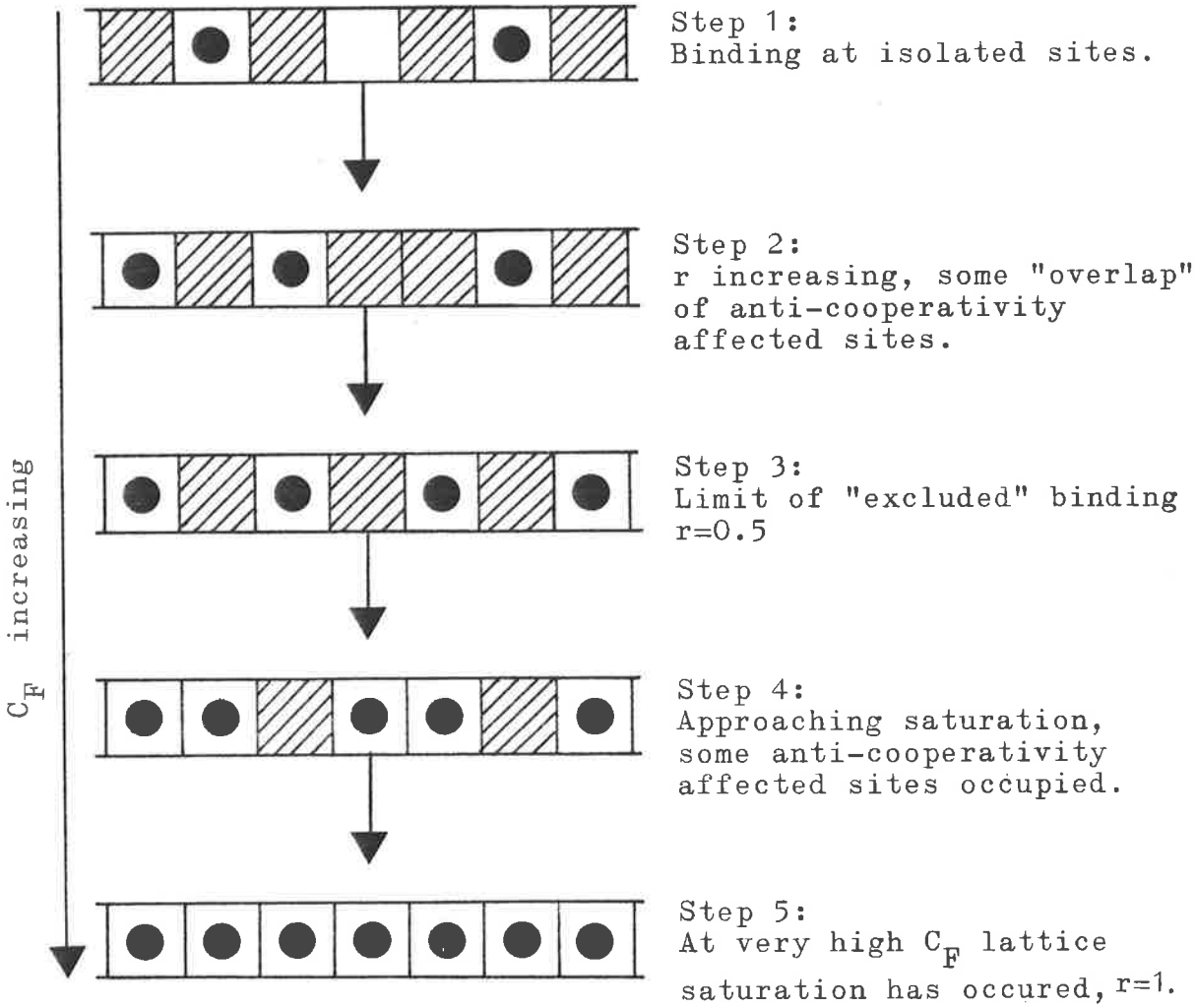

Figure 5-6. Schematic representation of anti-cooperativity effects in the Two State model (Model I).

The curves obtained for $0 < k < 1$ are a combination of these processes, which represent extremes of behaviour. The steps involved as C_F, and hence r, increases are shown in Fig. 5.6(c). The scale of C_F will depend on the value of k. The logical next step is to add true site-exclusion to this model to determine the effect of this on the behaviour of the model.

(2) MODEL II - Two state model with site-exclusion and cooperativity.

The introduction of the site-exclusion effect, through the use of Eqn. 5.38, means that ligand *cannot* bind to the lattice sites immediately adjacent to a bound ligand. Any cooperative effect, introduced if $k \neq 1$, will now act at sites removed from the bound site. Figure 5.4(b) shows the effects adjacent to a bound ligand.

The required SGF is given in Eqn. 5.38, where $m = N = 1$. The equation of $f(X,K,k,C_F)$, for t excluded sites, now becomes:

$$f(X,K,k,C_F) = 1 - \frac{KC_F}{(X-1)(X^{t+1} - kKC_F)}$$

$$= X^{t+2} - X^{t+1} - kKC_FX + (k-1)KC_F = 0$$

--- 5.49

and so r becomes:

$$r(X,K,k,C_F) = \frac{kKC_FX - (k-1)KC_F}{(t+2)X^{t+2} - (t+1)X^{t+1} - kKC_FX}\Bigg|_{X = X_1}$$

$$= \frac{X^{t+2} - X^{t+1} - f(X,K,k,C_F)}{(t+2)X^{t+2} - (t+1)X^{t+2} - kKC_FX}\Bigg|_{X = X_1}$$

$$= \frac{X^t(X-1)}{(t+2)X^{t+1} - (t+1)X^t - kKC_F}\Bigg|_{X = X_1}$$

--- 5.50

In the simplest case we consider a single excluded site, t = 1, so this result reduces to:

$$r(X,K,k,C_F) = \frac{X(X-1)}{3X^2 - 2X - kKC_F}\Bigg|_{X = X_1} \qquad \text{--- 5.51}$$

and the equation to be solved to find the critical value X_1, Eqn. 5.49, is:

$$f(X,K,k,C_F) = X^3 - X^2 - kKC_FX + (k-1)KC_F = 0 \qquad \text{--- 5.52}$$

Although the roots of this cubic can be found analytically and the largest positive root selected, a faster numerical procedure has been developed and is detailed in Appendix V.

This expression has been evaluated for the same values of K and k as were used for model I and the resultant curves are presented in Figs. 5.7 and 5.8. In this model there is no linear isotherm, the case of k = 1 corresponding exactly to the limiting case of k = 0 in model I. The concave curvature typical of cooperative interactions only appears for k > 1.65, a situation which arises because of the effect of site-exclusion. This can be conceived of as a limiting case of adjacent anti-cooperativity so that the two effects are opposed. It should be noted that for k values in the range 1.65 - 1.75 the isotherm will appear linear unless data for very high r values can be obtained (see Fig. 5.8). Only if this is possible can the distinction between an independent binding type and the more complex model described here be drawn.

The limiting values obtained from this model as $k \to 0$ are an abscissa intercept of 0.33 and the slope at low r corresponds to an abscissa intercept of 0.2. Consideration of the limiting anti-cooperative binding behaviour, as was done for model I, leads to an explanation of these values.

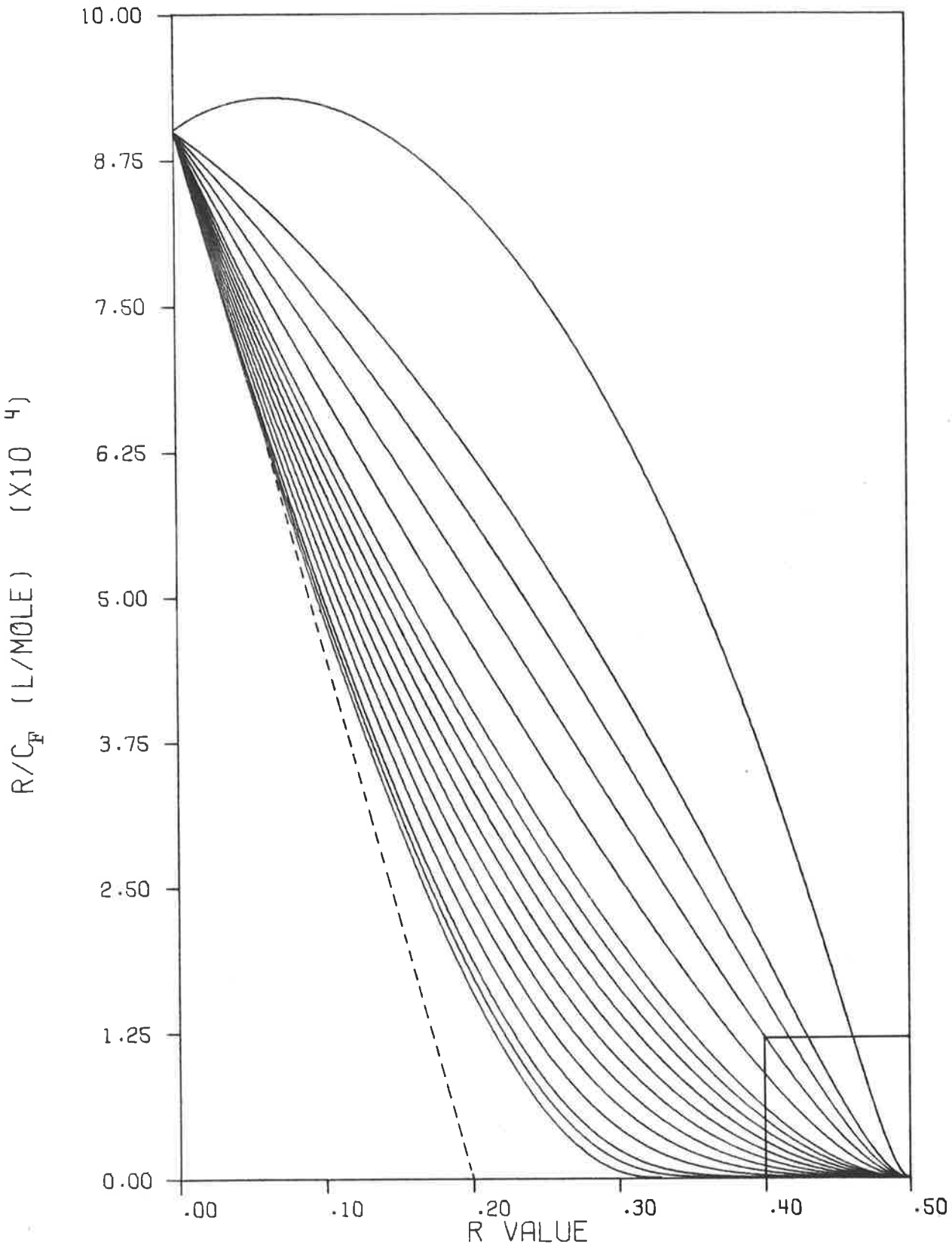

K = 9.0 x 10^4 M^{-1}; k values are 3, 2, 1.75, 1.5, 1.25, 1, 0.9, 0.8, 0.7, 0.6, 0.5, 0.4, 0.3, 0.2, 0.1, 0.05 and 0.0001 from top to bottom respectively. The dashed line is the upper limiting slope of the k = 0.0001 curve. The boxed section at high r values is that section plotted in Fig. 5-8 on an expanded scale.

Figure 5-7. Scatchard plots of SGF model II.

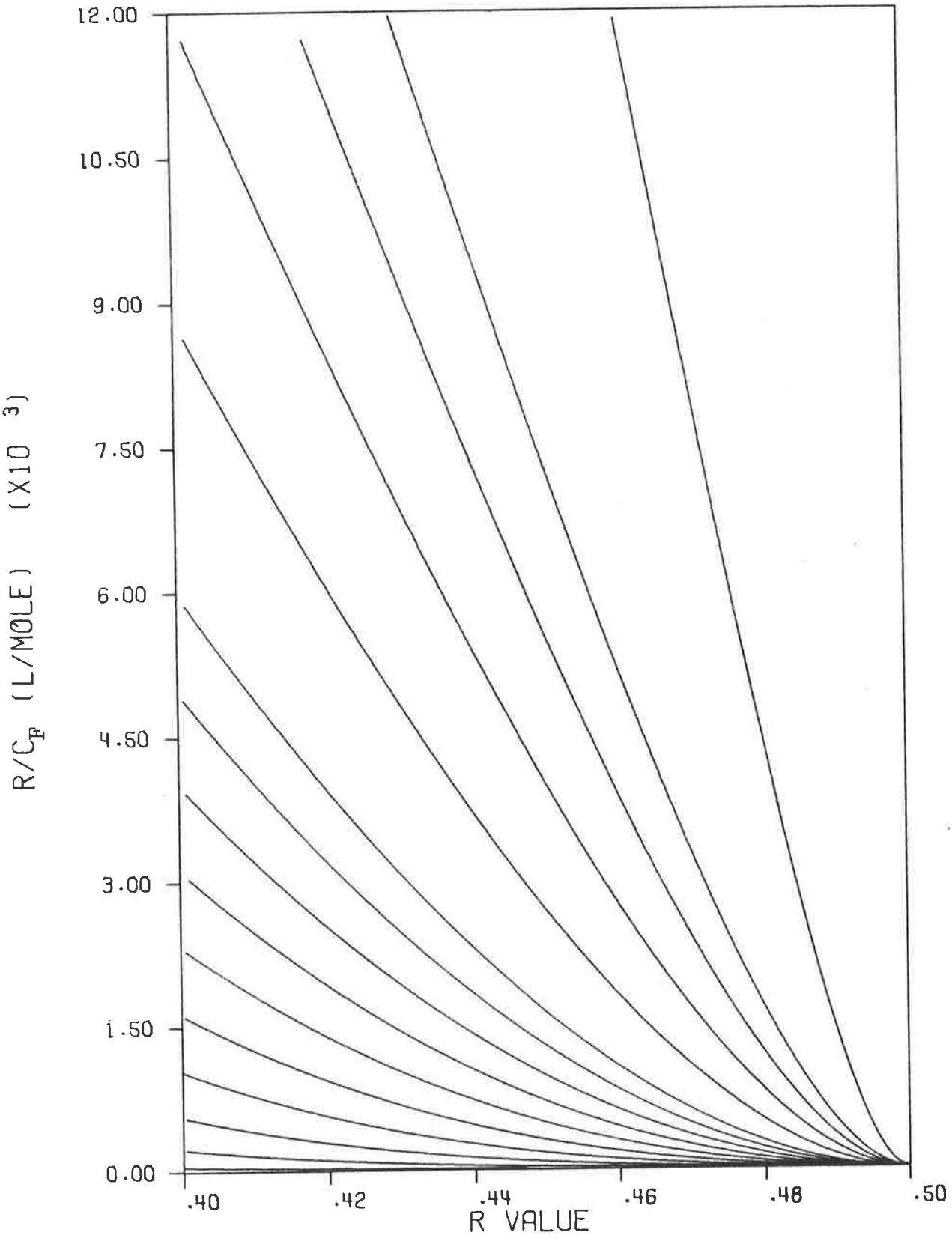

Figure 5-8. The expanded section of Fig. 5-7 showing that all the curves display curvature convex to the axes at high r values.

(i) For low r the "isolated" binding leads to a limit of one ligand bound per five lattice sites. This is illustrated in Fig. 5.9(a) and explains the lower limiting slope abscissa intercept of r = 0.2.

(ii) For higher r values the sites affected by anti-cooperativity may overlap and so each ligand may effectively occupy 3 sites without yet overlapping excluded sites. This situation is shown in Fig. 5.9(b).

(iii) For very high C_F, and hence r, only excluded sites will not be bound and, since these will overlap, the eventual abscissa intercept for all curves will be r = 0.5. This is shown in Fig. 5.9(c).

The curves obtained with this model for $0 < k < 1.65$ are the result of a combination of the limiting behaviours listed above, being somewhat more complex than for the first model due to the effect of site-exclusion. More than one site may be excluded simply by changing the value of t and rewriting Eqns. 5.49 and 5.50. This would only be warranted if experimental binding data appeared to have an intercept of $(t + 1)^{-1}$ on the abscissa, a situation not encountered in this work. The only other model not already covered which may be applicable to 9-aminoacridines/native DNA/0.10 M NaCl systems will extend the cooperative effect beyond a single site.

(3) MODEL III - Two state model with site-exclusion and dual cooperativity factors.

The extension of cooperativity to a second site is achieved by defining a second cooperativity weighting parameter, s. The SGF for this situation was previously defined, Eqn. 5.39. Assuming one excluded site, t = 1, the two equalities required are:

(a)

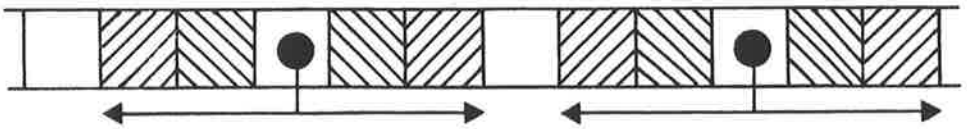

k → o, low r For this situation when the ligands bind in isolation on the lattice each ligand effectively occupies 5 sites.

(b)

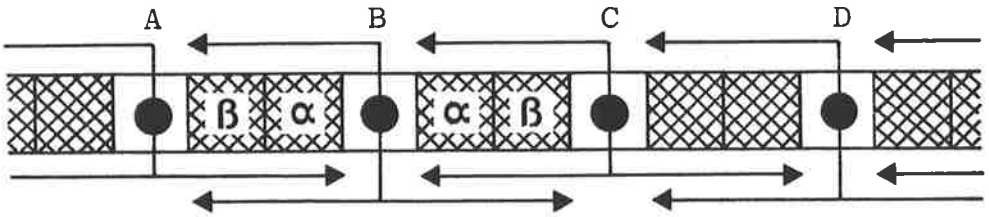

k → o, high r Double overlap of excluded sites and anti-cooperativity effected sites occurs so that sites excluded by ligand B, marked α, are subject to anti-cooperativity from ligands A and C and sites excluded by A and C, marked β, are subject to anti-cooperativity from B.

(c)

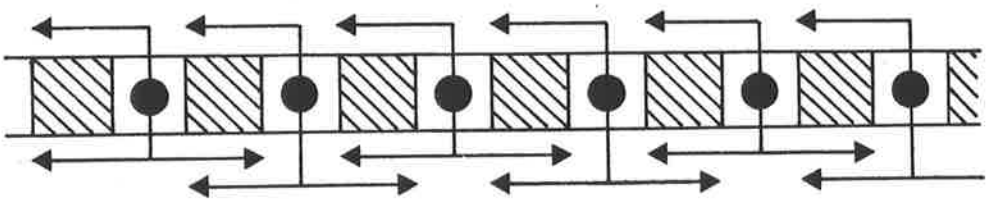

Lattice saturation occurs as $C_F \rightarrow \infty$. Note that every ligand has a vacant, excluded site on either side and that one ligand effectively occupies 2 sites. Overlap of excluded sites has occured.

Figure 5-9. Schematic Representation of anti-cooperative effects in the Two State excluded site with cooperativity model (MODEL II).

$$f(X,K,k,s,C_F) = 1 - \frac{KC_F + (KC_F)^2k(1-s)X^{-2}}{(X^2-ksKC_F)(X-1)}$$

$$= X^5 - X^4 - ksKC_FX^3 + (ks-1)KC_FX^2 + (KC_F)^2k(s-1) = 0$$

--- 5.53

and

$$r(X,K,k,s,C_F) = -\frac{K}{X}\left[\frac{-ksC_FX^3 + (ks-1)C_FX^2 + 2KC_F^2k(s-1)}{5X^4 - 4X^3 - 3ksKC_FX^2 - 2(1-ks)KC_FX}\right]\Bigg|_{X=X_1}$$

--- 5.54

A fast, numerical procedure to determine the critical largest root, X_1, has been developed and is given in Appendix V.

This model, which has not, to my knowledge, been described in the literature, may be tested for validity using the limiting case of $s \to 1$ when it should be identical to the previous model. This has been verified numerically. There are now two separate parameters to describe the cooperative effect so that analysis of the behaviour of the model is more complex. If we restrict the limits of the parameters as:

(1) If $k < 1$, then $1 \geq s > k$

(2) If $k > 1$, then $1 \leq s < k$

This essentially requires that cooperative effects fall off as the number of sites from a bound site increases. This need not be a requirement of the model as formulated, however I have not tested the behaviour of the model for conditions other than those listed above.

There are now two co-operativity parameters so that a simple set of related curves to illustrate the behaviour of this model, such as those presented for models I and II, is not possible. Rather than attempt a limiting behaviour analysis, I shall consider model III as an extension of model II. The salient difference between this model and

model II lies in the type of curvature which can be obtained in the curves when both k and s are used to generate a co-operative effect. Figure 5.10 shows a set of curves for $k = 0.5$ and $0.5 < s < 1$. The effect of gradually introducing the second anti-cooperative weight, s, is seen to modify the slope of the curves. The initial slope as r increases from zero becomes steeper as s decreases and the final slope is less steep, relative to the initial slope, than in the case of only one anti-cooperative weight factor. A second feature is how closely curves from model III can be made to match those of model II. Since there are two weights associated with model III, the k value used will always be greater than that for model II. If we chose a k of 0.5 for model II then the effective total weight for two sites, the one affected by k and its adjacent unaffected site of weight 1, is 1.5. We may compare this curve with one generated from model III using $k = 0.74$ and $s = 0.76$, again a total weight of 1.5 for the two sites. These curves are shown in Fig. 5.11. Although agreement between these two curves is good, the curve from model III is lower in r/C_F values until $r = 0.33$ is reached. This reflects the fact that in model III the second site is subject to an anti-cooperative effect whereas this site is unaffected in model II. Once all the second sites are occupied, i.e. $r > 0.33$, then as expected the model II curve is of lower r/C_F values. This kind of behaviour leads to the more pronounced curvature observed for curves from model III.

5. Analytical solution models

An analytical solution for some models of the type presented in the previous section has been published by McGhee and von Hippel[13]. Their interest in binding models

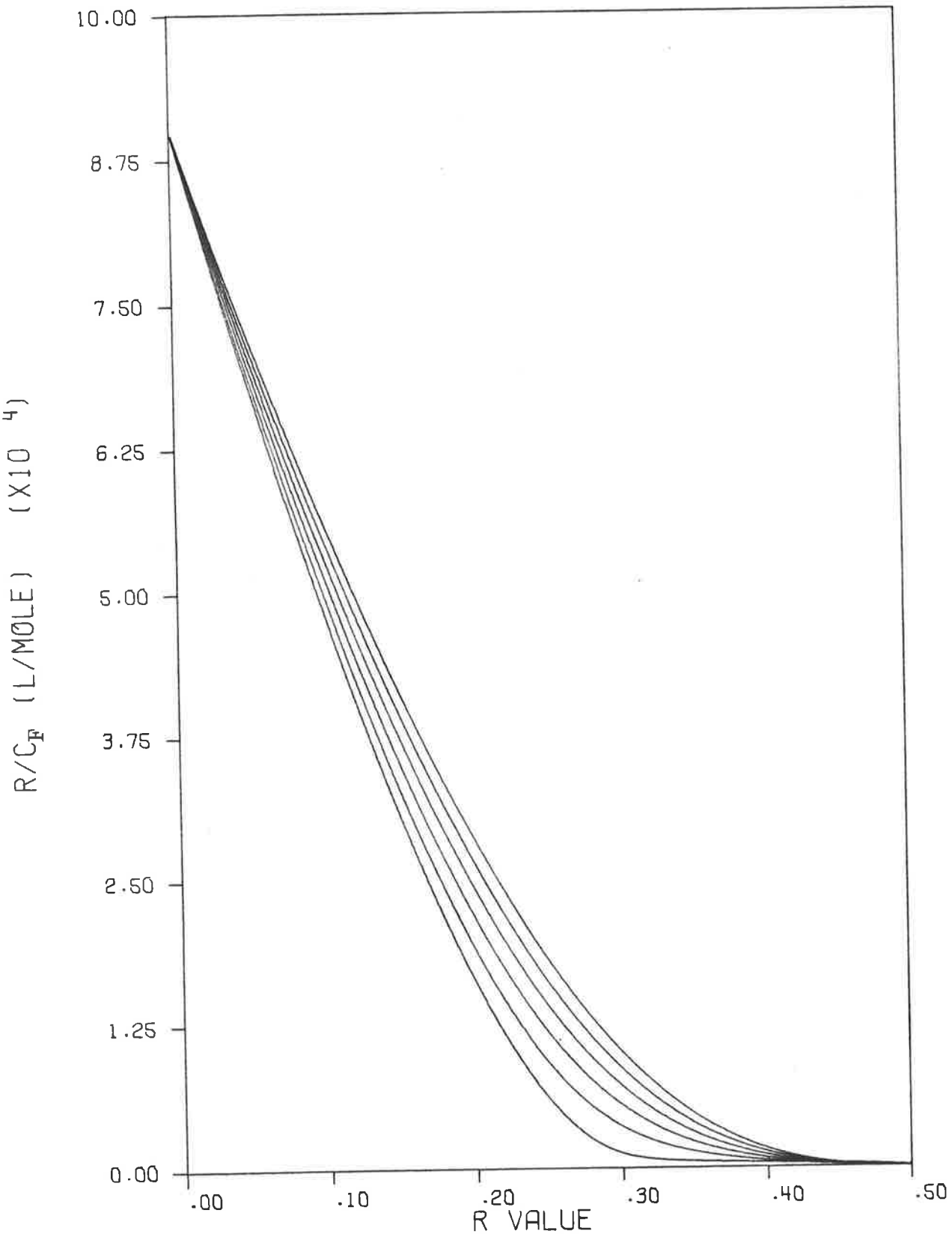

$K = 9.0 \times 10^4\ M^{-1}$, k = 0.50, s values are 0.999, 0.9, 0.8, 0.7, 0.6 and 0.51 from top to bottom respectively.

Figure 5-10. Scatchard plots of SGF model III.

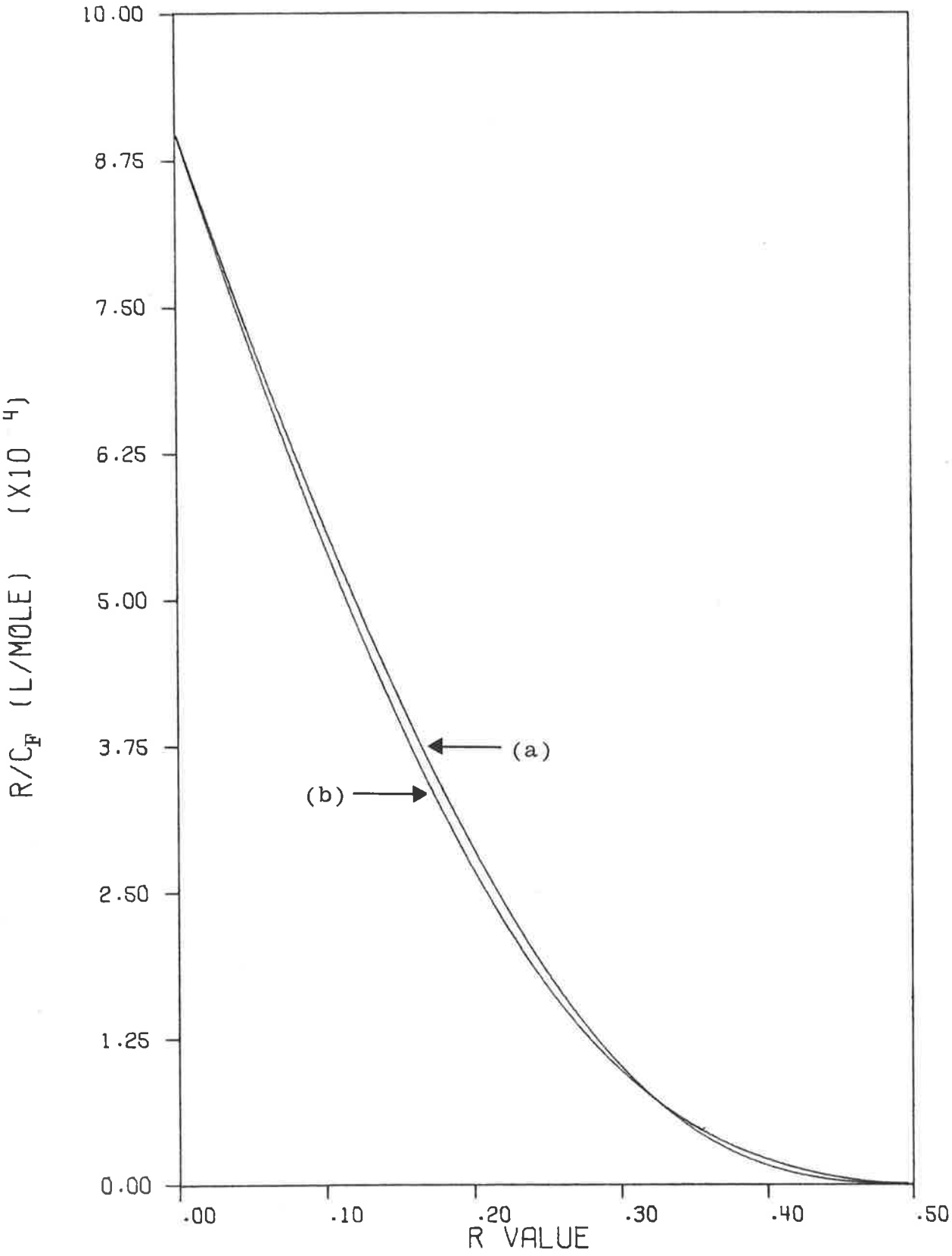

(a) SGF model II; $K = 9.0 \times 10^4\ M^{-1}$, $k = 0.50$.

(b) SGF model III; $K = 9.0 \times 10^4\ M^{-1}$, $k = 0.74$, $s = 0.76$.

Figure 5-11. Scatchard plots of SGF model II and SGF model III of comparable anti-cooperative weighting (see text).

arose from a need to treat the binding of multi-valent ligands to DNA. They proposed that the curvature observed in Scatchard plots arose from either effective site overlap when binding multi-valent ligands, or cooperativity in the binding process, or a combination of both these effects. From the consideration of conditional probabilities for site occupation when binding n-valent ligand to an infinite, one-dimensional, homogeneous lattice of binding sites, they arrived at two expressions relating the fraction of occupied binding sites, r, to the free ligand concentration, C_F.

The first of these describes the binding of n-valent ligand to the lattice assuming a single type of binding and no inter-ligand interactions. Their equation 10 may be written, with the nomenclature used here, as:

$$\frac{r}{C_F} = K(1-nr).\left[\frac{1 - nr}{1 - (n-1)r}\right]^{n-1} \qquad \text{--- 5.55}$$

where n is the number of sites occupied by *each* ligand. For n = 1 this equation reduces to the Scatchard equation[10] for a single binding mode. For n = 2 or greater the values of r/C_F produced are always less than for n = 1 so the characteristic binding curve convex to the axes is obtained. The abscissa intercept is 1/n and the ordinate intercept is K. This expression may be expanded to cover i different binding modes for i different ligands[13].

Nearest neighbour co-operativity may now be introduced and the model reformulated as:

$$\frac{r}{C_F} = K(1-nr).\left[\frac{(2k-1)(1-nr) + r - R}{2(k-1)(1-nr)}\right]^{n-1}.\left[\frac{1-(n+1)r + R}{2(1-nr)}\right]^{2} \qquad \text{--- 5.56}$$

where $$R = \sqrt{[1 - (n+1)r]^2 + 4kr(1-nr)} \qquad \text{--- 5.57}$$

This expression is equivalent to equation (15) of McGhee and

von Hippel although it should be noted that Eqn. 5.56 is the correct form as the published equation contains typographical errors. This equation reduces to Eqn. 5.55 for k = 1[13]. The cooperativity factor, k, applies only to nearest neighbour site interactions. The ordinate and abscissa intercept are as for Eqn. 5.55 although for very low values of k the abscissa intercept may appear to be lower than 1/n for experimentally obtainable C_F values. Equation 5.56 produces identical numerical results with those of SGF model II for the same K and k values when n = 2. Figure 5.7 then applies equally to Eqn. 5.56 with n = 2. This indicates that Eqn. 5.56 with n = 2 exactly simulates single site-exclusion for a uni-valent ligand. This simulation of site-exclusion is quite general and multi-site-exclusion effects are treated by setting the n of Eqn. 5.56 equal to the (t+1) parameter of the SGF model II. This provides a convenient alternative to the treatment of site-exclusion effects, especially if a large number of excluded sites are involved. In these cases the order of the polynomial which must be solved to apply the SGF model II, becomes large with rapidly increasing numerical complexity. The cost involved in by-passing the SGF method is the loss of the many other average properties of the system which can be obtained via the SGF method.

(a) The implicit conditions

Before applying the Eqns. 5.55 and 5.56, two important conditions must be considered.

(1) The lattice on which the derivation is based is a lattice of binding sites and so the unit binding site on a macromolecule must be defined before applying the equations. All experimentally obtained binding data must be expressed in

terms of this unit binding site, it is not sufficient to use any macromolecular repeating unit.

(2) The probability expressions on which the derivation is based do *not* allow for fractional site occupation. A site is either occupied or vacant as these are time-independent models. Therefore, solutions involving non-integer n values have no meaning in the context of these models.

A simple example may help to clarify the importance of point (1). If we supposed that a ligand bound to 8 consecutive phosphate groups on the same strand of a native DNA double helix, and that ligands could bind independently on both strands, then n would be 8 and binding data calculated on the basis of DNA phosphate residues as the unit binding sites could be fitted to Eqn. 5.55. We may now use Eqn. 5.55, a K value of 4.5×10^4 M^{-1} and an n value of 8 to calculate some "perfect" data for our paper experiment. Figure 5.12 shows the curve for these parameter values and the "data points" taken from this curve. These data are now transformed by considering two phosphate residues to be the unit binding site. We would now expect to find n = 4 and $K = 9.0 \times 10^4$ M^{-1}. The result of this transformation of the data and the attempted fit of the new parameter values is shown in Fig. 5.13, together with the original data and fit for comparison. It is obvious that the curve does not fit the data. The use of n = 4 has under-estimated the site overlap effect. Indeed no combination of values of K and n can be found to fit this transformed data. If the range of the r values is reduced and experimental error introduced, so more closely approaching a real experimental data set, apparently good fits may be obtained, especially if fractional n values are allowed in the fitting procedure. The original choice of the unit

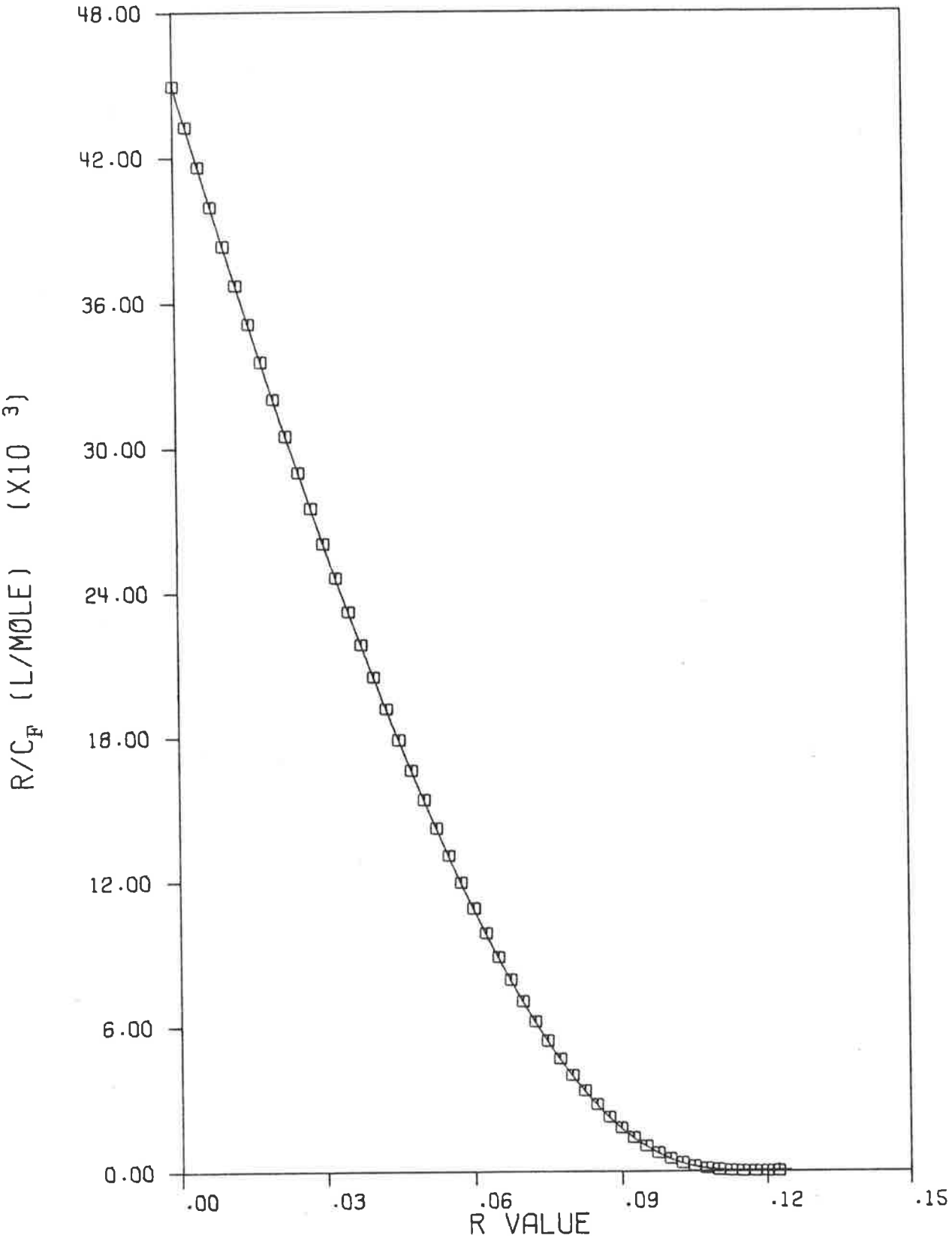

Figure 5-12. Scatchard plot from the application of McGhee and von Hippel's first equation (ie. Eqn. 5.55) with $K = 4.5 \times 10^4\ M^{-1}$ and $n = 8$. The "data points" selected are marked on the curve.

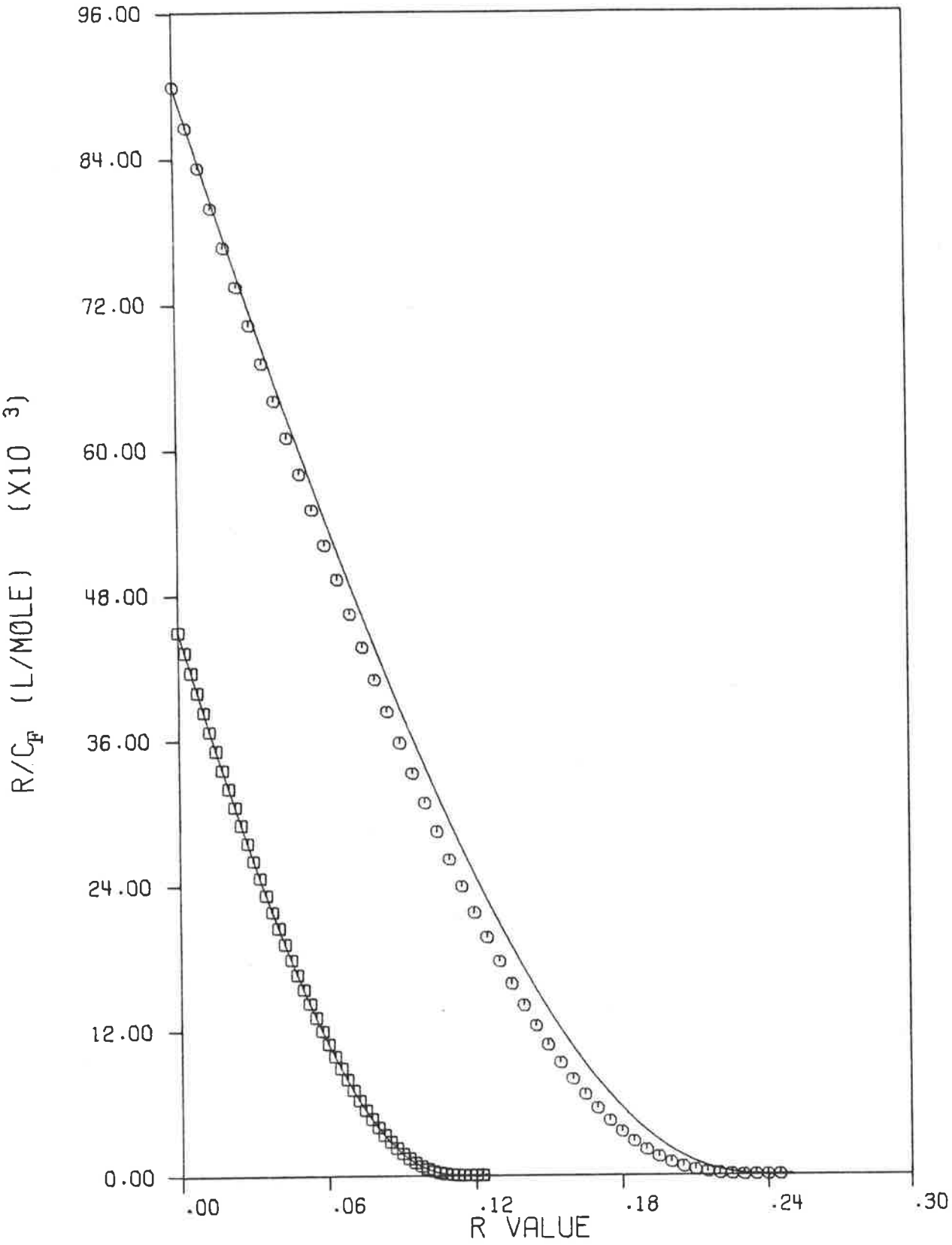

Figure 5-13. Scatchard plots of the "data points" transformed to K = 9.0 x 10^4 M^{-1} and n = 4 and the fitted curve for these parameters. The original data and curve are shown for comparison.

binding site and strict adherence to integer n values are crucial to a meaningful modelling of the physical processes using these equations. Providing these conditions are recognised, the analytical solutions of McGhee and von Hippel present a convenient alternative to the SGFs for the two simple models they describe. They suffer the disadvantages of being unable to evaluate other system average properties and cannot describe more complex binding models.

6. Heterogenous lattice methods

Before proceeding to examine possible models for the binding of 9-aminoacridines to native DNA I shall briefly mention the method of modelling heterogenous lattices. Crothers[4] has presented a method for such modelling in which a heterogenous lattice is generated using random number methods. This lattice can be constrained to have the same GC content as the DNA being modelled, however the distribution of "bases" along the lattice is random and as such is only an approximation to the DNA sequence which is not random in natural DNA. For very large DNA molecules the approximation of a random base sequence will generally not represent a serious error. How well such a lattice approaches true randomness and the appropriate base composition, depends on the number of units in the lattice which must in any case be large enough to enable end-effects to be ignored. Crothers[4] states that a length of 500 gives a base-composition within 2% of the desired figure. Furthermore a statistical fluctuation of 2% is observed between different lattices so generated, which represents the departure from true randomness of the lattices. These errors could be reduced by increasing the length of the lattice. However the lattice length must be increased geometrically to obtain linear decreases in the error.

The binding parameters are calculated using Montroll's Matrix methods to calculate a partition function and hence, by differentiation, r. This method of calculating binding parameters is, by its nature, inexact. It does however represent the best available method of formulating binding models in terms of heterogenous lattice types.

7. Concluding remarks

In this Chapter I have examined various techniques for the derivation of mathematical models to describe the binding of ligands to DNA. Of these methods the SGFs are the most fruitful approach to the problem. This technique allows both simple and more complex models to be developed and has the potential to provide any desired average property of a model. The analytical solutions of McGhee and von Hippel[13] have the advantage of being more easily applied to systems for which either of their two models is suitable. Analytical solutions are, however, less flexible than the SGF approach.

The emphasis in this work is on models of a single equilibrium constant binding to a homogeneous lattice. A number of such models which may describe the interaction of 9-aminoacridines with DNA are presented. In Chapter VI I shall examine the application of these models to the binding data determined in this work, choose the model of best fit and discuss the parameters derived from this model.

REFERENCES

1. Langmuir I., *J.A.C.S.*, 38, 2221 (1916).
2. Langmuir I., *J.A.C.S.*, 39, 1848 (1917).
3. Peacocke A.R. and Skerrett J.H.N., *Trans. Farad. Soc.*, 52, 261 (1956).
4. Crothers D.M., *Biopolymers*, 6, 575 (1968).
5. Armstrong R.W., Kurucsev T. and Strauss U.P., *J.A.C.S.*, 92, 3174 (1970).
6. Lifson S., *J. Chem. Phys.*, 40, 3705 (1964).
7. Lifson S. and Bradley D.F., in "Molecular Associations in Biology", ed. B. Pullman, Academic Press, New York, pp. 261-270.
8. Tanford C., in "The Physical Chemistry of Macromolecules", J. Wiley and Sons Inc., Chapter 8.
9. Blake A. and Peacocke A.R., *Biopolymers*, 6, 1225 (1968).
10. Scatchard G., *Ann. N.Y. Acad. Sci.*, 51, 660 (1949).
11. Schellman J.A., *Isr. J. Chem.*, 12, 219 (1974).
12. Ramstein J.M., Leng M. and Kallenbach N.R., *Biophys. Chem.*, 5, 319 (1976).
13. McGhee J.D. and von Hippel P.H., *J. Mol. Biol.*, 86, 469 (1974).

CHAPTER VI

Mathematical models and thermodynamic parameters for the interaction.

CONTENTS

1. Introduction

In order to simplify the choice of the mathematical model which best fits the experimental binding curves, the information available concerning the binding process will be examined with a view to defining constraints to be placed on the model. The systems studied are all 9-aminoacridines binding to *E. Coli* native DNA in 0.10 M NaCl at temperatures between 10°C and 50°C. The reader is referred to Chapter II of this work, which contains a summary of the considerable literature dealing with the binding of aminoacridines to DNA, for specific references which will not in general be duplicated here for the sake of brevity.

2. Constraints on the model

The pertinent points which serve to define suitable models are summarized as follows:

(1) A basic observation is that the binding process in high ionic strength solvent is by intercalation of the aminoacridine molecule between adjacent base pairs of the native DNA helix. The lattice for the binding model then must represent consecutive interstices between adjacent base pairs of the helix.

(2) In the case of most of the 9-aminoacridines studied in this work the sets of spectra used to define the binding curves are internally linear throughout the accessible range of T_L/T_A. This observation implies that there are only two spectrally distinct forms of the aminoacridine in solution, one of which will be free aminoacridine. The implication is therefore that either there is a single unique bound form of

(2) (Continued)

aminoacridine or if more than one spectrally distinct bound form exists then the ratio of those forms to one another is invariant. In either case there will be a single, unique apparent equilibrium constant for the interaction.

(3) The Scatchard plots of the binding data show marked curvature convex to the axes and indicate that effective binding saturation occurs at less than one aminoacridine bound per base pair. The highest observed r value is about 0.33. These observations indicate that there is either an anti-cooperative effect or a site exclusion effect or both operating in the system. A subjective observation of the binding curves suggests that the curvature is not due to site-exclusion alone since this effect produces sharp curvature as $r/C_F \rightarrow 0$, and less apparent curvature at lower r values than is observed experimentally.

To summarize, the model must represent the intercalation of aminoacridine molecules into a lattice of the interstices between the DNA base pairs. The interaction will be described by a single K value and be subject to site-exclusion and/or anti-cooperativity effects.

3. Trial models

The following models may describe the interaction.

(1) Single K, one or two excluded sites.

(2) Single K, one or two anti-cooperativity affected sites.

(3) Single K, one excluded site with one or two anti-cooperativity affected sites.

These trial models were fitted to the experimentally observed binding curves using a non-linear fitting procedure, program NONLIN. Appendix V contains details of the algorithm and methods used to assess convergence of the fit. A plot of the residuals is used as the single most useful diagnostic of the goodness of fit of the model to the experimental binding data, both for individual models and for comparison between different models. Figures 6.1, 6.2 and 6.3 contain the resultant curves for the fitting of these models to the 9-aminoacridine/*E. Coli* DNA/0.10 M NaCl system at 22°C as an example. The behaviour of this system is typical of all the 9-aminoacridines studied. Taking each of the three types of model, the following observations may be made.

(1) The use of site-exclusion alone is unsatisfactory. The residuals are large and systematic and the type of curvature produced in the fitted curve does not match that of the experimentally observed binding data. These curves are shown in Fig. 6.1.

(2) The use of one anti-cooperativity affected site is not indicated since k tends to zero and the result is similar to one excluded site. Two anti-cooperativity affected sites produces a better result, although one of the parameters tends to zero indicating again that a single excluded site is required. These curves are shown in Fig. 6.2.

(3) The single excluded site, single anti-cooperativity affected site model fits the data well, there being only small residuals when compared to the maximum possible experimental error. These small residuals however, systematically deviate from the observed data. The

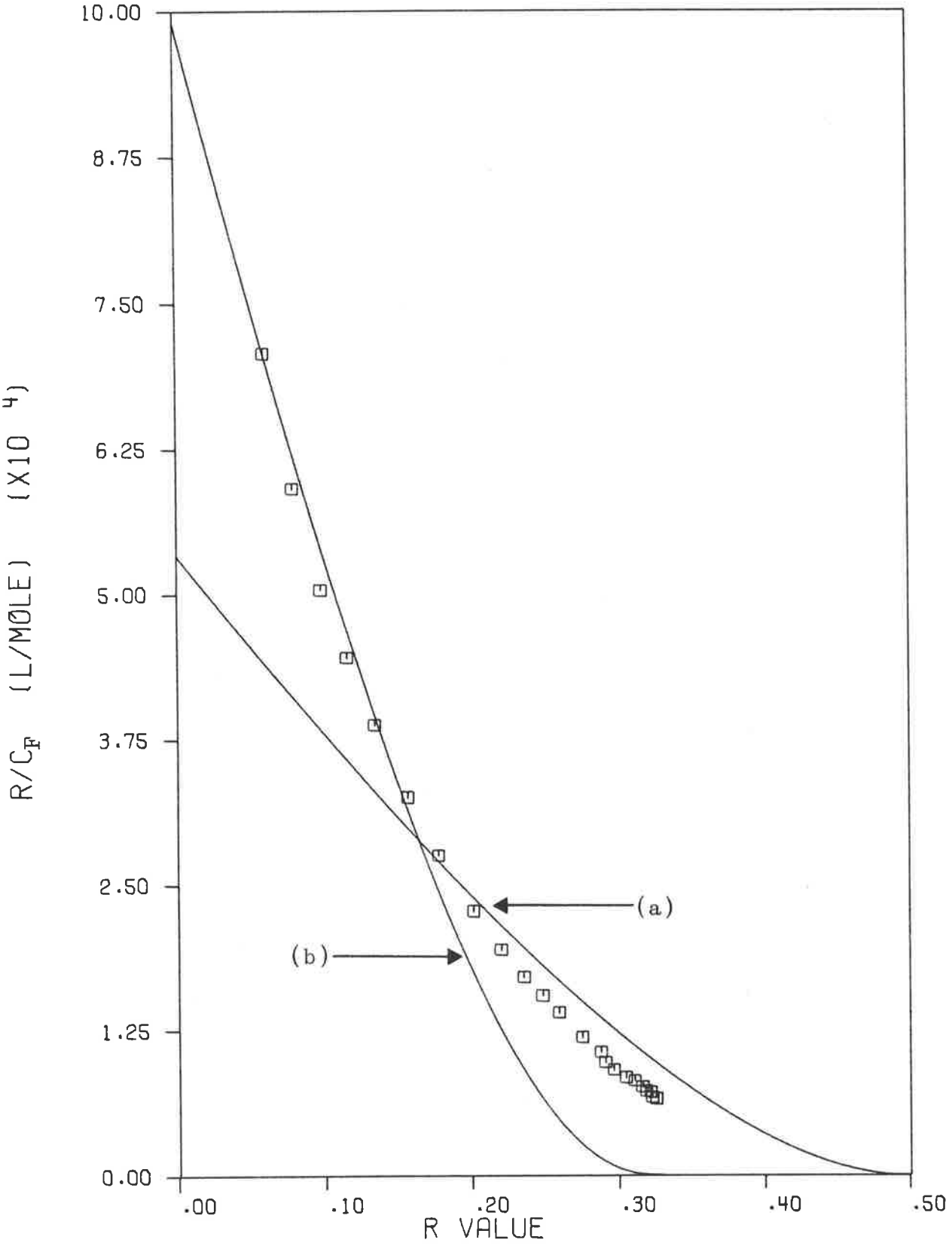

(a) $K = 5.23 \times 10^4\ M^{-1}$; one type of binding with one excluded site.
(b) $K = 9.89 \times 10^4\ M^{-1}$; one type of binding with two excluded sites.

Figure 6-1. Scatchard plots of binding data for the 9AA/*E Coli* DNA/0.10 M NaCl system at 22°C together with fitted curves for excluded site models.

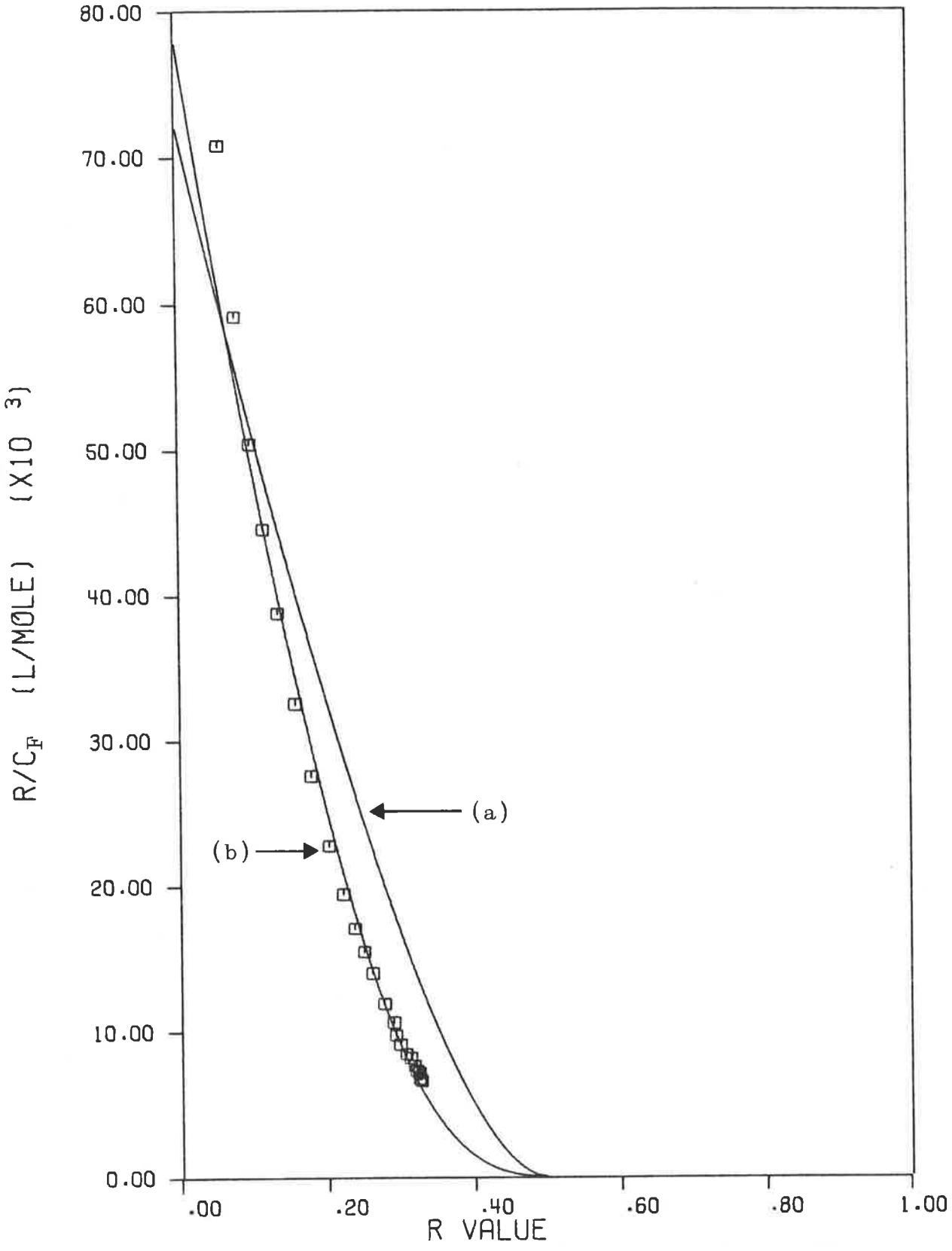

(a) $K = 7.21 \times 10^4\ M^{-1}$, $k = 1 \times 10^{-6}$; one type of binding with one anti-cooperativity affected site.
(b) $K = 7.80 \times 10^4\ M^{-1}$, $k = 1 \times 10^{-5}$, $s = 0.51$; one type of binding with two anti-cooperativity affected sites.

Figure 6-2. Scatchard plots of binding data for the 9AA/*E Coli* DNA/0.10 M NaCl system at 22°C together with fitted curves for anti-cooperativity affected site models.

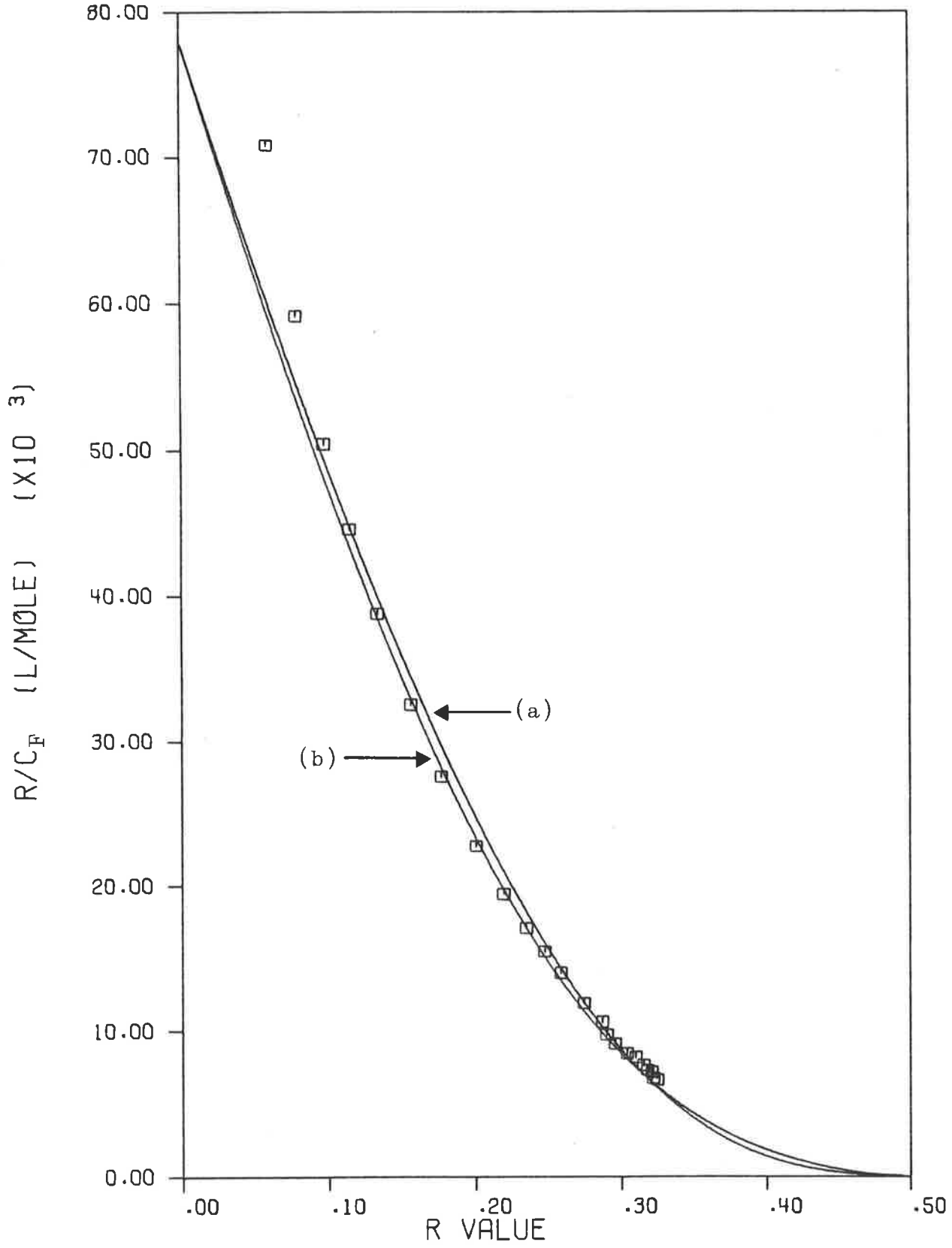

(a) $K = 7.799 \times 10^4\ M^{-1}$, $k = 0.495$; one type of binding with one excluded site and one anti-cooperativity affected site.
(b) $K = 7.81 \times 10^4\ M^{-1}$, $k = 0.74$, $s = 0.75$; one type of binding with one excluded site and two anti-cooperativity affected sites.

Figure 6-3. Scatchard plots of binding data for the 9AA/*E Coli* DNA/0.10 M NaCl system at 22°C together with fitted curves for excluded site with anti-cooperativity affected site models.

(3) (Continued)

curvature generated allowing only one anti-cooperavity affected site will not precisely fit the experimentally observed curvature in some cases. As a refinement of this model the anti-cooperative effect was extended to two sites. This results in a better fit to the experimental data in cases where small systematic deviations were observed with the single anti-cooperativity affected site.

4. The model of best fit

From these trial models it is concluded that the models which best fit the experimental binding data include a single excluded site and one or two anti-cooperativity affected sites. The model with only two anti-cooperativity affected sites may also fit the data. Two points which require further discussion arise from these conclusions. The first concerns the difference between the single excluded-site model with a single anti-cooperativity affected site and the model with two anti-cooperativity affected sites. Within the range over which experimental binding data can be collected, that is up to an r value of about 0.35, the former of these two models is essentially identical to the limiting case of the latter when the first cooperativity parameter tends to zero. The difference between the two occurs at very high, probably physically unattainable, aminoacridine concentrations when the former model reaches an ultimate r value of 0.5 and the latter an ultimate r value of 1.0. The essence of the difference lies in whether binding above an r value of 0.5 is forbidden in site-exclusion or whether this site has become so unfavourable due to anti-cooperativity that an unresolveable

increment in binding is possible above r = 0.5 if the aminoacridine concentration is extremely high. This difference between these two situations is of little consequence to a physico-chemical study of the binding since it is unlikely that this difference could be discerned by physico-chemical techniques. The question of whether there is any biological consequence of this difference is beyond the scope of this work. The preferred model is the site-exclusion case since this involves fewer parameters and describes the physico-chemical situation as well as the two anti-cooperativity affected sites model.

The second point concerns the extent of the anti-cooperativity effect. It is observed that some of the aminoacridines studied showed small systematic variations between the observed data and the fitted curves for the one excluded-site and one anti-cooperativity affected site model at some temperatures. Further, the introduction of a second anti-cooperativity affected site removes this deviation. However this deviation is very small and may be due to small systematic errors in the binding data arising, for instance, from a choice of ϵ_B^{λ}. It is not observed for most of the systems studied. In the light of these observations, the introduction of this second anti-cooperativity affected site is probably an unwarranted complication of the model. The preferred model is that with a single anti-cooperativity affected site since this model adequately describes all the systems studied in terms of two parameters.

The resultant best fit curves for this model to each experimentally determined binding curve are plotted as lines on the data presented in Appendix III. The chosen values for the equilibrium constants, K, and the cooperativity factors, k,

are displayed in tabular form in Section 5(b) of this Chapter.

5. Thermodynamic parameters

(a) Introduction

A study of the temperature variation of the equilibrium constant, K, governing the reaction yields values of the thermodynamic parameters for the reaction. The parameters which can be evaluated are ΔG°, ΔH° and ΔS°, the free energy, enthalpy and entropy of reaction respectively. The following fundamental thermodynamic relationships are used to obtain the required parameters.

$$\Delta G^\circ = -RT\ln K \qquad \text{--- 6.1}$$

$$\Delta G^\circ = \Delta H^\circ - T\Delta S^\circ \qquad \text{--- 6.2}$$

ΔG° is obtained from Eqn. 6.1. Substitution of Eqn. 6.1 into Eqn. 6.2 yields:

$$\ln K = -\frac{\Delta H^\circ}{R}\left(\frac{1}{T}\right) + \frac{\Delta S^\circ}{R} \qquad \text{--- 6.3}$$

A plot of lnK versus $^1/_T$ will yield a straight line of slope $-\Delta H^\circ/R$ if the enthalpy change of the reaction is independent of temperature over the temperature range studied. This relationship is often called the Van't Hoff plot. The error in K was obtained from the non-linear fitting program as the standard deviation of the fitted value of K. The error in ΔG° is obtained from the error in K, through Eqn. 6.1, assuming that T is free of error. The error associated with ΔH° is obtained from a weighted linear regression of the lnK versus $^1/_T$ plot where T is assumed to be free of any error. This error is then the standard error of the slope of this regression line.

The evaluation of ΔS° is more complex. This value has often been obtained[1,2] from substitution of ΔG°, ΔH° and T into Eqn. 6.2. In the absence of any independently measured value of ΔH° this procedure yields a poor estimate of ΔS° associated with large errors. This is clearly seen from Eqn. 6.3. The value of ΔS° is obtained as the intercept of the Van't Hoff plot. The extrapolation required is unacceptably large as is reflected in the standard error of the intercept obtained from such extrapolations. A better method of evaluating ΔS° is from Eqn. 6.2. A plot of ΔG° versus T will yield a straight line of slope $-\Delta S^\circ$. This method requires no extrapolation from the range of measured data and the error is obtained as the standard error of the slope from the weighted linear regression line.

(b) Parameter values

The values of K and the cooperativity parameter k obtained from the non-linear fitting procedure for the 9AA/*E. Coli* DNA/0.10 M NaCl system are shown in Table 6.1. The plots associated with the determinations of ΔH° and ΔS° are shown in Fig. 6.4. The same parameters and plots for the methyl, butyl, n-hexyl and cyc-hexyl derivatives are shown in Tables 6.2 to 6.5 and Figures 6.5 to 6.8 respectively.

The ΔG° for the interaction is similar for all the compounds studied, falling in the range -26 to -28.5 kJ/mole. These values may be compared to values for Proflavine[1,4] and Acridine Orange[2] in the range -32 to -42 kJ/mole and to the values obtained by Turner[3] for 9-aminoacridine under similar conditions of -35 kJ/mole by equilibrium spectrophotometry and

TABLE 6.1

The equilibrium constants, cooperativity parameters and the thermodynamic parameters for the 9AA/*E Coli* DNA/0.10 M NaCl system.

Temperature (°C)	10	22	35	50
K x 10^{-4} (M^{-1})	12.810	7.799	4.567	2.657
S.D. x 10^{-4} (M^{-1})	0.339	0.197	0.102	0.081
k	0.532	0.495	0.572	0.517
S.D.	0.161	0.021	0.024	0.039
$\Delta G°$ (kJ $mole^{-1}$)	-27.687	-27.642	-27.489	-27.371
S.D. (kJ $mole^{-1}$)	0.061	0.062	0.058	0.083
$\Delta H°$ (kJ $mole^{-1}$)	-30.991			
S.E. (kJ $mole^{-1}$)	0.332			
$\Delta S°$ (J deg^{-1} $mole^{-1}$)	-8.2_8			
S.E. (J deg^{-1} $mole^{-1}$)	0.9_9			

TABLE 6-2

The equilibrium constants, cooperativity parameters and the thermodynamic parameters for the 9(Me)AA/*E Coli* DNA/0.10 M NaCl system.

Temperature (°C)	10	22	35	50
K x 10^{-4} (M^{-1})	9.346	6.251	4.182	2.730
S.D. x 10^{-4} (M^{-1})	0.503	0.246	0.177	0.060
k	0.826	0.807	0.874	0.788
S.D.	0.056	0.044	0.055	0.033
$\Delta G°$ (kJ $mole^{-1}$)	-26.945	-27.099	-27.263	-27.445
S.D. (kJ $mole^{-1}$)	0.127	0.097	0.108	0.059
$\Delta H°$ (kJ $mole^{-1}$)	-23.417			
S.E. (kJ $mole^{-1}$)	0.033			
$\Delta S°$ (J deg^{-1} $mole^{-1}$)	12.4_6			
S.E. (J deg^{-1} $mole^{-1}$)	0.1_3			

TABLE 6.3

The equilibrium constants, cooperativity parameters and the thermodynamic parameters for the 9(Bu)AA/*E Coli* DNA/0.10 M NaCl system.

Temperature (°C)	10	22	35	50
K x 10^{-4} (M^{-1})	12.419	8.917	6.259	4.154
S.D. x 10^{-4} (M^{-1})	0.542	0.124	0.089	0.058
k	0.383	0.393	0.426	0.401
S.D.	0.026	0.009	0.011	0.037
$\Delta G°$ (kJ $mole^{-1}$)	-27.614	-2 .971	-28.296	-28.572
S.D. (kJ $mole^{-1}$)	0.103	0.034	0.036	0.037
$\Delta H°$ (kJ $mole^{-1}$)	-21.535			
S.E. (kJ $mole^{-1}$)	0.529			
$\Delta S°$ (J deg^{-1} $mole^{-1}$)	22.9_6			
S.E. (J deg^{-1} $mole^{-1}$)	1.8_3			

TABLE 6.4

The equilibrium constants, cooperativity parameters and the thermodynamic parameters for the 9(n-Hex)AA/*E Coli* DNA/0.10 M NaCl system.

Temperature (°C)	10	22	35	50
K x 10^{-4} (M^{-1})	9.698	6.494	4.389	2.923
S.D. x 10^{-4} (M^{-1})	0.343	0.279	0.339	0.092
k	0.645	0.686	0.670	0.532
S.D.	0.027	0.036	0.075	0.033
ΔG° (kJ $mole^{-1}$)	-27.028	-27.189	-27.383	-27.624
S.D. (kJ $mole^{-1}$)	0.085	0.108	0.206	0.086
ΔH° (kJ $mole^{-1}$)	-23.466			
S.E. (kJ $mole^{-1}$)	0.156			
ΔS° (J deg^{-1} $mole^{-1}$)	14.9_5			
S.E. (J deg^{-1} $mole^{-1}$)	0.4_2			

TABLE 6.5

The equilibrium constants, cooperativity parameters and the thermodynamic parameters for the 9(cyc-Hex)AA/*E Coli* DNA/0.10 M NaCl system.

Temperature (°C)	10	22	35	50
K x 10^{-4} (M^{-1})	6.961	5.144	3.946	2.642
S.D. x 10^{-4} (M^{-1})	0.062	0.123	0.124	0.033
k	0.544	0.600	0.595	0.500
S.D.	0.007	0.030	0.029	0.013
ΔG° (kJ $mole^{-1}$)	-26.247	-26.617	-27.114	-27.353
S.D. (kJ $mole^{-1}$)	0.021	0.059	0.081	0.034
ΔH° (kJ $mole^{-1}$)	-18.902			
S.E. (kJ $mole^{-1}$)	0.946			
ΔS° (J deg^{-1} $mole^{-1}$)	28.2_2			
S.E. (J deg^{-1} $mole^{-1}$)	3.3_8			

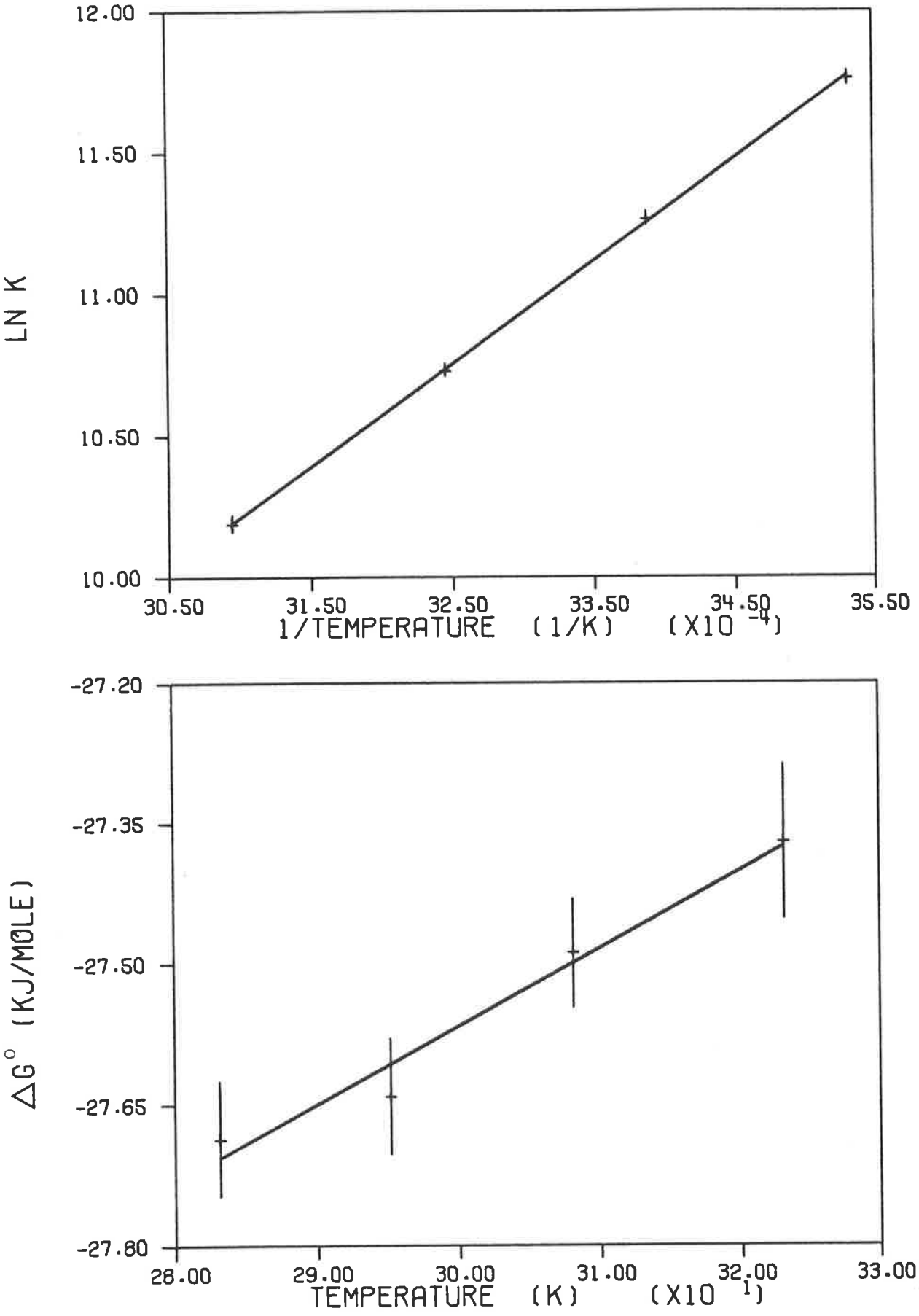

Figure 6-4. The plots of lnK versus T^{-1} and ΔG° versus T associated with the determination of ΔH° and ΔS° respectively for the 9AA/*E Coli* DNA/0.10 M NaCl system.

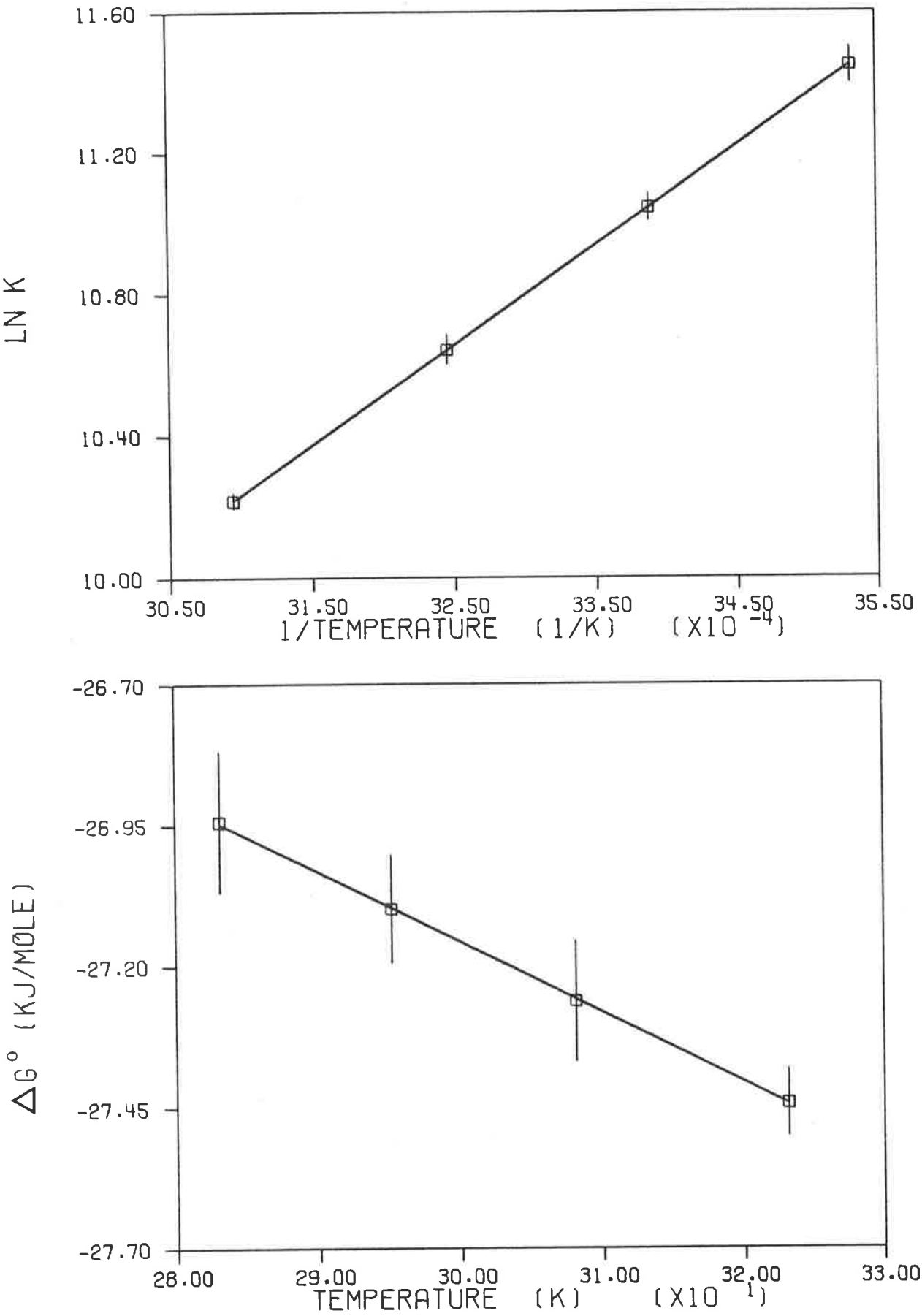

Figure 6-5. The plots of lnK versus T^{-1} and $\Delta G°$ versus T associated with the determination of $\Delta H°$ and $\Delta S°$ respectively for the 9(Me)AA/*E Coli* DNA/0.10 M NaCl system.

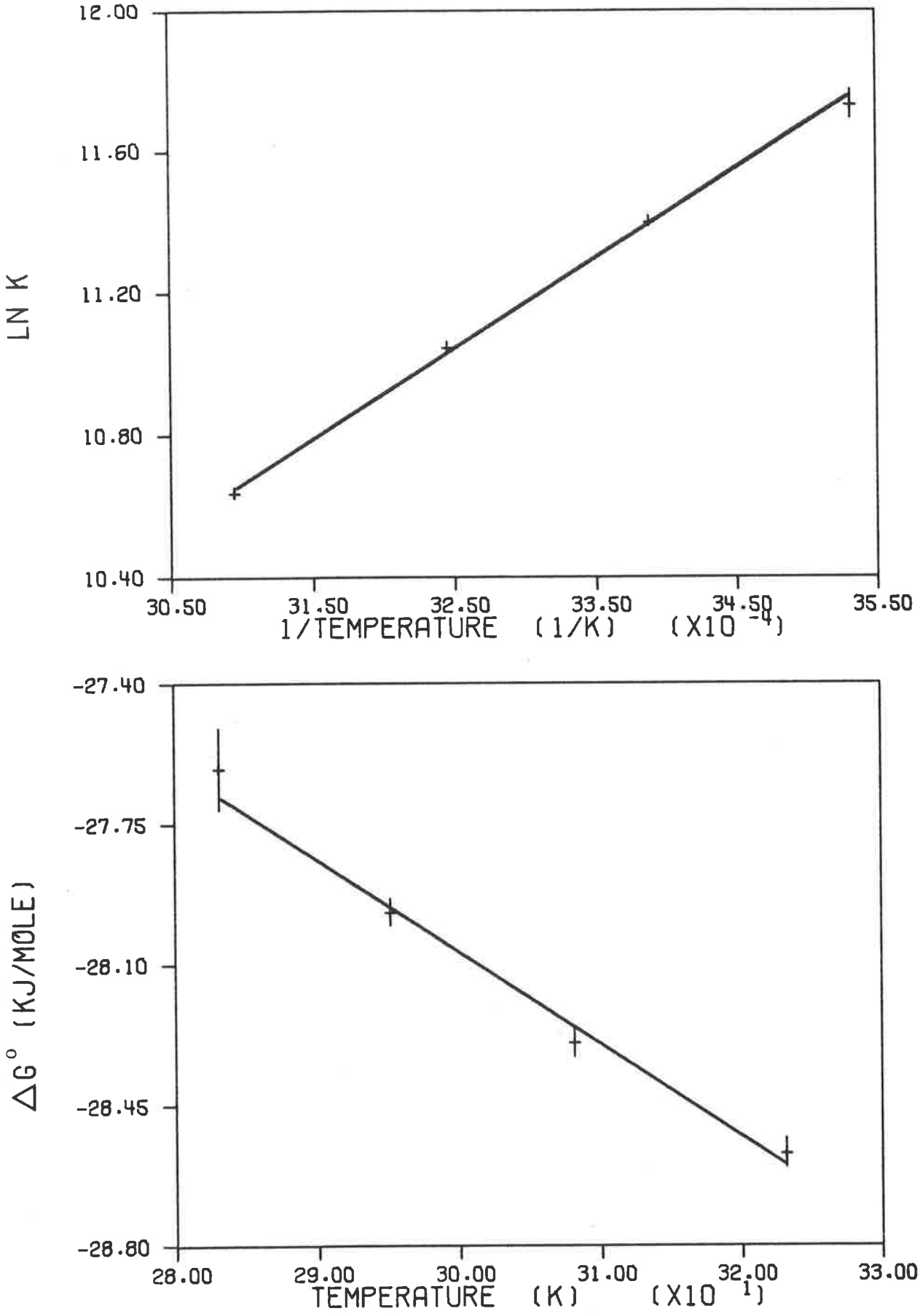

Figure 6-6. The plots of lnK versus T^{-1} and ΔG° versus T associated with the determination of ΔH° and ΔS° respectively for the 9(Bu)AA/*E Coli* DNA/0.10 M NaCl system.

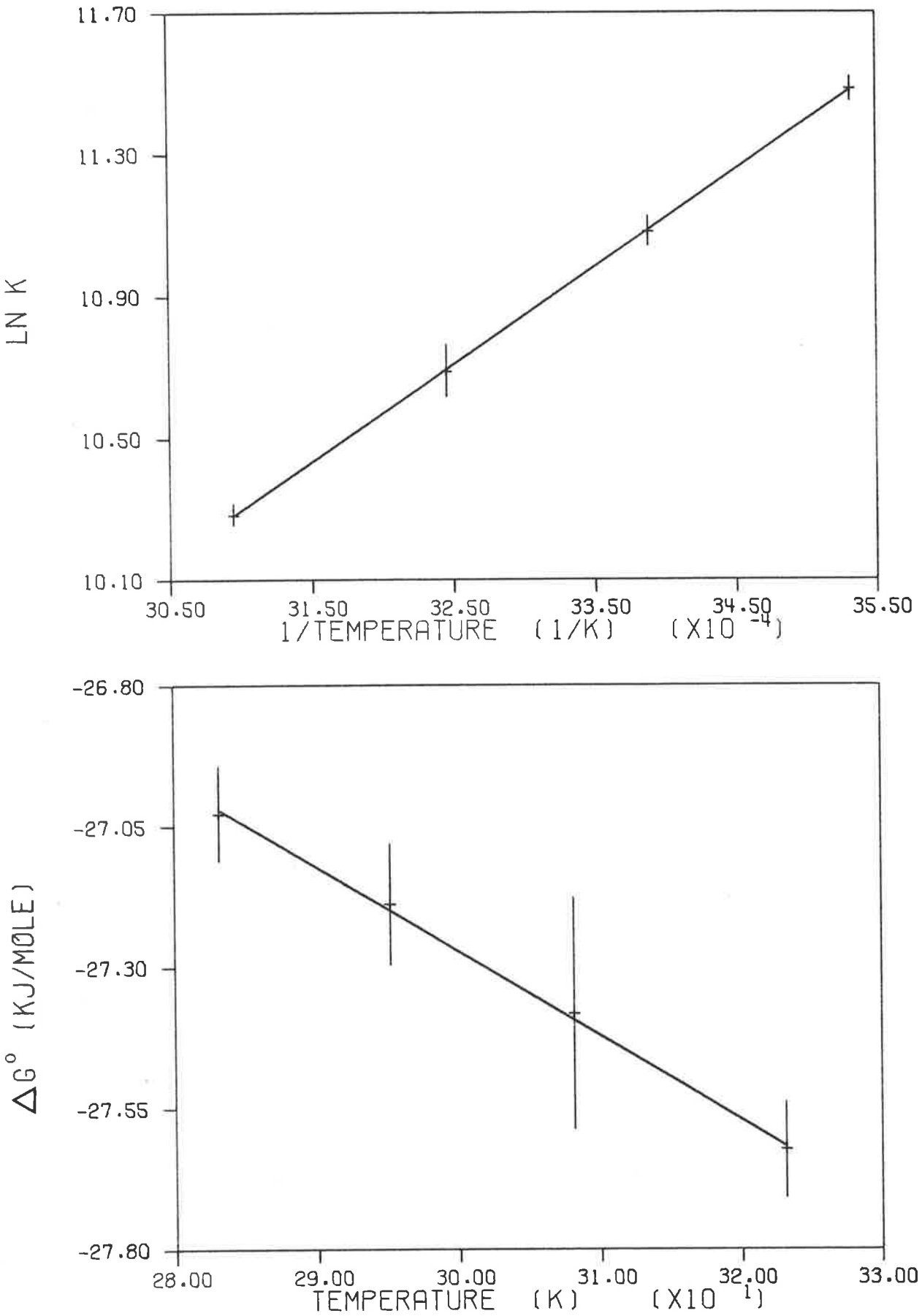

Figure 6-7. The plots of lnK versus T^{-1} and ΔG° versus T associated with the determination of ΔH° and ΔS° respectively for the 9(n-Hex)AA/*E Coli* DNA/0.10 M NaCl system.

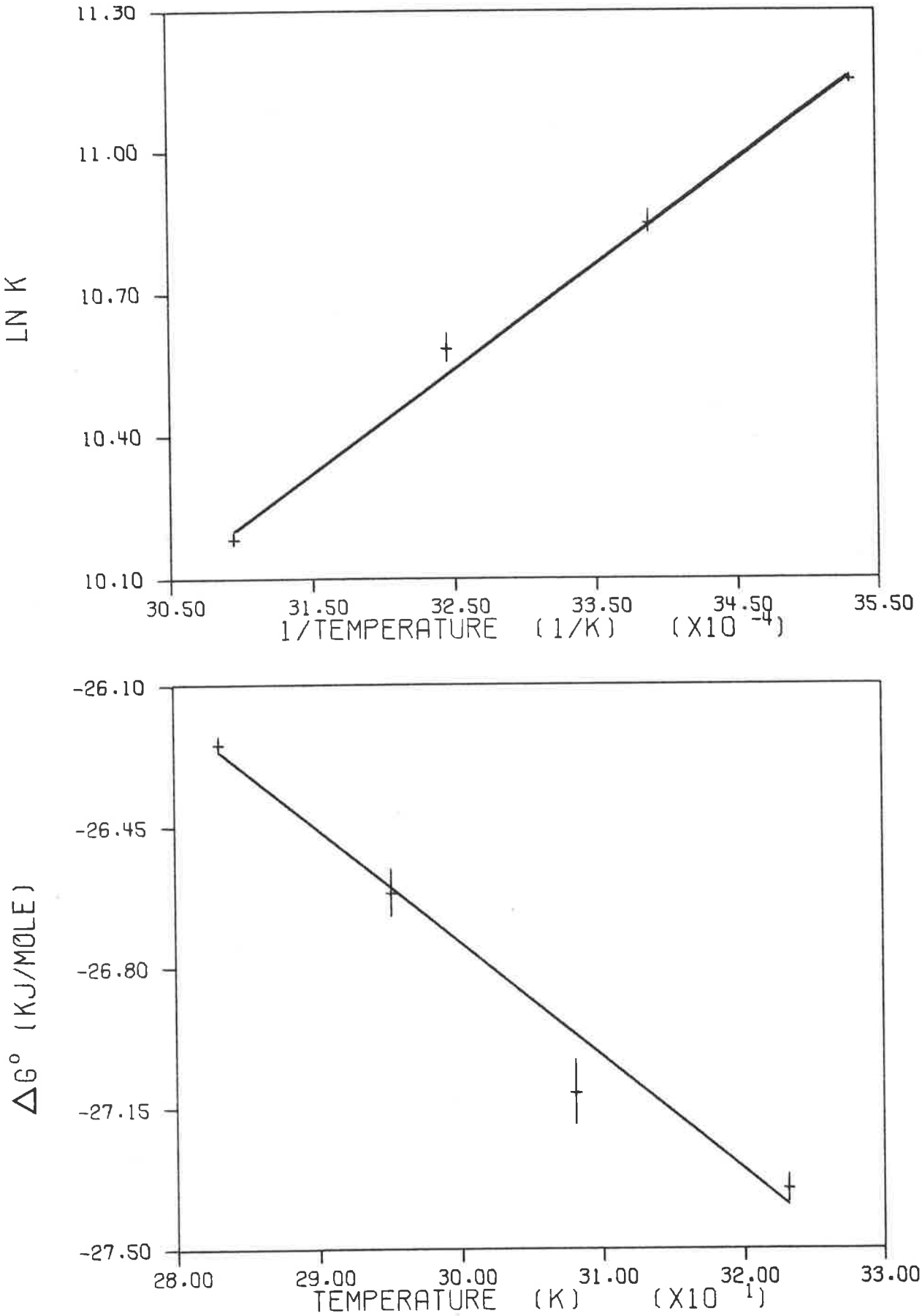

Figure 6-8. The plots of lnK versus T^{-1} and $\Delta G°$ versus T associated with the determination of $\Delta H°$ and $\Delta S°$ respectively for the 9(cyc-Hex)AA/*E Coli* DNA/0.10 M NaCl system.

-29 kJ/mole from T-jump kinetic studies. The value for ΔG° obtained from equilibrium spectrophotometry by Turner[3] was based on an assumed "binding in isolation" model in which the low r portion of the binding curve was assumed to be linear. This linear portion of the curve was fitted to a one-site Langmuir isotherm. If these data of Turner[3] are fitted to the model used in this work, the resultant ΔG° values are within 1 kJ of the values cited in Table 6-1.

The values obtained for ΔG° are similar to values reported for the interaction of other aminoacridines with native DNA and are indicative of a strong interaction. There is little variation in ΔG° among the compounds studied in this work. At 22°C the strongest interaction is that of 9(Bu)AA and the weakest 9(cyc-Hex)AA. With the exception of 9(Bu)AA all the alkyl derivatives show slightly weaker binding than 9-aminoacridine. This observation, that the binding affinities of the 9-substituted 9-aminoacridines differ only slightly from the binding affinity of 9-aminoacridine, is in general agreement with previous work on the binding of 9-substituted 9-aminoacridines[17-19]. This work found that the attachment of long and bulky side chains to the 9-amino group of 9-aminoacridine did not hinder their binding to DNA (see Chapter II 3(b)).

(c) Discussion

The component ΔH° and ΔS° values of these systems fall into two distinct groups. The first of these groups contains 9-aminoacridine itself. It is characterized by a large favourable ΔH° value and a small unfavourable ΔS° value. This results in relatively stronger interaction at lower temperatures and the reaction can be said to be entirely

"enthalpy driven". The dominant bonding interaction is made up of the sum of electrostatic, dipole and induced dipole interactions between the intercalated aminoacridine and the adjacent DNA bases and backbone groups. The unfavourable entropy change must result from an overall reduction in the number of degrees of freedom of the system when binding occurs. The simplest view of the system, that of two separate species interacting to form a single complex, would be expected to result in an unfavourable entropy change. Although such an unfavourable entropy change is observed it is of lower magnitude than would be predicted by this simple view of the system. This suggests that changes in solvent interactions on complexation make a significant contribution to the entropy change. The observed ΔS° of -8 J deg^{-1} $mole^{-1}$ for 9-aminoacridine may be contrasted with values of about -30 J deg^{-1} $mole^{-1}$ observed for the interaction of Proflavine[1,4] and Acridine Orange[2] with native DNA at high ionic strength. A value of -30 J deg^{-1} $mole^{-1}$ is closer to the expected value of ΔS° for a bimolecular complexation.

The second group contains all of the substituted 9-aminoacridines studied. This group is characterized by a smaller favourable ΔH° and a larger but favourable ΔS° when compared to 9-aminoacridine. The interaction is still predominantly but not entirely "enthalpy driven". The positive ΔS° means that the interaction becomes relatively more favourable with increasing temperature.

The reduction in ΔH° is systematic, the values being close to -22 kJ $mole^{-1}$ except for 9(cyc-Hex)AA which is somewhat lower with a value of -19 kJ $mole^{-1}$. The reduction in ΔH° for these 9-substituted 9-aminoacridines may be due either to systematic changes in the dipoles and induced

dipoles of the substituted compounds when compared with the parent compound, or to a different intercalated position within the helix or to a combination of both effects. There have been suggestions[5] that the 9-aminoacridine cation may exist partly or wholely as the imino tautomer in solution. Albert[6] rejects these suggestions in his excellent review of the electronic and spectral properties of the aminoacridines. X-ray structure determinations of hydrated single crystals of 9-aminoacridine hydrochloride[7] locates the H(10) proton on the ring nitrogen atom, N(10), and defines the acridine nucleus as nearly planar. The planarity of the acridine nucleus may be contrasted with structure determinations for a number of 9-substituted 2-methoxy-6-chloro-9-aminoacridines[8-10] which show degrees of deviation from planarity of the acridine nucleus of between 5° and 10°. Whilst no structure determinations have been reported for simple 9-alkylaminoacridines it is possible that they will show a degree of distortion of the acridine nucleus. Such distortion may adversely affect the strength of the bonding interactions. If the acridine nucleus is not planar and/or if steric hindrance due to the 9-alkyl group prevents the acridine nucleus from maximizing the overlap with the heterocyclic DNA bases then a reduction in the strength of bonding interactions would be expected.

The $\Delta H°$ values determined in this work do not reveal any definite trend within the group of substituted compounds. However it is tempting to suggest that the lower $\Delta H°$ found for 9(cyc-Hex)AA supports the suggestion of a limited steric hindrance to the intercalation of these compounds. It can be stated unambiguously that alkyl substitution of the 9-amino group of 9-aminoacridine leads to a reduction of the $\Delta H°$ for the interaction to about $^2/_3$ of the value found for the parent compound.

The inversion of the sign as ΔS° for the substituted compounds is presumably substantially a solvent effect. The major features of the interaction remain unaltered. This suggests that changes in solvation on binding are the major factors contributing to ΔS°. This is not surprising since these compounds all contain alkyl groups which would be expected to exert a considerable effect on the solvation properties of both the free aminoacridine and its complex with DNA in a solvent of high dielectric constant.

Finally it should be pointed out that the thermodynamic parameters which have been obtained for these compounds are not very model dependent. If no model was assumed, or indeed a different and perhaps inappropriate model was chosen, the same relative order of the K values and hence thermodynamic parameters would result. The simplest approach would be to linearly extrapolate the low r region of each curve to the ordinate axis and hence obtain estimates of K. This procedure would yield similar relative values of the thermodynamic parameters although at a much reduced accuracy.

6. Anti-cooperativity parameters

The anti-cooperativity parameter, k, is a measure of the hindrance to binding to an affected site. In the model chosen as the model of best fit this site is two potential sites from an intercalated aminoacridine since nearest neighbour site-exclusion is operating. The binding of aminoacridine to this affected site will occur with an apparent association constant of kK. The origin of the nearest neighbour site-exclusion and the next neighbour anti-cooperativity is almost certainly due to strain induced in the native DNA helix in the vicinity of the intercalated aminoacridine.

Since the effects of this strain are evident at two potential intercalation sites adjacent to an intercalated aminoacridine it is probably transmitted through the sugar-phosphate backbone of the helix. This local distortion of the backbone induced by intercalation is such as to prevent the nearest neighbour sites from opening sufficiently to accept an intercalated aminoacridine and to restrict intercalation at the next neighbour sites. It is possible that this restricting effect on the binding may extend even further than these next neighbour sites (see Section 4 of this Chapter). Alternative explanations of the origin of site-exclusion and anti-cooperativity involve ionic interactions, either by preventing an intermediate "outside bound" complex forming adjacent to an intercalated aminoacridine and so providing a mechanistic barrier to intercalation at this site, or as a simple repulsion between the cationic aminoacridines. Although such explanations can account for nearest neighbour site-exclusion, they are less tenable when a further anti-cooperativity affected site is involved.

The values found for k for the compounds studied in this work are all in the range 0.4 - 0.65 with the exception of those found for 9(Me)AA which were about 0.82. There is no discernable trend with temperature suggesting that the anti-cooperative effect is relatively independent of temperature. This observation may be consistent with the suggestion that a conformational change in the helix backbone structure is the origin of site-exclusion and anti-cooperative effects. Such conformational changes will presumably be characteristic for each of the aminoacridines. If the group of 9AA, 9(Me)AA, 9(Bu)AA and 9(n-Hex)AA are considered then there is a trend for an inverse correlation between K and k

suggesting that stronger binders exert stronger anti-cooperative effects, although the trend is not pronounced.

The k values found for 9(Me)AA are significantly higher than those found for the other compounds studied. The value of k is most dependent on the binding data determined at high r values which are in turn most affected by the values of ε_F^λ calculated from the absorbance versus concentration data. The fitted models for 9(Me)AA at 10°C and 22°C are the poorest fits for all the compounds studied. Further, these relatively poor model fits result from the significantly higher r values found at high T_L/T_A when compared to the other compounds. The higher k values for 9(Me)AA are a result either of small errors in ε_F^λ which have adversely affected the binding data determined at high T_L/T_A or, if this is not the case then the model apparently breaks down at high r values for this compound.

7. Concluding remarks

In this Section I shall briefly summarize the most important points from the earlier Chapters and then discuss the results presented in this Chapter as they relate to other work on the binding of aminoacridines to native DNA.

In Chapter III experimental techniques for the determination of data from which binding curves can be calculated are critically examined, with emphasis on spectrophotometric and equilibrium dialysis methods. In the practical application of both methods the utmost care is required with attention to all the experimental techniques involved from the preparation and handling of materials and solutions to the recording of absorbances from a properly calibrated spectrophotometer. While both methods yield good results the spectrophotometric method is preferred since it

involves less quantities of materials, less handling of solutions and less time than equilibrium dialysis experiments. In addition the spectrophotometric method is potentially usable over a wider range of solvents than equilibrium dialysis and also provides valuable information concerning the system under study through the internal linearity analysis. The problem of extrapolating to ε_B^λ is thoroughly discussed. The prefered method of determining ε_B^λ is the method of plotting $\varepsilon_{OBS}^\lambda/\varepsilon_M^\lambda$ against T_L/T_A and extrapolating to $\varepsilon_B^\lambda/\varepsilon_M^\lambda$. This method is validated by comparison with other methods of determining ε_B^λ.

The transformation of the experimental data into binding data is the subject of Chapter IV. Emphasis is placed on the use of correct ε_F^λ values for the calculations on data in the region of high r, the region most important to the modelling of site-exclusion and anti-cooperativity effects. A detailed discussion of the effect of errors in the experimental data and the ε_B^λ value on the calculated parameters shows the complex way in which such errors are propagated.

The conditions placed on, and the derivation of, mathematical models for the binding of ligand into linear lattices is the subject of Chapter V. Emphasis is on the relatively new SGF method and the advantages it offers over other methods. Several models are derived and thier properties discussed.

In the preceding sections of this Chapter the fit of several potential models for the binding to native DNA of the 9-aminoacridines studied has been examined. A model, which embodies a single, apparent equilibrium constant, nearest neighbour site-exclusion and next neighbour anti-cooperativity is chosen as the model of best fit for the binding data.

The model parameters for each 9-aminoacridine at each temperature studied are used to calculate the thermodynamic parameters which characterize the binding of each compound in terms of the chosen model for the interaction. These parameters are discussed in terms of the two groups they fall into and their implications for physical models of the interaction.

The equilibrium and thermodynamic parameters describing the interaction of 9AA and the substituted 9AAs with native *E Coli* DNA in 0.10 M NaCl can be considered in the context of previously published work in this field. The parameters which characterize the interaction of 9AA may be compared with data determined by Turner from a T-jump kinetic study of the 9AA/native *E Coli* DNA/0.1 M NaCl system[3]. Turner found that the mechanism of the interaction could be adequately described by a single bimolecular reaction step. This work, however, was weakened somewhat by the failure to obtain good agreement between parameters determined from kinetic and from equilibrium methods with a binding in isolation model used as a basis for the calculation. If equilibrium and related thermodynamic parameters obtained by Turner are recalculated in terms of the binding model used in this study then better agreement between the parameters found from equilibrium and kinetic studies is obtained. This adds weight to Turner's finding of a single step mechanism for the intercalation of 9AA into native DNA[3], a finding at variance with kinetic studies of Proflavine/native DNA systems which yield two step mechanisms[4].

The observation that a single step mechanism for the intercalation of 9AA into native DNA yields kinetic parameters consistent with the equilibrium parameters adds support to Peacocke's proposal[11] that there may be two major

classes of aminoacridine/DNA interactions, one containing the 1,2 and 9-aminoacridines and the other the aminoacridines with a 7-aminoquinoline sub-structure such as Proflavine. While there is considerable evidence of heterogeniety among the strong binding sites of Proflavine and Proflavine-like aminoacridines this thesis presents a strong case that no such heterogeneity exists among the strong binding sites for the 9AAs, especially when taken with the results of the kinetic study of Turner.

A very recent study[12] of the interaction of the substituted 9-aminoacridine Quinacrine with native DNA modelled the interaction with the same model as used in this work using the less general equation of McGhee and von Hippel. Although these workers exercised care in the determination of binding curves they did not correct for dimerization of Quinacrine and hence did not use the appropriate ε_F^λ values.* They do not mention correcting for DNA background absorbance when using the spectrophotometric method. Further considerably lower precision is evident in their equilibrium dialysis than was achieved in this work. These factors will affect the accuracy of the values they report, however that study and this work are in agreement about the model to best describe the interaction of 9AAs with native DNA. Unfortunately no study of the variation with temperature of the interaction of Quinacrine was undertaken and so no thermodynamic parameters were reported.

---

* Wilson and Lopp[12] reported a dimerization constant of 500 M^{-1} for Quinacrine in an ionic strength of 0.12 which may be compared to a dimerization constant of 650 ± 50 M^{-1} for 9AA at ionic strength 0.1 (determined by the author). The importance of this correction and the method of applying it have been fully discussed in Chapter IV 4(c).

The implication of this study to the studies of bis-intercalating 9AAs must be mentioned. The work of Le Pecq *et al*[13] on the bis-intercalation of Quinacrine-like dimers linked through the 9-amino side chain found definite evidence of nearest neighbour site-exclusion. Conversely the work of Wakelin *et al*[14] on the bis-intercalation of 9-aminoacridines linked through simple alkyl 9-amino side chains found no evidence for nearest neighbour site-exclusion. Even the most careful equilibrium study of the interaction of aminoacridines with native DNA cannot determine between true site-exclusion and extreme anti-cooperativity. For example if true site-exclusion is considered not to occur in the systems studied in this work, the anti-cooperativity factor which is then applied to the nearest neighbour site is about 10^{-6} yielding an effective association constant for this site in the range 0.05 - 0.1. If typical concentrations of aminoacridine and DNA are considered then one would expect to find one nearest neighbour bound aminoacridine about every 10^5 base pairs, that is on average somewhat less than one such occurrence per DNA molecule even in the highly polymerized DNA used in this work. This suggests that the mono-functional 9-alkylaminoacridines cannot be directly compared with their bi-functional bis-intercalating analogues.

The problem of inaccuracy in binding data for these systems and its effect on the determination of model fits and parameter values has been recognised by Schellman[15]. Many of the attempts to model experimentally determined binding data[12,15,16] have been unconvincing because of this problem and the associated problem of the restricted range over which usable data was obtained. For the first time this study has

shown that it is possible to experimentally determine binding data with sufficient accuracy and precision to enable choices to be made between potential models for the interaction. Furthermore such accurate data yield more precise estimates of model parameters than have been possible previously. This will enable binding data to assume a more important role in deciding whether proposed models for the interactions of chromophores with DNA are appropriate.

REFERENCES

1. Chambron J., Daune M. and Sadron C., *Biochim. Biophys. Acta*, 123, 306 (1966).
2. Ichimura S., Zama M., Fujita H. and Ito T., *Biochim. Biophys. Acta*, 190, 116 (1969).
3. Turner D.R., Ph.D. Thesis, University of Adelaide (1975).
4. Li H.J. and Crothers D.M., *J. Mol. Biol.*, 39, 461 (1969).
5. See for example: Capomaccia A.C., Casper J. and Schulman S.G., *J. Pharm. Sci.*, 63, 1272 (1974).
6. Albert A., "The Acridines", 2nd ed., Arnold (publishers) Ltd., (1966).
7. Talacki R., Carrell H.L. and Glusker J.P., *Acta Cryst.*, B30, 1044 (1974).
8. Glusker J.P., Minkin J.A. and Orehowsky W., *Acta Cryst.*, B28, 1 (1972).
9. Berman H.M. and Glusker J.P., *Acta Cryst.*, B28, 590 (1972).
10. Carrell H.L., *Acta Cryst.*, B28, 1754 (1972).
11. Peacocke A.R., *Chem. Heterocycl. Comp.*, 9, 723 (1973).
12. Wilson W.D. and Lopp I.G., *Biopolymers*, 18, 3025 (1979).
13. Le Pecq J.B., Le Bret M., Barbet J. and Roques B., *Proc. Nat. Acad. Sci. U.S.A.*, 72, 2915 (1975).
14. Wakelin L.P.G., Romanos M., Chen T.K., Glaubiger E.S., Canellakis E.S. and Waring M.J., *Biochemistry*, 17 5057 (1978).
15. Schellman J.A., *Isr. J. Chem.*, 12, 219 (1974).
16. Ramstein J., Leng M. and Kallenbach N.R., *Biophys. Chem.*, 5, 319 (1976).
17. Drummond D.S., Simpson-Gildemeister V.F.W. and Peacocke A.R., *Biopolymers*, 3, 135 (1965).
18. Peacocke A.R., *Stud. Biophys.*, 24/25, 213 (1970).

19. Filipski J., Chorazy M. and Mendecki J., *Stud. Biophys.*, 24/25, 249 (1970).

CHAPTER VII

Materials and methods

CONTENTS

Part A - Preparation of materials

1. Synthesis of 9-alkylaminoacridines

The substituted 9-aminoacridines were prepared by condensation of the corresponding alkylammonium chlorides and 9-phenoxyacridine free base, a synthesis described by Albert[1]. The alkylamines were all Fluka A.G. purum grade and converted to the ammonium chloride salt by saturation of a solution of the free amine base in dry ether with dry HCl gas. The product was recovered by vacuum filtration and stored in a desiccator over phosphorus pentoxide until required. Methylamine was purchased as the hydrochloride salt. The following syntheses were used.

Diphenylamine-2-carboxylic acid

Synthesized according to the method of Albert[1] except that three extractions with active charcoal were required. The yield was 70% of a pale yellow product which melted at 182°C.

9-chloroacridine

Synthesized according to the method of Albert[1] from diphenylamine-2-carboxylic acid using phosphoryl chloride as the cyclizing agent. It should be noted that extreme care is required in the work-up step involving the ammonia solution. In one incident in this laboratory the chloroform layer failed to mix with the ice-cold ammonia solution for about 2 minutes despite vigorous stirring. After this time the reaction occurred suddenly with explosive force. It is suggested that the ammonia solution be added slowly with vigorous stirring to ensure a controlled reaction. The product was recrystallized once from benzene to yield 90% of a pale green crystalline material which melted at 121°C. The product was

stored in a desiccator over sodium hydroxide pellets.

9-phenoxyacridine

Synthesized from 9-chloroacridine according to the method of Albert[1]. The yield was 80 - 90% of a grey powder which melted at 126°C.

9-alkylaminoacridines

The synthesis is adapted from the method of Albert[1] for 9-methylaminoacridine. 13.6 g of freshly prepared 9-phenoxyacridine was dissolved in 50 g of freshly redistilled phenol in a 200 ml round-bottomed flask at 80°C. 0.1 M of the appropriate alkylamine hydrochloride, thoroughly dried over phosphorus pentoxide, was added to the mixture, an air condenser fitted and the temperature raised to 120°C. After one hour the mixture was cooled to 60 - 80°C and poured into 500 ml of ice-cold 2 M NaOH with rapid stirring. The resultant product was quickly filtered off and washed with ice-cold hydroxide solution and several portions of ice-cold water. The crude base was sucked dry on the filter and twice recrystallized from petroleum spirit (bp. 80 - 100°C). Yields were in the range 75% - 85%. The hydrochlorides were obtained by dissolving the dry base in anhydrous ether and bubbling dry hydrogen chloride gas through the solution until the supernatant ether was clear. The product was then filtered off and dried. All of the 9-alkylaminoacridine hydrochlorides were bright yellow except the tert-octyl compound which was scarlet in colour. The structures were verified by the infra-red and proton NMR spectra of the free bases.

2. Purification of 9-aminoacridines

9-aminoacridine hydrochloride was Fluka puriss grade and recrystallized from 20% aqueous ethanol. The purity of the compounds was followed by paper chromatography using two solvent systems. These solvent systems were 3% aqueous ammonium chloride and a 70 : 30 mixture of redistilled butanol and 5 M acetic acid[1]. The resultant spots were visualized by their fluorescences under UV light from a low pressure mercury lamp. Repeated recrystallization from aqueous ethanol was sufficient to purify all compounds except the methyl and cyclo-hexyl derivatives which showed persistent traces of 9-aminoacridine. These compounds were purified by column chromatography using neutral alumina as a support phase and methanol as the eluting phase. The column was 1 cm x 50 cm. The compounds treated in this way each showed a single spot with both solvent systems, with no trace of 9-aminoacridine.

The degree of hydration of the pure crystalline hydrochlorides was determined by weighing 0.5 g samples which were repeatedly dried and rehydrated. Drying was accomplished alternately by storing the samples for 48 hours, *in vacuo* over phosphorus pentoxide and storage at 120°C overnight. Samples were rehydrated by storage at 100% relative humidity at room temperature. It was determined that 9AA.HCl and 9(Me)AA.HCl were mono-hydrates and 9(Bu)AA.HCl was a tri-hydrate. All the other 9-aminoacridines prepared were anhydrous.

3. DNA extraction

The DNA samples used throughout this work were prepared by modifications of the method described by Marmur[2]. The bacterium used was an *E. Coli* K12 strain. This bacterium

strain was cultured in a standard aerobic complete growth medium in 10 or 20 litre containers. The culture was grown from a heavy, stationary state inoculum for 24 to 36 hours and harvested by continuous flow centrifugation. The bacteria were stored at -20°C until required. The following two extraction methods were used to purify the DNA. The first method was used to obtain samples for general use and the second to prepare samples for use in equilibrium dialysis experiments.

(a) Method I

The bacteria (100 g) were lysed by gentle shaking with sodium dodecyl sulphate. The method of Marmur[2] was followed except that one or two additional phenol extractions were performed as recommended by Hirschman and Felsenfeld[3]. The DNA, after the final "wind-out" of solution was washed with redistilled ethanol and then redistilled acetone and dried *in vacuo*. The dry solid samples were stored in tightly sealed vials at -20°C. The yield of DNA was generally about 100 mg from 100 g of bacteria.

(b) Method II

The bacteria were lysed by 6 hours incubation at 37°C with lysozyme (Sigma Biochemicals). The work up of this lysate was then according to Marmur[2] until the chloroform extractions were complete. At this stage the DNA was precipitated from solution, washed and resolvated in standard saline citrate. The ribonuclease digestion step was performed and then the solution was incubated for 12 hours with a 0.5% solution (final concentration) of the non-specific protease Pronase A (Calbiochem, nucleic acid free grade). This solution was then chloroform extracted until protein free and given three phenol extractions. The product was then treated as in Method I.

4. Characterization of DNA

The DNA, extracted and purified as described previously, was characterized by ultracentrifugation, UV absorbance the protein analysis. Sedimentation velocity experiments showed that the samples had an $\bar{M}_w$ of between 8×10^5 and 1.2×10^6 daltons. Equilibrium density gradient experiments on caesium chloride gradients were consistent with a GC content of 49%. The UV absorbance experiments showed that the DNA had a λ_{max} at 258 nm. Typical results of the spectral analysis of Hirschman and Felsenfeld[3] are given in Part B (2) of this Chapter. Thermal denaturation experiments, using 0.10 M NaCl as solvent, yielded melting temperatures of between 86.5°C and 88°C accompanied by a hyperchromicity of 49%. The protein analysis yielded a protein content of less than 0.2%, the lower sensitivity limit of the ninhydrin test employed.

Part B - Preparation of solutions

1. DNA solutions

DNA solutions were prepared by dissolution of solid DNA samples in 0.001 M NaCl with gentle stirring using a teflon coated stirring magnet at 4°C. After 24 to 48 hours the neutral salt concentration was increased to 0.10 M NaCl by addition of the appropriate volume of a 1.00 M NaCl solution. This solution was stirred at 4°C for at least 12 hours. The solution was then centrifuged for 45 minutes at 16000 RCF in polycarbonate centrifuge tubes. The resultant DNA solution was carefully decanted and stored at 4°C. The final concentration of these DNA stock solutions was about 2 mg/ml. All glassware, the centrifuge tubes and the teflon coated

stirrers were carefully cleaned and steamed for at least 30 minutes prior to use. DNA solutions prepared by this method were very stable and were unchanged, as judged by their spectral properties, over periods of several months.

2. Determination of DNA concentration

The concentration of DNA in solution was determined by the 3-term UV spectral analysis of Hirschman and Felsenfeld[3]. In this technique absorbances are recorded at a series of wavelengths and used to calculate both the DNA concentration in the solution and the GC content of the DNA. The method also provides an error function, Δ, which is a measure of the goodness of fit of the experimentally observed absorbances to the equations of Hirschman and Felsenfeld[3]. This function should ideally equal zero for a perfect set of spectral data. This method of DNA solution analysis also provides a 3-term hyperchromic analysis which analyses both the native and denatured spectrum of a DNA solution. A computer program, DNANAL, was written to make these calculations. Every new preparation of DNA was examined using the hyperchromic analysis and the concentration of each DNA stock solution was determined and periodically checked using the native analysis. Considerable experience was gained during the course of this work in using this spectral analysis. The results were very good. The following results were obtained from the concentration determinations of a DNA stock solution over a period of six weeks.

	Average	S.D.
Concentration (Moles of DNA phosphorus)	$1.987_6 \times 10^{-3}$	6.16×10^{-6}
GC content (%)	48.7	0.43
Δ	0.018	0.002

These results were obtained from approximately 25 fold dilutions of the stock solution, determined exactly by weight. The reproducibility of concentration determination by this method is excellent. The accuracy of the method depends on the coefficients originally determined by Hirschman and Felsenfeld[3]. No attempt was made to check the accuracy of the method since absolute concentration determination methods are difficult to perform and generally not very precise. There is no reason to doubt the accuracy of the original data and the internal consistency of concentration determinations observed throughout this work indicate that this method is superior to the more generally used single wavelength concentration determination technique.

3. Aminoacridine solutions

Stock solutions of 9-aminoacridines were made initially by dissolving accurately weighed solid samples of the corresponding hydrochloride salt in water using 'A' grade volumetric flasks. The neutral salt concentration of the solution was adjusted to the final required concentration with 1.00 M NaCl solution before the solution was made up to the marked volume. The solid samples were weighed on a Cann microbalance which was periodically checked with standard

weights. Three such solutions were used to determine molar absorptivities of the aminoacridines in the range 5×10^{-6} to 1×10^{-5} M. These molar absorptivities were then used to determine stock solution concentrations during any subsequent work.

4. Aminoacridine/DNA solutions

All solutions of aminoacridine and DNA stock solutions were made by weight using a Mettler H4 balance. Pipettes were used to obtain approximately the desired final dilution which was then exactly determined by weighing the additions.

All solutions were assumed to have the same density. Since all solutions used were dilute this approximation is consistent with the accuracy required in this work. The aminoacridine/DNA mixtures were made by adding the aminoacridine stock aliquot, followed by the solvent aliquot and lastly the DNA stock aliquot. The series of solutions made for each experiment were generally required to have a constant aminoacridine concentration. In practise the final aminoacridine concentration varied slightly as determined by weight. A typical result from a 26 solution series was $5.495_9 \times 10^{-5}$ M $\pm$ 1.47×10^{-7} M. All aminoacridine/DNA solutions were stored at 4°C. The pH of these solutions was monitored periodically throughout this work. The pH values were always within the range 5.9 - 6.5.

Part C - Experimental techniques

1. Spectrophotometry

(a) Apparatus

Two spectrophotometers were used during this work. They were a Zeiss PMQII single beam and a modified Zeiss DMR-10 double beam recording spectrophotometer. The calibration, accuracy and precision of these instruments is discussed in Chapter III (2) (e). The modifications to the DMR-10 are discussed in Appendix IV. The DNA melting curves were recorded on a Gilford model 220 single beam spectrophotometer equipped with an electrically operated cell heating assembly and proportional temperature control described elsewhere[4].

A variety of quartz spectrophotometer cells were used. The effective optical path length of these cells was determined to ± 0.001 mm using a microcomparator. In a few cases where the internal surfaces of the cell walls were not easily visible the measurement was made through the frosted bottoms of the cells which were wetted with paraffin oil to enhance visibility. The parallelism of the cell walls was also checked using the microcomparator.

(b) Methods

The spectra of all solutions were recorded on the DMR-10 using the following regime. The cells containing the solutions were allowed 15 minutes to obtain thermal equilibrium after which time the spectrum was recorded twice in wavelength increments of 1 nm between the preset wavelength limits. An integration time of 3 seconds was allowed at each wavelength after which the integrated absorbance was read by the microcomputer system. These

duplicate spectra were compared and if any discrepancy of 0.002 or more absorbance units was found at any wavelength the spectra were rejected and the experiment repeated. The cell correction spectrum was determined in the same way but with three recordings of the spectrum. This correction was redetermined every time the cells were positioned in the cell housing or the temperature of the cell block changed. Once the cells were positioned and the correction spectrum determined solutions were removed from the sample cell with the aid of fine polythene canulla tubing connected to a water pump. Solutions were added to the cell with a pasteur pipette. In this way the position of the cells relative to the light beams did not alter between the recording of the cell correction spectrum and the recording of sample solution spectra. None of the aminoacridines used was adsorbed onto the walls of the spectrophotometer cells as determined by an unchanged cell correction spectrum after cells had contained concentrated aminoacridine solution. As an additional precaution only new silica spectrophotometer cells and pyrex flasks were used to contain these solutions.

The temperature of solution in the cell was determined by constructing a calibration curve which compared the temperature of the circulating water bath, as read on a calibrated thermometer, with the temperature of the solution in the cell. This latter temperature was determined from the resistance of a thermocouple placed so that the couple was in the middle of the cell. This thermocouple cell assembly had been previously calibrated. The temperature of the water bath was controlled to ± 0.1°C. A similar variation was found about the mean temperature of the cell solution. For work below ambient temperature the sample compartment of the DMR-10 was

continuously flushed with dry nitrogen to prevent moisture condensation on the lenses and cell windows.

The resultant data from the collection system was punched on paper tape and further processed by a number of computer programs, which are briefly described in Appendix V.

2. Equilibrium dialysis

(a) Apparatus

The apparatus used was a Kontron Diapack. A schematic diagram of a dialysis cell, which was constructed of teflon, is shown in Chapter III. These dialysis cells were mounted in banks of five cells into a holder which enabled the cells to be rotated at a preselected speed. The entire assembly was then immersed in a thermostated water bath and allowed to reach equilibrium.

The dialysis membrane was prepared by the following pretreatment. The tubing or cut flat sections were boiled in a 5% solution of sodium bicarbonate for 30 mins. The membrane was then rinsed several times with distilled water and boiled in distilled water for a further 30 mins. It was again rinsed several times and allowed to stand in distilled water for 24 hours. Following this period it was rinsed several times with 0.10 M NaCl solution and leached for a further 24 hours in this solution. The membrane was then further rinsed with 0.10 M NaCl and stored in this solution. Membrane treated in this manner showed no leaching of UV absorbing material over a 48 hour period. The membrane, once pretreated, was only handled with gloved hand or stainless steel tweezers. This treated membrane could be stored for up to 4 weeks at room temperature.

(b) Methods

The DNA stock solutions used for dialysis were exhaustively dialysised against 0.10 M NaCl solution. The DNA solution was placed into prepared tubing tied to form sacks. The filled sacks were placed in glass tubes filled with solvent and gently rocked, to ensure constant mixing, at 4°C. The volume of solvent contained in the glass tube was at least 20 times the volume of solution in the dialysis sack to ensure that sink conditions were maintained. The dialysis was continued for 7 - 10 days with two changes of solvent each day. The DNA solution was then diluted by weight to the required concentration for use in the equilibrium dialysis experiments.

Solutions were loaded into the equilibrium dialysis cells using glass syringes which were weighed before and after discharging the solution into the dialysis cell to determine the exact volume filled into each side of the cell. The precision syringes used were capable of delivering 3.00 ml ± 0.01 ml as determined by weighing. After equilibration the solutions were discharged from the dialysis cells directly into spectrophotometer cells for analysis. A new membrane was mounted in each cell for each experiment.

3. Liquid scintillation counting

The machine used was an Isocap model 300 counter equipped for 3 channel counting with fixed or variable windows. Since the planned experiment was to detect a small difference in the total observed count, a preliminary investigation of the properties of the counter and the scintillation medium was undertaken. The aqueous samples for counting were incorporated into a commercially available gel scintillation medium,

PCS (Searle Aust. Ltd.) and counted in low potassium glass vials. Using a tritiated water standard it was determined that the efficiency of the counting medium was dependent on the amount of aqueous phase in the mixture. All solutions for counting were prepared by incorporating 1.00_0 g of water into 10.0 ml of scintillant. A second experiment was conducted in which 10 samples, prepared as above, with total activities in the range 10^3 - 10^6 dpm and 3 tritium standards in a toluene-based scintillation medium were counted for ten minute periods over 48 hours in a continuous cycle. A small diurnal variation in the apparent counting efficiency of the gel scintillant was observed. This variation was related to the ambient temperature and all future counting experiments were confined to an 8 hour overnight period in which the greatest temperature stability was observed.

Data collected in this period were used to calculate observed standard deviations among the ten minute counts. The expected standard deviation of a count is related to the square root of the number of counts observed. These experiments showed that the lowest standard deviations were observed when the activity of the solutions was maintained between 5000 and 40000 counts per minute.

Using this technique the observed deviation could be maintained at 10% or less of the difference in the observed counts hence ensuring the accuracy of the determination (see Chapter III, Table 3-5). The tritium counting efficiency of the medium employed under these conditions was 28%.

Part D - General

1. Materials

All reagents used were analytical grade. Water was prepared by distilling deionized water through a well seasoned all glass still and stored in a seasoned polypropylene container. The conductivity of the water was continuously monitored and found to be consistently less then 2.5×10^{-6} mho cm^{-1}. Methanol used to wash and dry spectrophotometer cells was distilled in an all glass still equipped with a fractionating column and operating with a reflux ratio of 2 : 1. The middle $^2/_3$ cut was collected for use.

2. Cleaning

General glassware was cleaned by soaking in a solution of 2% w/v of $KMnO_4$ in 10% w/v NaOH for 12 hours. The glassware was then thoroughly rinsed with deionized water and leached for 24 hours in acidified sodium metabisulphite solution (0.1% w/v). It was then further rinsed with deionised water, then distilled water and dried and stored in a stainless steel oven at 160°C until required. The oven was used only for storing clean glassware. Apparatus used for DNA solutions was further steamed immediately before use with a well seasoned all glass steamer charged with distilled water.

Optical glassware was cleaned by overnight immersion in a 5% solution of Decon-90 detergent. It was then thoroughly rinsed with distilled water and stored in distilled water until required. Before use it was rinsed with distilled water followed by several portions of distilled methanol and dried in a gentle stream of warm air.

Teflon and stainless steel was cleaned by immersion in 5% Decon-90 solution followed by rinsing and leaching in

distilled water. To aid in cleaning the teflon dialysis cells a soft, natural bristle toothbrush was used which enabled the inner surfaces to be thoroughly cleaned without damaging the sealing rings. Syringe needles were cleaned by sucking Decon-90 solution through the needle followed by copious quantities of distilled water.

Pipettes and volumetric flasks were cleaned with a 5% solution of Decon-90 and leached with distilled water. The flasks were stored full of distilled water and the pipettes were dried at 160°C and stored in sealed glass containers. Glass syringes with metal Luer-lok fittings required special attention since prolonged soaking in Decon-90 led to deterioration of the metal fitting. The syringe bodies were soaked in 2% Decon-90 for 10 minutes and then brushed with a test-tube brush. They were then rinsed with and stored in distilled water. Before use they were oven dried at 100°C.

3. pKa determination

Approximate pKa values of those 9-aminoacridines which had not been previously reported in the literature were determined by the following method. A solution of the appropriate 9-aminoacridine hydrochloride of approximately 1×10^{-4} M was made up in 0.10 M NaCl. A series of ammonium chloride buffers with pH values of 8.8, 9.2, 9.6, 10 and 12.5 and a total ionic strength of 0.1 were made up from stock solutions of 1 M HCl and 2 M ammonia solution. One ml of the aminoacridine stock solution was made up to 100 ml with the appropriate buffer solution and the spectrum was immediately recorded in cells of a 5 cm pathlength. All solutions were stable for at least 30 minutes as determined by unchanged spectral properties. The spectrum of a similar dilution in

0.10 M NaCl, acidified with a drop of hydrochloric acid, was taken to be the spectrum of the pure hydrochloride and the spectrum at a pH of 12.5 to be that of the pure free base. These spectra were used to calculate apparent molar absorptivities at two wavelengths for each form of the aminoacridine. The spectra recorded at intermediate pHs were used to obtain apparent molar absorptivities at these pHs. These values were used to construct and solve equations of the following form:

$$\varepsilon_I^\lambda = (1 - x)\varepsilon_H^\lambda + x\varepsilon_B^\lambda$$

where the subscripts I, H and B refer to the intermediate pH, the hydrochloride and the free base. The two determinations of x were averaged. The pKa was expressed as being greater than the lowest pH tested which produced an x value of less than 0.5. Since the value was only required to ensure that the aminoacridine was sufficiently basic to be completely ionized at neutral pHs, it was not necessary to define the value more closely.

REFERENCES

1. Albert A., "The Acridines", 2nd ed. Arnold (London).

2. Marmur J., *J. Mol. Biol.*, 3, 208 (1961).

3. Hirschman S. and Felsenfeld G., *J. Mol. Biol.*, 16, 347 (1966).

4. Turner D.R., Ph.D. Thesis, University of Adelaide (1975).

Appendix I

The relationship between observable and derived parameters for the binding in isolation model.

Consider the simple equilibrium

$$AA + DNA \underset{\leftarrow}{\overset{K}{\rightarrow}} AA\text{-}DNA$$

For any known total aminoacridine and DNA concentration the equilibrium state may be written in terms of equilibrium concentrations as:

$$K = \frac{x}{(T_L - x)(T_A - x)} \qquad \text{--- 1}$$

hence $$Kx^2 - (KT_L + KT_A + 1)x + KT_LT_A = 0 \qquad \text{--- 2}$$

The general solution for the two roots of a quadratic equation such as Eqn. 2 is:

$$x = \frac{1}{2a}(-b \pm \sqrt{b^2-4ac})$$

$$x = \frac{1}{2K}[(KT_L+KT_A+1) \pm \sqrt{(T_L-T_A)^2K^2 + 2(T_L+T_A)K + 1}] \qquad \text{--- 3}$$

For positive values of T_L, T_A and K both roots of the quadratic are real and positive, that is:

$$-b > \sqrt{b^2 - 4ac} > 0 \quad \text{and} \quad a > 0$$

A condition that must be met is that $x < T_L$ and so the smaller of the two solutions is the only physically real solution. The known parameters are ε_F, T_L and T_A and the value of ε_{OBS} is experimentally observed. The unknown parameters are K and ε_B which are constants of the system. The following equality relates these parameters:

$$\varepsilon_{OBS} = [(T_L - x)\varepsilon_F + x\varepsilon_B]/T_L \qquad \text{--- 4}$$

$$x = \frac{[(KT_L+KT_A+1) - \sqrt{(T_L-T_A)^2K^2 + 2(T_L+T_A)K + 1}]}{2K} \qquad \text{--- 5}$$

ε_{OBS} then is a function of the known values (T_L,T_A,ε_F) and the unknown constants (K,ε_B). Equation 4 is fitted to values of K and ε_B using a non-linear fitting program. Since T_L was constant within each set of data the dependent variable, ε_{OBS}, is fitted as a function of the independent variable, T_A. Several curves of $\varepsilon_{OBS} = f(T_A,T_L)$ may be fitted together since K and ε_B are assumed to be constant for all values of T_A and T_L.

Appendix II

PART A

The spectral properties of the 9-aminoacridines in 0.10 M NaCl solution.

This part of the Appendix summarizes the spectral properties of 9AA, 9(Me)AA, 9(Bu)AA, 9(n-Hex)AA and 9(cyc-Hex)AA in tabular form. There are three tables for each aminoacridine. The first table contains the coefficients of the polynomials that describe absorbance as a function of concentration at each of the four temperatures used in this work. The other tables list the molar absorbances at, and the wavelengths of, each of the three peaks of the ^1L_a band for both the monomer (free aminoacridine), and DNA bound form of each compound at the four temperatures. The following notes apply to all these tables.

(1) All absorbance and molar absorbance values quoted, or calculated from polynomials, have been corrected for solution thermal expansion or contraction to their equivalent values at 22°C to enable direct comparison of the values. Those values for the temperatures other than 22°C may be corrected to their actual values at these temperatures by dividing the value by the following factors. At 10°C by 0.999072, at 35°C by 1.003760 and at 50°C by 1.017562.

(2) All maxima wavelengths are quoted to the nearest whole nm. A fixed bandwidth of 0.4 nm was used to determine all the absorbances at the wavelengths quoted.

(3) The polynomials quoted are of the lowest order which gave acceptable fits, as determined by the criteria that no calculated absorbance deviated from a measured

(3) (Continued)

absorbance by more than 0.0010 absorbance units. These polynomials were fitted to data from no fewer than 20 different concentrations in the range 5×10^{-6} M to 8×10^{-5} M and are valid for interpolations within this range. Aminoacridines at concentrations below 5×10^{-6} M were assumed to be monomeric and assigned absorbances calculated from monomer molar absorptivities.

(4) To facilitate any comparison of the values recorded in these tables with values of absorbances or molar absorptivities that may be determined on other spectrophotometers the reader is referred to the discussion of spectrophotometer accuracy and precision in Chapter III 2(e).

TABLE A2-1

9AA/0.10 M NaCl

$$A_F^{401} = aC_F^3 + bC_F^2 + cC_F + d$$

T (°C)	a x 10^{-10}	b x 10^{-6}	c x 10^{-4}	d x 10^5
10		-13.1729	1.06220	1.00337
22		-6.74106	1.03717	3.57829
35	1.18903	-5.46069	1.02293	0.430529
50	1.171985	-4.36697	1.00425	0.391722

Monomer Spectrum

T (°C) \ λ_{max} (nm)	381	401	423
10	6860	10590	8530
22	6780	10400	8315
35	6700	10190	8085
50	6650	10040	7900

E Coli Bound Spectrum

T (°C) \ λ_{max} (nm)	387	407	430
10	3090	4850	4175
22	3060	4760	4055
35	3040	4695	3975
50	3035	4635	3900

TABLE A2-2

9(Me)AA/0.10 M NaCl

$$A_F^{410} = aC_F^3 + bC_F^2 + cC_F + d$$

T (°C)	a x 10^{-10}	b x 10^{-5}	c x 10^{-3}	d x 10^{6}
10		-45.7945	10.1894	23.38042
22	1.53429	-41.9800	10.0746	5.73485
35	-1.48401	-6.19034	9.93664	-7.84923
50		-10.2344	9.83065	-3.87358

Monomer Spectrum

T (°C) \ λ_{max} (nm)	391	410	432
10	6275	10200	8820
22	6235	10050	8655
35	6200	9930	8525
50	6190	9830	8340

E Coli Bound Spectrum

T (°C) \ λ_{max} (nm)	396	416	439
10	3090	5265	4890
22	3085	5195	4765
35	3070	5145	4715
50	3070	5085	4615

TABLE A2-3

9(Bu)AA/0.10 M NaCl

$$A_F^{408} = aC_F^3 + bC_F^2 + cC_F + d$$

T (°C)	a x 10^{-10}	b x 10^{-6}	c x 10^{-4}	d x 10^{6}
10		-9.18230	1.33320	66.5744
22		-5.21840	1.31313	60.1085
35		-3.74216	1.30034	34.6187
50	3.03120	-5.26818	1.28845	4.40368

Monomer Spectrum

λ_{max} (nm) / T (°C)	389	408	430
10	8500	13350	11090
22	8455	13175	10905
35	8415	13000	10720
50	8405	12850	10550

E Coli Bound Spectrum

λ_{max} (nm) / T (°C)	394	414	438
10	4135	6555	5895
22	4145	6465	5790
35	4155	6410	5710
50	4205	6360	5595

TABLE A2-4

9(n-Hex)AA/0.10 M NaCl

$$A_F^{410} = aC_F^3 + bC_F^2 + cC_F + d$$

T (°C)	a x 10^{-9}	b x 10^{-5} *	c x 10^{-4}	d x 10^{6}
10	-8.74643	-31.0762	1.10852	8.88123
22		-21.5520	1.10402	-57.9485
35	-24.0989	4.00765	1.10206	-48.1393
50	-29.6454	34.4103	1.07564	-48.9004

Monomer Spectrum

T (°C) \ λ_{max} (nm)	392	410	432
10	6835	11100	9590
22	6860	11040	9515
35	6935	11020	9465
50	6800	10730	9190

E Coli Bound Spectrum

T (°C) \ λ_{max} (nm)	396	416	439
10	3500	5940	5475
22	3485	5845	5340
35	3480	5810	5295
50	3480	5760	5230

* It should be noted that the occurrence of positive b coefficients at 35°C and 50°C is indicative of the unusual behaviour of this compound at these temperatures in as much as the ϵ_F^{410} actually increases with increasing C_F to a C_F of about 3 x 10^{-5} M.

TABLE A2-5

9(cyc-Hex)AA/0.10 M NaCl

$$A_F^{412} = aC_F^3 + bC_F^2 + cC_F + d$$

T (°C)	a x 10^{-10}	b x 10^{-6}	c x 10^{-4}	d x 10^{6}
10		-5.49922	1.23884	40.7036
22	1.63150	-5.27458	1.23100	3.84679
35		-2.53841	1.21798	0.339796
50	2.55596	-3.82320	1.20707	-14.4245

Monomer Spectrum

T (°C) \ λ_{max} (nm)	393	412	434
10	7675	12410	10835
22	7660	12300	10690
35	7645	12180	10540
50	7615	12030	10350

E Coli Bound Spectrum

T (°C) \ λ_{max} (nm)	397	417	441
10	3885	6655	6190
22	3865	6545	6050
35	3835	6465	5960
50	3835	6401	5890

PART B

The spectra of the 9-aminoacridines and their mixtures with *E Coli* DNA in 0.10 M NaCl as solvent.

This part of the Appendix contains plots of the spectra of 9AA, 9(Me)AA, 9(Bu)AA, 9(n-Hex)AA and 9(cyc-Hex)AA and their mixtures with *E Coli* DNA in 0.10 M NaCl as solvent. These plots include the results of internal linearity analysis of each set of spectra. The following notes apply to all these composite plots.

(1) The lines representing the spectra were produced as an exact spline fit of experimental data spaced at 1 nm intervals. Refer to Appendix V, program PLOTT for further details.

(2) Only every second spectrum has been plotted in each set for the sake of clarity of the plots.

(3) All molar absorptivities are corrected to 22°C. Refer to part A of this Appendix, note (2).

(4) The spectra of the monomer free aminoacridine and the calculated spectrum of the DNA bound aminoacridine have been included on the plots. The monomer spectrum has the highest ε^{λ} at the λ_{max} and the bound spectrum the lowest.

(5) The mean T_L values, which can be used to calculate the absorbances actually recorded at any point, were:

9AA $5.370_8 \times 10^{-5}$ M; 9(Me)AA $5.407_8 \times 10^{-5}$ M.
9(Bu)AA $5.377_7 \times 10^{-5}$ M; 9(n-Hex)AA $5.513_6 \times 10^{-5}$ M.
9(cyc-Hex)AA $5.366_2 \times 10^{-5}$ M.

(6) The internal linearity plots cover the range governed by the conditions set out in Chapter IV 3(a). The $\bar{\delta}_{\lambda}$

(6) (Continued)

values are plotted in absorbance units since these relate directly to the expected experimental error.

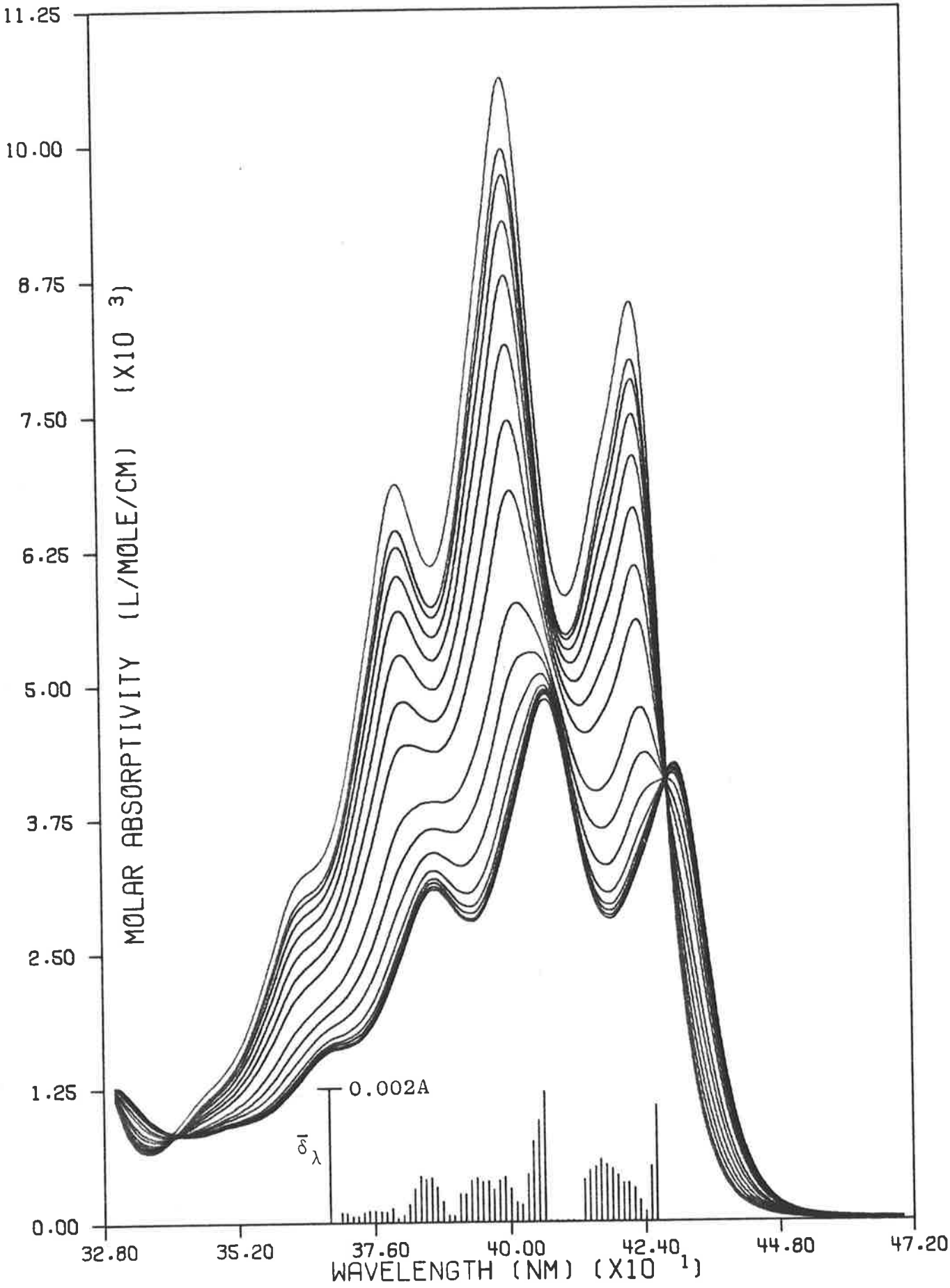

Figure A2-1. The spectra and internal linearity deviation plot for the 9AA/*E Coli* DNA/0.10 M NaCl system at 10°C.

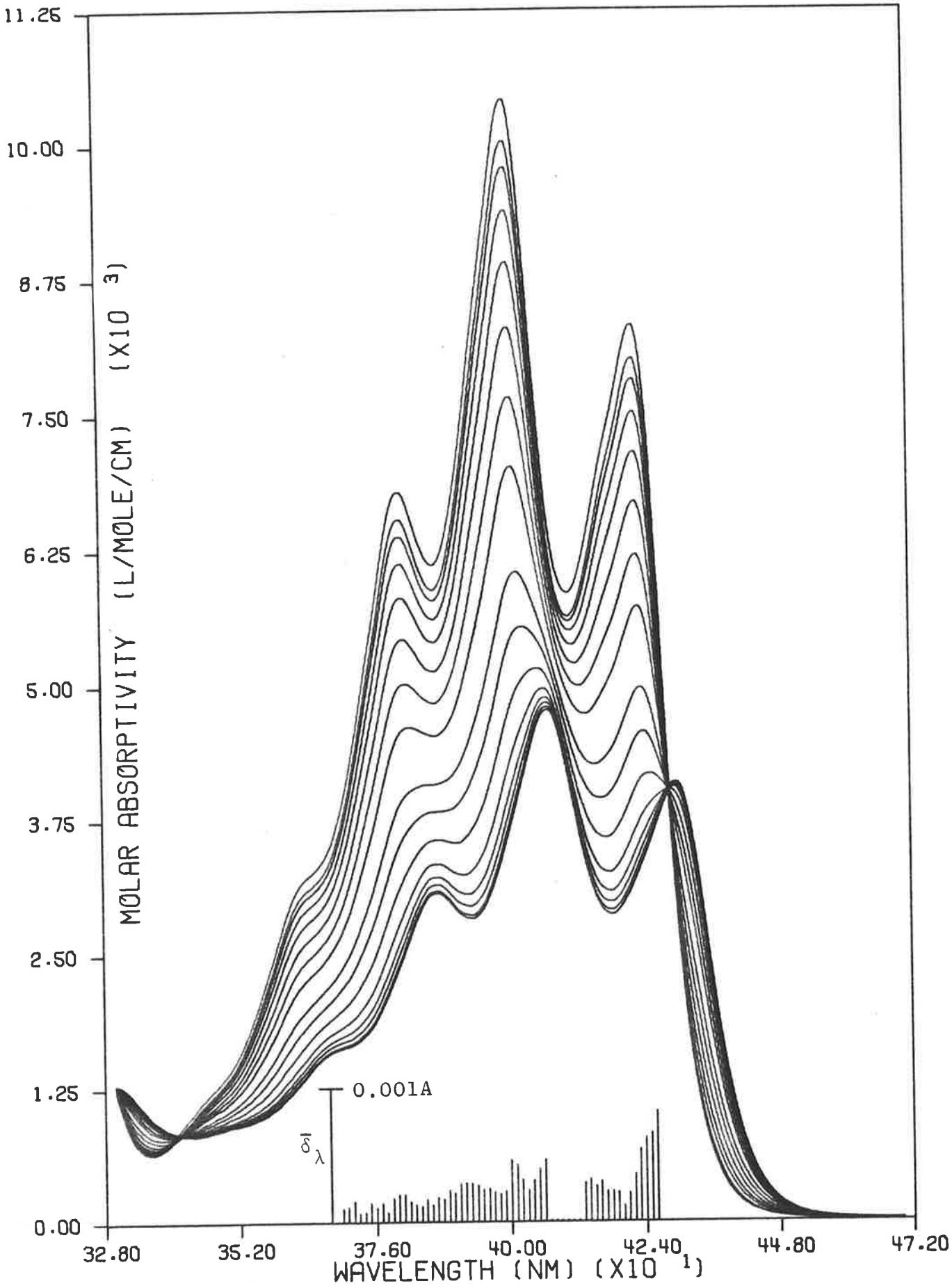

Figure A2-2. The spectra and internal linearity deviation plot for the 9AA/*E Coli* DNA/0.10 M NaCl system at 22°C.

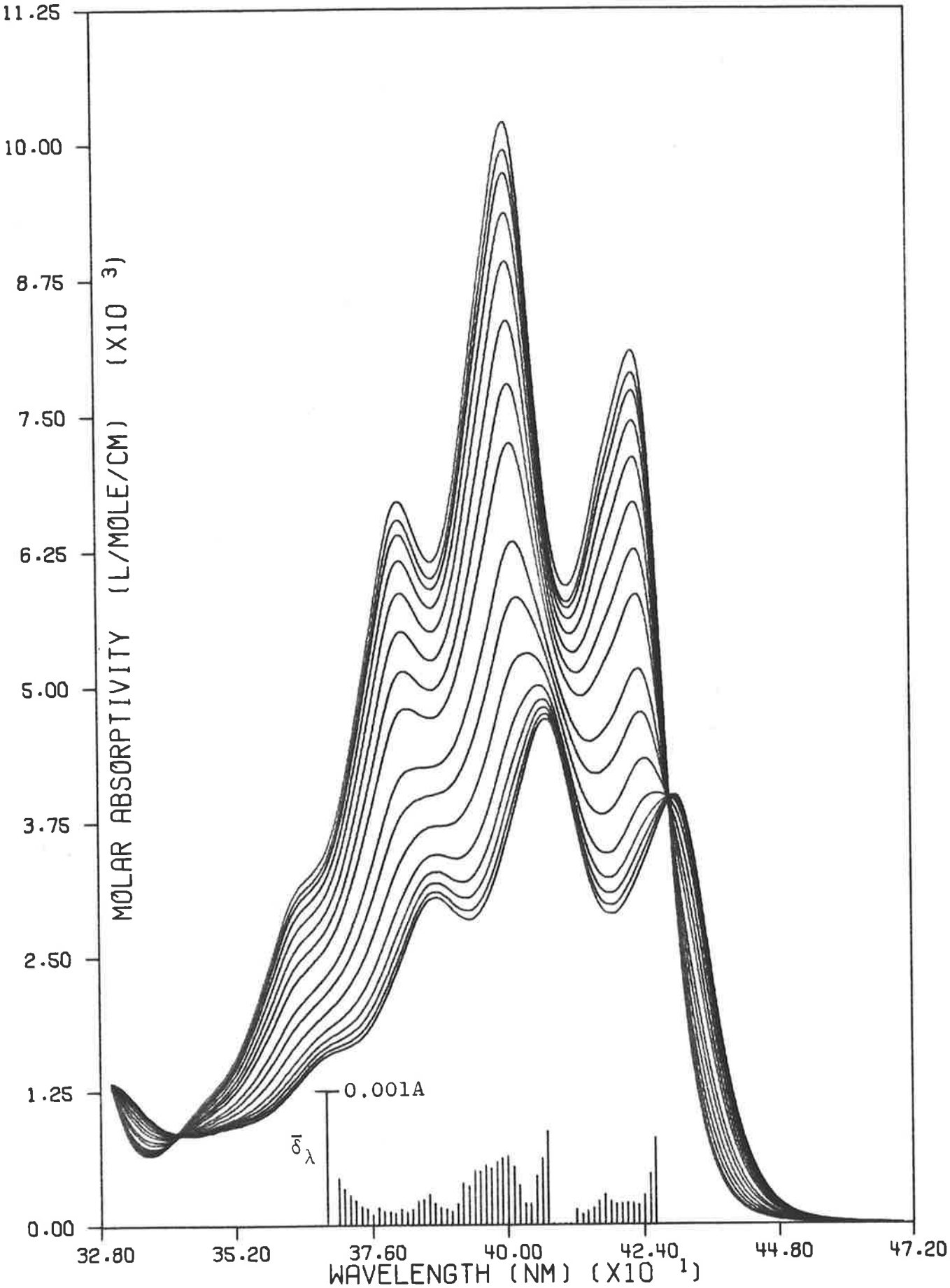

Figure A2-3. The spectra and internal linearity deviation plot for the 9AA/*E Coli* DNA/0.10 M NaCl system at 35°C.

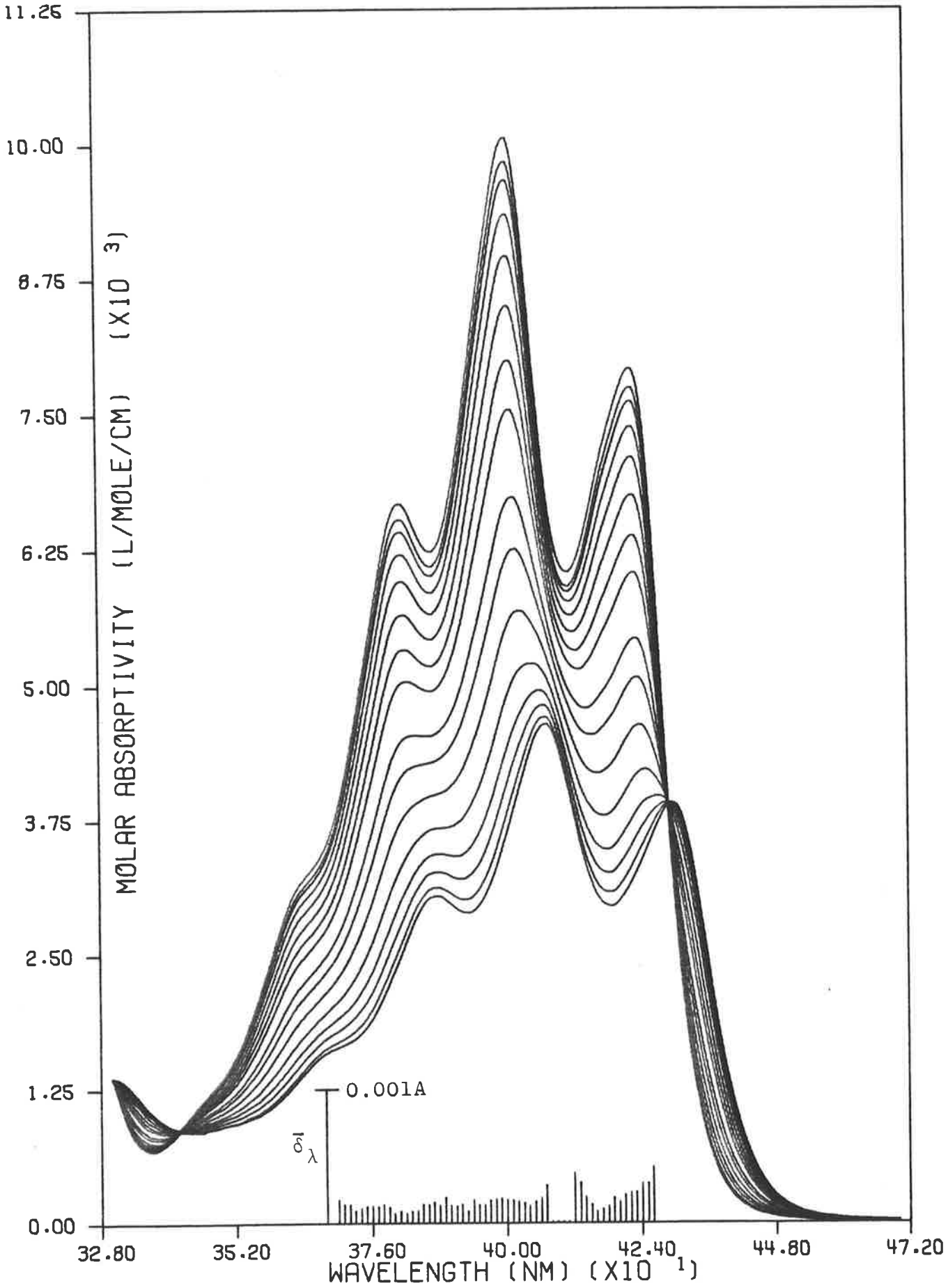

Figure A2-4. The spectra and internal linearity deviation plot for the 9AA/*E Coli* DNA/0.10 M NaCl system at 50°C.

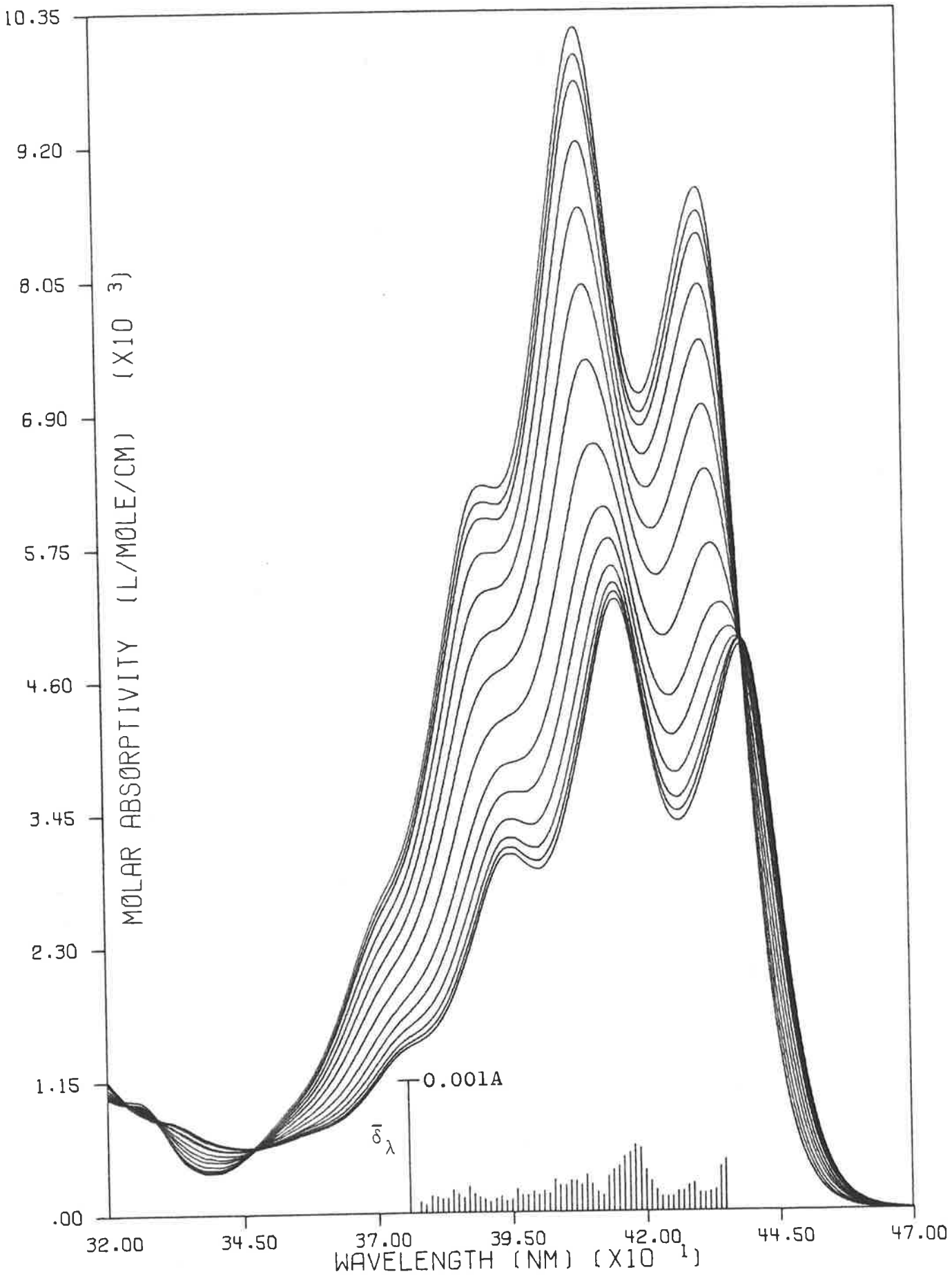

Figure A2-5. The spectra and internal linearity deviation plot for the 9(Me)AA/*E Coli* DNA/0.10 M NaCl system at 10°C.

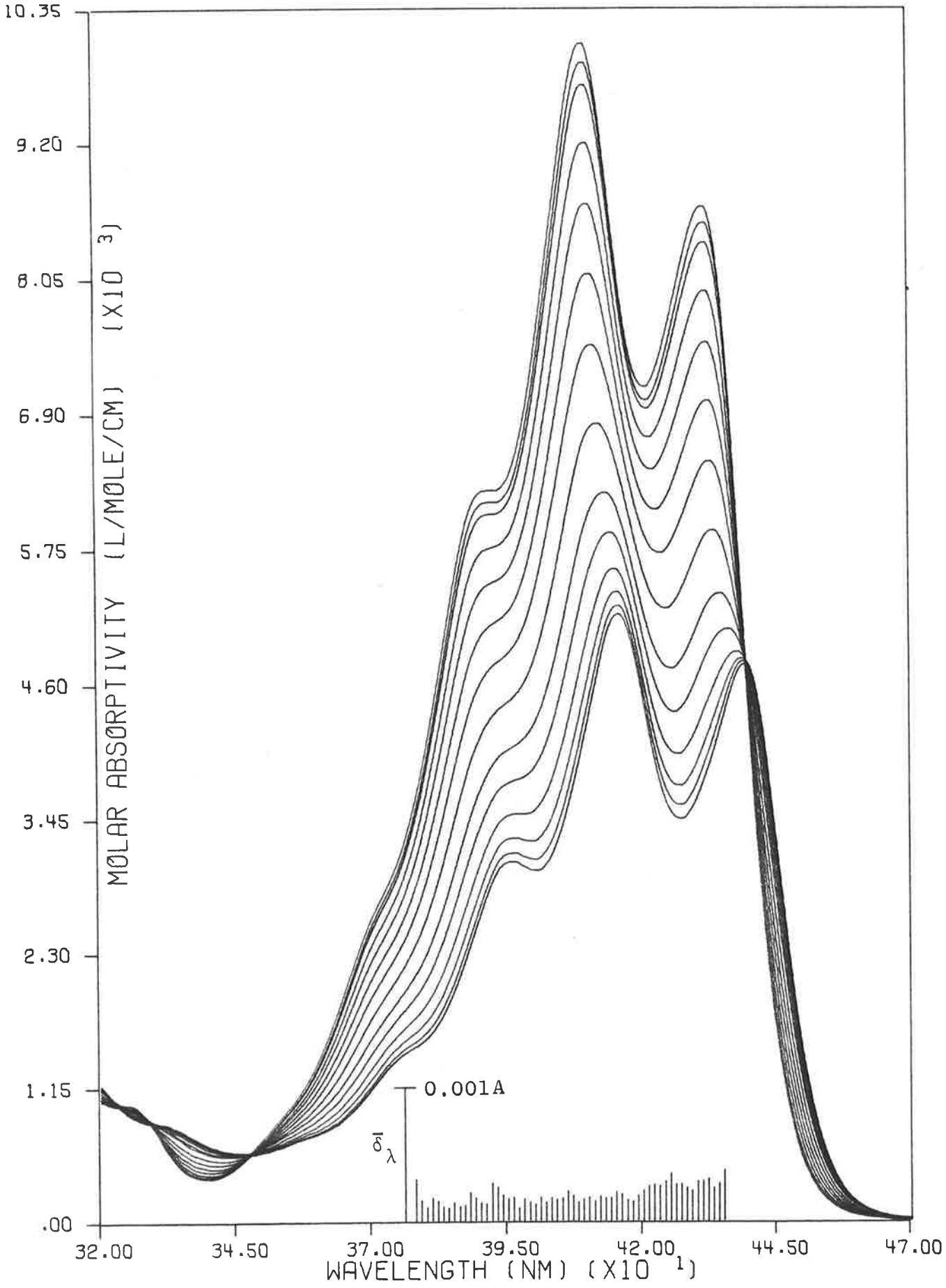

Figure A2-6. The spectra and internal linearity deviation plot for the 9(Me)AA/*E Coli* DNA/0.10 M NaCl system at 22°C.

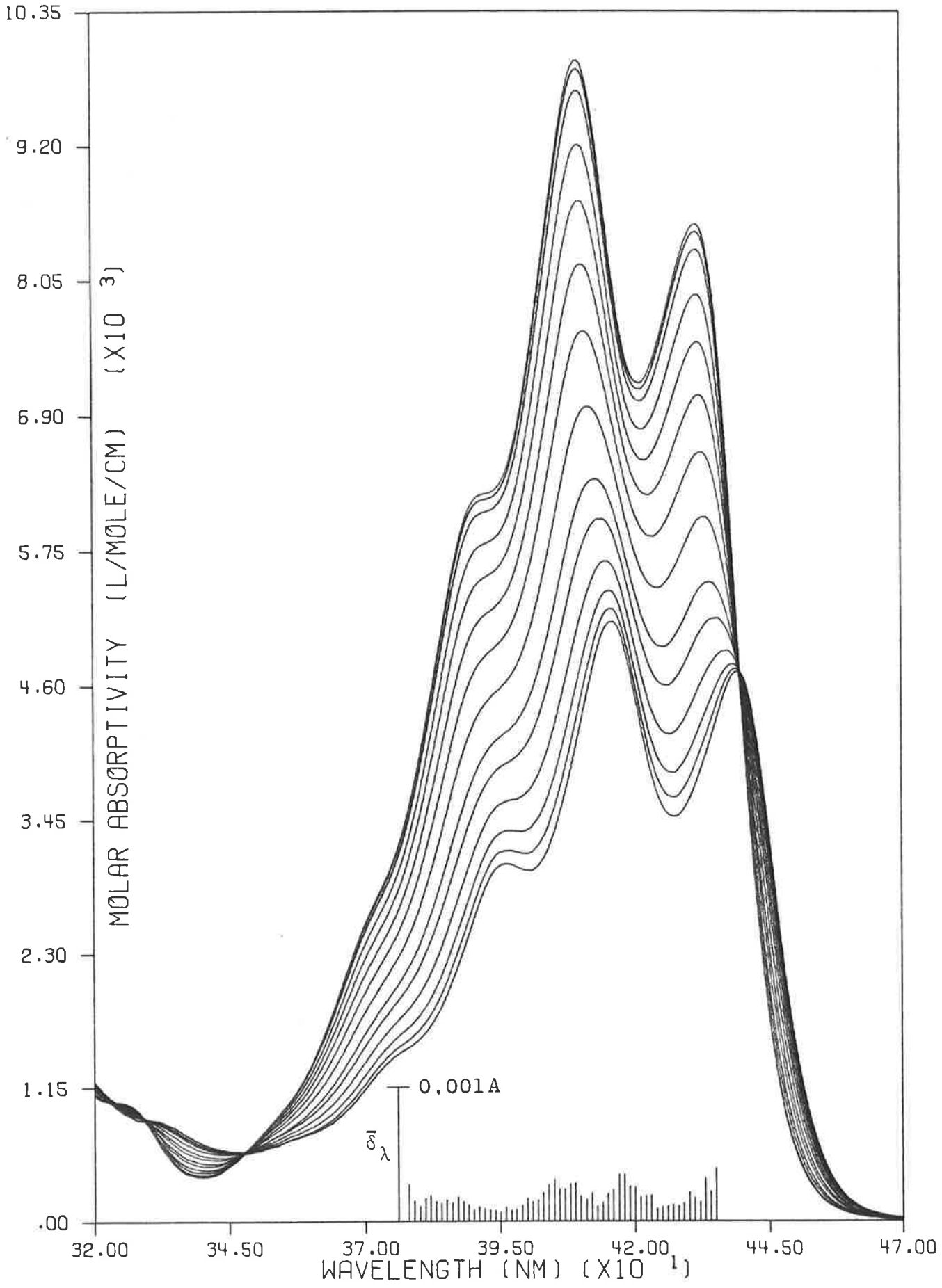

Figure A2-7. The spectra and internal linearity deviation plot for the 9(Me)AA/*E Coli* DNA/0.10 M NaCl system at 35°C.

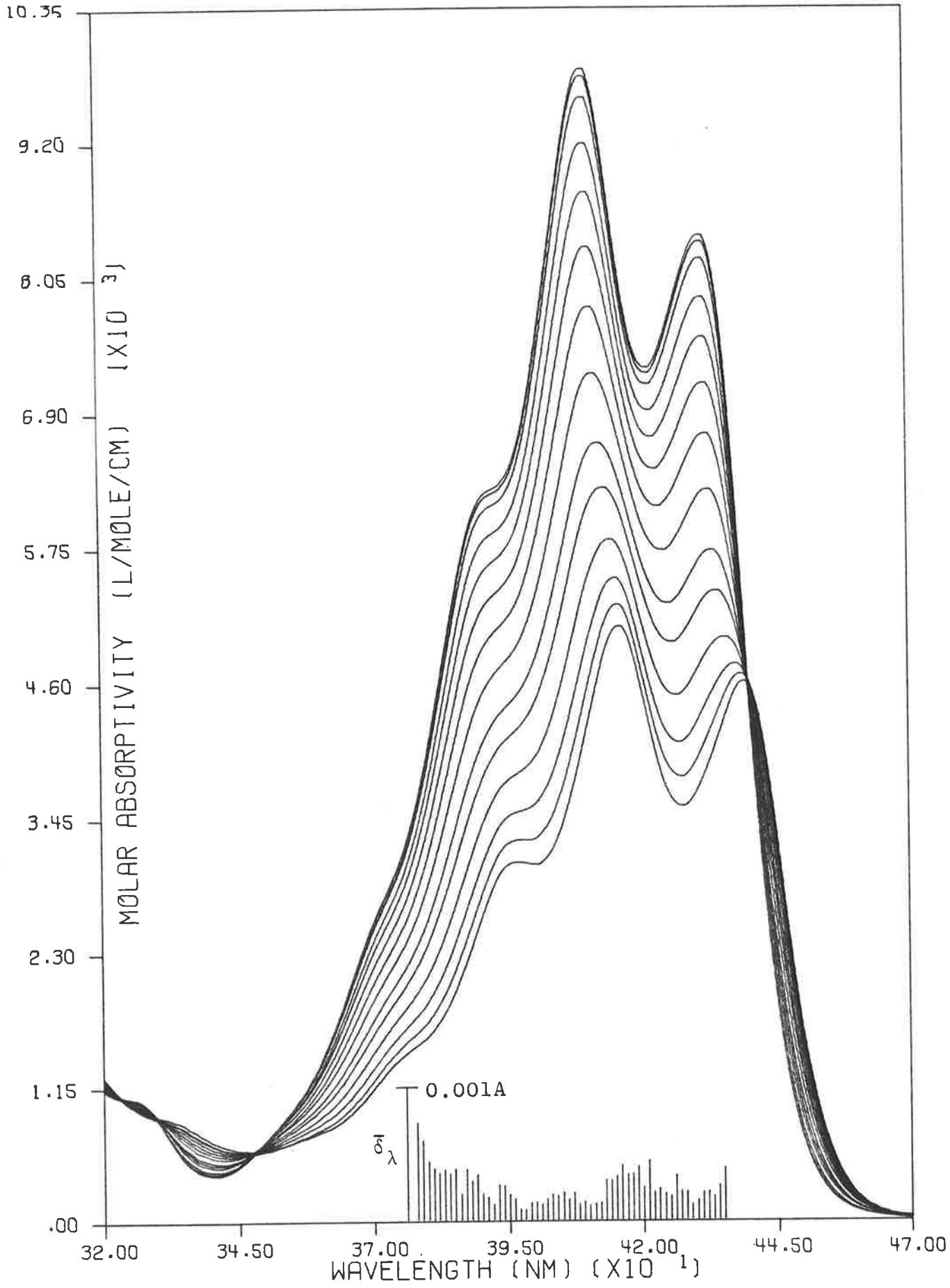

Figure A2-8. The spectra and internal linearity deviation plot for the 9(Me)AA/*E Coli* DNA/0.10 M NaCl system at 50°C.

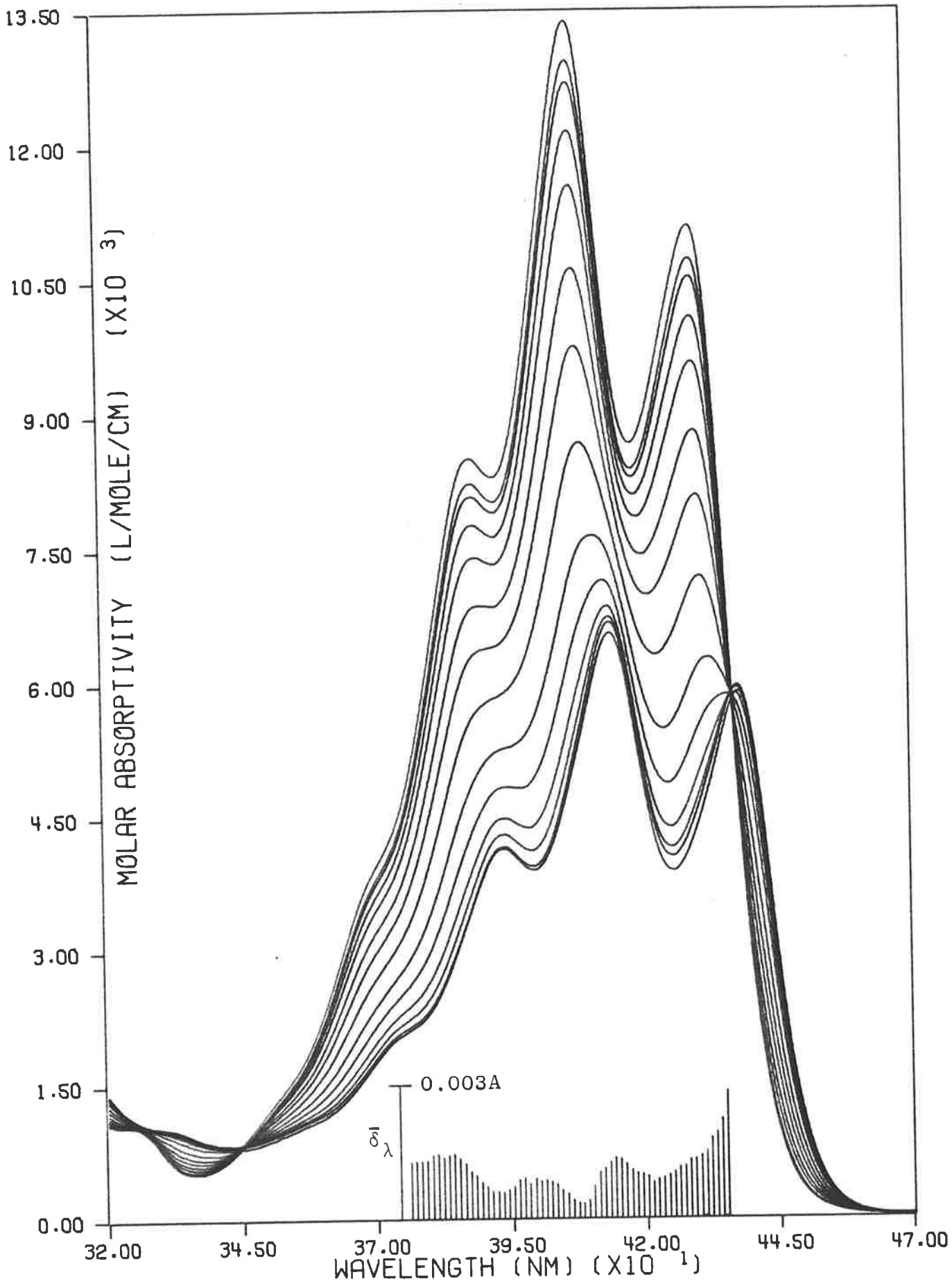

Figure A2-9. The spectra and internal linearity deviation plot for the 9(Bu)AA/*E Coli* DNA/0.10 M NaCl system at 10°C.

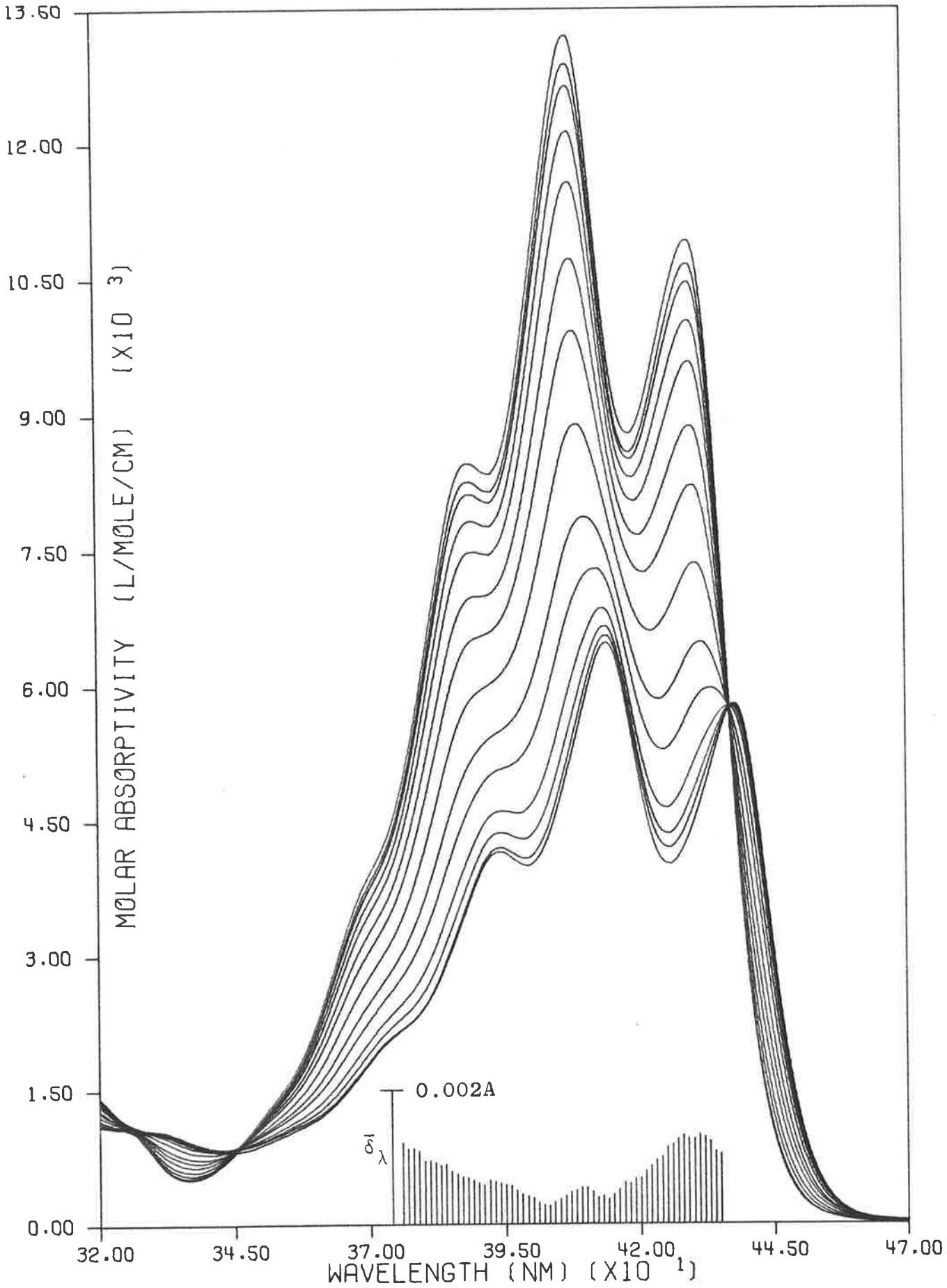

Figure A2-10. The spectra and internal linearity deviation plot for the 9(Bu)AA/*E Coli* DNA/0.10 M NaCl system at 22°C.

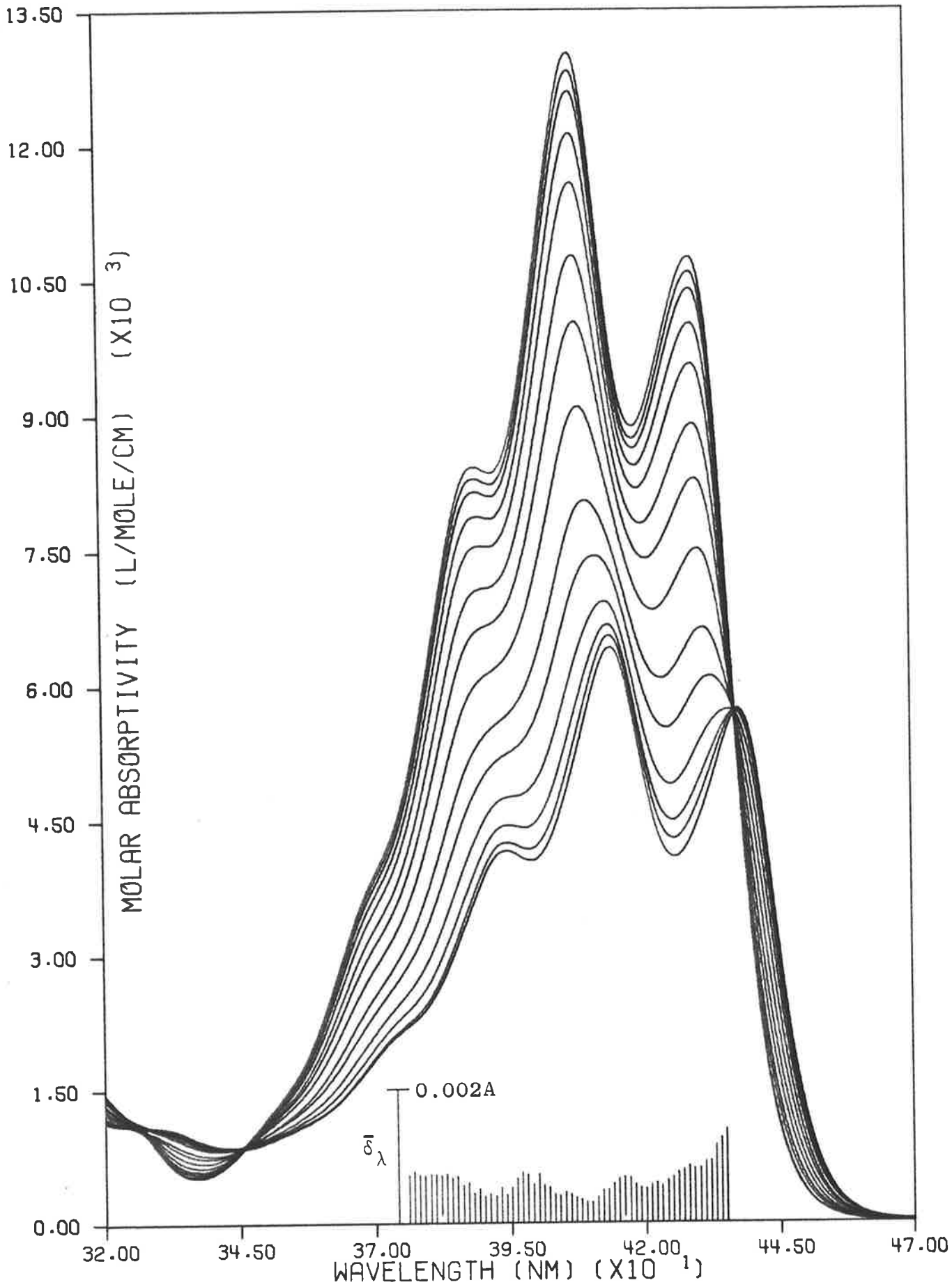

Figure A2-11. The spectra and internal linearity deviation plot for the 9(Bu)AA/*E Coli* DNA/0.10 M NaCl system at 35°C.

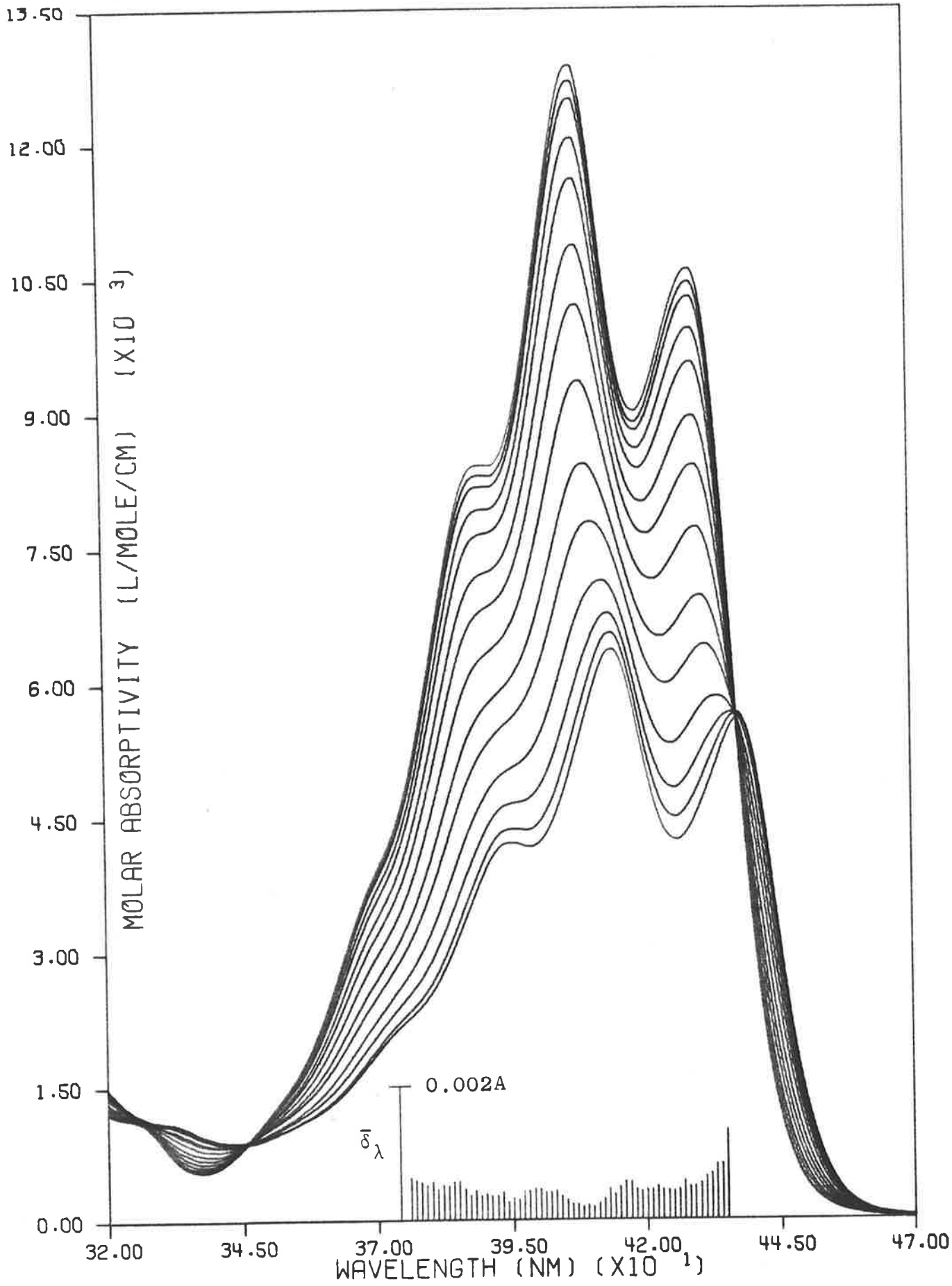

Figure A2-12. The spectra and internal linearity deviation plot for the 9(Bu)AA/*E Coli* DNA/0.10 M NaCl system at 50°C.

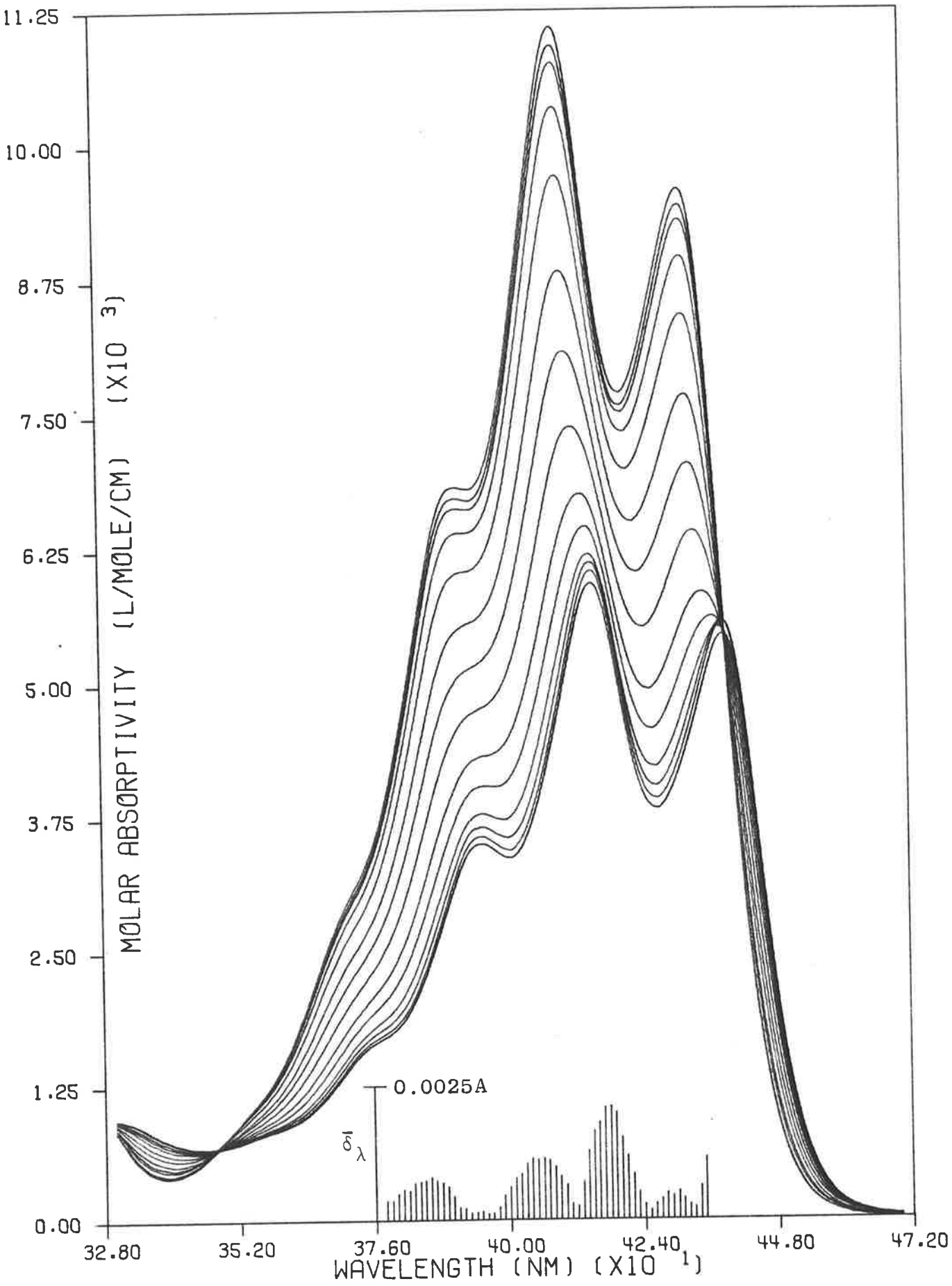

Figure A2-13. The spectra and internal linearity deviation plot for the 9(n-Hex)AA/*E Coli* DNA/0.10 M NaCl system at 10°C.

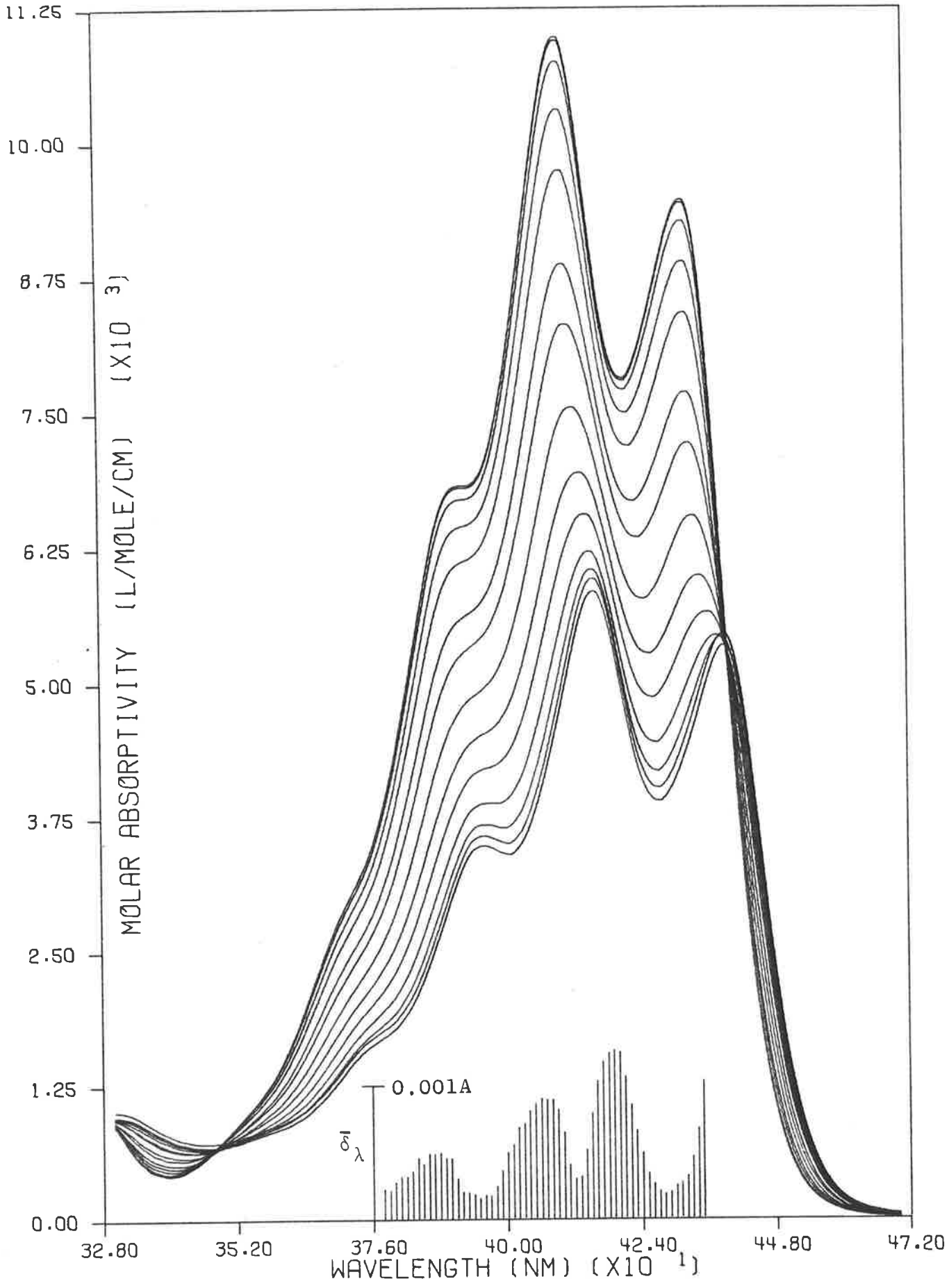

Figure A2-14. The spectra and internal linearity deviation plot for the 9(n-Hex)AA/*E Coli* DNA/0.10 M NaCl system at 22°C.

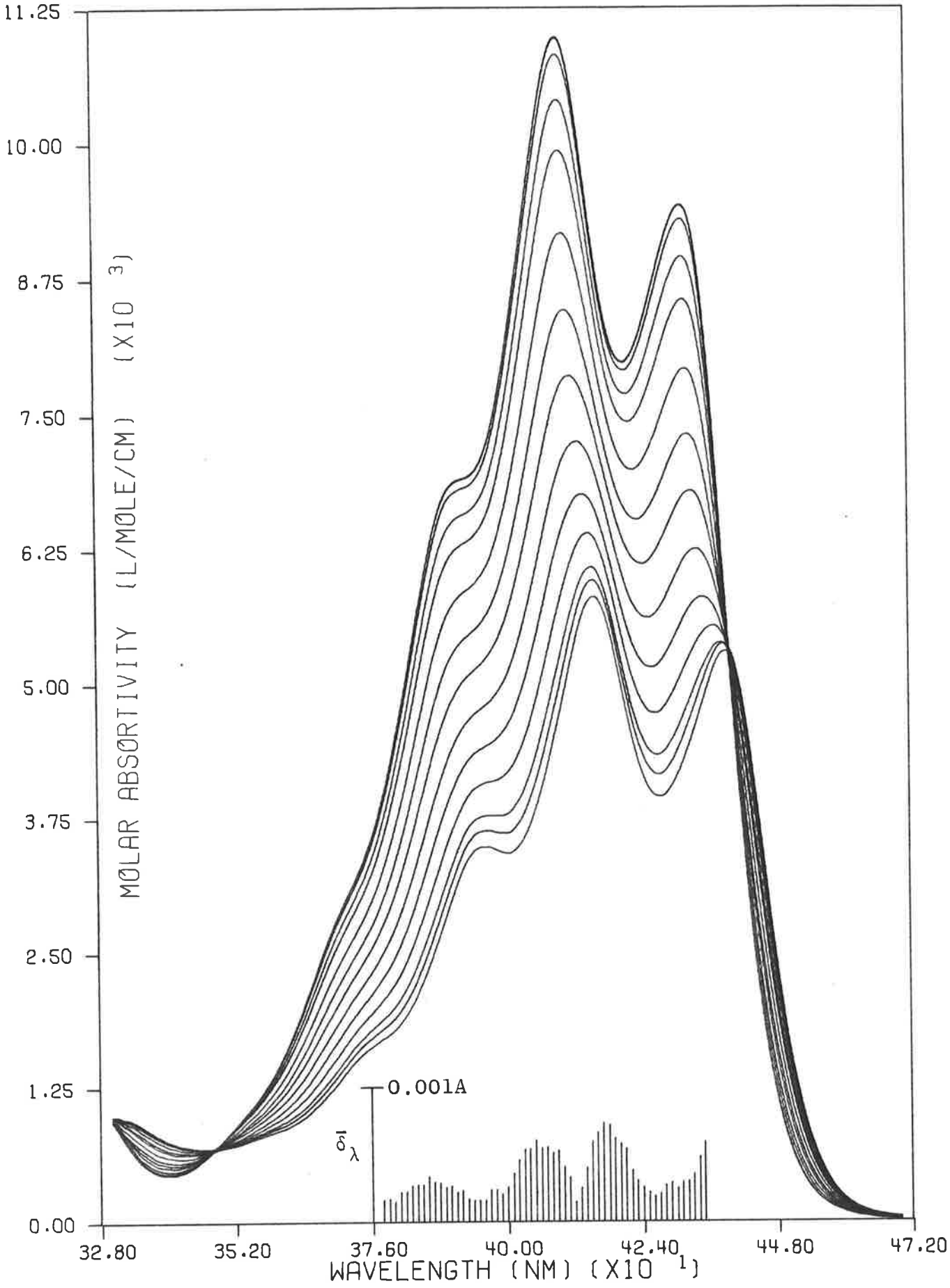

Figure A2-15. The spectra and internal linearity deviation plot for the 9(n-Hex)AA/*E Coli* DNA/0.10 M NaCl system at 35°C.

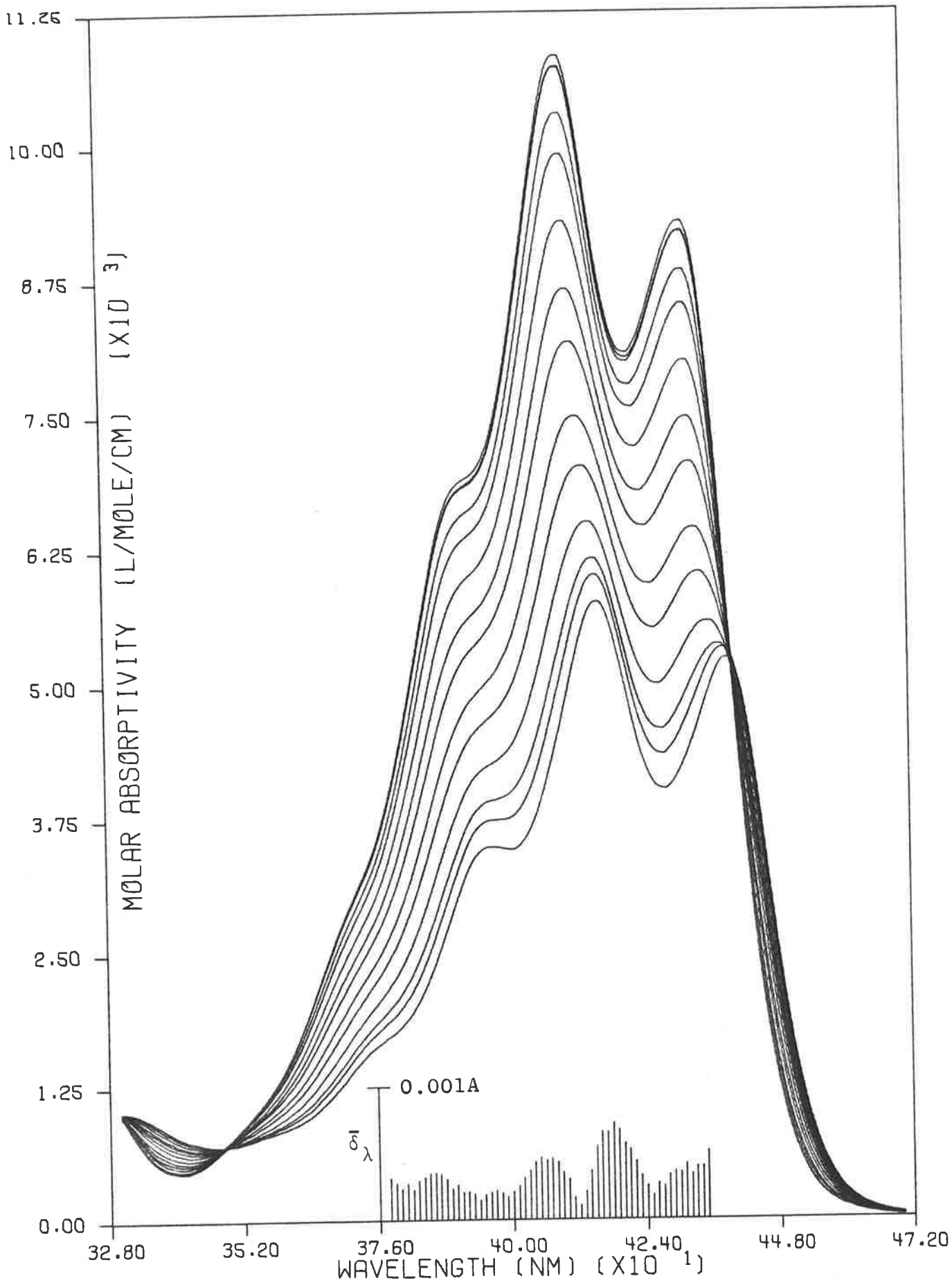

Figure A2-16. The spectra and internal linearity deviation plot for the 9(n-Hex)AA/*E Coli* DNA/0.10 M NaCl system at 50°C.

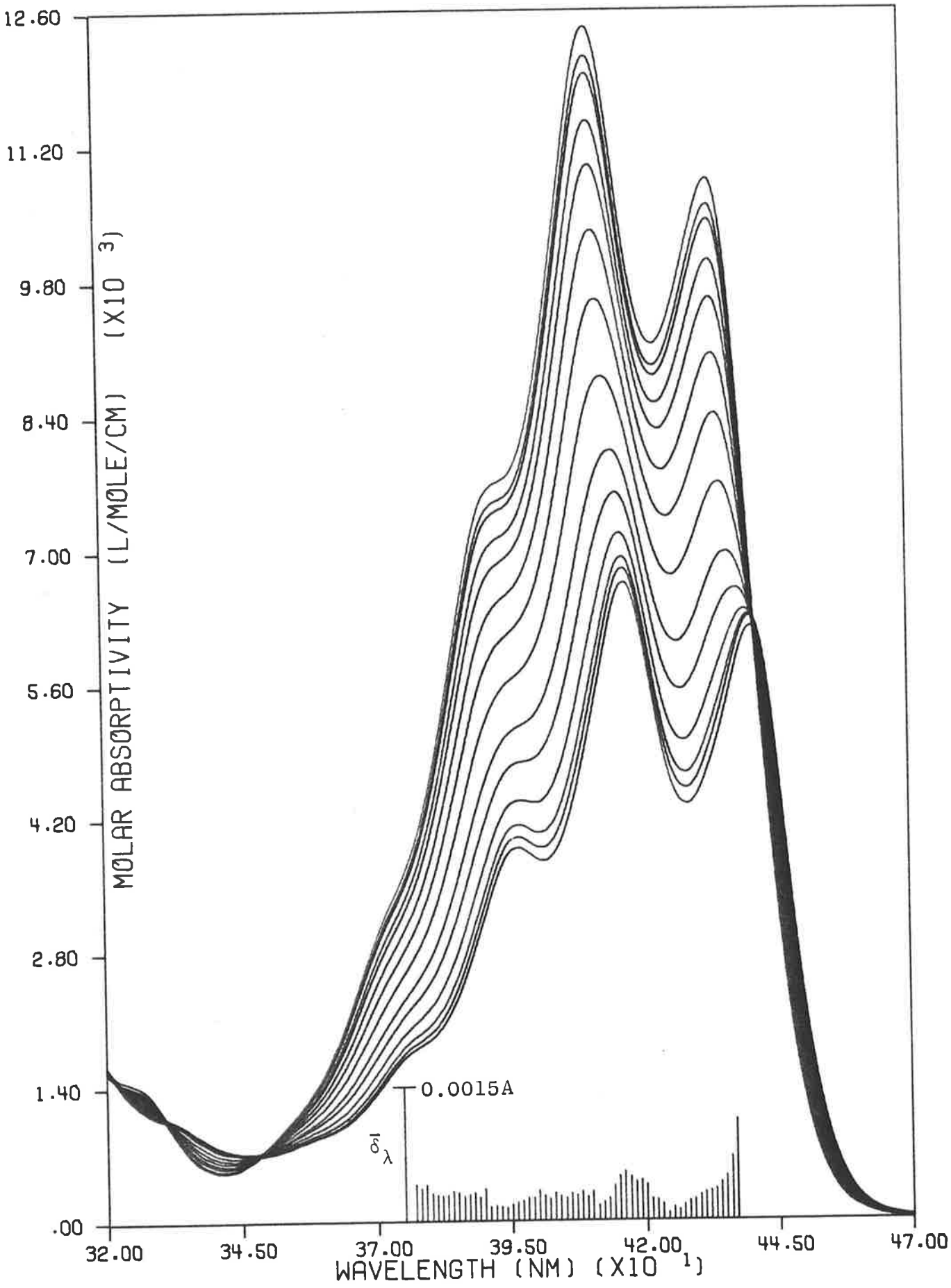

Figure A2-17. The spectra and internal linearity deviation plot for the 9(cyc-Hex)AA/*E Coli* DNA/0.10 M NaCl system at 10°C.

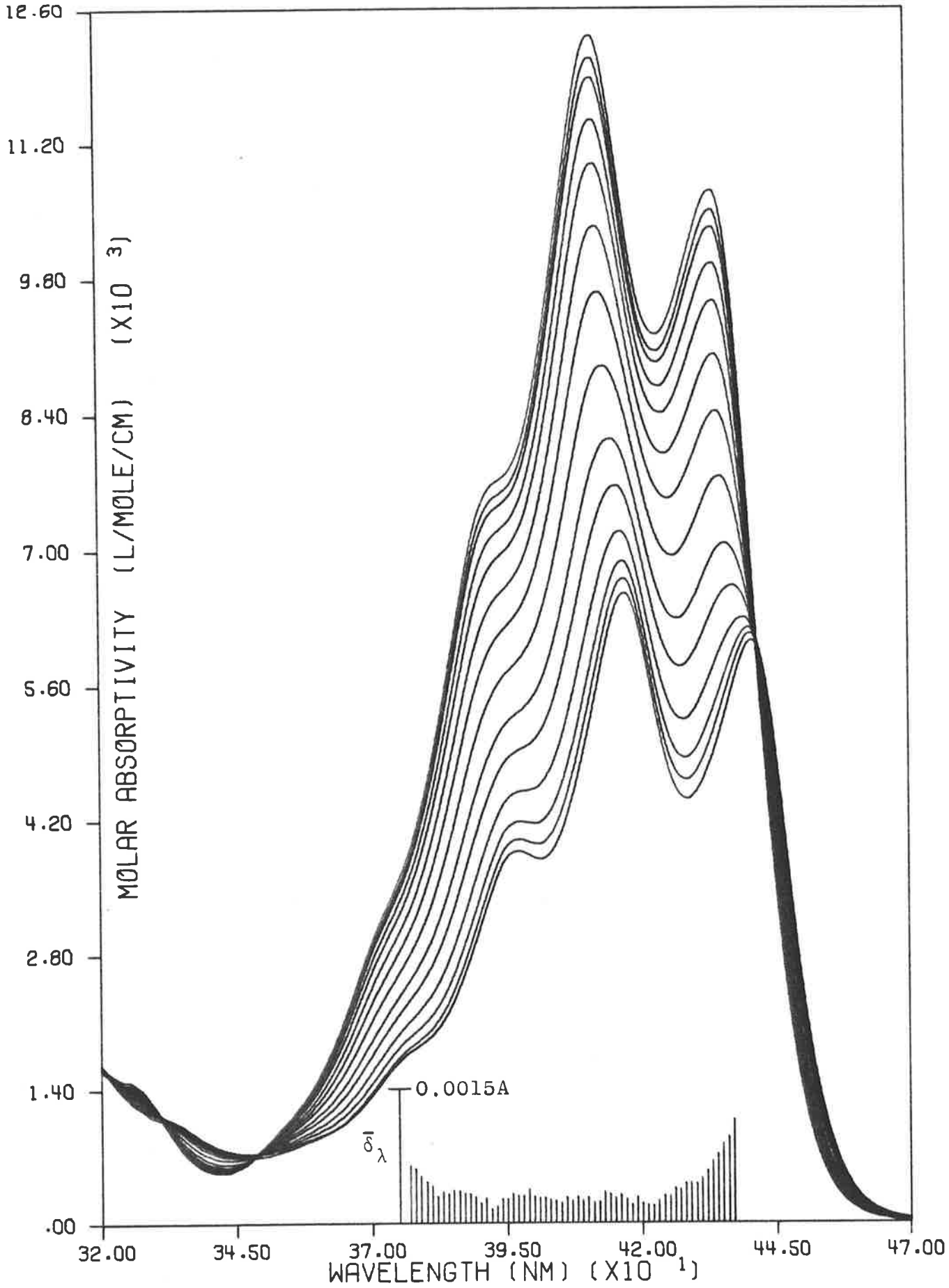

Figure A2-18. The spectra and internal linearity deviation plot for the 9(cyc-Hex)AA/*E Coli* DNA/0.10 M NaCl system at 22°C.

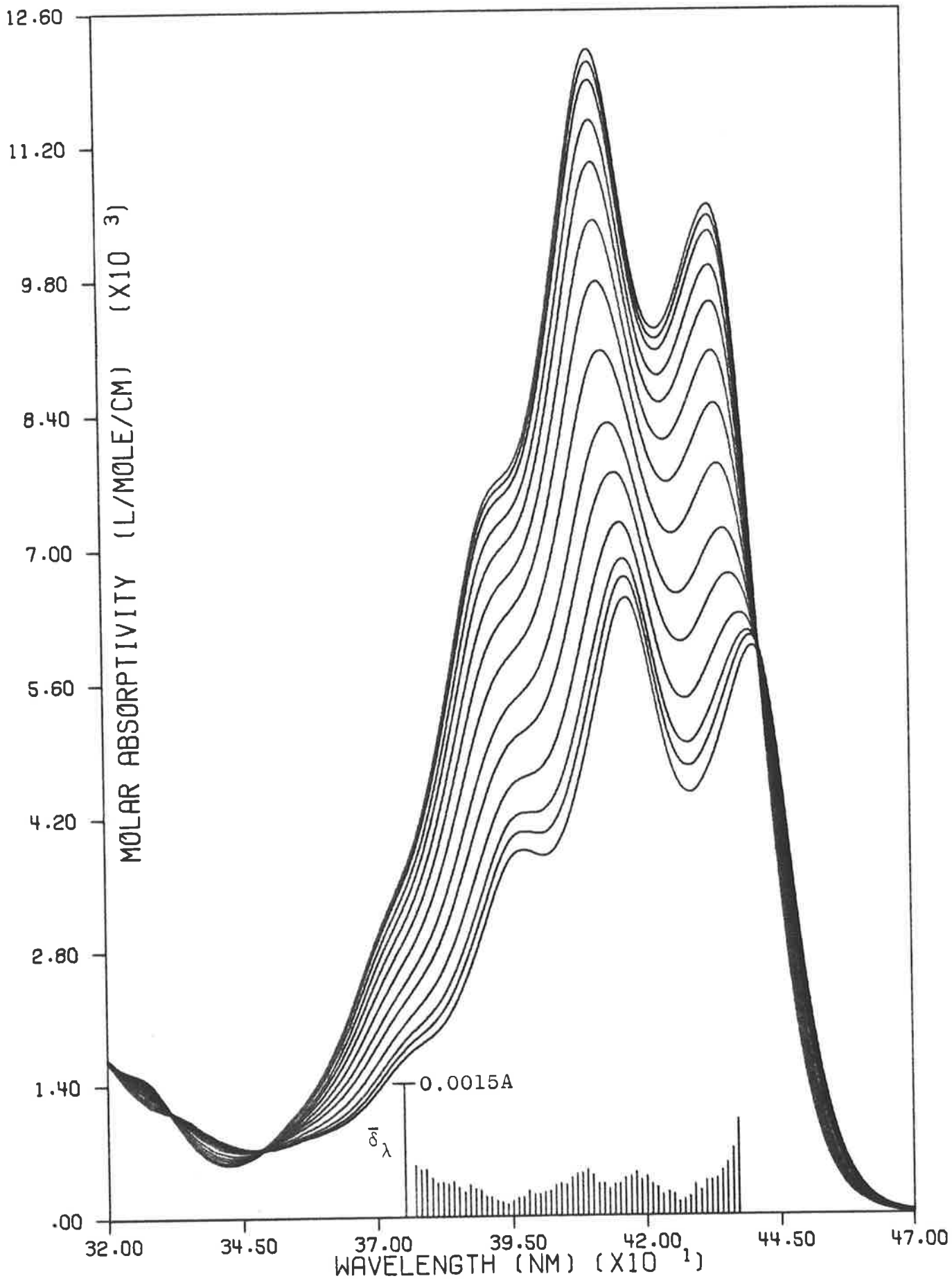

Figure A2-19. The spectra and internal linearity deviation plot for the 9(cyc-Hex)AA/*E Coli* DNA/0.10 M NaCl system at 35°C.

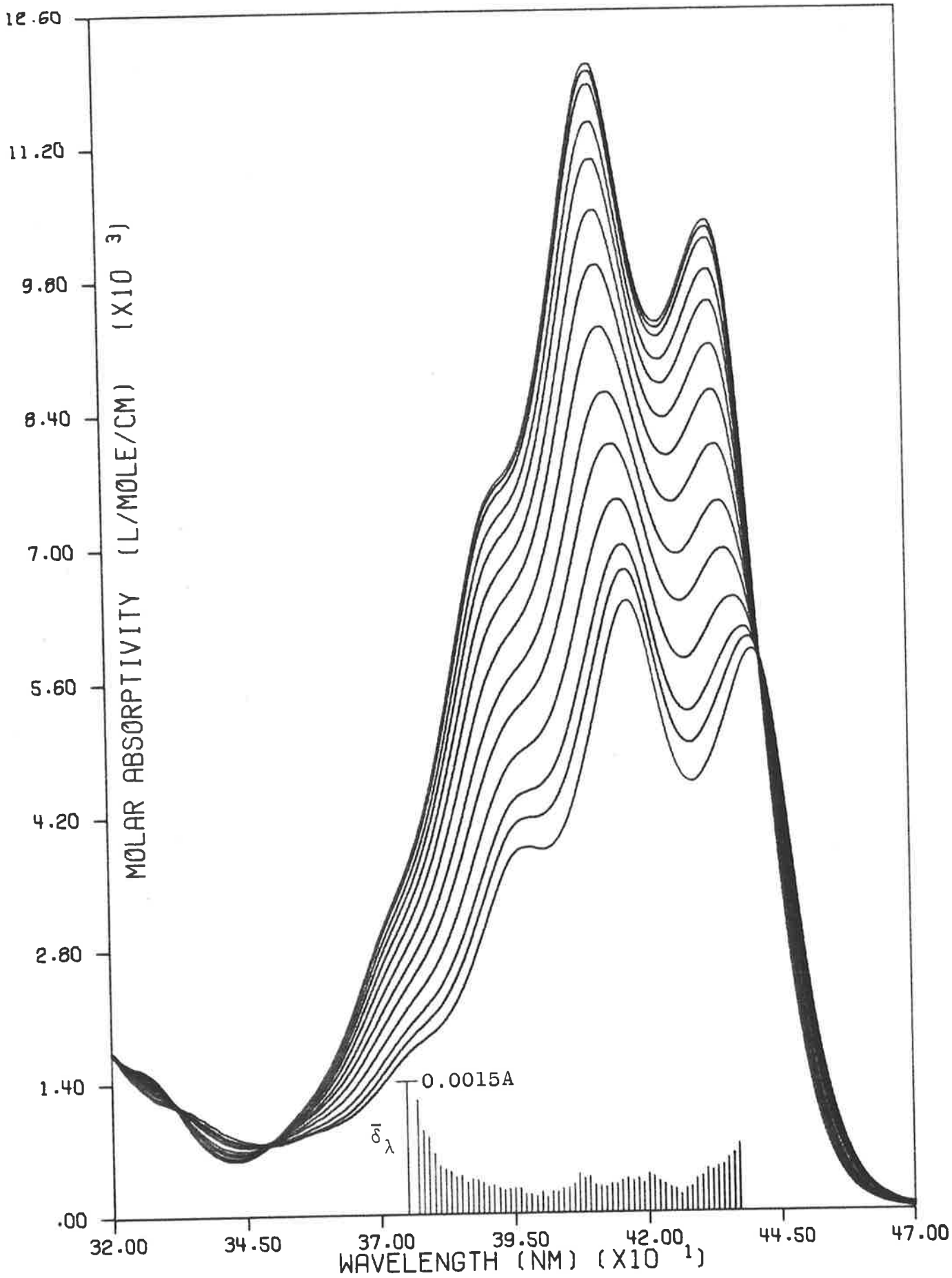

Figure A2-20. The spectra and internal linearity deviation plot for the 9(cyc-Hex)AA/*E Coli* DNA/0.10 M NaCl system at 50°C.

Appendix III

Scatchard Plots of the binding data and the mathematical models of best fit.

This Appendix contains Scatchard plots of the experimentally determined binding data for the binding of 9AA, 9(Me)AA, 9(Bu)AA, 9(n-Hex)AA and 9(cyc-Hex)AA to native *E Coli* DNA in 0.10 M NaCl at 10°C, 22°C, 35°C and 50°C. For each data set the curve of the mathematical model of best fit is also plotted. The parameter values of the model curves are included on these plots only for convenience. These models and the parameters obtained from them are tabulated and discussed in Chapter VI. These binding curves are plotted two per figure in figures numbered A3.1 to A3.10 inclusive.

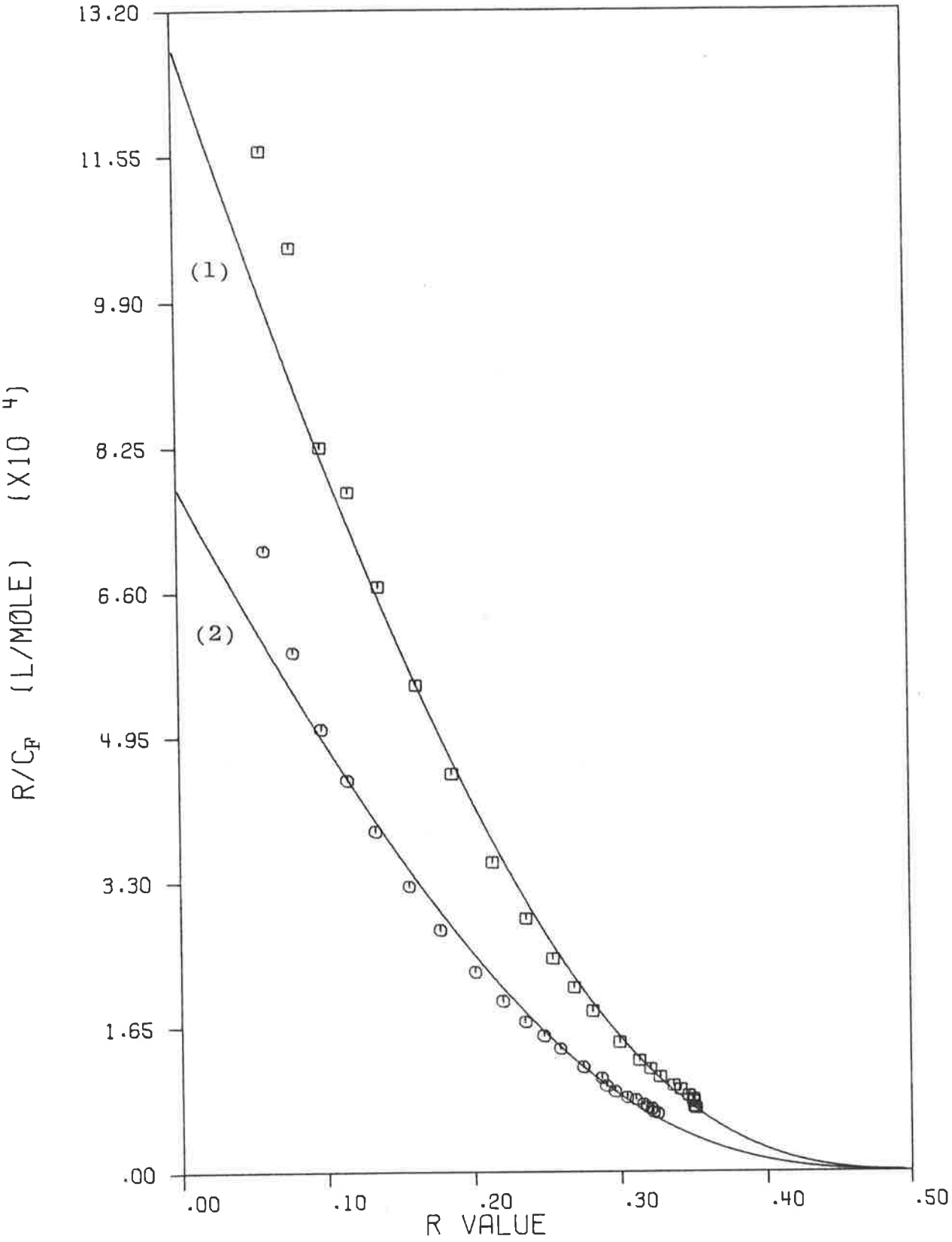

Figure A3-1. The Scatchard plots of the binding data and mathematical model curves for 9AA/*E Coli* native DNA/0.10 M NaCl.
(1) = 10°C; (2) = 22°C.

K_1 = 128100 M^{-1}; k_1 = 0.53_2
K_2 = 77990 M^{-1}; k_2 = 0.49_5

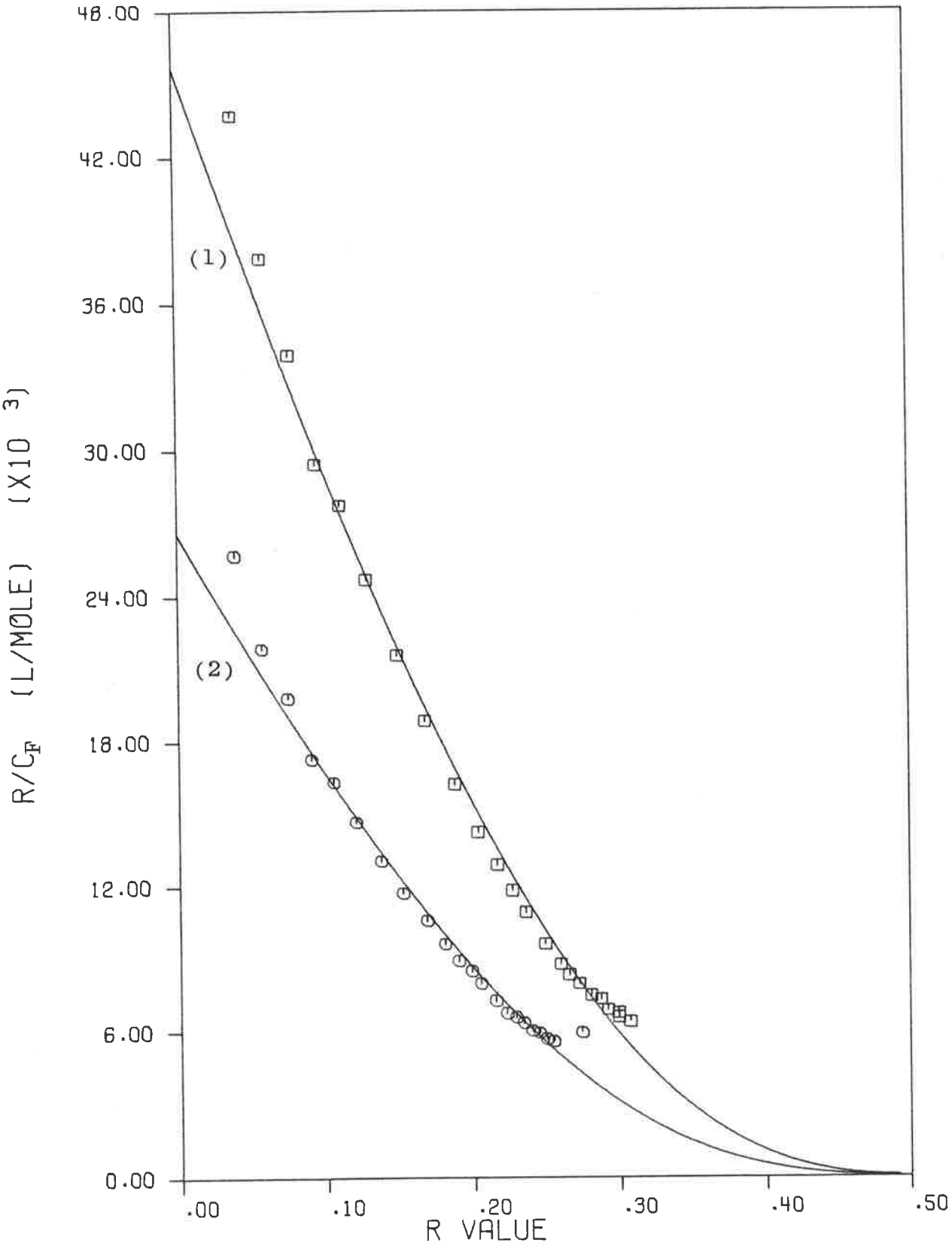

Figure A3-2. The Scatchard plots of the binding data and mathematical model curves for 9AA/*E Coli* native DNA/0.10 M NaCl.
(1) = 35°C; (2) = 50°C.
K_1 = 45670 M^{-1}; k_1 = 0.57$_2$
K_2 = 26570 M^{-1}; k_2 = 0.51$_7$

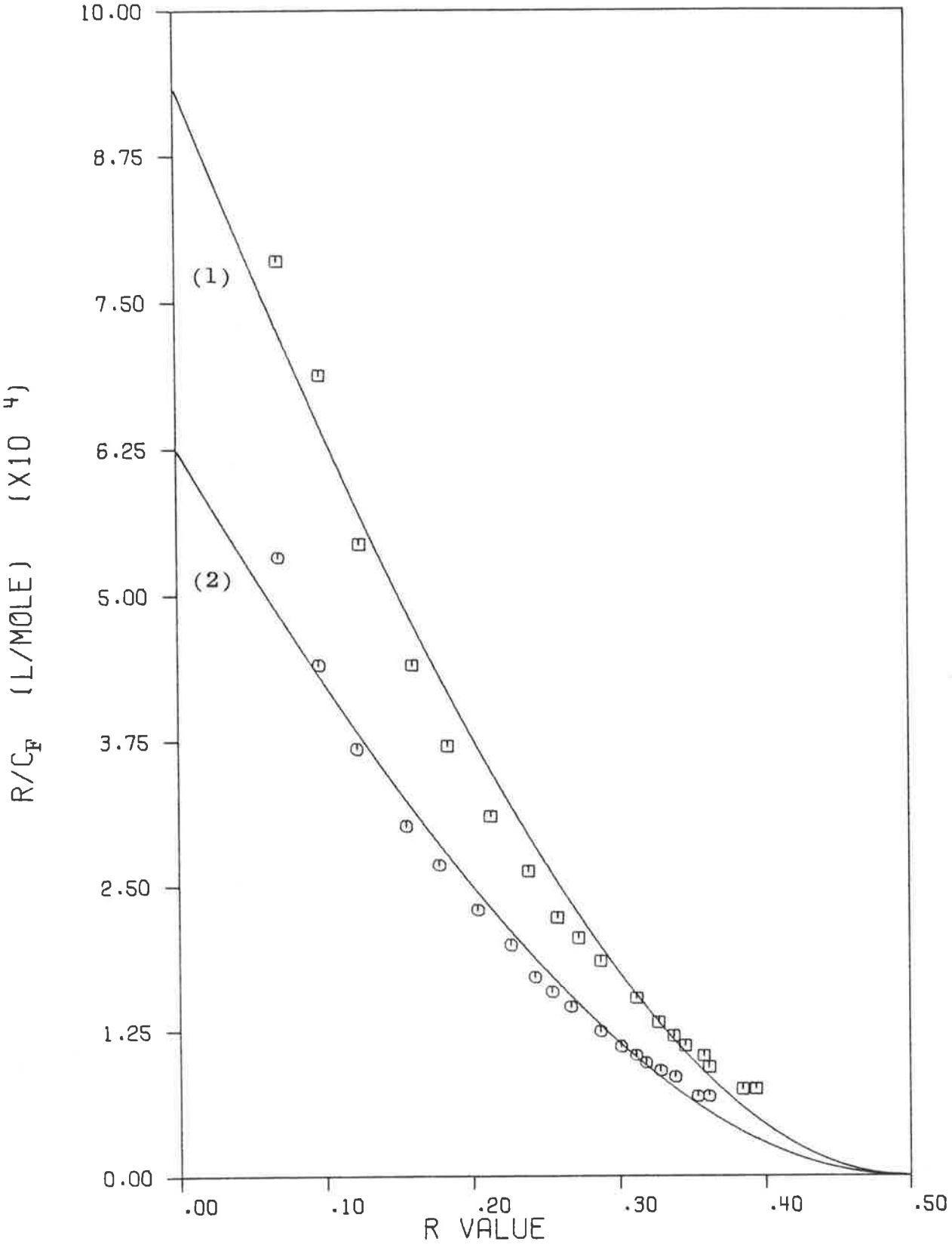

Figure A3-3. The Scatchard plots of the binding data and mathematical model curves for 9(Me)AA/*E Coli* native DNA/0.10 M NaCl.
(1) = 10°C; (2) = 22°C.
K_1 = 93460 M^{-1}; k_1 = 0.82$_6$
K_2 = 62510 M^{-1}; k_2 = 0.80$_7$

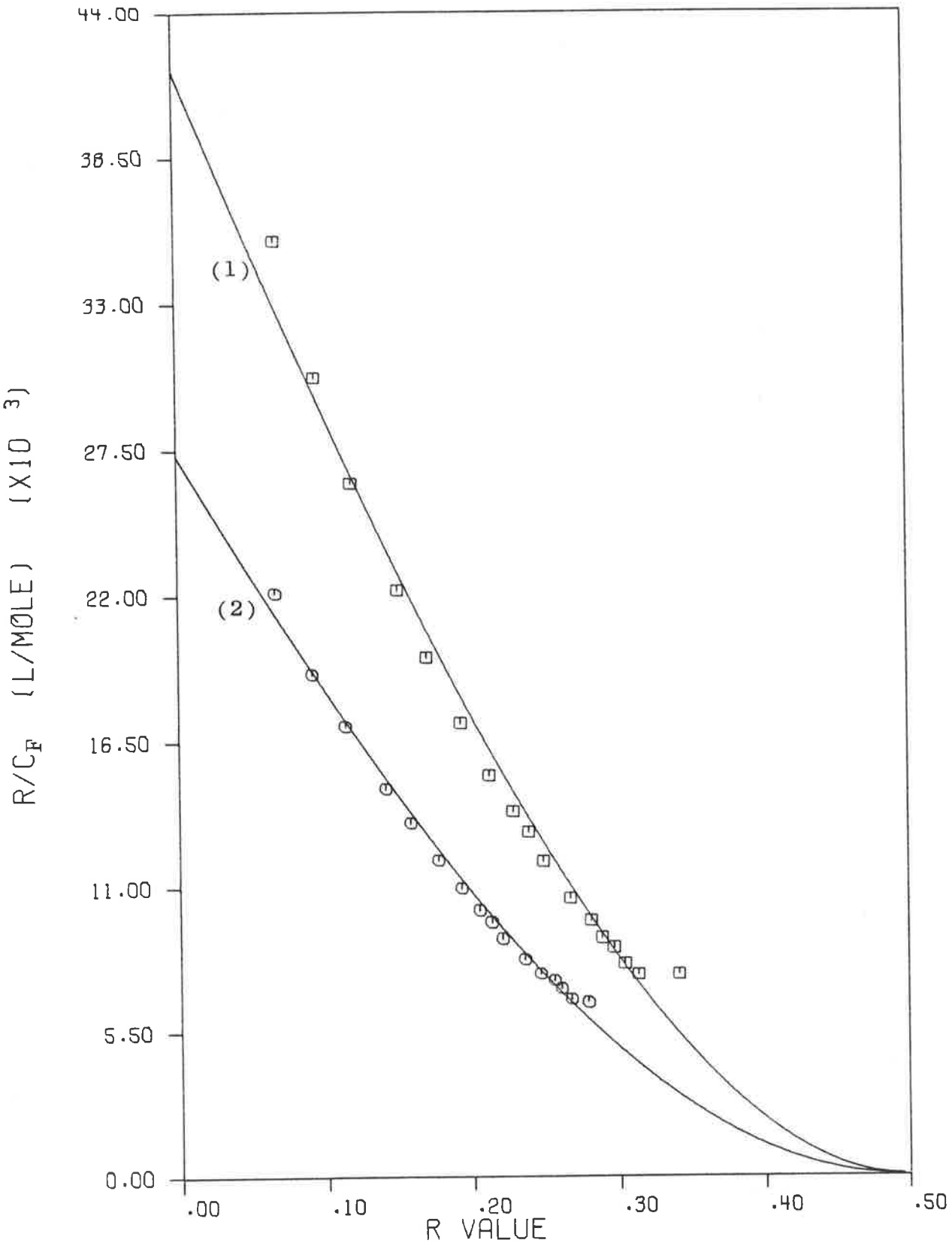

Figure A3-4. The Scatchard plots of the binding data and mathematical model curves for 9(Me)AA/*E Coli* native DNA/0.10 M NaCl.
(1) = 35°C; (2) = 50°C.
K_1 = 41820 M^{-1}; k_1 = 0.87$_4$
K_2 = 27300 M^{-1}; k_2 = 0.78$_8$

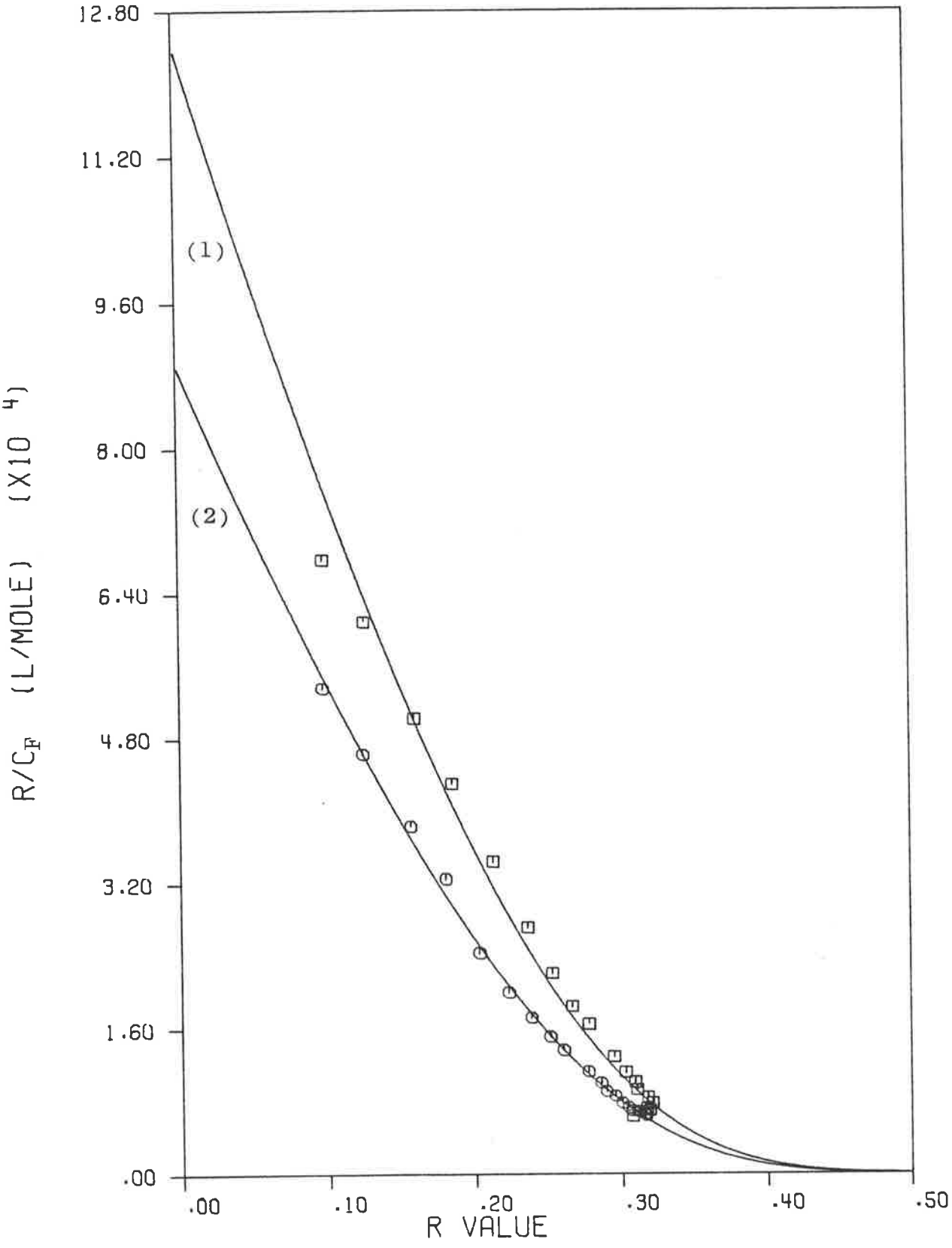

Figure A3-5. The Scatchard plots of the binding data and mathematical model curves for 9(Bu)AA/*E Coli* native DNA/0.10 M NaCl.
(1) = 10°C; (2) = 22°C.
K_1 = 124190 M^{-1}; k_1 = 0.38$_3$
K_2 = 89170 M^{-1}; k_2 = 0.39$_3$

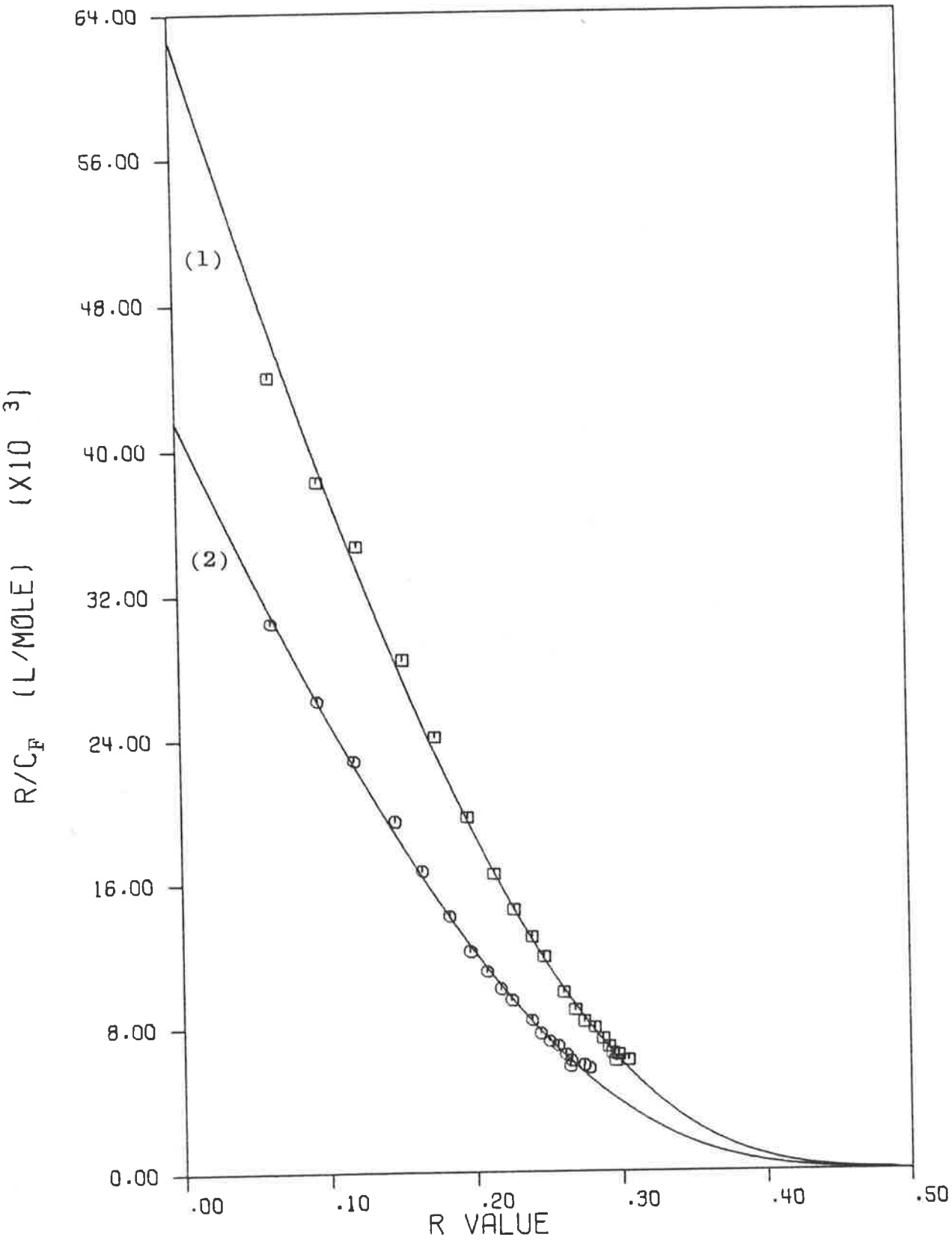

Figure A3-6. The Scatchard plots of the binding data and mathematical model curves for 9(Bu)AA/*E Coli* native DNA/0.10 M NaCl.
(1) = 35°C; (2) = 50°C.
K_1 = 62590 M^{-1}; k_1 = 0.42_6
K_2 = 41540 M^{-1}; k_2 = 0.40_1

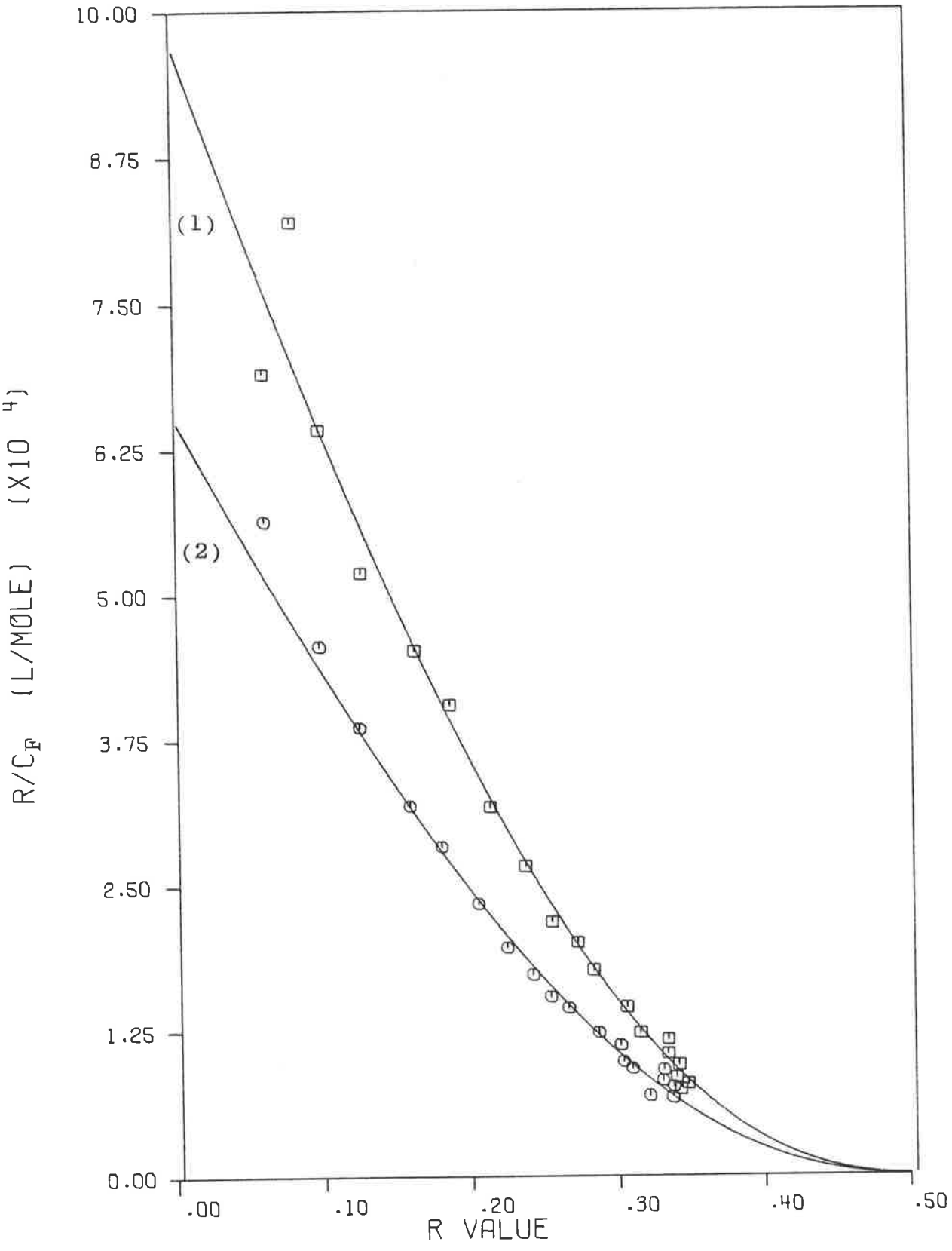

Figure A3-7. The Scatchard plots of the binding data and mathematical model curves for 9(n-Hex)AA/*E Coli* native DNA/0.10 M NaCl.
(1) = 10°C; (2) = 22°C.
K_1 = 96980 M^{-1}; k_1 = 0.64$_5$
K_2 = 64940 M^{-1}; k_2 = 0.68$_6$

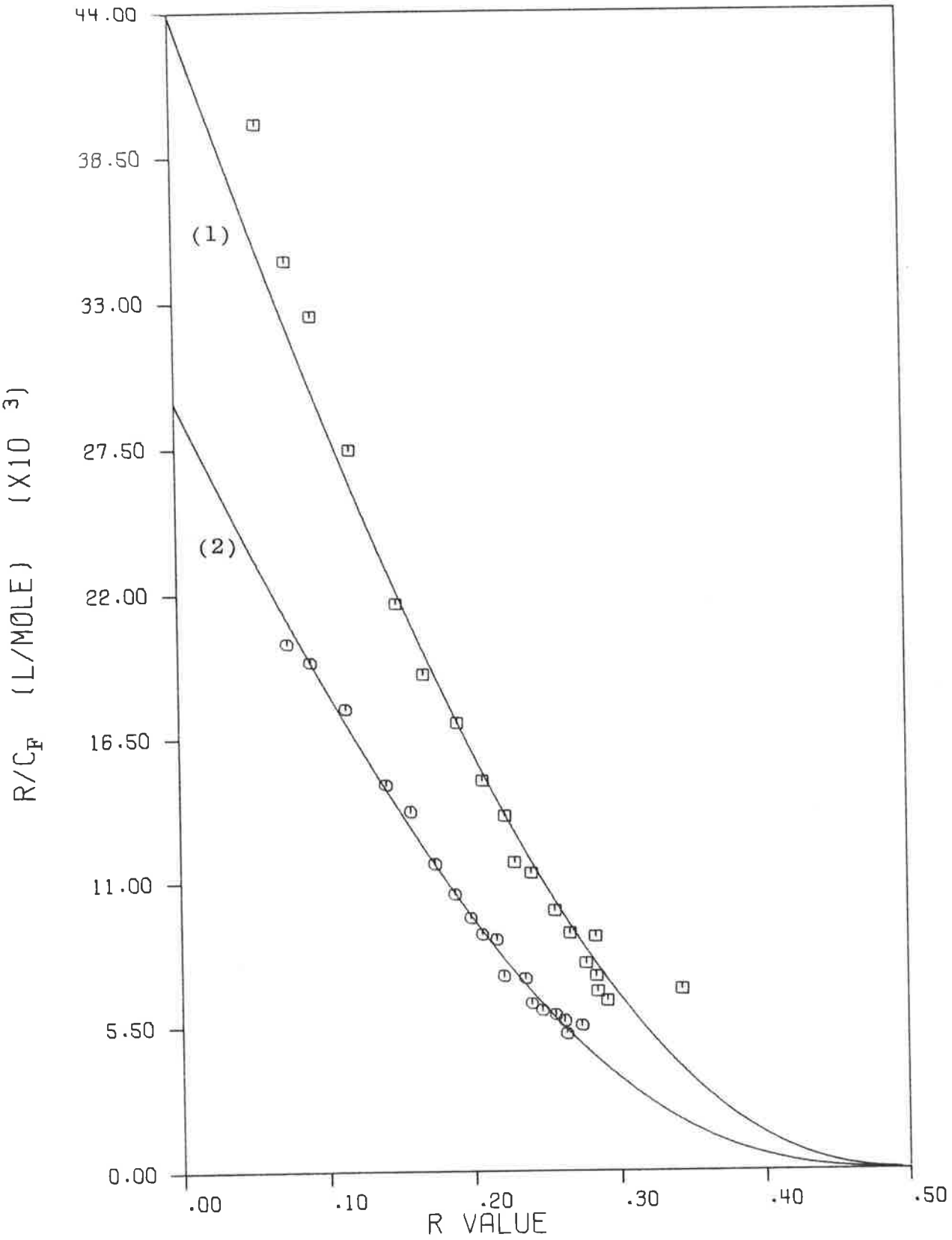

Figure A3-8. The Scatchard plots of the binding data and mathematical model curves for 9(n-Hex)AA/*E Coli* native DNA/0.10 M NaCl.
(1) = 35°C; (2) = 50°C.
K_1 = 43890 M^{-1}; k_1 = 0.67$_0$
K_2 = 29230 M^{-1}; k_2 = 0.53$_2$

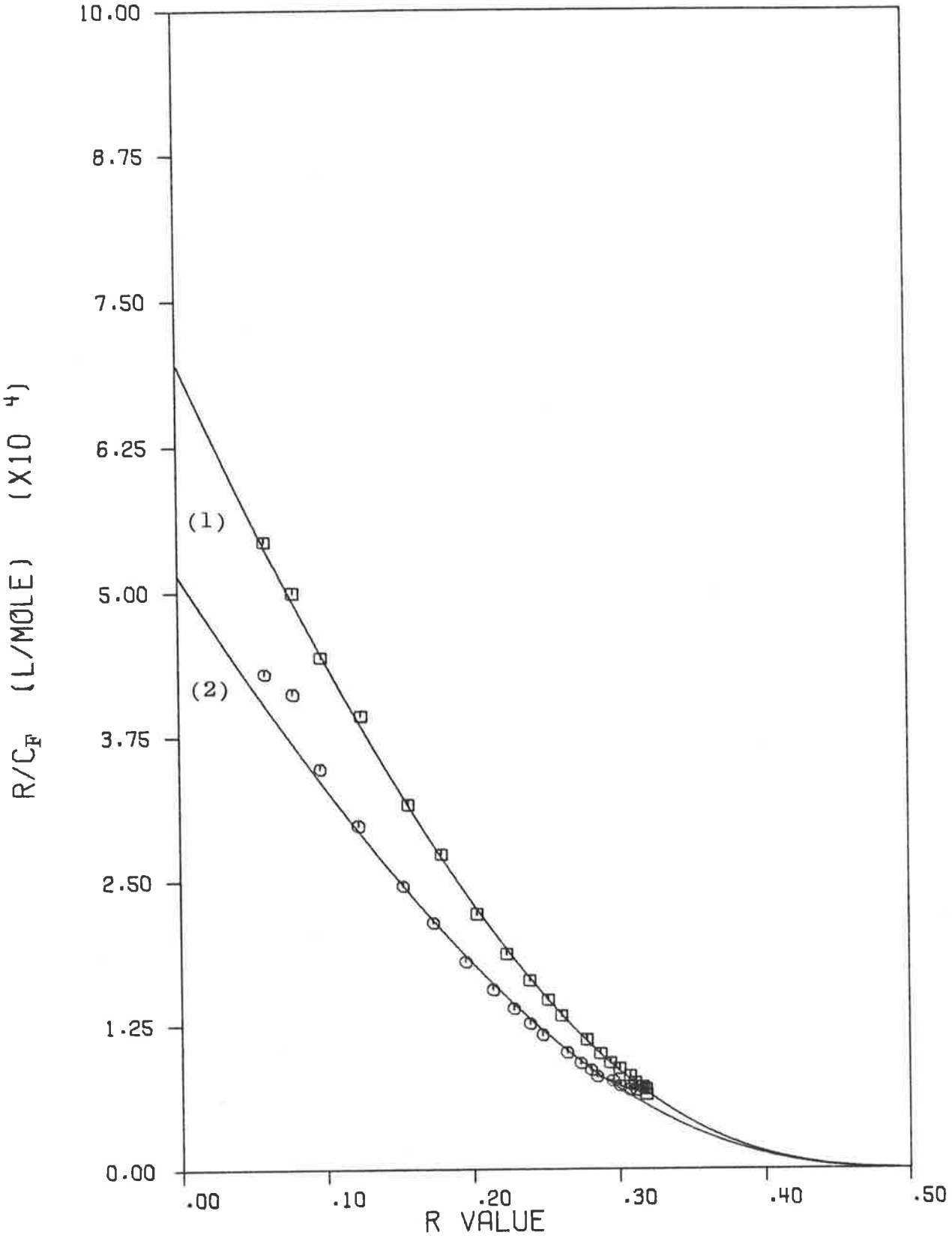

Figure A3-9. The Scatchard plots of the binding data and mathematical model curves for 9(cyc-Hex)AA/*E Coli* native DNA/0.10 M NaCl.
(1) = 10°C; (2) = 22°C.
K_1 = 69610 M^{-1}; k_1 = 0.54$_4$
K_2 = 51440 M^{-1}; k_2 = 0.60$_0$

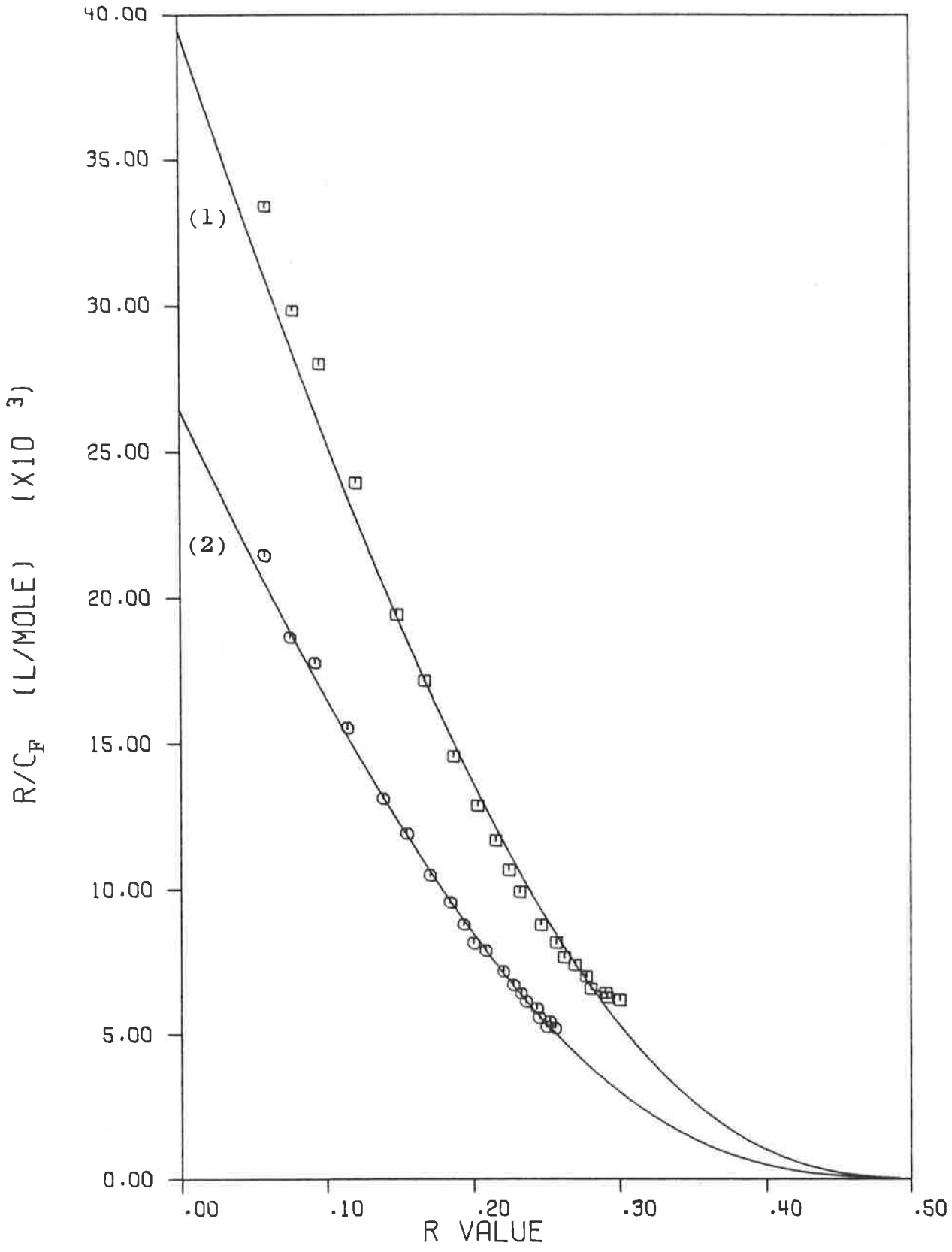

Figure A3-10. The Scatchard plots of the binding data and mathematical model curves for 9(cyc-Hex)AA/*E Coli* native DNA/0.10 M NaCl.
(1) = 35°C; (2) = 50°C.
K_1 = 39460 M^{-1}; k_1 = 0.59_5
K_2 = 26420 M^{-1}; k_2 = 0.50_0

Appendix IV

The micro-computer based control and data collection system for the Zeiss DMR-10 double-beam spectrophotometer.

In order to collect the very large amount of accurate spectral data required for this work, it was necessary to automate the DMR-10 spectrophotometer. The instrument was a basic DMR-10 with the optional digital readout accessory. This option provides a digital readout of the measured absorbance (or transmittance) based on a true integration of the absorbance/transmittance for a preselected time interval. The optimum integration time was three seconds. This was determined by using the micro-computer system described here to collect successive integrated readings, using various integration times between 0.2 seconds and 6 seconds, for a fixed total time interval and calculating the average reading and its standard deviation. From these observations it was determined that there was no improvement in standard deviation of the reading by using the computer to average successive readings taken with shorter integration times. There was no improvement in the observed standard deviation of readings of longer integration times than 3 seconds for absorbances between 0.1 and 0.8.

All of the normal functions of the spectrophotometer and the digitizing accessory can be controlled or accessed via TTL (Transistor-Transistor Logic) level signals at plug points provided on the instrument. The automation requires collection and storage of absorbance readings at predetermined wavelengths after an initial waiting period, required to attain thermal equilibrium of the sample. The data collection sequence is then repeated as frequently as desired, usually

once or twice. The data must then be transferred to some computer-readable form, in this case punched paper tape, for further processing.

The system chosen to perform the automation was an Intel SDK-80 system design kit, fully expanded, with an additional memory expansion. This micro-computer system is based on the Intel 8080A micro-processor circuit with 1K bytes of Read Only Memory (ROM), 3K bytes of Electrically Programmable Read Only Memory (EPROM) and, with expansion, 9K bytes of Random Access Memory (RAM). Also provided were three Programmable Peripheral Interface (PPI) circuits. One PPI was dedicated to the four figure BCD digital readout and associated "hand-shake" signals. Another was used for instrument control and status checking. The third controlled several switches and indicator lights on the computer front panel. User communication was provided through these switches and lights and via an ASR-33 Teletype equipped with a paper tape punch.

A program was written in 8080A machine language to provide all the necessary machine instructions to control and collect data, as a real-time operating system, from the DMR-10. The program listings and circuit diagrams are too large to be reproduced here, however copies are available on request. To use the system the sample and reference cells are loaded into the DMR-10, the temperature controller set (and the nitrogen flow if operating at temperatures below ambient). The monochromator limit switches are set to just above and below the required wavelength range and the integration time and monochromator step size switches are set. The computer is then turned on and an instruction entered to begin executing the program. An abridged flow diagram of the program operation, with emphasis on the interaction between the

computer and the operator, is contained in Fig. A4.1. The mode of communication is indicated by the boxed letter alongside the function, T for teletype and S for front panel switch and/or light. The Abort function can be entered at any time between the beginning of a collection sequence and the end of punching the data.

A complete collection sequence generally takes 30-45 minutes and the operator is only required to change the sample solution at the end of each collection. At the end of a work period the user has a punched paper tape containing all of the absorbance data collected. This tape is used to transfer the data to another computer for further processing.

This micro-computer based system provides an automated, absolutely reproducible operating regime for using the spectrophotometer. It has operated for three years without fault.

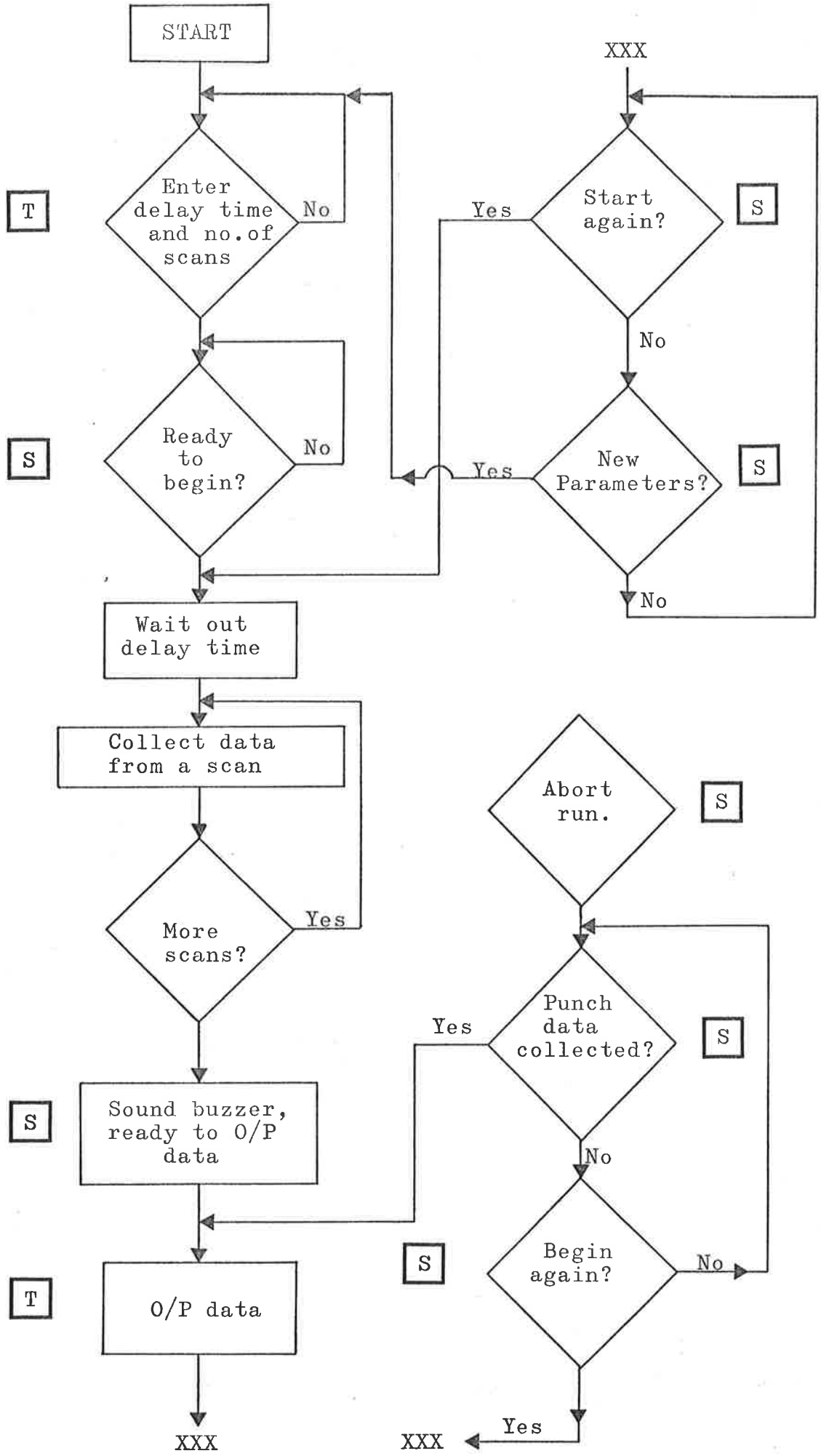

Figure A4-1. Flow diagram of Micro-computer operation.

Appendix V

Summary of computer programs written as part of this work.

The intention of this Appendix is to provide a brief summary of the computer programs written in the course of this work. It is not practical to reproduce full listings here since the total package contains over 8000 lines of code. Emphasis is on programs central to the calculation of binding data and where numerical or unusual alogrithms are employed. All the programs were written in FORTRAN EXTENDED and were run on either a CDC 6400 computer or, more latterly a CDC CYBER 173 computer. Extensive use was made of the CDC utilities UPDATE, EDITLIB and CCL in the creation and maintenance of both program and data libraries.

In addition to programs specifically described in this Appendix a number of other programs, for the most part trivial in nature, were written to perform tasks such as generating synthetic data sets for program testing.

PROGRAM BINDING

This program calculates binding data from spectral data. The primary data was obtained from program DMR02 and input values of monomer and bound ε^{λ} values and absorbance versus concentration polynomials. It used the algorithm detailed in Chapter IV to calculate values of ε_F^{λ}, α, C_B, C_F, r and r/C_F. On a user supplied option it also output data files suitable for plotting and/or as input to program NONLIN.

PROGRAM DMR01

This program reads the punched paper tape containing absorbance data. The data sets for each spectrum are averaged with a check that the maximum absorbance difference

at any wavelength does not exceed 0.002. The cell correction spectrum is subtracted and solution thermal expansion correction is made. The data are then added, in compressed format, to a data base file held on disc.

PROGRAM DMR02

This program takes data sets from the data base as input together with the DNA background correction spectrum, if appropriate. The program produces a set of tables of wavelength, absorbance, molar absorptivity, difference spectrum and normalized absorbance. It will also assemble disc files of corrected molar absorptivity values at particular wavelengths for use by program BINDING.

PROGRAM DMRI01

This is an interactive program used to interactively prepare a variety of data types for plotting through program PLOTT.

PROGRAM DNANAL

This program performed the Hirschman and Felsenfeld spectral analysis of DNA (see Chapter VII part B(2)). Absorbance data was input together with the temperature(s) at which they were collected. The program then performed the appropriate analyses. It was written in such a way that it recognised the types of analyses for which there were sufficient data input and performed all these analyses. For example, data collected to perform the hyperchromic analysis also contains sufficient data to perform the native and denatured analyses as subsets of the data.

PROGRAM GENER8

This routine generates spectra using linear combinations. It is used principally to generate bound spectra from data sets

from the data base using either "fraction bound" values for specified spectra or value(s) of ε_B^λ.

PROGRAM INTLIN

The calculation of the internal linearity conditions, according to the algorithm described in Chapter IV (3)(a). The program also prepared a file suitable for plotting.

PROGRAM NONLIN

This program was used to calculate best fit parameter values for non-linear equations. The program was a modified version of a program written by C.M. Metzler of the Upjohn Company. The program uses a modification of the Newton-Rapson method of linearizing equations due to Hartley*. A subroutine which contains the equation(s) to be fitted is supplied along with the data. The program was always used as a weighted non-linear fit. Extensive use of this program was made in many aspects of this work.

Convergence of the fit was assessed on minimizing the sum squares of the deviations and full statistical error calculations were performed on the fitted values. The only major alteration made from the original version concerns the use of a precision factor. This factor was used to truncate values of the calculated independent variable(s) to the level of significance of the original data. The intention of this truncation is to avoid attempting to refine fitted parameter values beyond the significant figures of the experimental data. There is no theoretical justification for such truncation, which inevitably changes the values contained in the solution matrix. This facility was removed from the program.

---

* Hartley H.O., *Technometrics*, 3, 269 (1961).

The equation subroutines supplied for fitting data to the sequence generating functions are unusual in that a numerical solution of the roots of a polynomial are required for each calculation of a fitted value of the equation. Since many thousands of such calculations are made in each fitting exercise, the solution must be rapid and precise. The relevant code used for each of the sequence generating functions is reproduced below. These same algorithms were used in the equation subroutine of program PLOTT to produce the curves shown in figures in Chapters V and VI and in Appendix III.

PROGRAM PLOTT

This program is a versatile plotting routine which produces plots on 10" or 75 cm Calcomp digital plotters. Plots can be produced containing any combination of data points, curves from equations supplied in an equation subroutine, polynomial fits or lines fitted to data points by an exact cubic spline. All of the computer produced diagrams used in this thesis were produced on the 75 cm plotter which has a resolution of 0.1 mm. The exact cubic spline was used to produce the plots of spectra contained in this work. This routine was originally obtained from the Defence Research Establishment, Salisbury, South Australia. It was extensively modified to suit the needs of this plotting program. The lines produced by the spline exactly represent the spectra which they fit since the line is constrained to pass exactly through each datum point. These data points are at 1 nm intervals. Tests showed that the 2000 points per spectrum interpolated by the spline exactly represented spectrum to within the resolution of the plotter. Similar tests showed that 2000 points

calculated from functions contained in the equation subroutine exactly represent the function to within the resolution of the plotter. The plots reproduced in this thesis may be used to obtain data to within the precision from which measurements can be taken from them.

```
      SUBROUTINE DFUNC(T,I,J,K,P,VAL)
      DIMENSION P(16),VAL(10),NAME(4)
      COMMON NP,NC,NIV,NDE,NIT,NTP,PM,IP,IT,SS,WS
      COMMON PL(32),CON(8),IW(10),NPT(11),Y(10),IDIG(10)
      COMMON NAME,LPLOT,LDEQ,TEST,DEL
      COMMON YOBS(400),X(800),DV(400),W(400),YCALC(400)
C
C     SEQUENCE GENERATING FUNCTION FOR A ONE SITE BINDING MODEL WITH
C       NEAREST NEIGHBOUR SITE EXCLUSION AND NEXT SITE CO-OPERATIVITY.
C
C     CONTAINS AN ALGORITHM TO FIND THE LARGEST ROOT OF THE CUBIC
C       EQUATION CONTAINED IN THE SOLUTION.  THIS INVOLVES FINDING THE
C       GREATEST TURNING POINT AND TAKING 3 TIMES THIS VALUE OF X AS THE
C       FIRST GUESS FOR A <NEWTON'S ITERATION> TECHNIQUE.
C
C       FKASS -- INTRINSIC ASSOCIATION CONSTANT.
C       FKCOP -- CO-OPERATIVITY FACTOR.
C       CF    -- FREE LIGAND CONCENTRATION.
C
       FKASS=P(1)
       FKCOP=P(2)
       CF=X(I)
       A=FKASS*CF
       B=A*FKCOP
       C=(1.0-FKCOP)*A
       XO=2.0*(1.0+SQRT(1.0+3.0*B))/3.0
C
C      XO IS NOW THE INITIAL ESTIMATE OF THE LARGEST POSITIVE ROOT OF
C       THE CUBIC POLYNOMIAL.
C
       XN=XO
    10 XSQ=XN*XN
       F=XSQ*XN-XSQ-B*XN-C
       DF=3.0*XSQ-2.0*SN-B
       XINC=F/DF
C
C      XINC IS THE NEW ESTIMATE FROM THIS ITERATIVE STEP.  IF NO
C       SIGNIFICANT CHANGE HAS OCCURRED ON THIS ITERATION, THEN THIS
C       IS THE ROOT.
C
       XTEST=ABS(XINC)
       IF(XTEST.LE.1.0E-7) GO TO 20
       XN=XN-XINC
       GO TO 10
    20 X1=XN-XINC
C
C      DEPENDENT VARIABLE VALUE IS RETURNED AS T.
C
       T=(B*X1+C)/(X1*(3.0*X1*X1-2.0*X1-B))
       RETURN
       END
```

```
      SUBROUTINE DFUNC (T,I,J,K,P,VAL)
      DIMENSION P(16),VAL(10),NAME(4)
      COMMON NP,NC,NIV,NDE,NIT,NTP,PM,IP,IT,SS,WS
      COMMON PL(32),CON(8),IW(10),NPT(11),Y(10),IDIG(10)
      COMMON NAME,LPLOT,LDEQ,TEST,DEL
      COMMON YOBS(400),X(800),DV(400),W(400),YCALC(400)
C
C     SEQUENCE GENERATING FUNCTION FOR A ONE SITE MODEL WITH NEAREST
C       NEIGHBOUR SITE EXCLUSION AND THE NEXT TWO SEQUENTIAL SITES HAVE
C       CO-OPERATIVITY FACTORS.
C
C     DEVISED AND WRITTEN BY G. BOEHM FROM AN IDEA FROM M. WAGNER.
C
C     CONTAINS AN ALGORITHM TO SOLVE THE QUINTIC INVOLVED IN THE
C       EXPRESSION.  THIS CONTAINS A CUBIC,THE GREATEST TURNING POINT
C       OF WHICH CAN BE CALCULATED. THIS VALUE IS USED AS AN ESTIMATE
C       TO CALCULATE THE LARGEST POSITIVE ROOT OF THE CUBIC. TWICE THIS
C       VALUE IS THEN USED AS AN INITIAL ESTIMATE FOR THE LARGEST
C       POSITIVE ROOT OF THE QUINTIC WHICH IS THEN COMPUTED FROM A
C       <NEWTON'S ITERATION> TECHNIQUE.
C
C     FKASS  -- INTRINSIC ASSOCIATION CONSTANT.
C     FKCOP1 -- BETA SITE CO-OPERATIVITY FACTOR.
C     FKCOP2 -- GAMMA SITE CO-OPERATIVITY FACTOR.
C     CF     -- FREE LIGAND CONCENTRATION.
C    (NB. THE SITES ADJACENT A BOUND SITE ARE DESIGNATED <ALPHA,BETA,ETC.>)
C
      FKASS=P(1)
      FKCOP1=P(2)
      FKCOP2=P(3)
      CF=X(I)
      A=FKCOP1*FKCOP2
      B=A-1.0
      C=FKASS*CF
      D=FKCOP1*(1.0-FKCOP2)
      T1=A*C
      T2=B*C
      T3=C*C*D
      TERM1=3.0*T1
      TERM2=2.0*T2
      XP=(4.0+SQRT(16.0+45.0*T1))/5.0
C
C     XP IS THE LARGEST TURNING POINT OF THE CUBIC CONTAINED WITHIN
C      THE QUINTIC EXPRESSION.
C
    5 XSQ=XP*XP
      G=5.0*XSQ*XP-4.0*XSQ-TERM1*XP+TERM2
      DG=15.0*XSQ-8.0*XP-TERM1
      XINC=G/DG
      XTEST=ABS(XINC)
      XP=XP-XINC
      IF(XTEST.GT.1.0E-7) GO TO 5
      XN=2.0*XP
C
C     XN IS NOW THE LARGEST POSITIVE ROOT OF THE SUB-EXPRESSION CUBIC
C      POLYNOMIAL.
```

```
C
   10 XSQ=XN*XN
      XCB=XSQ*XN
      X4=XSQ*XSQ
      F=XSQ*XCB-X4-T1*XCB+T2*XSQ+T3
      DF=5.0*X4-4.0*XCB-TERM1*XSQ+TERM2*XN
      XINC=F/DF
      XTEST=ABS(XINC)
      XN=XN-XINC
      IF(XTEST.GT.1.0E-9) GO TO 10
      X1=XN
C
C     XN IS NOW THE LARGEST POSITIVE ROOT OF THE QUINTIC POLYNAMIAL.
C
      XSQ=X1*X1
      XCB=XSQ*X1
      X4=XSQ*XSQ
      FNUM=T1*XCB-T2*XSQ+2.0*T3/FKASS
      DENOM=XSQ*(5.0*XCB-4.0*XSQ-TERM1*X1+TERM2)
C
C     THE VALUE OF THE DEPENDENT VARIABLE IS RETURNED AS T.
C
      T=FNUM/DENOM
      RETURN
      END
```